The Synthesis and Characterisation of Novel Amide Initiators for the ATRP of OEGMA

Aaron J Kliene

A thesis submitted to the University of Kent in partial fulfilment of the requirements for the degree of Doctor of Philosophy.

University of Kent
Canterbury
Kent
CT2 7NH

September 2015

Abstract

Whilst atom transfer radical polymerisation (ATRP) has been shown to be a robust and versatile technique for the creation of a wide range of polymers from many different initiators, there is relatively little previous research into the usage of initiators containing amide functionality. Low initiator efficiencies, often resulting in higher than predicted molecular weight parameters, and slow polymerisations with variable rates of reaction are generally reported when amide initiators have previously been used. Various reasons have been proposed in the literature for poor performance of amide initiators including; interactions of the catalytic system of ATRP and the amide bond in the initiator, the irreversible loss of catalyst activity, a rapid initiation causing an overabundance of radicals and poor initiator efficiencies. No suitable solution for these problems had been put forward and the poor performance observed was a major hindrance for any work with amide initiators.

This work describes the development of a system that enabled the usage of novel amide initiators for the ATRP of oligo (ethylene glycol) methyl ether methacrylate (OEGMA) with high levels of success. The development of an ideal set of reactions conditions was shown to produce materials with low dispersities and molecular weight parameters in close agreement to theoretical values. Through the usage of UV-visible spectroscopy and quantum chemical calculations the reason for poor amide initiator performance was determined to be as a result of the high bond dissociation energy of the initiator's halide as a result of its proximity to the amide bond. This effect could be mitigated, but not eliminated, by performing reactions in polar solvent systems. Optimised reaction conditions were utilised in the synthesis of a block copolymer of POEGMA and polyethyleneimine, which shows potential as a stabiliser for superparamagnetic nanoparticles and as a controlled drug delivery system due to the materials high solubility and thermoresponsive properties.

Acknowledgments

Firstly I would like to thank my parents, grandparents and brother. Throughout all the trials and tribulations of the last few years, your constant support and love have kept me going, no matter how many setbacks I encountered.

Sarah, there is no way I would have been able to finish this work without the love and care you have given me over the past five years.

Jan and Sandra, thank you so much for making me feel welcome within your family, and for being there for me when my parents couldn't immediately make it as my appendix and gallbladder decided they no longer wanted to be my organs.

Marc, Toddy, Greg, Ben, Mark, Guy, and Ed; you guys are the best (worst) people I know. Thank you for agreeing to live with me throughout my time at university and for being constant sources of stress-relief and humour, even while things were bleak.

Thank you to the entire functional materials group, and more specifically everyone I shared my time in the lab with. David, Beulah, Anica, Mat, girl Charlie, Gemma, Darren, Adrian, Steve, Chris, boy Charlie, Liv, Christina, Tom, Kate and Marc; you have all taught me something, and made the experience of working in a lab something I will never forget. In particular I need to thank Kate and Marc for going through hell with me, continually giving me support, and convincing me that I could finish this.

Thank you to all the academic and technical staff within Physical Sciences at the University of Kent. You have always offered help when I have asked for it, and your chemical and technical knowledge is a resource that made this work possible. More specifically I am indebted to J.J. who not only freely offered advice on technical matters, but actually employed me part-time during my write up.

I would like to thank all of my collaborators; Tom Ashton during his masters at the University of Kent, Cem Atlan and Nico Sommerdijk at the Eindhoven University of Technology, U. Ecem Yara and Seyda Bucak at Yeditepe University in Istanbul.

Finally I need to thank Simon Holder, my supervisor, for convincing me to continue when I tried to quit. I know that I have not been an ideal student over the years, but without your invaluable support and guidance throughout this PhD I would never have been able to make it to this point.

Declaration

I declare that this thesis is my own work and effort, and has been written in my own words. Due care has been taken to properly reference the work of others wherever necessary.

Aaron J Kliene

5th June 2016

Abbreviations

ARGET	-	Activators regenerated by electron transfer
ATRP	-	Atom transfer radical polymerisation
BDE	-	Bond dissociation energy
$CDCl_3$	-	Chloroform-d
CuCl	-	Copper (I) chloride
DP	-	Degree of polymerisation
Đ	-	Dispersity
DLS	-	Dynamic light scattering
dNBpy	-	4,4'-Dinonyl-2,2'-bipyridine
EBriB	-	Ethyl 2-bromoisobutyrate
EtOH	-	Ethanol
I_{eff}	-	Initiator efficiency
k_{act}	-	Activation rate coefficient
k_{atrp}	-	Rate coefficient of ATRO
k_{deact}	-	Deactivation rate constant
k_p	-	Propagation rate coefficient
k_t	-	termination rate coefficient
LCST	-	Lower critical solution temperature
PEG	-	Polyethylene glycol
PEI	-	Polyethyleneimine
PEI-macroinitiator	-	Poly(ethylene imine)-*graft*-(2-bromo-2-methyl)propanamide
PMDETA	-	*N*,*N*,*N*′,*N*″,*N*″-Pentamethyldiethylenetriamine
PNIPAAm	-	Poly(N-isopropylacrylamide)
POEGMA	-	Poly(oligo ethylene glycol) methyl ether methacrylate
PRE	-	Persistent radical effect
MeOH	-	Methanol
M_n	-	Number average molecular weight
MBriP	-	Methyl 2-bromo-2methylpropanoate
MBriPA	-	*N*-methyl 2-bromo-2-methylpropanamide

MBriPA2	-	*N*,*N*-dimethyl 2-bromo-2-methylpropanamide
MBrPA	-	2-bromo-2-methyl-*N*-propylpropanimde
MBrPBr	-	2-bromo-2-methyl-propionyl bromide
MCliP	-	methyl 2-chloro-2-methylpropanoate
MCliPA	-	*N*-methyl 2-chloro-2-methylpropanamide
MEO_2MA	-	2-(2-methoxyethoxy)ethyl methacrylate
MMA	-	Methyl methacrylate
NMR	-	Nuclear magnetic resonance
RAFT	-	Reversible-addition fragmentation chain transfer
SARA	-	Supplemental activator and reducing agent
SEC	-	Size exclusion chromatography
SET-LRP	-	Single electron transfer living radical polymerisation
$Sn(EH)_2$	-	Tin 2-ethylhexanoate
T_{CP}	-	Cloud point temperature
THF	-	Tetrahydrofuran
wt%	-	Weight percentage

Table of Contents

Chapter 1: Introduction to polymers

1.1 Polymers

Since the mid-1800s it was known that by using certain chemical reactions it was possible to affect the bulk properties of some materials, but it was not until 1922 that Hermann Staudinger first proposed that polymers consisted of long chains of atoms that are covalently bonded together into "macromolecules".[1] A polymer is now defined as a macromolecule that is composed of repeated smaller structural subunits, monomers, which are covalently bonded together. The number of monomer units within a polymer chain is known as the degree of polymerisation (DP), and by increasing this, the overall polymer molecular weight also rises. Perhaps the most well-known example of a polymer is that of polyethylene which is composed of the monomer unit ethylene and sees global usage in packaging, such as plastic bags and bottles (Figure 1.1).

The physical properties of polymers are dependent on the monomer subunits within them, the architecture that the units are arranged in, and the molecular weight of polymer chains. Monomers can be found from a wide array of sources, but can be roughly defined into two categories: natural and synthetic. It was monomers derived from natural sources that were first experimented on in the 1800s which led to the usage of materials such as natural rubber (via vulcanisation) and celluloid (through treatment with camphor).

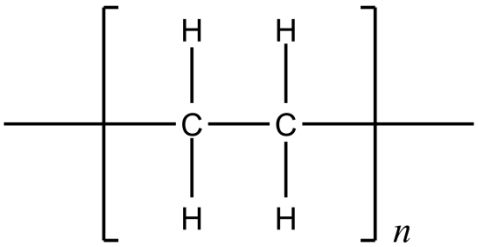

Figure 1.1: Ethylene monomer unit in part of a polyethylene polymer. The degree of polymerisation is denoted by the value *n*.

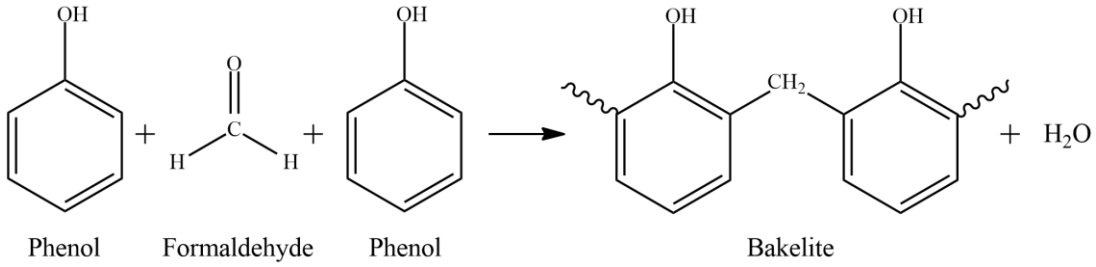

Scheme 1.1: Condensation reaction of phenol and formaldehyde to produced Bakelite and eliminate water.

The first synthetic polymer was created in the early 1900s when Leo Baekeland used a condensation reaction of phenol and formaldehyde to create Bakelite (Scheme 1.1).[2]

Interest into synthetic polymers dramatically increased with the onset of the Second World War where an alternative to silk was required. Work by DuPont solved this, with the introduction of nylon, a high tensile strength polymer that could be easily extruded into threads to replicate the properties of natural fibres.

Due to the large number of monomers available for polymerisation, and the different structural architectures that they can be arranged in, materials can be found for almost any application, and this has caused a subject to be created to study these materials: polymer science.

1.1.1 Copolymers

Whilst many applications can be completed by changing the monomer composition of a polymer, by carefully selecting two or more monomers and combining them in one macromolecule, specific functionality can be introduced. This can be ideal in situations where arrays of traits are desired in the final material but using simple homopolymers is impossible due to either chemical or physical restrictions.

The term copolymer applies when a polymer chain is composed of two or more distinct monomers. Various types of copolymer are possible and selection of

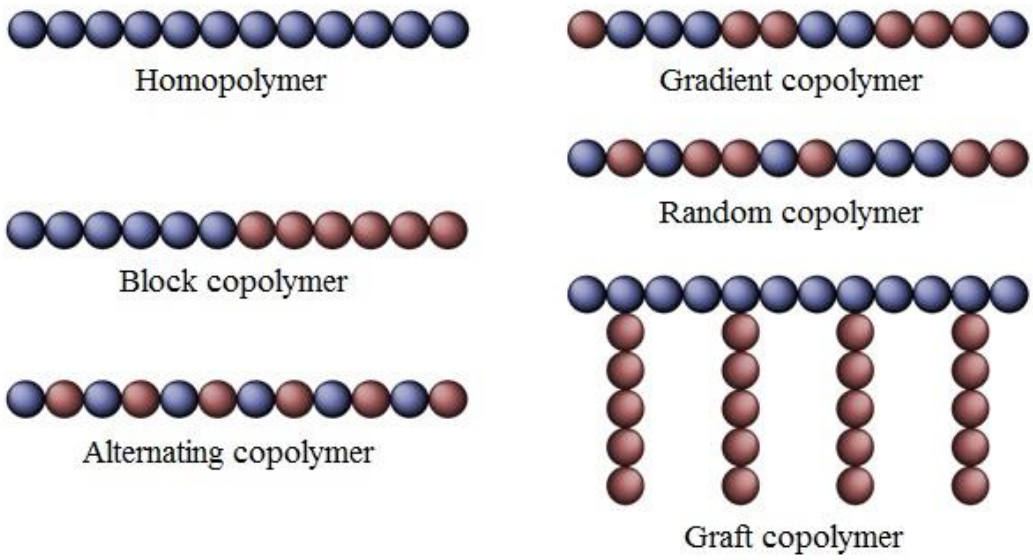

Figure 1.2: Common types of copolymers, where distinct monomer units are displayed as blue and red circles.[3]

architecture is either the result of the polymerisation process or reactivity of monomers. Block copolymers are comprised of two or more different monomers polymerised in distinct segments that are covalently bonded. An alternating copolymer consists of a regularly repeating pattern of monomer types throughout the whole structure of a polymer chain. Gradient copolymers are formed when one type of monomer tends towards one end of a polymer chain. Random copolymers have no order or pattern as to where individual monomer units will be placed. Graft copolymers involve a central structure of one monomer type that has one of more other monomers attached to the central core. All of these can be seen in Figure 1.2.

The mechanical and physical characteristics that polymers possess can be drastically changed by adjusting the architecture of monomer units within it. In general block and graft copolymers tend to maintain most of the original properties of each monomer whereas alternating and random copolymers display more of a compromise of the monomer qualities. Polymeric topology is another effect that can affect the functionality of materials.

Polymers can be described as linear, comb-like, star-shaped and dendritic depending on the structure that they exhibit. Some examples of this can be seen in Figure 1.3 on the following page. These differing topologies can be created by controlling the number of initiating sites that are present for polymerisation to occur from, adjusting the method of synthesis, or controlling the ratio of monomer feedstocks.

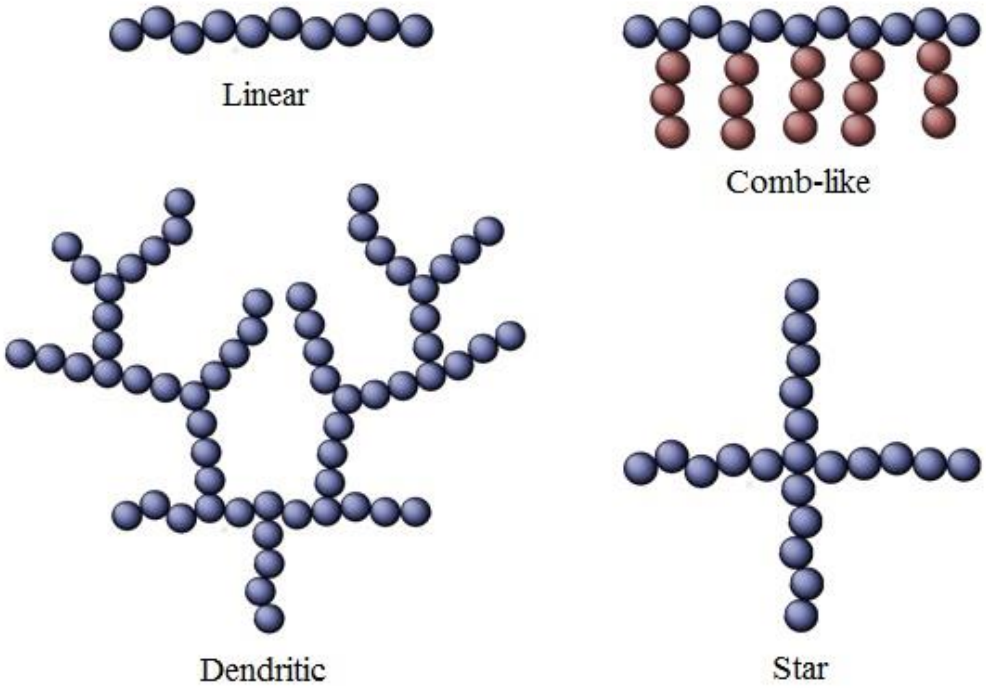

Figure 1.3 – Common architectures of polymers, where distinct monomer units are displayed as blue and red circles.[3]

1.1.2 Block Copolymers

As polymer science advanced there was a greater desire to create materials that could combine multiple benefits of different monomers in one material. Block copolymers that are created from two or more chemically different monomers tend to keep the properties of both parent monomers and open up access to multiple functionalities.[3] A diblock copolymer consists of two monomer blocks, whilst a three monomer unit copolymer is known as a triblock. The general notation for block copolymers is of the form shown in Figure 1.4 below.

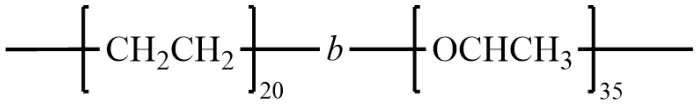

Polyethylene-*block*-Polyethylene glycol

Figure 1.4: General notation for block copolymers. This structure denotes 20 polyethylene units as one block, then a further 35 polyethylene glycol units, as part of one whole block copolymer.

Block copolymers can be formed into various topologies, both linear and non-linear, depending on the number of active sites where polymerisation can occur on initiating and propagating species.

The key advantage of block copolymers over mechanically mixed homopolymers is that block copolymers are covalently linked at the interface of each block. The result of this is that the chemical and physical properties of both blocks can be utilised.

For example, it is possible to create polymers that are hydrophilic and hydrophobic in each block respectively, which leads to the creation of complex morphologies when introduced to aqueous solvent systems.[4] Likewise, it is also possible to shield both polymer components and payloads in drug delivery vehicles *in vivo* by using protein resistant monomers bound to cores that are able to carry pharmaceuticals.[5, 6]

One method for the preparation of block copolymers is by synthesising each polymer component separately, then coupling them together to form single macromolecules.

The advantage of this is that each homopolymer can be synthesised exactly to the parameters desired. A variation of this is the synthesis of a macroinitiator, where a previously prepared polymer is functionalised to act as an initiator in a subsequent polymerisation.[3]

1.2 Polymerisation Techniques

In order to synthesise polymers with desired topology and functionality new techniques for polymerisation had to be developed. There is no catch-all mechanism to create functional polymers, and the techniques that are used tend to be a direct consequence of the traits desired in the final product.

Free radical polymerisations (FRP) have remained some of the most commercially successful reactions due to their ability to work with high levels of impurity, at a wide range of temperatures and in the presence of water and other solvents. This flexibility enables the operation of manufacturing plants that do not have to work under the rigorous conditions of many more recent techniques, lowering the cost of production. This has led to FRP being used to produce over 100 million tonnes of polymer, from numerous different monomers, each year.[7]

Polymerisation reactions can be described as either "step-growth" or "chain-growth", with the distinction between the two being described by Flory in 1953.[8] Primarily the difference is that a step-growth polymerisation occurs by a reaction of the functional groups present in the monomers, whilst a chain-growth reaction is the results of a reaction with an ion or radical. It is important to not get this principle confused with the terms "addition polymerisation" and "condensation polymerisation", which do not relate to the mechanisms involved, but to the products of the reaction. In an addition polymerisation only polymer is produced, whereas in a condensation reaction polymer is produced along with a leaving group (often water).[9]

Free radical polymerisations can be described as a three step process: initiation, propagation and termination, as displayed in Scheme 1.2 on the following page. At initiation, reactive species are created with an unpaired electron (radical) that will be present to attack the vinyl bonds of the monomer units. This occurs through the homolytic fission of the initiator through; thermal decomposition, photoinitiation, or chemical reaction. Once the unsaturated bond has been opened, the monomer unit acquires an unpaired electron of its own, causing the initiator-monomer molecule to become the new reactive centre. This enables another monomer unit to react with this new site, and the free electron is passed along the chain with each successive addition. In an ideal circumstance this propagation continues until the monomer feedstock is used.[3] Termination generally occurs either through bimolecular termination, disproportionation or chain transfer processes. Bimolecular termination occurs when reactive sites on two growing chains come into contact with each other instead of a monomer unit. This causes a loss of reactive sites from the overall reaction as the charge cannot be passed onto a further reactive site and propagation stops. Alternatively disproportionation occurs when a reactive site interacts with a hydrogen atom present on another chain, causing a new unsaturated monomer unit at the terminus of the chain. Similarly to disproportionation, chain transfer processes involve an interaction with hydrogen atoms present within the system, though not necessarily in another growing chain. Chain transfer can occur to the solvent, monomer, initiator or polymer. When chain transfer occurs it results in the removal of a radical from the propagating system, and the generation of a radical that is likely unable to continue reacting due to either; being on a solvent molecule or resonance

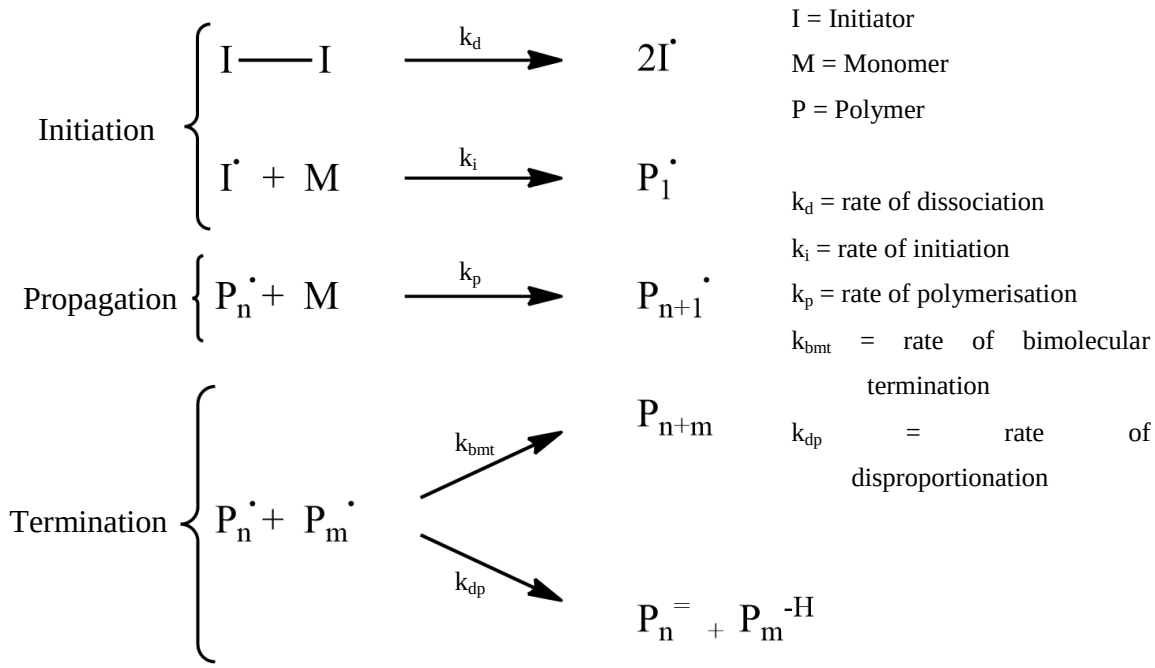

Scheme 1.2: The three stages involved in a radical polymerisation

stabilised on the monomer. If the chain transfer is to the initiator then further propagation may be possible, and chain transfer to the polymer can induce branching due to the radical activation site now situated in the middle of a polymer chain. The largest effect this has on a polymerisation is a decrease in the polymer chain lengths produced.[3]

In practice ideal polymers (with well-defined topology and a controlled degree of polymerisation) are impossible to make using FRP due to a number of factors. It is clear from Scheme 1.2 that by having a high number of reactive sites (radicals) present within the system the chances of bimolecular termination are increased. Further to this, unless the rate of propagation is slower that the rate of initiation there will always be a surplus of reactive sites on chains when compared to active initiator units. The rate at which bimolecular termination occurs is primarily controlled by diffusion within the system, and as such is solvent dependent, and can be in the range of $10^8 M^{-1}s^{-1}$ whereas the rate of propagation tends to be around $10^3 M^{-1}s^{-1}$, again causing chains to terminate faster than they grow.[10]

The effect of these issues is that polymers produced by FRP tend to terminate early and as a result have very broad distributions of molecular weights (dispersity, Đ).

Early termination also means it is difficult to create complex topologies as terminated chains cannot easily be reactivated, excluding the possibility of simple block copolymerisation. If there have been multiple active sites on polymer chains as a result of chain transfer processes, then the material will most likely have crosslinked and have significantly different physical properties to a linear polymer.[8]
These hindrances were not an issue in most bulk industrial applications, and in fact the mild conditions that FRP can operate under were economically desirable. However, as more complex polymeric architectures were desired to fulfil emerging applications in fields such and engineering, electronics and medicine, new polymerisation methods were required.

1.2.1 Controlled Polymerisation Techniques

In order to create polymers with complex well-defined architectures, several methods for controlled polymerisation were developed. Often, these techniques limited the termination reactions that occurred in the early stages of polymerisation, narrowing the dispersity of polymers produced.
The first system that overcame these problems was demonstrated by Szwarc *et al* in 1956, an anionic polymerisation that utilised a rapid simultaneous initiation.[11] He noted the electron transfer properties of polystyrene chains in the presence of a naphthalene-sodium initiator and used this mechanism to produce ABA type block copolymers. The initiation step can also be triggered through the usage of a strong anion and successful reactions have been carried out using metal amides, alkoxides and amines amongst other functional groups.[12] The mechanism for anionic polymerisation is displayed in Scheme 1.3 on the following page. Unlike FRP, anionic polymerisations have no obvious termination reactions; they will progress until all monomer is used up. However, reactions sometimes undergo termination through quenching of the active ion due to impurities such as oxygen, carbon dioxide or water in the system. Quenching can also be used to prematurely terminated a reaction at determined time through the addition of water or an alcohol.[12]
Methods similar to this but using radicals instead of anions were soon developed, and the new systems became known as “controlled free radical polymerisation” (CFRP) or “living radical polymerisation” and yielded polymers with well-defined

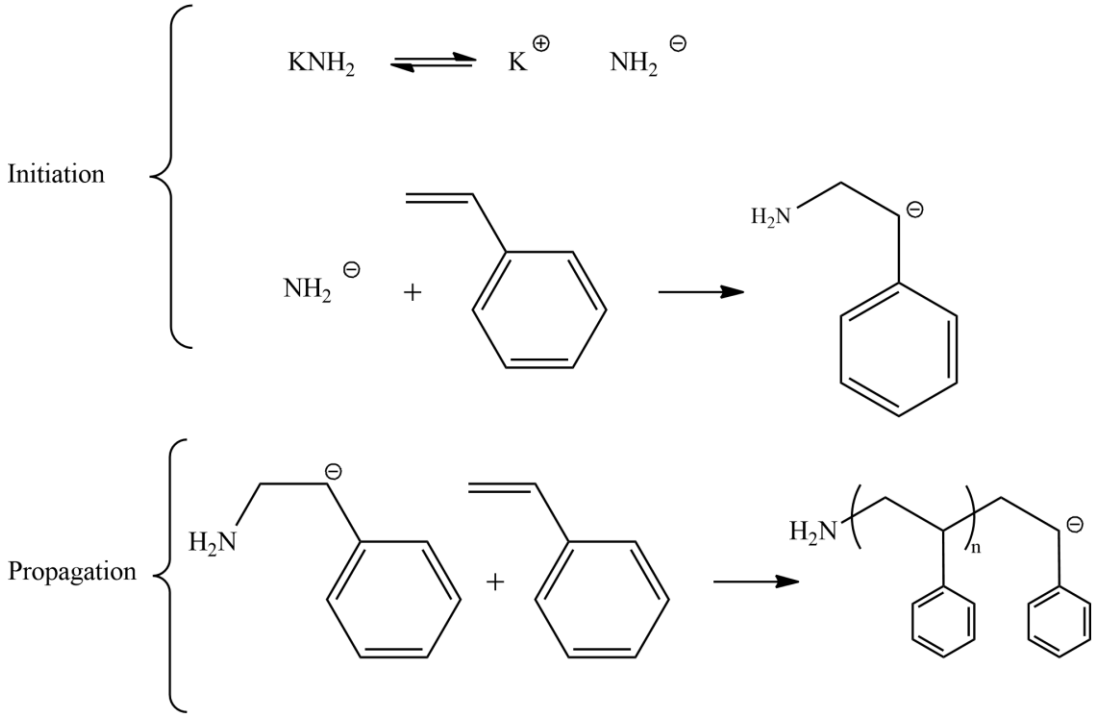

Scheme 1.3: Anionic polymerisation of styrene using a strong anion initiator.

molecular structure and narrow dispersities ($M_w/M_n < 1.5$) compared to previous conventional methods.

The full requirements for a polymerisation to be described as "living" were outlined by Quirk in 1992.[13] Simply put, for a polymerisation to be considered living it must:

- Have a linear increase of molecular weight with conversion.
- Continue propagation until all monomer has been polymerised.
- Have a constant concentration of active radical species.
- Produce polymers with narrow dispersities ($M_w/M_n < 1.5$)
- Retain the functionality of the polymer end group.
- Produce block copolymers with the addition of an additional, differing, monomer.

Living polymerisations are generally controlled by having a low concentration of active propagation sites within the reaction. This means that the dynamic

equilibrium that forms between dormant polymer chains and active species favours the dormant chains, limiting the chance of bimolecular termination, or any other side reaction that could prematurely stop the reaction. In many techniques this dynamic equilibrium is brought about through either a degenerative transfer process or a mediating species.

The degenerative transfer process involves moving the active centre from a growing polymer chain to either another molecule or a different site on the same molecule. This affords some level of control of the polydispersity of the system depending on the specific methods used. The most widely used form of this is reversible addition-fragmentation chain transfer polymerisation (RAFT),[14] although other techniques exist such as iodine-transfer radical polymerisation (ITRP)[15] and telluride-mediated polymerisation (TERP).[16]

In a mediated process radicals are switched between an activated and terminated state, ensuring that there can only ever be a small number of propagating species. Perhaps the most widespread usages of this process are atom transfer radical polymerisation (ATRP),[17] where transition metal halides are used to reversibly generate radicals for propagation, and nitroxide mediated polymerisation (NMP).[18] Whilst other techniques include variations of ATRP such as activator regenerated by electron transfer ATRP (ARGET-ATRP),[19] or copper (0) mediated systems such as supplemental activator reducing agent ATRP (SARA-ATRP)[20] and single electron transfer living radical polymerisation (SET-LRP).[21]

The overall mechanisms for the degenerative transfer and radical mediation processes are displayed in Scheme 1.4 on the following page.

For these techniques to be successful the rate of propagation during polymerisation must be lower than the rate of dormant to active species exchange, and the number of self-terminating reactions must be kept to a minimum, leading to all polymer chains retaining their end-group functionality. Ideally this enables polymers created by CFRP to be re-initiated in the presence of a new monomer feedstock in order to either increase the molecular weight of a homopolymer, or create desirable copolymers. When CFRP is successful it also enables the synthesis of polymers with extremely narrow dispersities due to the uniform, simultaneous, growth of all polymer chains within the reaction.

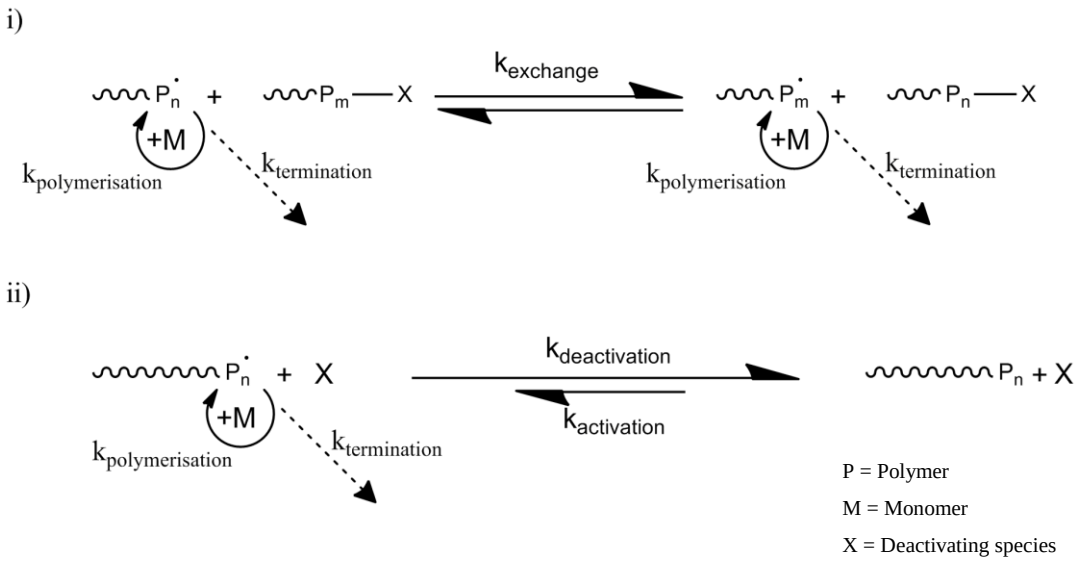

Scheme 1.4: Mechanisms for i) degenerative transfer and ii) radical mediated processes

The downside to this is that CFRP struggle to produce polymers with high molecular weights due to the total number of radicals at any given moment being limited in the system. With a low radical population the time-scale for reactions to reach high molecular weights is increased. Whilst this can be adjusted by optimizing reaction conditions, any increase to the rate of polymerisation by temperature or solvent could directly influence the ratio of dormant to active species, adversely affecting the control of the system.

It should be noted that whilst the terms "living" and "controlled" are often used synonymously within polymer science, but there are some key differences between the two. Matyjaszewski notes that a "living" polymerisation does not inherently provide control over the architecture of the polymer synthesised, nor its molecular weight parameters.[22] A controlled polymerisation can be defined as one where the final polymer created has a targeted molecular weight that is determined upon initiation by the ratio of monomer to initiator used. It should also have a well-defined structure and maintain end group functionality. This is achieved by a fast initiation step but relatively slow propagation and is generally carried out through the transfer of the active site of polymerisation. The result of this is the uniform, simultaneous, growth of all polymer chains resulting in a low dispersity for the material that is produced.

Whilst these traits can be desirable in "living" polymerisation they do not fully match what Quirk outlined as essential.[13] A slow initiation step similar to FRP is possible, and this brings with it the problems associated with that reaction mechanism.

The difference between these two terms can be clearly highlighted when looking at the kinetics of a specific reaction. A reaction that shows "living" characteristics under a set of specific conditions can vary drastically when temperature or solvent changes, elucidating the "non-living" nature of the polymerisation. In an effort to get around this, the term "controlled/living" can be used to describe systems where characteristics of both are present, and IUPAC recommends the usage of reversible-deactivation radical polymerisation (RDRP) when talking about any mechanism in which: "*chain polymerisation is propagated by radicals that are deactivated reversibly, bringing them into active-dormant equilibria*", and only using the term "controlled" when talking specifically about the topology of a polymer or the kinetics of the reaction.[23]

1.2.2 Reversible-addition fragmentation chain transfer polymerisation (RAFT)

The reversible-addition fragmentation chain transfer polymerisation (RAFT) system was first published by Rizzardo *et al* in 1998.[14] The RAFT process relies on a free radical initiator to start the polymerisation, and then the active site of a growing polymer chain is temporarily transferred to the RAFT agent forming a dormant species. Upon reinitiation the radical group "R" can react with monomer to form a second growing polymer chain, allowing polymerisation and chain transfer from both sides of the RAFT agent.

The radical stabilisation by the RAFT agent is a reversible process, and the dynamic equilibrium that forms between dormant and active chains is comparable to the dynamic equilibriums that form in other RDRP such as NMP or ATRP.

The specific chain transfer reagent that is used in the polymerisation is critical in controlling the molecular weight parameters and dispersities of polymer that are synthesised. Most commonly used RAFT agents are composed of dithioesters, dithiocarbamates or dithiobenzoates, but all require three properties to be successful:

a reactive C=S bond, a "Z" group stabiliser (often a phenyl group), and a free radical leaving group "R".[14, 24] Due to the importance of the role the RAFT agent plays within the polymerisation, they are often tailored to the monomer and solvent system that is used in the synthesis.

The RAFT system is probably the most commonly used degenerative transfer process polymerisation, and has been utilised in the synthesis of controlled polymers and block copolymers with, and without, complex morphologies.[25] Block copolymers are formed by reinitiation of a dormant polymer chain with a new monomer, whilst star shaped polymers can be prepared by using a RAFT agent with multiple dithio moieties.[26] A simplified mechanism for the RAFT process is shown in Scheme 1.5 on the following page.

Due to the RAFT agent being composed of dithio moieties, polymers produced by the RAFT process often retain some sulphur following synthesis. The results of this are polymers that are often highly coloured or possess an unpleasant smell, making them undesirable for applications where these factors are detrimental. As the process developed it was found that the RAFT agent could be regenerated by using a free radical source, reducing the sulphur moieties leftover in the polymer.[27] Furthermore, the chain transfer agent could be functionalised following polymerisation to give materials produced increased utility.[28] These advances were shown to mitigate the colouration of synthesised polymers, as well as opening up new synthetic options due to increased functionality.

Besides the somewhat detrimental properties of polymers produced by the RAFT process, another major problem is that the chain transfer agents often have to be synthesised specifically for each unique reaction. Whilst some RAFT agents are now commercially available,[29] in order to create highly functional or specific topologies within a polymer the RAFT agent still needs to be synthesised for a specific set of conditions. In addition to this, as the amount of monomer in the system decreases the rate of bimolecular termination increases, especially when a free radical initiation source is used. In order for polymers produced by the RAFT process to maintain their chain activity for further reactions the polymerisation typically needs to be stopped at 70-90% conversion.

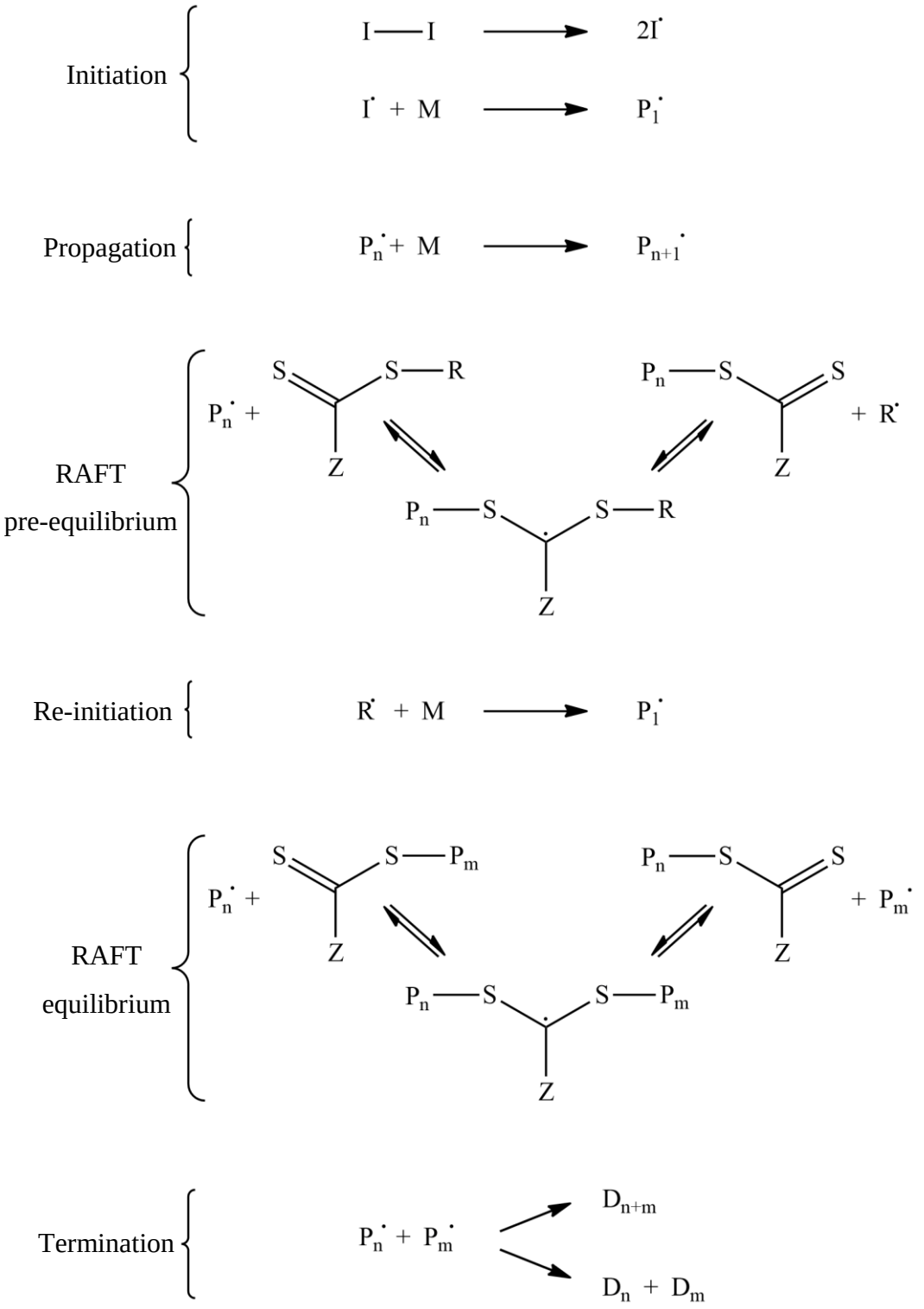

Scheme 1.5: Simplified mechanism for the RAFT process. The reaction is initiated with a free radical source, such as azobisisobutyronitrile (AIBN). Propagating polymer radicals are reversibly stabilised by the RAFT agent, producing leaving group "R" radicals which continue the polymerisation. Polymer chains P_n and P_m continue to be stabilised by the RAFT agent as chain growth continues until termination.

1.2.3 Nitroxide mediated polymerisation (NMP)

Nitroxide mediated polymerisation (NMP) utilises a dynamic equilibrium that forms between dormant alkoxyamines and active propagating polymer species in a similar fashion to other RDRP. The technique was developed by Hawker *et al* in 1994 and initially reported the use of 2,2,6,6,-tetramethylpiperidinyl-1-oxy (TEMPO) as a "*thermally labile capping agent for growing polymer chains*" used in the polymerisation of styrene.[30] Since then the technique has progressed and now the radical mediator can range from (arylazo)oxy, substituted triphenyl, verdazyl, triazolinyl or other nitroxides.[18]

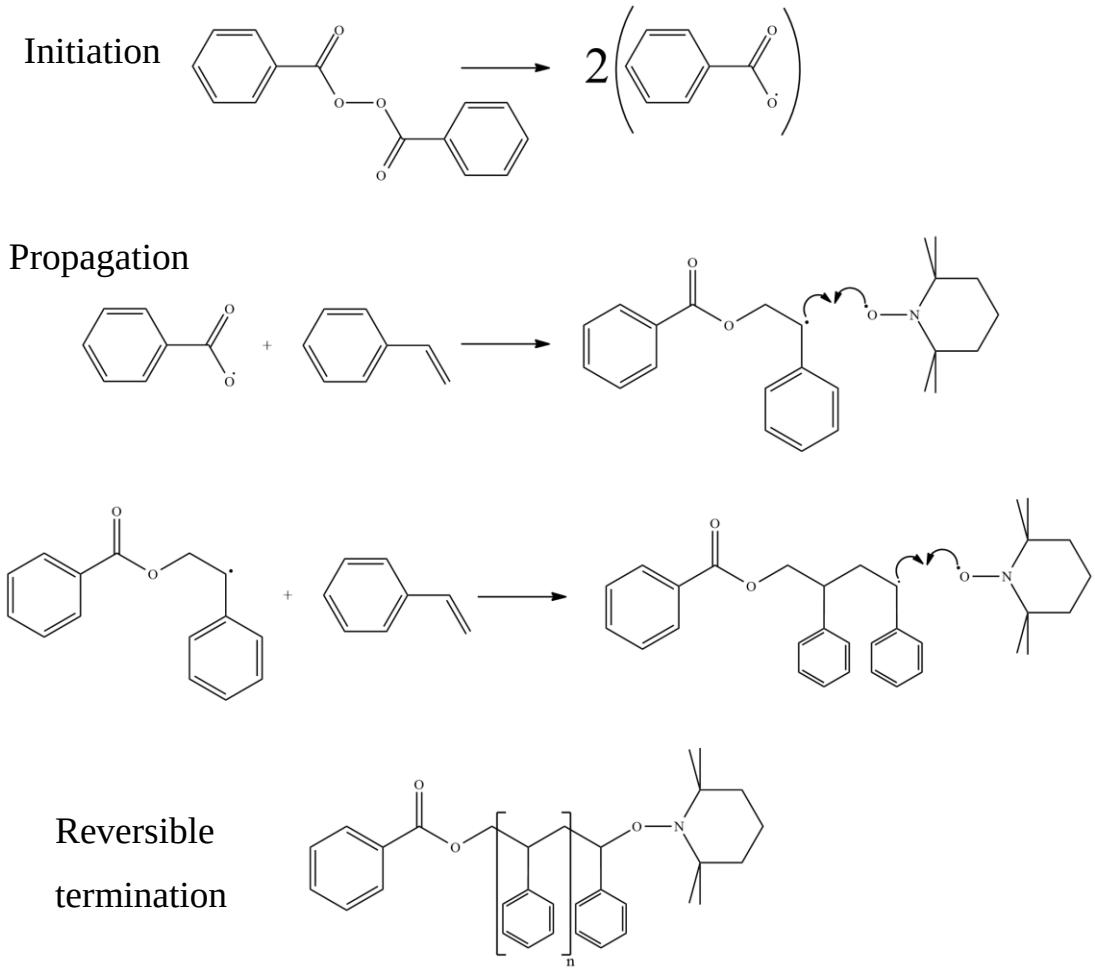

Scheme 1.6: Simplified mechanism for the NMP of styrene using BPO as an initiator. The reaction initiates with the thermally promoted homolysis of BPO to produce radicals. Generated radicals encounter styrene monomer and the propagating polymer chain has its active site mediated by the nitroxide radical (TEMPO). The nitroxide radical produces a thermally labile alkoxyamine, which acts as a reversible termination event, allowing the reaction to be reinitiated for further polymerisation or to create a block copolymer.

Within the mechanism TEMPO is often described as a persistent radical, an idea that shares similarities to the process within ATRP described later. Early reactions revolved around bimolecular initiators such as benzoyl peroxide (BPO), but as the technique progressed new research led to the synthesis of unimolecular initiators which could act as chain capping agents themselves, improving the functionality of synthesised materials.[18]

NMP is a relatively facile process and its ability to produce polymers in bulk with high molecular weights is very advantageous. In addition to this, NMP is an entirely thermally initiated process, requiring no external radical source or metal catalyst as in other RDRPs. The downside however is that many reactions require high temperatures (the seminal paper carried out NMP at 130 ºC), and the range of monomers that can be used is limited.[18] In fact, it was only in 2014 that the homopolymerisation of a group of methacrylates was carried out at relatively low temperatures (40-50 ºC) using NMP by Detrembleur *et al*.[31]

Also, similarly to RAFT, both the nitroxide mediating molecule, and the initiating radical source often have to tailored and synthesised for the required application, with only a small range of commercially available options on offer.

A simplified mechanism for NMP is shown on the previous page in Scheme 1.6.

1.2.4 Atom Transfer Radical Polymerisation

Since its development in the mid-1990s copper mediated atom transfer radical polymerisation (ATRP) has become a fascinating tool for the creation of well defined, controlled polymers due to its relatively facile experimental technique and the lack of stringent reaction conditions necessary for successful reactions.[32] ATRP was developed simultaneously and independently by Matyjaszewski and Sawamoto and has become one of the most intensively researched synthetic methods for creating well defined polymers and copolymers across a broad range of monomers.[32, 33]

The primary mechanism of ATRP involves the homolytic bond cleavage of a carbon-halogen bond, and the radical that is formed subsequent attack of a vinyl monomer. Propagation of the polymer proceeds through a stepwise addition of

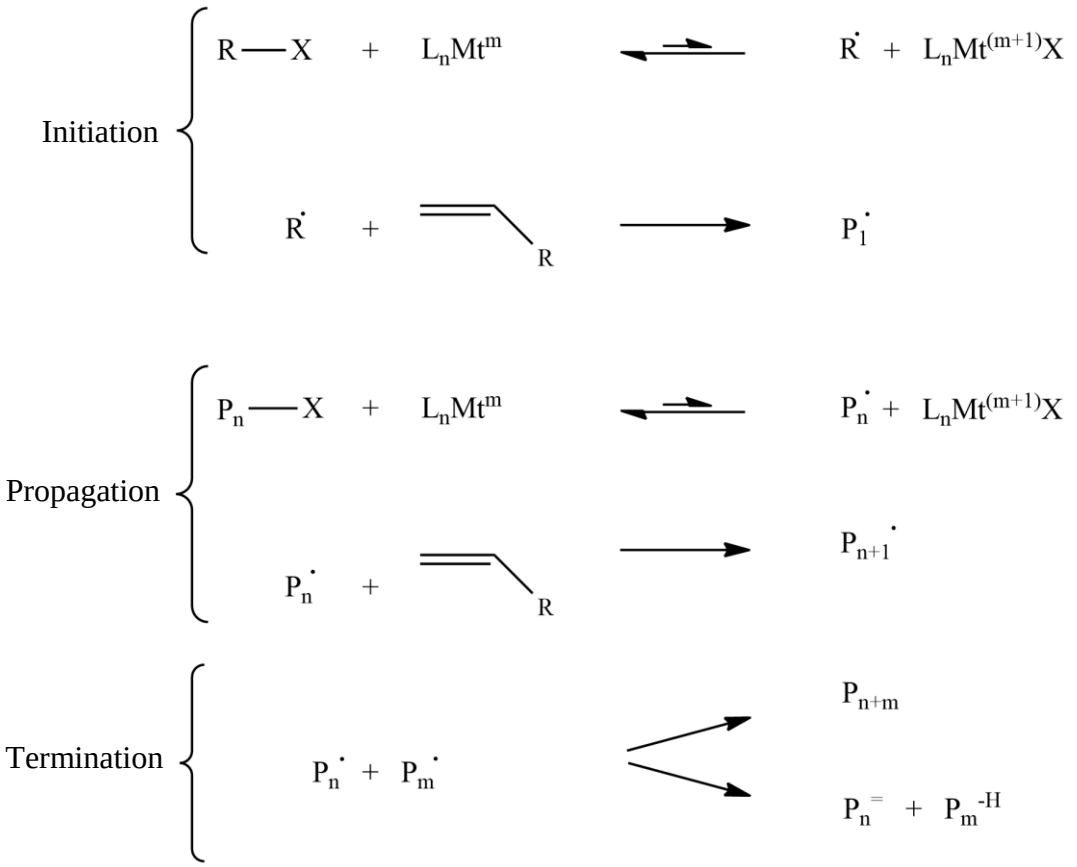

Scheme 1.7: Simplified mechanism for the ATRP of a vinyl monomer. R-X denotes an initiator where X is a halide, generally Cl or Br. L_nMt^m represents a complexing ligand with metal halide capable of adopting a higher oxidation state, often CuCl or CuBr. Initiation occurs due to the reversible disassociation of the alkyl halide and the metal halide catalyst. Alkyl radicals then encounter monomer to produce propagating polymer chains. Termination occurs leaving a halide capped chain or as an unwanted side reaction.

monomer units which are mediated by the re-addition of the halide.

This process was first studied using copper (Matyjaszewski) and ruthenium (Sawamoto) halides, but has now been proven to be successful using a wide array of transition metals including iron, nickel and palladium as well as the seminal ruthenium and copper.[34] Vinyl monomers are susceptible to this reaction and the most commonly studied are styrene, acrylates, and acrylamides.[7] ATRP is a RDRP technique that enables access to customised homo and block copolymers of controlled molecular weight and low dispersity. Polymers created by this technique have started finding applications in areas as widespread as drug delivery systems, electronics and even controlled nanocomposite synthesis.[35, 36] By using a functionalised initiator additional reactivity can be added to the α-end of polymer chains, increasing possible applications.

The ATRP system is a multicomponent package consisting of: halide initiator, transition metal halide, aliphatic amine ligand, monomer and solvent. Varying these components can have drastic effects on the outcome of materials produced, and in order to achieve successful "living/controlled" reaction reagents must be chosen carefully.

The basic mechanism of ATRP is that a transition metal halide complexed to a ligand in solution can reversibly react with an alkyl halide based initiator. As the halide atom dissociates from the alkyl halide, the transition metal undergoes oxidation and is complexed again with the ligand (and required halide or counter-ion) to force its dissolution into the solvent and balance the redox potential of the system. This produces a radical that will propagate the reaction via interaction with vinyl groups within a monomer unit and then return the halide from the transition metal (lowering it back to its original oxidation state) and placing the halide back on the end of the polymer chain.[34]

This causes the uniform growth of all polymer chains simultaneously as the monomer feedstock is used up. This is achieved by a rapid initiation step, creating many growing polymer chains at the very beginning of the reaction, but a fast reversible deactivation of radicals formed from initiation. The number of active radicals is controlled by a dynamic equilibrium that is formed between the number of chains that are capped with dormant halogen atoms, and the number of chains that contain a propagating radical. To ensure that there are fewer radicals present in the system, and that kinetic control is maintained, the equilibrium lies heavily in favour of the creation of dormant chains and a low number of propagating radicals. This is brought about due to the high strength of the carbon-halide bond, which requires a relatively large amount of energy to break and create a radical.[34, 37]

A key feature that brings about the kinetic and molecular weight control of ATRP is what is known as the "persistent radical effect" (PRE).[38] The PRE comes about due to the fact that at the start of a reaction there are very few higher oxidation state transition metal (Mt^{n+1}) species present in solution. This means that there is a chance of bimolecular termination between propagating polymer chains, causing an overall increase in the total amount of Mt^{n+1} relative to the number of polymer chains in the polymerisation, with no way of it being reduced back into the lower oxidation sate(Mt^{n}).[38] This accumulation of Mt^{n+1} adds control to the reaction by pushing the

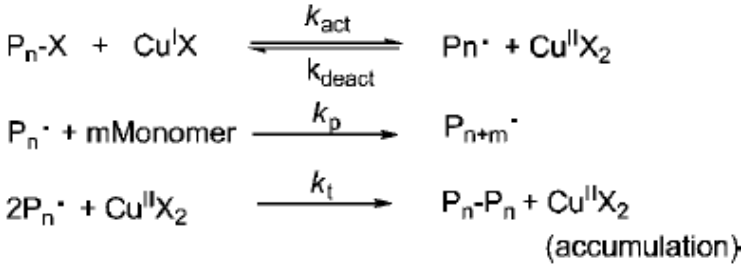

Scheme 1.8 : Mechanism by which the persistent radical effect occurs, leading to an accumulation of Cu(II) species within ATRP.[38]

dynamic equilibrium between active and dormant chains back towards the dormant side, as there is now a greater chance of interaction between Mt^{n+1} and any propagating species. A small percentage of termination reactions can occur which are attributed to either radical – radical bimolecular termination, or disproportionation of the metal halide leading to a C=C bond formation. The majority of the material should exhibit polymer chains end capped with the halide used in the system. This enables polymers produced by ATRP to be readily used as macro-initiators for subsequent polymerisations to synthesise block copolymers.

By using functional initiators, polymers produced can easily be tailored to the specific role that they are required to fill. The only real requirement for an initiator is that it is an alkyl halide where the radical will be stabilised by an electron withdrawing moiety. Typically this is achieved using; esters, amides, aryl, or cyano groups.[34]

1.2.4.1 Kinetics of ATRP

As has been mentioned previously in this chapter, the high degree of control that ATRP provides over molecular weight and dispersity is a result of the dynamic equilibrium that forms between activation and deactivation, shown in Scheme 1.9. The equilibrium can be described in terms of the rate of activation (k_{act}) and the rate of deactivation (k_{deact}), the ratio of which describes the overall rate of ATRP (k_{atrp}), as is shown in Equation 1.1 on the following page.

$$k_{ATRP} = \frac{k_{act}}{k_{deact}} = \frac{[P\bullet][Cu(II)]}{[PX][Cu(I)]}$$

Equation 1.1

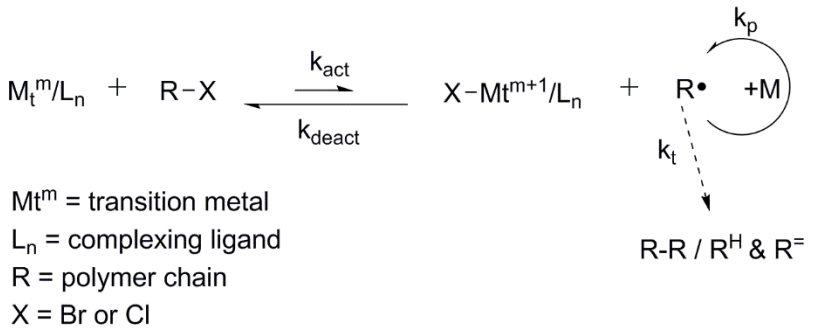

Scheme 1.9 : An illustration of the dynamic equilibrium involved in ATRP.[32]

where [P•] is the concentration of propagating polymer chains, [Cu(II)] is the concentration of Cu(II) halide, [PX] is the concentration of dormant polymer chains, and [Cu(I)] is the concentration of Cu(I) halide.

If control over the reaction is to be achieved k_{atrp} must be kept low, as this will reduce the chance of propagating radicals suffering termination reactions that are seen more often in a conventional radical polymerisation. If the value of k_{act} is too low however, the reaction will progress extremely slowly, whilst if k_{act} is too large then the reaction will progress rapidly but not possess living characteristics as termination reactions occur alongside polymer propagation.

The rate at which polymerisation occurs specifically (R_p) is defined by Equation 1.2:

$$R_p = k_p[P\bullet][M]$$

Equation 1.2

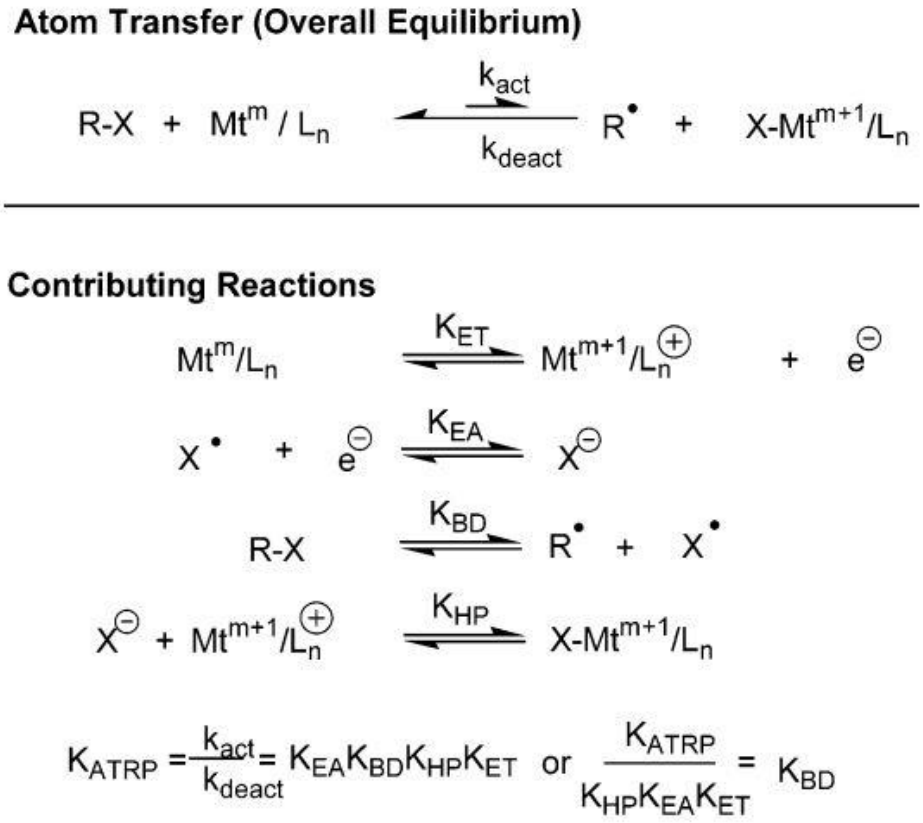

Scheme 1.10 : Reactions contributing to the atom transfer equilibrium.

where k_p is the rate of propagation, [P•] is the concentration of propagating species, and [M] is the concentration of monomer. Clearly, if the concentration of propagating species increases, then R_p will also increase. From Equation 1.1, if this is not countered by an increase in k_{deact}, then the total value for k_{atrp} will also rise and control of the system will be lost.

The overall dynamic equilibrium that is occurring within ATRP is actually composed of four separate equilibria (shown in Scheme 1.10), all of which have an effect on the total k_{atrp}.[39, 40] k_{ET} represents the electron transfer between low oxidation state metal halides, to the higher state, k_{EA} is the electron affinity of the halide, k_{BD} is the rate of homolysis of the alkyl halide bond, and k_{HP} is the association of the halide to the metal ligand complex.[40] A modification to any of these values, by variation of any component within a reaction, will affect the overall k_{atrp} causing an increase or decrease in the level of control present within the polymerisation. These equilibria are known to be very solvent dependent, with k_{EA} expected to be relatively high in protic solvents such as water or ethanol.[41] If it is assumed that k_{ET}, k_{EA} and k_{HP} are constants within a given

polymerisation, then k_{ATRP} is only really dependent on the bond dissociation energy of the halide bond (k_{BD}).[40, 42] From this, if the rate of polymerisation of a given monomer is known, the relative rates of polymerisation for different monomers can be calculated by using identical reaction conditions.[34, 42] The most common form of evidence provided as to whether a specific ATRP reaction is living is in the form of a kinetic plot created from samples recovered from polymerisations in progress. ATRP reactions should possess pseudo first order characteristics, as at any given time during the polymerisation the concentration of monomer is significantly greater than the concentration active propagation sites.

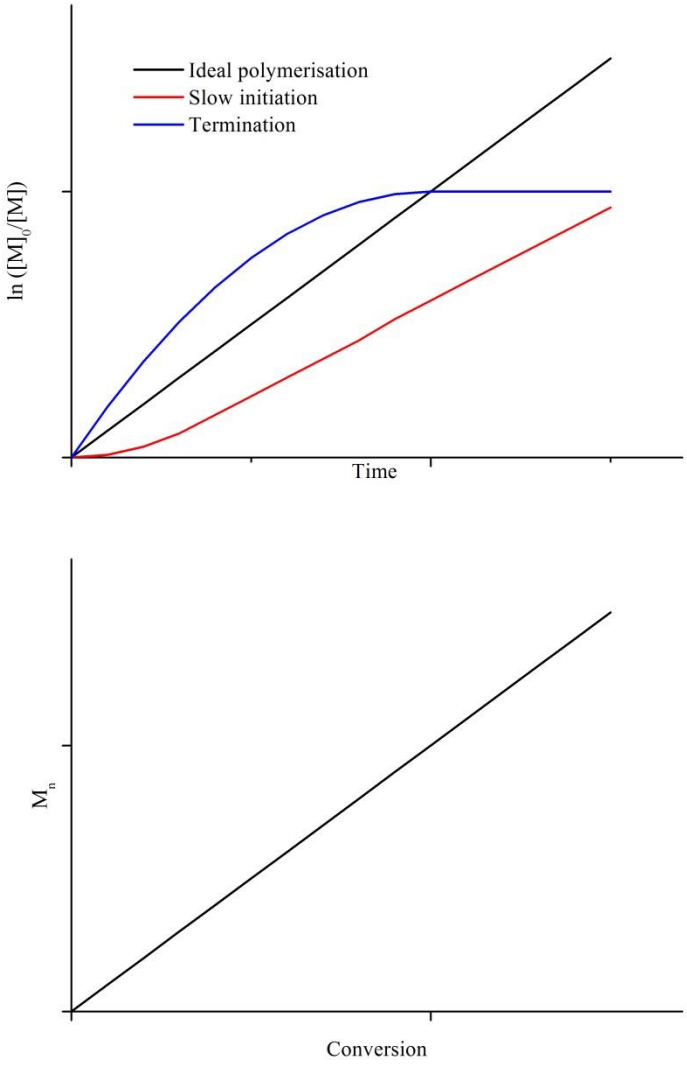

Figure 1.5: Semi-logarithmic kinetic plot (top) displaying relative monomer conversion against time, and a linear plot of molecular weight against conversion (bottom).

The only time this is not generally true is towards the end of the reaction, as the relative concentration of monomer decreases following its conversion to polymer. Due to the pseudo first order nature of the reaction a semi-logarithmic plot (where only one axis uses a log scale) of monomer conversion against time should be linear, and any deviations from this pattern suggest that polymerisation is occurring in an uncontrolled manner. If the semi-logarithmic plot shows a plateau after a period of linearity, then it is indicative of termination occurring, whilst if there is slow initiation, plots tend to only attain linearity after an inductive period.[40]

The semi-logarithmic plot is generally displayed alongside a plot of molecular weight against conversion, which is also expected to be linear due to the controlled manner in which monomer is added to propagating polymer chains. Examples of these plots are shown in Figure 1.5 on the previous page. If the rate of termination remains low in a reaction, and the concentration of propagating radicals is low compared to the concentration of monomer (pseudo first order), then Equation 1.3 describes the relationship between the semi-logarithmic plot and the equilibria parameters of the ATRP system:

$$ln\left(\frac{[M]_0}{[M]_t}\right) = \frac{k_p k_{act}[RX]_0[Cu(I)]_0}{k_{deact}[Cu(II)]_0}t$$

Equation 1.3

where $[RX]_0$ is the concentration of alkyl halide at initiation, [Cu(I)] is the concentration of Cu(I) species, [Cu(II)] is the concentration of Cu(II) species, k_p is the rate of propagation, k_{act} is the rate of activation, and k_{deact} is the rate of deactivation.[43]

The kinetics of ATRP using different reagents has been widely investigated, and the effect that a wide range of initiators, ligands, monomers and solvents have on rates of reaction have been experimentally demonstrated or theoretically predicted.[7, 44-47]

1.2.4.2 Metal halide catalyst system

Whilst recent pioneering work has demonstrated the metal free ATRP of vinyl monomers,[48] the catalytic systems for ATRP generally consists of a transition metal halide and an aliphatic amine ligand.[32, 33]

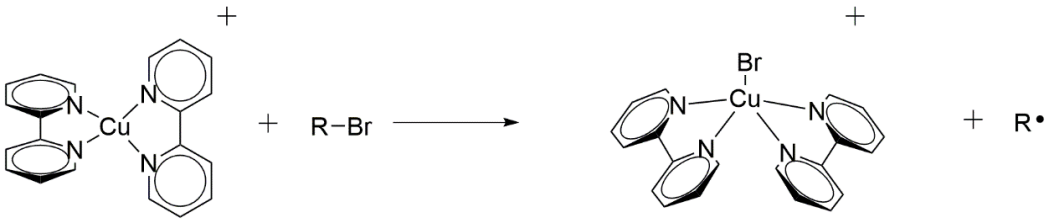

Scheme 1.11 : The proposed complexation between bidentate ligands and copper when acting as a catalyst for an ATRP system.[49]

The most commonly used metal halides are copper based, in part due to the volume of work that the Matyjaszewski group have produced following the discovery of copper mediated atom transfer radical polymerisation of styrene in 1995.[17] Simultaneously to this the Sawamoto group demonstrated a ruthenium mediated polymerisation of methyl methacrylate.[33] Since these seminal papers a wide array of transition metal halides have been proven to conduct ATRP successfully, although copper remains commonly used due to its ready availability and comparatively higher reactivity, and as such copper halides will primarily be discussed in the rest of this chapter.[50, 51]

The fundamental features that a metal halide must possess to catalyse an ATRP are: two valence states that are one electron apart, and an affinity for halogens. This allows the metal to undergo redox reactions: being oxidised from its lower state Mt^m, to its higher state Mt^{m+1}, when it accepts a halide from either the initiator or a propagating polymer chain, and then be reduced back to Mt^m when the halide is returned to deactivate a propagation site.

The overall activity of a catalyst system is dependent both on the redox potential of the metal halide, and the affinity of the transferred atom for the transition metal complex (k_{ET} and k_{HP} on Scheme 1.10).[39] It is important that the affinity of the transition metal towards halides is high in order to prevent the formation of organometallic derivatives through an alkyl radical interaction with the transition metal core.

If transition metal complexes possess similar values for the association of the halide to the metal ligand (k_{HP}), then the redox potentials can be used to indicate the relative activity of the catalytic system.[52] Matyjaszewski *et al* performed cyclic voltammetry studies of copper complexes with a wide array of ligands in order to

determine the redox potentials of ATRP catalyst systems. CuCl species typically showed lower redox potentials than CuBr species, and the overall redox potential of a species was observed to decrease as the number of coordination sites present on the ligand increased.[52] The reason given for this is that the lower the redox potential of the system, the large the apparent equilibrium constant for the oxidation reaction of Cu(I) to Cu(II) species, resulting in a higher activity in catalysing the system. In general it would be expected that the k_{ATRP} of CuBr systems would be many orders of magnitude greater than for CuCl, as a result of the difference in bond dissociation energies between C-Br and C-Cl, but it is actually much smaller as a result of the electron affinity of chlorine.[53]

The ligand that is selected has a contribution in determining the redox potential of the system, and acts to solubilize the transition metal complex in the reaction medium for efficient atom transfer.[34, 54] Numerous ligands have been developed, utilised, and characterised for ATRP, and the specific ligand selected is often chosen depending on the transition metal being used as catalyst. Copper and iron catalysed systems tend to be successful using multidentate aliphatic amine ligands, whilst ruthenium systems tend to use alkylidenes and metallocenes.[45, 55, 56]

Early ATRP reactions made use of the bidentate ligand 2,2'-bipyridine (Bpy). It was demonstrated that the ratio of ligand to copper affected the level of control over the reaction, with a Cu:ligand ratio of 1:2 being optimal for Bpy.[45, 57-60] It was observed

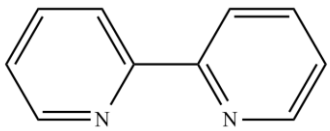

2,2'-bipyridine

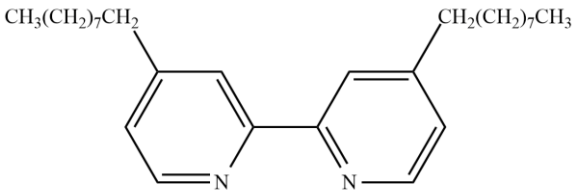

4,4'-dinonyl-2,2'-bipyridine

Figure 1.6 : Structures of Bpy (top) and dNBpy (bottom) which are common ligands used within ATRP.

that if the ratio of Cu:Bpy was altered to 1:3 the ATRP of oligo (ethylene glycol) methyl ether methacrylate occurred three times as fast, but the dispersity of prepared POEGMA was measured as 1.45 as opposed to 1.20 when a 1:2 Cu:Bpy ratio was used.[58] The addition of various substituents to the Bpy structure was shown to improve the solubility of copper halides in reaction mixtures, and resulted in narrower dispersities. The addition of alkyl chains with at least four carbon centres to the 4,4' position of Bpy produced a series of ligands that when used in the ATRP of styrene produced polymers with extremely narrow dispersities (Đ ≈ 1.05).[61] The attachment of these alkyl chains was also noted to increase the k_{act} of ligands, with a value of 0.2 being measured for 4,4'-dinonyl-2,2'-bipyridine compared to 0.066 for the original Bpy.[45] Eventually tri- and tetradentate ligands were developed, and displayed high relative k_{act} values again. The structure-related reactivity of various ligands were studied by Tang and Matjaszewsk.[62] In general ligand reactivity within ATRP follows a general principle of: tetradentate (cyclic-bridged) > tetradentate (branched) > tetradentate (cyclic) > tridentate > tetradentate (linear) > bidentate, starting with the highest activity (tetradentate) and ending with the lowest (bidentate).[62]

It is known that for the successful synthesis of controlled polymers via ATRP the k_{atrp} must be low. Investigations into the k_{atrp} of ligands, such as the one displayed in Figure 1.7, highlight the importance in selecting suitable reagents for specific reactions. In the experimental setup used by Tang *et al* to produce Figure 1.7 (ethyl 2-bromoisobutyrate (EBriB), Cu-X (where X is Br or Cl) and acetonitrile), values of 3.9×10^{-9}, 3×10^{-8}, 7.5×10^{-8} and 1.5×10^{-4} were recorded for Bpy, dNBpy, PMDETA and Me_6TREN respectively.[43] Even though the k_{atrp} values across these four ligands (in this system) vary by orders of magnitude, they have all been used in the synthesis of controlled polymers in other, different reaction conditions where alternate solvents, catalysts or varying monomers were used.[34]

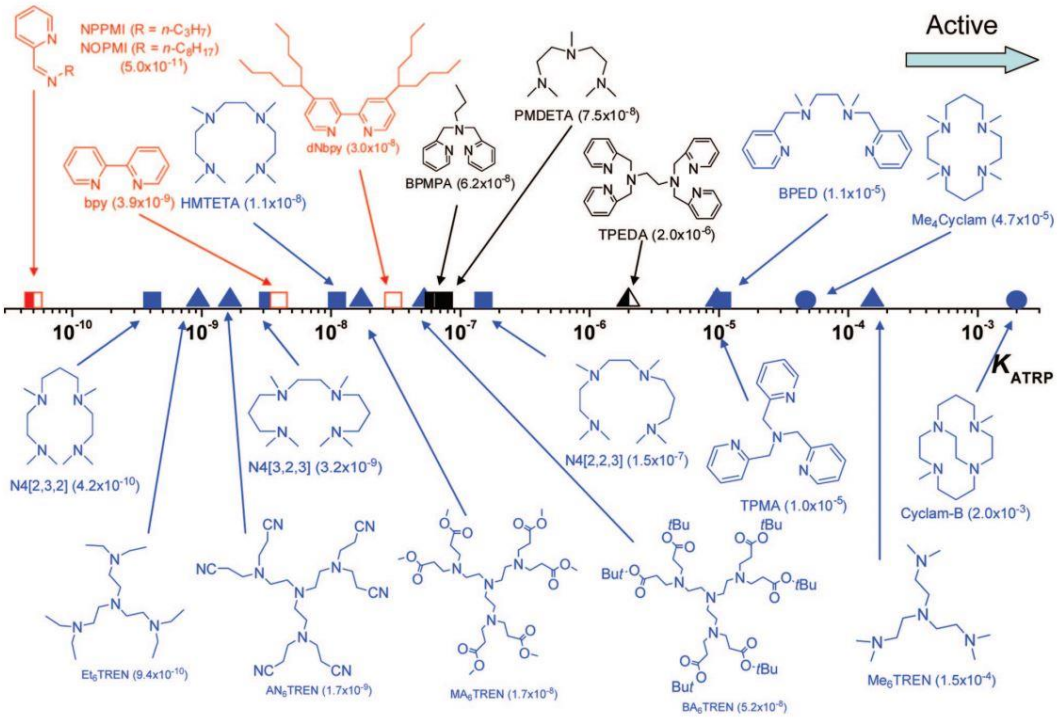

Figure 1.7: k_{ATRP} constants for various ligands when used in conjunction with CuBr catalyst, EBriB initiator, in acetonitrile.[43]

1.2.4.3 Initiators

In an ATRP reaction the degree of polymerisation (DP) of a prepared polymer can be defined by Equation 1.4;

$$DP = \frac{M_n}{M_0} = \frac{[M]}{[I]}$$

Equation 1.4

where [M] is the concentration of monomer, [I] is the concentration of initiator, M_n is the observed molecular weight of the synthesised polymer, and M_0 is the molecular weight on a single monomer unit. The DP of a produced polymer can be calculated by dividing the M_n by M_0 and if the polymerisation is "living" it should also be proportional to the ratio between concentrations of monomer and initiator added at the start of the reaction.

Initiators for ATRP are of the general form R-X, where R is an alkyl group and X is a halide (predominantly Br or Cl) which acts as an ATRP initiation site.[43, 46] The R-X bond tends to be adjacent to an electron withdrawing moiety (such as a carbonyl or benzyl group) which helps to activate the R-X bond by increasing its polarity and therefore allowing the creation of a more stable radical.[63] One way that this occurs is through the donation of an electron from a lone pair (as in an amide or ester initiator), which enables a resonance structure to form that distributes the positive charge of the carbocation. If this stabilisation effect is too strong then the high resulting bond dissociation energy of the R-X bond will result in poor initiator efficiency or a complete lack of polymerisation. The structure of the initiator is therefore of critical importance in determining the success of a polymerisation, due to its significance in the k_{act}. In a lot of cases the general molecular structure of an initiator is chosen to be similar to that of the monomer, such as EBriB for the ATRP of MMA or 1-phenylethyl chloride for the ATRP of styrene, so as to be analogous to a propagating chain.[17, 32]

The general trend in activities for ATRP initiators was elucidated by Tang and Matyjaszewski, and is in increasing order: amide < ester ≈ aryl < cyano, with the full plot of their results shown in Figure 1.8.[46] Initiators with the R-X bond found

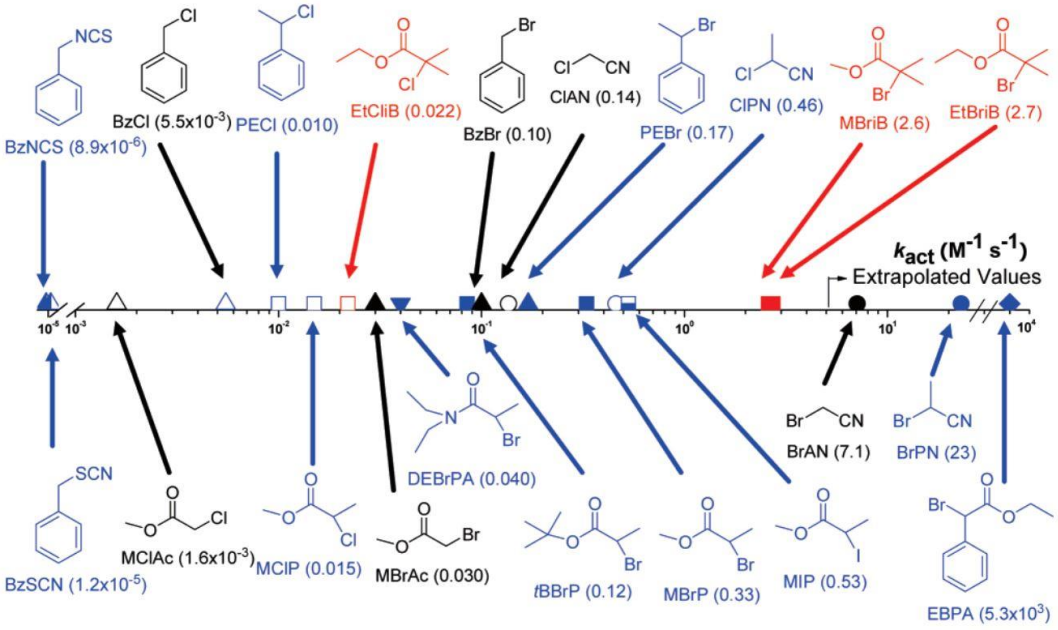

Figure 1.8 : k_{atrp} constants for a range of initiators using TPMA as ligand, acetonitrile as solvent and a Cu-X catalyst system.[46]

adjacent to a tertiary carbon exhibit the highest activities, followed by secondary and then primary carbon centres. This is again due to the increased stabilisation that a tertiary carbon centre provides to a radical when compared to the other two arrangements.[64]

For a successful ATRP the rate of initiation must be faster than the rate of propagation, and the R-X bond must be sufficiently transient in order to allow for the rapid generation of radicals. This means that when considering the polymerisation of a specific monomer the efficiency and reactivity of the initiator must be taken into consideration. Matyjaszewski *et al* demonstrated this principle with the ATRP of MMA using a range of initiators.[65] They found that using initiators with very high k_{atrp} (such as benzhydrylchloride) resulted in low monomer conversions, slow polymerisations and an apparent build-up of Cu(II) species immediately after initiation. EBriB on the other hand (which has a lower activity relatively) produced the fastest rate of polymerisation and produced controlled polymers with low dispersities.[65]

The most common choices of halogen for the initiator are Br and Cl. Alkyl iodides have shown to be effective for acrylate polymerisations in copper mediated ATRP, and for the polymerisation of styrene in ruthenium or rhenium mediated ATRP, but care must be taken with their usage due to their light sensitivity.[34, 64]

The desire to create functional polymers with complex molecular architectures led to the development of molecules with more than one ATRP initiating site.[34] This has enabled the synthesis of star or branched polymers that still possessed controlled kinetic characteristics throughout the polymerisation.[66] Additional functionality, aside from molecular architecture, can be introduced into polymers through careful design of the other end of an initiator. As long as the requisite activated R-X bond is incorporated into the molecular design, then the remainder of the initiator can be modified to produce specific α-end functionality in produced materials. This can serve a precise functional role in a desired application, or simply open the material up to further chemical reactions that can be performed post polymerisation. Due to materials being produced by ATRP retaining an activated C-Br bond, polymers produced by ATRP can themselves be reactivated to act as macroinitiators in subsequent polymerisations in order to easily synthesis block copolymers.[66]

Whilst initiators with an amide bond activating the R-X bond have previously attracted little interest in the literature, probably due to their known low activity (Figure 1.8 on the previous page), the presence of an amide bond would be beneficial in numerous circumstances. Not only is the chemistry of amide bonds well known, allowing additional synthetic routes to functionalisation, but it is a type of bond that is often found in biological chemistry.[67, 68] Whilst some amide initiated systems have been shown to be effective, many produced polymers that had broad dispersities, higher than predicted molecular weight parameters, and polymerisations that converted low percentages of monomer to polymer.[67-73] Many different possible explanations have been given for this effect within the literature, often in contradiction to each other, with no clear investigation into what is actually occurring. The problems with amide initiators and associated explanations for these problems will be talked about in greater detail in Chapter 3.

1.2.4.4 Monomer

ATRP has been shown to be effective in the polymerisation of a wide range of monomers, with the only requirement being a vinyl group that is susceptible to attack by the radicals produced upon initiation. ATRP was first demonstrated with the polymerisation of styrene by Matyjaszewski *et al*, and methyl methacrylate by Sawamoto *et al*.[32, 33] Since these seminal works, polymers based on styrene,[47, 74, 75] acrylates,[47, 76, 77] methacrylates,[32, 78, 79] isoprene,[80] butyl acrylates,[70, 81] acrylamides[69, 82] and many more, have all been synthesised through this process.

Each individual monomer has a unique k_{atrp}, which is highly dependent on the stabilisation of the propagating radical. The radical is stabilised by the presence of an electron withdrawing group (meth/acrylate, amide, etc.) in the same way as the initiators, often meaning that monomer and initiator share similar chemical structures. The rate of propagation is also unique to every specific monomer, so reaction conditions must be carefully chosen in order to maintain control over the polymerisation.[34]

1.2.4.5 Solvent

The main role that the solvent provides is in aiding the solubility of the catalytic system as well as the polymer. Under some conditions ATRP can be carried out in the bulk, as long as the catalyst/ligand is soluble in the monomer.[37, 83] Solvent is also an important part of the k_{EA} (sub equilibria for k_{atrp}, Scheme 1.10), as the electron affinity of a halide in known to be higher in protic solvent such as water or alcohols.[41] The total amount of solvent used within a reaction mixture is also expected to have an effect on the rate of polymerisation, as when monomer is more dispersed in a solution there is reduced chance of radical monomer interaction.[77]

Finally, solvent has also been proposed to be a differentiating factor in the mechanism that occurs when performing some Cu(0) mediated polymerisations. Percec *et al* demonstrated that a polymerisation of methyl acrylate in DMSO possessed characteristics of single electron transfer living radical polymerisation (>98% polymer bromine functionality indicating few bimolecular terminations), but if reaction conditions remained constant and MeCN was used as solvent, the reaction had characteristics in line with conventional ATRP (80% bromine functionality at 86% monomer conversion).[84]

1.2.5 Removal of catalyst from ATRP polymers

Overall ATRP is viewed as an extremely versatile technique that can be used to produce polymers from a wide range of monomers, with exacting control over polymer molecular weight parameters and topologies through the use of multi-functional initiators. The major drawback of ATRP is that often there are often significant amounts of catalytic system left in polymers that have been produced. Due to this, there has been a large amount of experimental effort put into either the removal of catalyst from products of ATRP, or analogous polymerisation systems using smaller amounts of catalyst such as; ARGET-ATRP, SARA-ATRP, or SET-LRP.

The most commonly used transition metal for ATRP is copper, and as such the rest of this chapter will discuss methods of copper removal or RDRP methods involving low catalyst quantities. Various industrial applications require the removal of excess copper as it is both expensive as a reagent and possibly undesirable aesthetically if the colour of a prepared material is important. In medical applications the presence

of copper is potentially hazardous, as while copper is found in trace amounts within some cells, free copper has been shown to catalyse highly reactive hydroxyl radicals *in vivo*.[85]

The most common methods of copper removal are precipitation into polar solvents, or running polymer solutions through columns containing alumina or silica. It is know that copper complexes formed with aliphatic ligands are highly soluble in polar solvents.[86] By precipitating the polymer into a solvent such as methanol, the polymer can be recovered by filtration whilst the copper/ligand complex remains in solution.

Ion-exchange resins have been shown to be highly effective in the removal of copper from ATRP polymers.[87, 88] The usage of a cationic macroporous exchange resin enabled the removal of over 95% of a CuBr/PMDETA catalyst system, but it was noted that the amount of CuBr removed was dependent on the polarity of the solvent, ionic character of the resin, pH of the solution, cross-linking degree of the resin, acidic strength, and the size of the ion exchange resins.[87] The down side of this is that it was observed that to achieve higher levels of copper extraction the polymer had to remain in contact with the resin for long periods of time.

An alternative method utilised a poly(ethyleneimine) (PEI) "macro-ligand" as part of a recoverable catalyst system for the ATRP of methyl methacrylate (MMA). The numerous amine sites within the PEI structure enabled complexation with cuprous halides, and the catalyst could be recovered by precipitating the synthesised polymer into methanol, where the macro-ligand remained soluble. Following filtration to remove the PMMA, the macro-ligand was recovered by exposing the remaining methanolic solution to a vacuum.[89] The strong affinity of PEI for copper is something that became extremely relevant with the synthesis of the PEI-graft-POEGMA copolymers that are discussed in Chapter 4.

The alternative to removing copper from synthesised polymers is reducing the amount of catalyst that is used for the reaction. To this end numerous low catalyst systems have been developed recently. Most notable amongst these systems are ARGET-ATRP, a variant of conventional ATRP that utilises a reducing agent to recover Mt^{n+1} that is part of the PRE, and a pair of copper (0) mediated systems: SARA-ATRP and SET-LRP.

1.2.5.1 Activator regenerated by electron transfer ATRP (ARGET-ATRP)

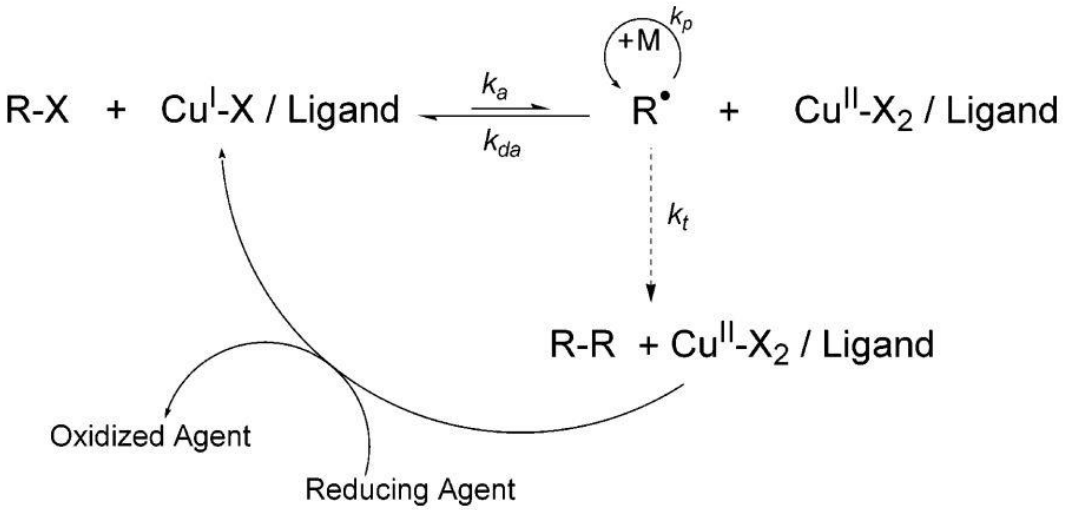

Scheme 1.12: Proposed mechanism for ARGET-ATRP.[84] The reducing agent acts to regenerate Cu(I) species by reducing inert Cu(II) back to its low oxidation state form, allowing it to react again with alkyl halides and continue propagation.

Activator regenerated by electron transfer ATRP (ARGET-ATRP) is a variant of ATRP that makes use of a reducing agent to mitigate the persistent radical effect. The result of this is that any Cu(II) species that form within the reaction are reduced back to Cu(I), and the total amount of copper halide that is required in the system is lowered.

ARGET-ATRP was first reported by the Matyjaszewski group in 2006, where tin(II) 2-ethylhexanoate ($Sn(EH)_2$) was used as a reducing agent in the ATRP of styrene. $CuCl_2$ was the only transition metal halide introduced to the system, and the dynamic equilibrium required for RDRP was created by it being reduced to CuCl by the $Sn(EH)_2$.[90] Polymers produced by this method showed low dispersities (<1.28), and experimental molecular weight values close to those predicted theoretically, whilst using copper amounts in the tens of parts per million range (ppm), as opposed to the typical 1000 ppm.

A side advantage of ARGET-ATRP is that the whole system is made more robust by allowing for a limited amount of oxygen to be present within the reaction. In conventional ATRP any unforeseen oxidation of Cu(I) to Cu(II) is detrimental, as it results in the permanent loss of a propagating chain. In ARGET-ATRP Cu(II) species are rapidly reduced back to Cu(I), allowing continued polymerisation.

The actual amount of reducing agent in the reaction has to be carefully managed. If too little is added, then any residual oxygen will not be mitigated, causing a lack of Cu(I) species for living polymerisation. On the other hand, if too much reducing agent is added then a significant loss of control is observed within the system due to the overabundance of Cu(I) species.[91]

1.2.5.2 Supplemental activator and reducing agent ATRP (SARA-ATRP)

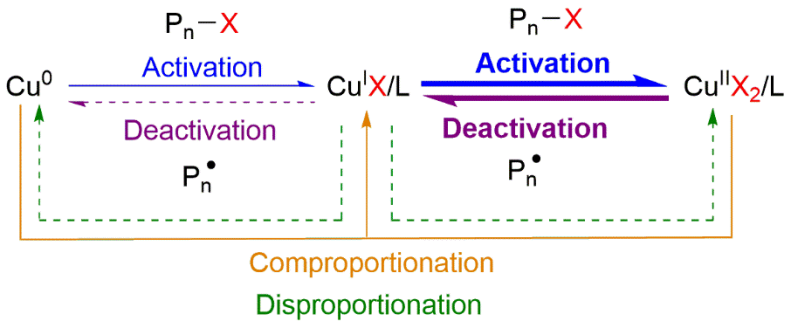

Scheme 1.13: Scheme showing the processes proposed to be occurring during SARA-ATRP – dashed lines indicate those which are not considered occurring, bold lines indicated being those which are dominant.[92]

Supplemental activator and reducing agent ATRP (SARA-ATRP) is a different variant of conventional ATRP that uses the addition of Cu(0) to act as an additional activator in the dynamic equilibrium between Cu(I) and Cu(II) species. Cu(0) is activated by the alkyl halide (initiator or propagating polymer) to form Cu(I), which then undergoes conventional ATRP to synthesise polymers. Again, the result of this is a reduced amount of non-zero valence copper required at the start of the synthesis.[93]

PMMA polymers with dispersities of 1.20 were prepared using only 250ppm of $CuBr_2$, *N*,*N*,*N*',*N*'',*N*''-pentamethyldiethylenetriamine (PMDETA) and zero valence copper wire as the catalyst system.[93] When the $CuBr_2$ was excluded from an analogous reaction, the level of control was reduced, as shown by pseudo-first order logarithmic plots which no longer displayed a linear correlation. This data shares a resemblance to similar results produced from ARGET-ATRP systems, where polymerisation rates are not dictated by the concentration of the catalyst, but by the quantity of reducing agent the relative ratio of Cu(I)/ligand and Cu(II)/ligand.[83]

It is proposed that the activation of alkyl halides by Cu(0) is very slow, and the comproportionation of Cu(II) with Cu(0) mitigates the small number of radicals that are lost in the early stages of the reaction due to the low quantity of starting Cu(II) species. Supplemental activation has been shown to be successful with various zero valence metals including; iron, magnesium and zinc.[20] Several polymerisation of methyl acrylate were carried out using the various metals and generally produced polymers with dispersities less than 1.3 and showed controlled characteristics from kinetic plots.

It should be noted that within the current literature there is some debate as to the exact mechanism at play in these circumstance.[92, 94] The alternative model is known as single electron transfer living radical polymerisation and will be discussed next, along with the differences between the two mechanisms.

1.2.5.3 Single electron transfer living radical polymerisation (SET-LRP)

Single electron transfer living radical polymerisation (SET-LRP) follows a reaction mechanism that varies slightly from traditional ATRP. The key process in SET-LRP revolves around the rapid *in situ* disproportionation of Cu(I) species to Cu(0) and Cu(II), and it is the Cu(0) species that activate the alkyl halide initiator to trigger polymerisation. The Cu(II) formed fulfils the same role as in conventional ATRP, by acting as a deactivator to a propagating radical. The result of this is an ultra-fast controlled polymerisation that can be used in the polymerisation of vinyl monomers.[21] Typical reaction times for SET-LRP are measured in minutes, as opposed to conventional ATRP which generally take hours.[21]

Typical SET-LRP reactions can be carried out in conditions that are milder than that of conventional ATRP, often operating at ambient temperatures, and in polar solvents such as dimethylsulfoxide (DMSO), water, or ethanol.[95-97] SET-LRP has even been carried out with significant amounts of oxygen within the system by the use of hydrazine as an additive.[98] The polymerisation of methyl acrylate in DMSO was conducted without any of the usual oxygen purging techniques (freeze-pump-thaw and nitrogen degassing) but with hydrazine added to reduce Cu_2O generated by air back to Cu(0). PMA produced displayed dispersities below 1.2 with good correlations between experimental and theoretical molecular weights.

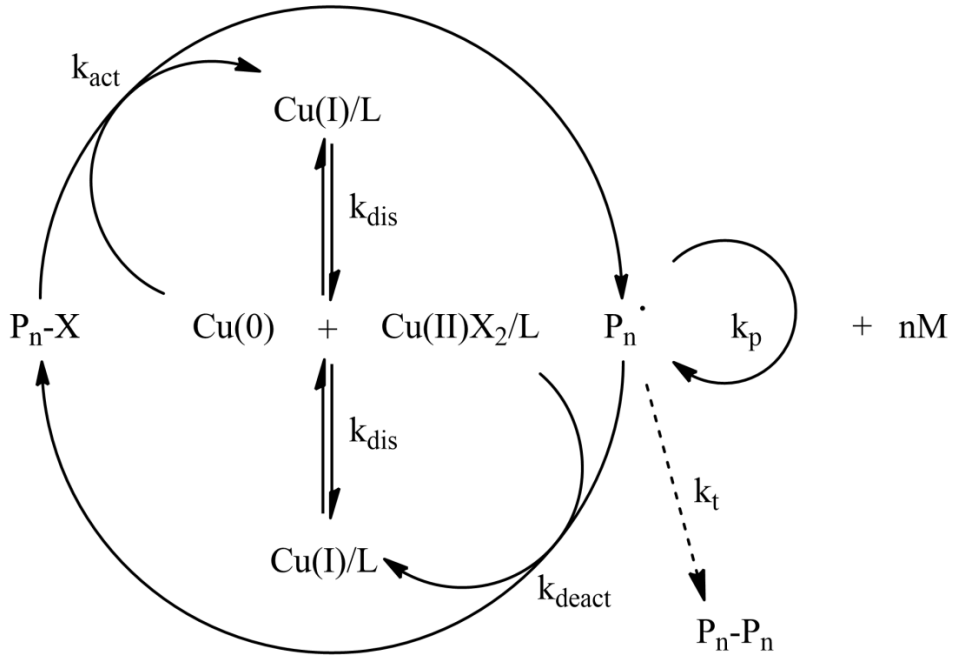

Scheme 1.14: Proposed mechanism for SET-LRP reproduced from the literature.[89] Cu(I) species undergo rapid disproportionation to produce Cu(0) and Cu(II). Cu(0) activates the alkyle halide moiety, producing radicals for propagation. Cu(II) acts to mediate the propagating radicals as in conventional ATRP.

Zero valence copper for SET-LRP can be introduced to the system in multiple ways. Reactions have proven to be successful using copper wire, copper powder, or by creating Cu(0) in situ through disproportionation. The addition of CuBr to tris[2-(dimethylamino)ethyl]amine (Me_6TREN) in water produced a reddish brown powder that was seen to precipitate out of solution, and the colour of the liquid changed to blue, indicative of $CuBr_2$.[99]

Whilst both SARA-ATRP and SET-LRP appear similar in terms of the components within the reaction, there is a significant difference in the mechanisms at play. Current consensus states that during SET-LRP an outer sphere electron transfer (OSET) occurs, whereas in SARA-ATRP an inner sphere electron transfer (ISET) is occurring. This means that during ATRP the alkyl halide and the metal catalyst form a transition state prior to the formation of the radical, whereas in SET-LRP there is no transition state formed, and the alkyl radical is produced before electron transfer can occur.[100] A representation of the different mechanisms is given in Scheme 1.15.

The result of the difference between OSET and ISET processes is a fundamental difference in the SET-LRP and SARA-ATRP reaction processes. SARA-ATRP relies on Cu(I) activating the alkyl halide, whilst there is little to no disproportionation observed. SET-LRP on the other hand requires disproportionation to be occurring as it is Cu(0) that is activating the halide.

Whilst the ultrafast synthesis of controlled polymers that SET-LRP can produce make it desirable as a polymerisation method, in order achieve optimal results the reaction conditions need to be optimised. Further to this, there is very little work within the literature that describes SET-LRP being used with methacrylates. When methacrylates, or long chain acrylates, have been polymerised with SET-LRP they often display signs of early bimolecular termination and can produce polymers with broad dispersities.[101, 102]

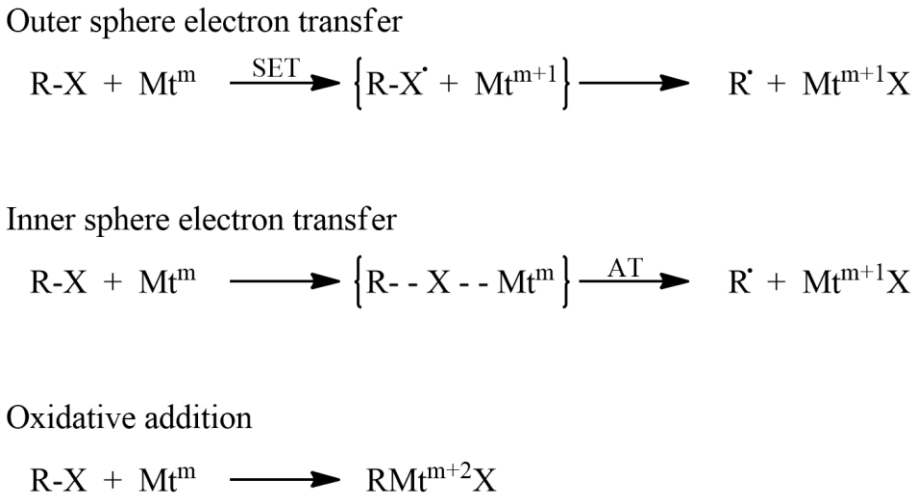

Scheme 1.15: Three possible mechanisms for the electron transfer between catalysts and alkyl halides in SET-LRP (OSET) and SARA-ATRP (ISET).[95]

1.2.6 Metal free atom transfer radical polymerisation

In 2012 Hawker and Fors published a paper titled "*Control of a Living Radical Polymerization of Methacrylates by Light*".[103] Previously reactions have been developed where initiation is triggered by a light source, but subsequent growth

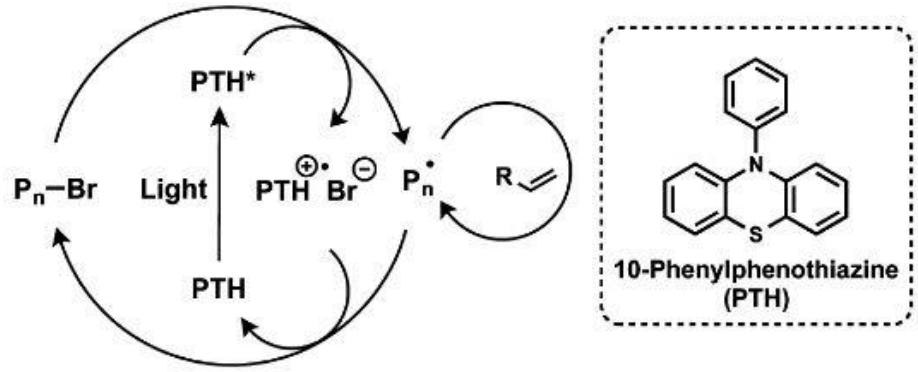

Scheme 1.16: The proposed mechanism for metal free photo-induced ATRP and the structure of 10-Phenylphenothiazine (PTH)[48]

steps could not be controlled by the same photo stimulus.[104-108] This was followed up in 2014 by a report of controlled radical polymerisation of acrylates by visible light, showing that the technique has potential across different monomer families.[109] The result of this work was a technique that was developed for the metal free ATRP of vinyl monomers, where polymerisations could be both activated and deactivated with light.[48]

The key component in the reaction is 10-phenylphenothiazine (PTH), which was synthesised from commercially available reagents. PTH's role within the reaction is analogous to CuBr/ligand in a conventional ATRP, except that without a source of light PTH remains inert. When the reaction is exposed to light, a radical is produced and ATRP carries on as normal.

Polymers produced by this method showed relatively narrow dispersities, and experimental molecular weights were in close agreement with theoretical values. In addition to this, the standard kinetic plots of conversion against molecular weight, and time against $\ln([M]_0/[M])$ displayed a linear relationship, suggesting the livingness of the reaction.

Although the paper does not detail if any effort was required to remove PTH from synthesised polymers, the reaction conditions state that catalyst concentration is only 10ppm. This value is significantly less that is found in conventional ATRP, and is similar to the values used in low catalyst concentration metal mediated polymerisation such as SET-LRP and ARGET-ATRP.[21, 48, 90]

1.3 Analytical methods used within this body of work

1.3.1 Size exclusion chromatography (SEC)

The most common method used for the analysis of polymers is through size exclusion chromatography (SEC), which can also be known as gel permeation chromatography (GPC). SEC is a chromatographic method that separates analysed polymers by their macromolecular size.

A SEC machine is typically composed of a series of columns packed with a stationary phase that is made up of particles with a known pore size, that are maintained within a thermally stable environment (oven), that lead to a detection system. For a sample to be analysed it must first be dissolved into a suitable solvent and then injected into the continuous phase (often THF) which runs all the way through the system. Higher molecular weight polymer chains pass through the columns more quickly than lower molecular weight chains, which are delayed in the column by their ability to pass through the pores of the stationary phase. As the sample is eluted from the column system it is analysed by a detector (usually refractive index or ultra-violet) which gives an intensity value dependent on the amount of material eluted.

The SEC system must be calibrated against known molecular weight standards, and for measurements to be accurate the standards used should be a similar polymer to the samples being analysed. The reason for this is that the hydrodynamic volume of materials in solution is dependent on the specific material.[110] Whilst a range of highly accurate standards are available commercially, they tend to be for common polymers such as polystyrene and poly methyl methacrylate. The analysis of highly functional polymers must often be carried out against an analogous standard due to the unavailability of standards with their exact molecular structure.

Branched and hyperbranched polymers are often measured by triple-detection SEC. SEC triple-detection utilises a concentration detector (again normally refractive index or ultra-violet), alongside a light scattering detector, and a viscometer. In this setup the viscometer is calibrated against a universal standard, derived from known values that are independent to any unknown properties of polymers to be analysed, and the light scattering result provides an absolute value for molecular weight.

Whilst high molecular weight branched polymers can show a large deviation in SEC results calibrated from linear standards, low molecular weight branched polymers tend to be similar to linear standards using conventional single channel SEC.[111]
SEC was used within this work to monitor the molecular weight parameters and dispersities of all polymers that were synthesised.

1.3.2 Nuclear magnetic resonance (NMR) spectroscopy

Nuclear magnetic resonance (NMR) spectroscopy is a highly versatile technique that enables the determination of the molecular structure of a sample. NMR relies on the measurement of the magnetic moment of nuclei located within a molecule. When the nuclei of a sample molecule are placed within an external magnetic field, they are forced into either aligning with (lower energy) or against (higher energy) the external field. If a radio frequency pulse is then applied across the sample the nuclei in the lower energy state absorb energy and jump up to the high energy state. This absorption of energy, or the resultant relaxation, can be observed and is used to generate a spectrum.[112] NMR can be performed on any nuclei that have a nuclear spin (I) of 1/2. In general it is commonly used to elucidate the local environments of hydrogen and carbon atoms within a molecule (^{1}H and ^{13}C NMR) and advanced techniques such as heteronuclear multiple-quantum correlation (HMQC), which utilises both ^{1}H and ^{13}C NMR, can be performed to provide correlations between directly connected carbon and hydrogen atoms.
In order to avoid unwanted nuclei signals in an NMR spectrum the solvent used is generally a deuterated form. Whilst a fully deuterated solvent would not produce any signals on ^{1}H NMR, the deuteration process never proceeds to 100%. This means there is often a residual solvent signal produced at a known chemical shift which can be used as a reference point for samples being analysed.[112]
When polymers are analysed by ^{1}HNMR the spectra that are produced often show broad peaks. This is due to the numerous, but not quite identical, proton environments present in polymer chains. The total area under the peak can still be correlated to the number of protons in the polymer specific to that signal, and when this is compared to the same signal from any monomer in the sample, a value of conversion from monomer to polymer can be calculated.

NMR was used within this work to elucidate the structure of novel initiators and macroinitiators, monitor the purity of synthesise, and calculate the conversion of monomer to polymer in polymerisations.

1.3.4 UV-visible and fluorescence spectroscopy

UV-visible (UV-vis) and fluorescence spectroscopy use the absorption and emission of light respectively to generate spectra.

In UV-vis the excitation of electrons by the absorption of light is measured. As a sample absorbs light electrons are elevated from the ground state to an excited one. Any molecule containing π-electrons can absorb UV light, so UV active molecules are often aromatic. The specific transitions that can occur are defined by the Beer-Lambert law, which is related to the concentration of absorbing groups in the sample. As the wavelength of light applied to the sample is varied, the recorded absorption also varies. Samples prepared for UV-vis must be of low concentration, as the Beer-Lambert law is only applicable when absorbance is less than or equal to 1.[113]

Fluorescence spectroscopy measures the amount of energy released as electrons fall back to a low energy state after absorbing UV radiation. As electrons in the sample are subjected to UV light they gain energy, becoming excited, and are promoted to a higher state. Initially the excited fluorophore loses some energy through vibrational interaction and heat, but eventually falls back from the excited state to the ground state through the emission of a photon. This photon has slightly less energy than when it was promoted up from the ground state, and as such has a longer wavelength. The difference in nanometres between excitation energy and emissions intensity is known as the Stokes shift. This process is displayed in Figure 1.9.[114]

UV-visible spectroscopy was used to monitor the reaction kinetics of amide and ester polymerisations, whilst fluorescence spectroscopy was used with the DNA binding assay in Chapter 4.

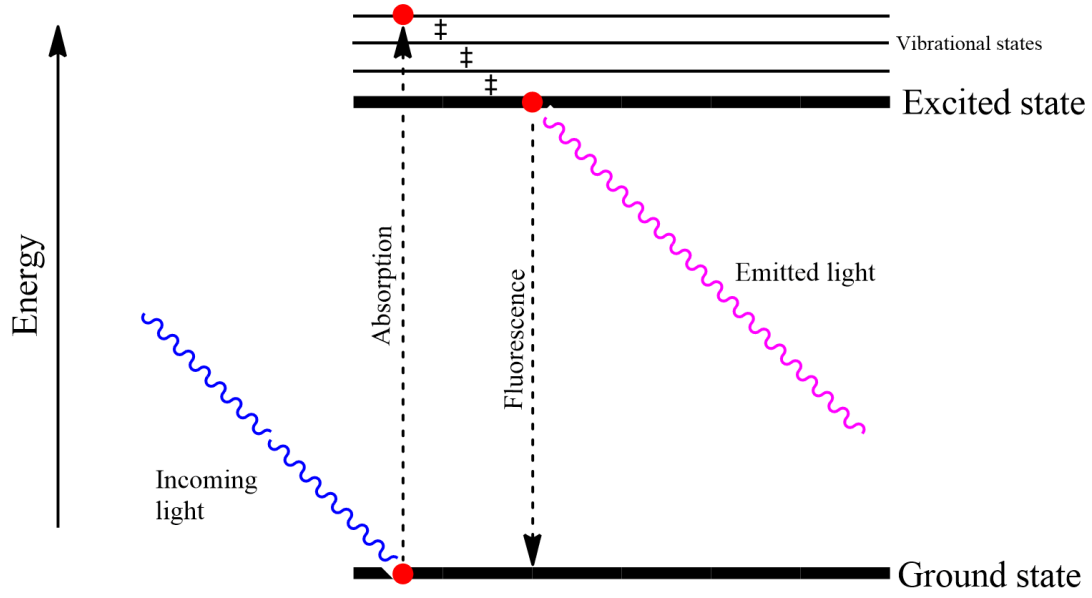

Figure 1.9 : Jablonski diagram showing how fluorescence occurs when a fluorophore is exposed to light.

1.3.3 Dynamic light scattering (DLS)

Dynamic light scattering (DLS) is a method used to measure the particle sizes of a material in solution due to the amount of light that they scatters. When a particle is in solution it will undergo Brownian motion, creating a random movement that is a result of the particle interacting with the solvent or other particles. This movement is tracked by a rapid series of scans by a laser, and by using the Stokes-Einstein equation the particle size can be calculated.[115]

During a measurement light emitted from the laser is shone into the sample solution and scattered onto a detector producing a speckle pattern of light and dark areas. Multiple patterns are collected and compared, and as particles move as a result of Brownian motion, the patterns change. The detector records these changes and this data is eventually used to calculate the particles sizes within the sample.

DLS measurements can produce data in three main size distributions: number, volume and intensity. A number average distribution takes into account the number of particles at a given size within a solution. For example, if a solution contained particles measuring 5 nm and 50 nm in equal amounts, two size distribution peaks would appear of equal area at their appropriate position on the x-axis. A volume

average distribution however will favour the larger particles as the total volume of the 50 nm particles is 1000 times larger than the 5 nm particles. An intensity average distribution would favour the 50 nm particles even more due to the increased scattering observed for large particles compared to small.[115]

DLS was used to measure particle sizes for polymers in solution, measure the size of magnetic nanoparticle and nanoparticle-polymer hybrids, and monitor the LCST of thermoresponsive polymers

1.4 Conclusions

The need for highly functional materials that can be produced cost effectively and without stringent reaction conditions has driven polymer science to great lengths, providing an array of possible techniques that can be used to fulfil these needs. This has enabled a whole range of monomers to be polymerised and specific materials to be designed to fit a previously assigned purpose.

Whilst early polymerisation techniques lacked finesse in producing controlled polymers, as the science advanced polymers with defined molecular weight, low dispersity, complex topology and multiple functionalities became increasingly possible to make. This was achieved by the realisation that the RDRP process is primarily controlled by the equilibrium that is present in a reaction between active propagating polymer chains, and dormant polymer chains.

ATRP is a technique that manages to control the rate of propagation through careful control of catalyst, initiator, solvent and monomer. The process works by the reversible halide transfer between a propagating polymer chain and a transition metal catalyst bound to a ligand in solution. It can also be used on a large array of monomers due to its mechanism that uses the vinyl bond for propagation.

Whilst several advances have been made from conventional ATRP (ARGET, SARA, metal free), the facile and robust nature of the system still makes it desirable for multiple syntheses. In addition to this, the kinetics of ATRP have been thoroughly investigated, meaning that within the literature there is a large amount of data on the effect that any part of the system has on the overall polymerisation.

1.4 References

1. H. Staudinger, *Berichte der deutschen chemischen Gesellschaft (A and B Series)*, 1920, **53**, 1073-1085.

2. L. H. Baekeland, *Method of making insoluble products of phenol and formaldehyde - Patent*, 1909.

3. J. M. G. Cowie and V. Arrighi, *Polymers: chemistry and physics of modern materials*, CRC press, 2007.

4. P. Alexandridis and B. Lindman, *Amphiphilic block copolymers: self-assembly and applications*, Elsevier, 2000.

5. T. M. Allen and P. R. Cullis, *Science*, 2004, **303**, 1818-1822.

6. F. F. Davis, *Advanced drug delivery reviews*, 2002, **54**, 457-458.

7. K. Matyjaszewski, *Macromolecules*, 2012, **45**, 4015-4039.

8. P. J. Flory, *Principles of polymer chemistry*, Cornell University Press, 1953.

9. W. H. Carothers, *J. Am. Chem. Soc.*, 1929, **51**, 2548-2559.

10. G. S. Moad, D. H., *The Chemistry of Free Radical Polymerization*, Pergamon: Oxford, 1995.

11. M. Szwarc, M. Levy and R. Milkovich, *J. Am. Chem. Soc.*, 1956, **78**, 2656-2657.

12. G. Odian, *Principles of polymerization*, John Wiley & Sons, 2004.

13. R. P. Quirk and B. Lee, *Polymer international*, 1992, **27**, 359-367.

14. E. Rizzardo, J. Chiefari, Y. Chong, F. Ercole, J. Krstina, J. Jeffery, T. P. Le, R. T. Mayadunne, G. F. Meijs, C. L. Moad and G. Moad, *Macromolecules*, 1998, **31**, 5559-5562.

15. S. G. Gaynor, J. S. Wang and K. Matyjaszewski, *Macromolecules*, 1995, **28**, 8051-8056.

16. A. Goto, Y. Kwak, T. Fukuda, S. Yamago, K. Iida, M. Nakajima and J.-i. Yoshida, *J. Am. Chem. Soc.*, 2003, **125**, 8720-8721.

17. J.-S. Wang and K. Matyjaszewski, *J. Am. Chem. Soc.*, 1995, **117**, 5614-5615.

18. C. J. Hawker, A. W. Bosman and E. Harth, *Chemical Reviews*, 2001, **101**, 3661-3688.

19. W. Jakubowski and K. Matyjaszewski, *Angewandte Chemie*, 2006, **118**, 4594-4598.

20. Y. Zhang, Y. Wang and K. Matyjaszewski, *Macromolecules*, 2011, **44**, 683-685.

21. V. Percec, T. Guliashvili, J. S. Ladislaw, A. Wistrand, A. Stjerndahl, M. J. Sienkowska, M. J. Monteiro and S. Sahoo, *J. Am. Chem. Soc.*, 2006, **128**, 14156-14165.

22. K. Matyjaszewski, *Introduction of living polymerization. Living and/or controlled polymerization*, DTIC Document, 1994.

23. A. D. Jenkins, R. G. Jones and G. Moad, *Pure and Applied Chemistry*, 2009, **82**, 483-491.

24. H. Arslan, *Block and Graft Copolymerization by Controlled/Living Radical Polymerization Methods*, 2012, 279.

25. G. Moad, E. Rizzardo and S. H. Thang, *Polymer*, 2008, **49**, 1079-1131.

26. S. Perrier and P. Takolpuckdee, *Journal of Polymer Science Part A: Polymer Chemistry*, 2005, **43**, 5347-5393.

27. S. Perrier, P. Takolpuckdee and C. A. Mars, *Macromolecules*, 2005, **38**, 2033-2036.

28. H. Willcock and R. K. O'Reilly, *Polymer Chemistry*, 2010, **1**, 149-157.

29. S. Aldrich, *RAFT: Choosing the Right Agent to Achieve Controlled Polymerisation*, 2015.

30. C. J. Hawker, *J. Am. Chem. Soc.*, 1994, **116**, 11185-11186.

31. C. Detrembleur, C. Jérôme, J. De Winter, P. Gerbaux, J.-L. Clément, Y. Guillaneuf and D. Gigmes, *Polymer Chemistry*, 2014, **5**, 335-340.

32. J. S. Wang and K. Matyjaszewski, *Macromolecules*, 1995, **28**, 7901-7910.

33. M. Kato, M. Kamigaito, M. Sawamoto and T. Higashimura, *Macromolecules*, 1995, **28**, 1721-1723.

34. K. Matyjaszewski and J. Xia, *Chemical Reviews*, 2001, **101**, 2921-2990.

35. K. Matyjaszewski and N. V. Tsarevsky, *J. Am. Chem. Soc.*, 2014, **136**, 6513-6533.

36. D. J. Siegwart, J. K. Oh and K. Matyjaszewski, *Progress in Polymer Science*, 2012, **37**, 18-37.

37. J.-S. Wang and K. Matyjaszewski, *Macromolecules*, 1995, **28**, 7901-7910.

38. H. Fischer, *Chemical Reviews*, 2001, **101**, 3581-3610.

39. N. V. Tsarevsky, W. A. Braunecker, A. Vacca, P. Gans and K. Matyjaszewski, *Macromol. Symp.*, 2007, **248**, 60-70.

40. M. B. Gillies, K. Matyjaszewski, P.-O. Norrby, T. Pintauer, R. Poli and P. Richard, *Macromolecules*, 2003, **36**, 8551-8559.

41. N. V. Tsarevsky, T. Pintauer and K. Matyjaszewski, *Macromolecules*, 2004, **37**, 9768-9778.

42. W. A. Braunecker and K. Matyjaszewski, *Journal of Molecular Catalysis A: Chemical*, 2006, **254**, 155-164.

43. W. Tang, Y. Kwak, W. Braunecker, N. V. Tsarevsky, M. L. Coote and K. Matyjaszewski, *J. Am. Chem. Soc.*, 2008, **130**, 10702-10713.

44. K. Matyjaszewski, A. K. Nanda and W. Tang, *Macromolecules*, 2005, **38**, 2015-2018.

45. W. Tang and K. Matyjaszewski, *Macromolecules*, 2006, **39**, 4953-4959.

46. W. Tang and K. Matyjaszewski, *Macromolecules*, 2007, **40**, 1858-1863.

47. K. A. Davis, H. J. Paik and K. Matyjaszewski, *Macromolecules*, 1999, **32**, 1767-1776.

48. N. J. Treat, H. Sprafke, J. W. Kramer, P. G. Clark, B. E. Barton, J. Read de Alaniz, B. P. Fors and C. J. Hawker, *J. Am. Chem. Soc.*, 2014, **136**, 16096-16101.

49. D. M. Haddleton, A. J. Clark, M. C. Crossman, D. J. Duncalf, A. M. Heming, S. R. Morsley and A. J. Shooter, *Chem. Commun.*, 1997, DOI: 10.1039/a702166f, 1173-1174.

50. M. Kamigaito, T. Ando and M. Sawamoto, *Chemical Reviews*, 2001, **101**, 3689-3746.

51. J. Queffelec, S. G. Gaynor and K. Matyjaszewski, *Macromolecules*, 2000, **33**, 8629-8639.

52. J. Qiu, K. Matyjaszewski, L. Thouin and C. Amatore, *Macromolecular Chemistry and Physics*, 2000, **201**, 1625-1631.

53. W. Jakubowski, J. F. Lutz, S. Slomkowski and K. Matyjaszewski, *Journal of Polymer Science Part A: Polymer Chemistry*, 2005, **43**, 1498-1510.

54. D. M. Haddleton, C. B. Jasieczek, M. J. Hannon and A. J. Shooter, *Macromolecules*, 1997, **30**, 2190-2193.

55. V. C. Gibson, R. K. O'Reilly, W. Reed, D. F. Wass, A. J. White and D. J. Williams, *Chem. Commun.*, 2002, 1850-1851.

56. T. Ando, M. Kato, M. Kamigaito and M. Sawamoto, *Macromolecules*, 1996, **29**, 1070-1072.

57. J. Xia and K. Matyjaszewski, *Macromolecules*, 1997, **30**, 7697-7700.

58. X. S. Wang and S. P. Armes, *Macromolecules*, 2000, **33**, 6640-6647.

59. K. Matyjaszewski, T. E. Patten and J. Xia, *J. Am. Chem. Soc.*, 1997, **119**, 674-680.

60. D. M. Haddleton, M. C. Crossman, B. H. Dana, D. J. Duncalf, A. M. Heming, D. Kukulj and A. J. Shooter, *Macromolecules*, 1999, **32**, 2110-2119.

61. T. E. Patten, J. Xia, T. Abernathy and K. Matyjaszewski, *Science*, 1996, **272**, 866-868.

62. W. Tang, N. V. Tsarevsky and K. Matyjaszewski, *J. Am. Chem. Soc.*, 2006, **128**, 1598-1604.

63. M. Mishra and Y. Yagci, *Handbook of vinyl polymers: radical polymerization, process, and technology*, CRC Press, 2008.

64. M. Ouchi, T. Terashima and M. Sawamoto, *Chemical Reviews*, 2009, **109**, 4963-5050.

65. K. Matyjaszewski, J.-L. Wang, T. Grimaud and D. A. Shipp, *Macromolecules*, 1998, **31**, 1527-1534.

66. V. Coessens, T. Pintauer and K. Matyjaszewski, *Progress in Polymer Science*, 2001, **26**, 337-377.

67. A. Limer and D. M. Haddleton, *Macromolecules*, 2006, **39**, 1353-1358.

68. Y. T. Li, Y. Q. Tang, R. Narain, A. L. Lewis and S. P. Armes, *Langmuir*, 2005, **21**, 9946-9954.

69. J. T. Rademacher, R. Baum, M. E. Pallack, W. J. Brittain and W. J. Simonsick, *Macromolecules*, 2000, **33**, 284-288.

70. D. Neugebauer and K. Matyjaszewski, *Macromolecules*, 2003, **36**, 2598-2603.

71. M. Senoo, Y. Kotani, M. Kamigaito and M. Sawamoto, *Macromolecules*, 1999, **32**, 8005-8009.

72. D. J. Adams and I. Young, *J. Polym. Sci. Pol. Chem.*, 2008, **46**, 6082-6090.

73. G. J. M. Habraken, C. E. Koning and A. Heise, *J. Polym. Sci. Pol. Chem.*, 2009, **47**, 6883-6893.

74. M. Rajan, U. Agarwal, C. Bailly, K. George and P. Lemstra, *Journal of Polymer Science Part A: Polymer Chemistry*, 2005, **43**, 575-583.

75. L. H. High, S. J. Holder and H. V. Penfold, *Macromolecules*, 2007, **40**, 7157-7165.

76. Y. Kotani, M. Kato, M. Kamigaito and M. Sawamoto, *Macromolecules*, 1996, **29**, 6979-6982.

77. H. Bergenudd, G. Coullerez, M. Jonsson and E. Malmstrom, *Macromolecules*, 2009, **42**, 3302-3308.

78. C. R. Becer, R. Hoogenboom, D. Fournier and U. S. Schubert, *Macromol. Rapid Commun.*, 2007, **28**, 1161-1166.

79. J. L. Wang, T. Grimaud and K. Matyjaszewski, *Macromolecules*, 1997, **30**, 6507-6512.

80. J. Wootthikanokkhan, M. Peesan and P. Phinyocheep, *Eur. Polym. J.*, 2001, **37**, 2063-2071.

81. S. Coca and K. Matyjaszewski, *Abstr. Pap. Am. Chem. Soc.*, 1996, **211**, 87-POLY.

82. G. Masci, L. Giacomelli and V. Crescenzi, *Macromol. Rapid Commun.*, 2004, **25**, 559-564.

83. K. Min, W. Jakubowski and K. Matyjaszewski, *Macromol. Rapid Commun.*, 2006, **27**, 594-598.

84. G. Lligadas, B. M. Rosen, M. J. Monteiro and V. Percec, *Macromolecules*, 2008, **41**, 8360-8364.

85. L. M. Gaetke and C. K. Chow, *Toxicology*, 2003, **189**, 147-163.

86. Y. Shen, H. Tang and S. Ding, *Progress in Polymer Science*, 2004, **29**, 1053-1078.

87. K. Matyjaszewski, T. Pintauer and S. Gaynor, *Macromolecules*, 2000, **33**, 1476-1478.

88. I. Ydens, S. Moins, F. Botteman, P. Degée and P. Dubois, *e-Polymers*, 2004, **4**, 414-420.

89. Z. Shen, Y. Chen, H. Frey and S.-E. Stiriba, *Macromolecules*, 2006, **39**, 2092-2099.

90. W. Jakubowski, K. Min and K. Matyjaszewski, *Macromolecules*, 2006, **39**, 39-45.

91. K. Matyjaszewski, H. Dong, W. Jakubowski, J. Pietrasik and A. Kusumo, *Langmuir*, 2007, **23**, 4528-4531.

92. D. Konkolewicz, Y. Wang, P. Krys, M. Zhong, A. A. Isse, A. Gennaro and K. Matyjaszewski, *Polym. Chem.*, 2014, **5**, 4409-4430.

93. A. J. Magenau, Y. Kwak and K. Matyjaszewski, *Macromolecules*, 2010, **43**, 9682-9689.

94. D. Konkolewicz, Y. Wang, M. Zhong, P. Krys, A. A. Isse, A. Gennaro and K. Matyjaszewski, *Macromolecules*, 2013, **46**, 8749-8772.

95. N. H. Nguyen, B. M. Rosen and V. Percec, *Journal of Polymer Science Part A: Polymer Chemistry*, 2010, **48**, 1752-1763.

96. G. Lligadas and V. Percec, *Journal of Polymer Science Part A: Polymer Chemistry*, 2008, **46**, 2745-2754.

97. G. Lligadas, B. M. Rosen, C. A. Bell, M. J. Monteiro and V. Percec, *Macromolecules*, 2008, **41**, 8365-8371.

98. S. Fleischmann, B. M. Rosen and V. Percec, *Journal of Polymer Science Part A: Polymer Chemistry*, 2010, **48**, 1190-1196.

99. Q. Zhang, P. Wilson, Z. Li, R. McHale, J. Godfrey, A. Anastasaki, C. Waldron and D. M. Haddleton, *J. Am. Chem. Soc.*, 2013, **135**, 7355-7363.

100. V. Percec, A. V. Popov, E. Ramirez-Castillo and O. Weichold, *Journal of Polymer Science Part A: Polymer Chemistry*, 2003, **41**, 3283-3299.

101. C. Boyer, A. Atme, C. Waldron, A. Anastasaki, P. Wilson, P. B. Zetterlund, D. Haddleton and M. R. Whittaker, *Polymer Chemistry*, 2013, **4**, 106-112.

102. A. Anastasaki, C. Waldron, V. Nikolaou, P. Wilson, R. McHale, T. Smith and D. M. Haddleton, *Polymer Chemistry*, 2013, **4**, 4113-4119.

103. B. P. Fors and C. J. Hawker, *Angewandte Chemie International Edition*, 2012, **51**, 8850-8853.

104. Y. Kwak and K. Matyjaszewski, *Macromolecules*, 2010, **43**, 5180-5183.

105. J. C. Scaiano, T. J. Connolly, N. Mohtat and C. N. Pliva, *Canadian journal of chemistry*, 1997, **75**, 92-97.

106. A. Goto, J. Scaiano and L. Maretti, *Photochem. Photobiol. Sci.*, 2007, **6**, 833-835.

107. E. Yoshida, *Colloid and Polymer Science*, 2010, **288**, 73-78.

108. M. A. Tasdelen, Y. Y. Durmaz, B. Karagoz, N. Bicak and Y. Yagci, *Journal of Polymer Science Part A: Polymer Chemistry*, 2008, **46**, 3387-3395.

109. N. J. Treat, B. P. Fors, J. W. Kramer, M. Christianson, C.-Y. Chiu, J. R. d. Alaniz and C. J. Hawker, *ACS Macro Letters*, 2014, **3**, 580-584.

110. P. C. Painter and M. M. Coleman, *Essentials of polymer science and engineering*, DEStech Publications, Inc, 2008.

111. M. Gaborieau and P. Castignolles, *Analytical and bioanalytical chemistry*, 2011, **399**, 1413-1423.

112. J. Keeler, *Understanding NMR spectroscopy*, John Wiley & Sons, 2011.

113. A. Owen, *Fundamentals of UV-visible spectroscopy*, 1996.

114. J. R. Lakowicz, *Principles of fluorescence spectroscopy*, Springer Science & Business Media, 2013.

115. W. Burchard and W. Richtering, in *Relaxation in Polymers*, Springer, 1989, pp. 151-163.

Chapter 2: Applications of functional materials

2.1 Applications for materials created by ATRP

With the flexibility of the ATRP system being well established, it is obvious that the ability to specify initiator and monomer has the potential to create highly customisable materials tailored for specific applications.[1]

One of the largest areas of interest is in bio-medical applications where there is an ongoing effort to create systems with higher bio-compatibility, bio-stability, and increased efficacy.[1-4] Possible applications are numerous and can range from; drug delivery systems that are able to deliver payloads of drugs to the active site where medicine is needed,[2, 5-7] the stabilisation of medical imaging contrast agents,[8-11] scaffolds for the growth of cell cultures or tissues[12-15] and improved dressings and sutures for wounds.[16, 17]

Biomedical engineering such as this has often been concerned with increasing the biocompatibility of materials in order to reduce any adverse effect that may be triggered in the host. However, through careful selection of initiator and monomer "smart" materials can be created that respond to one or more biological stimuli such as temperature, pH, and enzyme over-expression.[18-20] Often these characteristics can be activated by an external source, enabling the stimuli to be triggered at a desired time or location *in vivo*.[4]

This chapter will provide a brief overview of the current state of stimuli responsive polymers for drug delivery, focusing on thermoresponsive materials, and then discuss stabilisation of magnetic nanoparticles by polymers for magnetic resonance imaging contrast agents and targeted drug delivery.

2.1.1 Principles of biomedical polymers

In order for a polymer to be viable *in vivo* it needs to be resistant to the host's enzymatic attack, stable in the pH range it is required to operate, stable at body temperature, and non-toxic.[19, 20] If these goals are achieved the material that is produced can be said to be bio-compatible.

Within nature precedent for this already exists, with proteins being perfect polymeric structures. They are composed of defined sequences of amino acids that are selectively arranged with ideal molecular weights, molecular weight distributions, functionality and chemical composition. Ideally any bioengineered material would have as many properties in common to a polypeptide as possible, in order to mimic its biocompatibility.

The two main causes for a polymeric material to degrade *in vivo* are hydrolysis and enzymatic action on the chain structure.[21] Both processes cause polymer chains to be cleaved into shorter units that are generally excreted from the body via the renal system. Hydrolysis occurs on both ester and amide moieties in acidic and basic conditions, found freely inside a body. Enzymatic action can vary wildly depending on the location *in vivo* that the material is active and the functional groups making up the polymer structure.[22] Esters are cleaved by the presence of esterase, and amines by protease, to produced chains that are much shorter than the original.[23] This is detrimental to many functional polymers, as the physical properties of a polymer can be dependent on the functional groups in its structure, along with its molecular weight and dispersity.[24]

A common method that is used to reduce the rate of degradation of materials *in vivo* is by "pegylation", the process of attaching polyethylene glycol (PEG) chains to candidate molecules.[25, 26] PEG shows little toxicity to biological systems and can be cleared from the body through the renal system (for PEGs < 30 kDa) or in faeces (for PEGs > 20 kDA) so as not to accumulate permanently *in vivo*.[27] A variant method of protecting labile molecules is by using drug delivery vehicles such as liposomes, spherical vesicles composed of at least one lipid bilayer.[28-30] Therapeutics can be enclosed in the aqueous core (encapsulation), in the lipid bilayer (embedded), or on

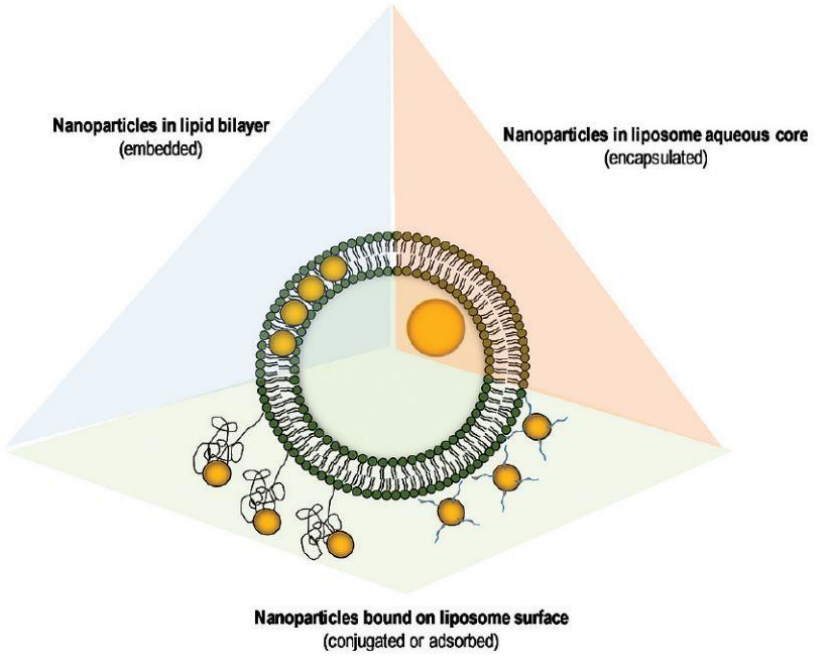

Figure 2.1 : A schematic diagram produced by Al-Jamal *et al* showing three different approaches to engineering a liposome for biomedical applications showing embedding (blue, left) encapsulation (pink, right) and conjugation (green, bottom).[31]

the surface (conjugation or adsorption), as is displayed in Figure 2.1. Whilst early liposomal systems suffered from issues with loaded drug molecules leaking from the vesicle structure, advances within the field of material preparation have reduced this effect, making liposomes the most clinically established nanometre-scale system used to deliver cytotoxic drugs, genes, vaccines and imaging agents.[31, 32]

Non-liposomal drug delivery systems can be created by using water soluble polymers that are composed of monomer units that are responsive to external stimuli.[4] The most widely researched polymers in this field possess thermoresponsive or pH-responsive activities, which cause a change in the hydrodynamic volume or internal structure of a polymer as the stimulus is applied.[4, 33-36]

2.2 pH-responsive polymers

Within a biological system there is significant variation in the pH values encountered. Whilst the stomach is well known to have a low pH (1.5-3.5), the small intestine is around pH 6 and the colon tends to have a pH neutral environment.[37] The pH values found in tumours are also known to be of a lower value than those of in blood.[38] This variation in pH environment means that a well-designed pH-responsive polymer drug delivery system can potentially be synthesised to inhibit payload release in systemic circulation (pH 7.4) and release when an acidic environment is encountered (such as in tumours).[39]

pH responsive polymers are often in the form of hydrogels, crosslinked polymers that possess hydrophilic groups and can absorb large amounts of water without losing their three dimensional structure.[40] When in an aqueous solution hydrogels often mimic biological tissues due to their high water content and soft consistency.[36, 41] Drugs are loaded into the hydrogel through a series of swelling and de-swelling

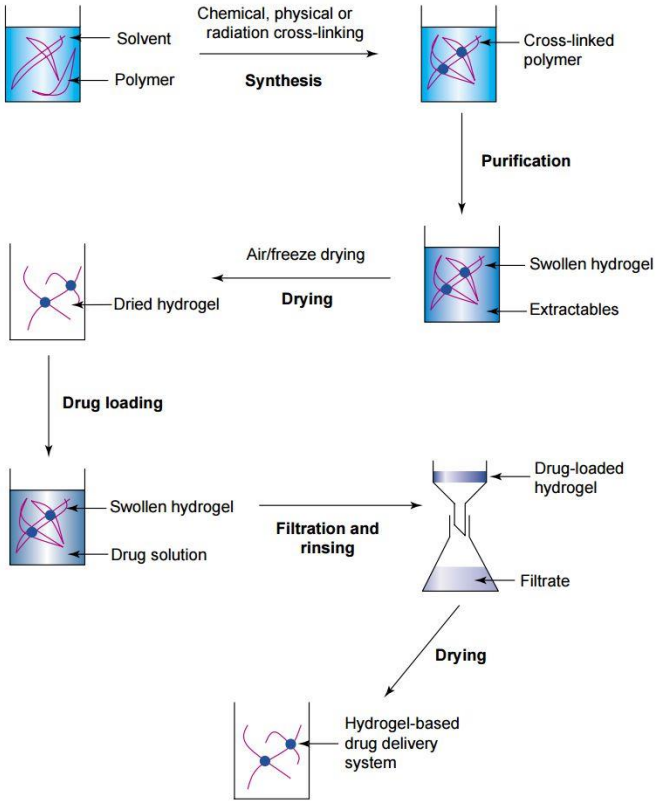

Figure 2.2 : A schematic representation of the steps involved with the preparation of a hydrogel drug release system.[40]

(drying) reactions as is displayed in Figure 2.2, with the drug loaded hydrogel being in a collapsed state before its released *in vivo*. Typical pH-responsive drug delivery hydrogels release their payloads through a swelling-controlled mechanism involving the simultaneous absorption of water and desorption of the drug when the stimulus is encountered.[42]

pH-sensitive polymers that have been used for drug delivery possess pendant acidic or basic groups that either accept or release protons in response to the pH of the environment they are in.[36] Depending on the monomer used, the pH-sensitivity of the polymer is controlled, providing the ability to release therapeutics at a range of pH values.

For example, the homo- and copolymerisation of 2-(dimethylamino)methyl methacrylate (DMAEMA) has been shown to be possible via ATRP,[43] whilst other research has shown that at low pH DMAEMA copolymers are highly soluble, but form micelles at high pH (>8).[44] Poly(methacrylic acid) based copolymers offer a reversed stimulus, being more soluble at high pH and less soluble at low pH (<6).[45] These effects are as a result of the ionisation of amino or acid groups present within the polymeric structures, as is displayed in Figure 2.3.[36]

Whilst pH-sensitive materials have been shown to be useful drug-delivery systems, the stimuli response is generally only controlled by the environment *in vivo*, not externally.[35, 39] Thermo-responsive drug delivery systems can be activated by the application of an external heating source, and therefore have seen a large of amount of interest.[34, 35, 46-48]

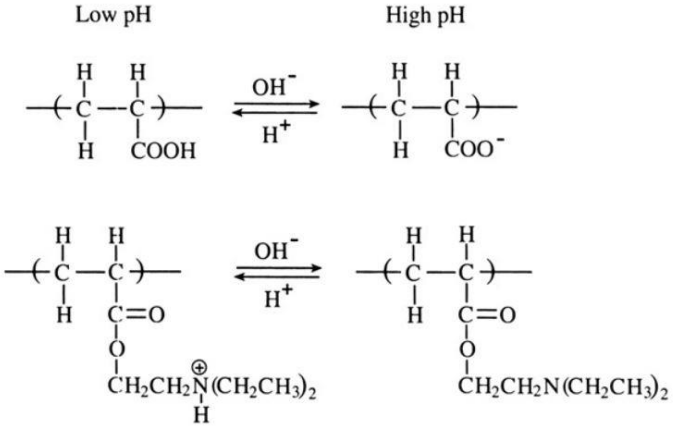

Figure 2.3 : pH dependent ionization of PAA (top) and PDMAEMA (bottom).[36]

2.3 Thermoresponsive polymers

A key advantage of a thermoresponsive polymer system is that the stimulus response (temperature) can easily be externally applied.[34] The main biomedical applications for thermoresponsive polymers are drug delivery, gene delivery and tissue engineering.[9, 12, 49-51] Polymers that are sensitive to thermal stimulus can either possess an upper critical solution temperature (UCST), or a lower critical solution temperature (LCST).

A polymer that possesses an LCST will be completely miscible below its critical temperature, and becomes immiscible above it. UCST polymers on the other hand are immiscible below their critical temperature, and become fully miscible above it.[34] This is displayed in Figure 2.4. UCST is a process driven by the enthalpy of the system, whilst LCST is an entirely entropic effect.[52] When a material with a LCST is brought above its critical temperature the formerly homogenous solution appears to become cloudy, as such the LCST is often referred to as the cloud point of a polymer (T_{CP}). However, LCST and T_{CP} are not necessarily the same thing, as due to the particles sizes that a polymer forms in when it becomes immiscible, clouding may not immediately (or ever) become apparent. LCST refers to the specific temperature where immiscibility occurs; whilst T_{CP} is the temperature this effect is apparent. Due to the fact that LCST is an entropically driven system it can be considered in terms

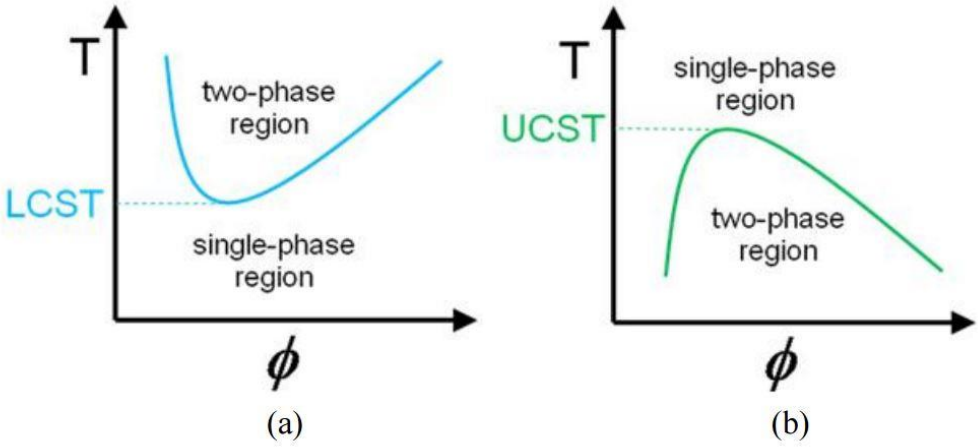

Figure 2.4 : Schematic illustration of phase diagrams for LCST polymers (left (a)) and UCST polymers (right (b)). Φ represents increasing polymer fraction in solution.[34]

of the Gibbs free energy equation:

$$\Delta G_{mix} = \Delta H_{mix} - T\Delta S_{mix}$$

Equation 2.1

where: G_{mix} is the Gibbs free energy, H_{mix} is the enthalpy, S_{mix} is the entropy and T is the temperature.

The main factor in the mixing of solutions in these circumstances relates to the entropy of the solvent (mainly hydrogen bonding in water). Below the LCST the polymer is mixed into solution with the water, creating a more ordered system and lowering the overall entropy. Above the LCST the polymer and solvent are in separate phases, creating a more disordered system and increasing entropy. Polymers that possess LCST are generally only able to mix into solution as a result of hydrogen bonding between the solvent and the polymer chains. As the temperature is raised this effect can no longer mitigate the relative hydrophobicity of the polymer chain and the polymer moves into a separate phase.

Thermoresponsive polymers investigated for biomedical applications generally make use of LCST, as triggering immiscibility by raising temperature is facile to accomplish and allows micelles formed by combining hydrophilic and hydrophobic homopolymers to be collapsed, forcing encapsulated therapeutics to be released.[53, 54] Materials with a UCST are also of possible importance, as they can be used as drug delivery vehicles by preparing them in a similar method to that proposed in Figure 2.2, where above the UCST swelling will occur as the polymer becomes miscible and the absorption of water triggers the desorption of the payload.[55]

The most widely studied polymers that present an LCST are ones where the transition temperature is similar to that of a biological system (≈37 ºC), chiefly this has been poly(*N*-isopropylacrylamide) (PNIPAAm) which has an LCST around 32 ^{o}C.[46, 49, 56-60] This value has been shown to be controllable by the copolymerisation of PNIPAAm with either more hydrophobic or hydrophilic monomers.[61-65] Other polymers that have been investigated include poly(*N*-vinylcaprolactam) (LCST 25 – 35 ºC),[66, 67] poly(2-(dimethylamino)ethyl methacrylate (DMAEMA) (LCST ≈ 50

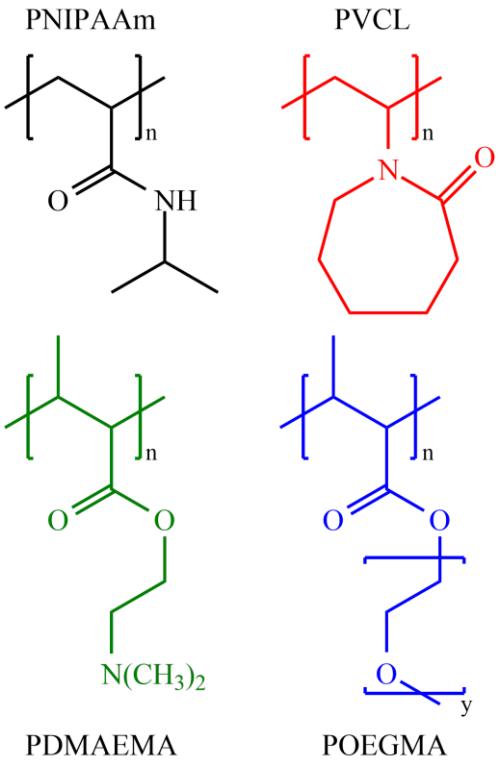

Figure 2.5 : Structures of commonly investigated polymers that possess an LCST. poly(*N*-isopropylacrylamide) (black, top left), poly(*N*-vinylcaprolactam) (red, top right), poly(2-(dimethylamino)ethyl methacrylate (green, bottom left), poly(oligo ethylene glycol)methyl ether (blue, bottom right).

ºC), which is also pH sensitive,[68-70] and poly(ethylene glycol) (PEG or PEO) (LCST ≈ 85 ºC).[71, 72] The LCST of PEG can be lowered through the placement of ethylene oxide units as a pendant chain, displayed as "POEGMA" in Figure 2.5. The value of y, the length of the pendant chain, affects the LCST of the polymer with 2 units giving an LCST of ≈ 26 ºC and 4-5 units giving an LCST of ≈ 64 ºC.[73] The LCST can be fine-tuned even further through copolymerisation between OEGMAs with differing ethylene oxide chain lengths. Lutz *et al* demonstrated that an LCST of 37 ºC was attainable by the polymerisation of OEGMA and 2-(2'-methoxyethoxy)ethyl methacrylate in an 8:92 ratio of monomers respectively.[74] The value of LCST is also affected by the total molecular weight of a polymer, the architecture of the polymer chains and the concentration of polymer in solution.[75-78]

2.4 Polymer stabilisation of magnetic nanoparticles

Magnetic nanoparticles are used in numerous biomedical applications including as MRI contrast agents,[10, 79] cell labelling and tracking,[80, 81] and targeted drug delivery systems.[82, 83] Polymer coatings are applied to magnetic nanoparticles in order to improve their biocompatibility and stabilise the particle in solution.

Magnetic nanoparticles can be synthesised using various types of magnetic materials such as magnetite (Fe_3O_4), maghemite (Fe_2O_3) or cobalt ferrite ($CoFe_2O_4$).[84] The rest of this chapter will discuss magnetite nanoparticle systems as they are one of the more frequently used. Magnetite contains both Fe^{2+} and $(Fe^{3+})_2$ ions, where Fe^{2+} ions occupy half of the octahedral sites within the lattice structure and $(Fe^{3+})_2$ fill the remainder of the octahedral sites and all of the tetrahedral sites.[85] If the grain size of a magnetite particle is less than around 15 nm, then the particle may possess a single magnetic domain which causes superparamagnetic behaviour.[86] This is important as if a superparamagnetic particle is exposed to an external magnetic field the entire magnetic moment of the particle aligns parallel to the field, and when the field is removed the alignment is full lost, resulting in no remanence or coercivity. This is important in biomedical applications because it ensures that outside of an external field there are no ferromagnetic attractions between particles and agglomeration of particles *in vivo* is reduced.[87]

2.4.1 Synthesis of magnetite nanoparticles

Co-precipitation methods are frequently used in the synthesis of magnetite nanoparticles as they have been shown to be both experimentally simple to perform and consistently produce low grain size nanoparticles.[88] In a co-precipitation, particle formation occurs as a result of the addition of a concentrated base to a solution of metal salts and is described by the reaction described in Equation 2.2.[89]

$$Fe^{2+} + (Fe^{3+})_2 + 8OH^- \rightarrow Fe_3O_4 + 4H_2O$$

Equation 2.2

The reaction typically takes place under an inert atmosphere to reduce the likelihood of the formation of maghemite, which is also a superparamagnetic iron oxide, but has a lower magnetic saturation value.

2.4.2 Stabilisation of magnetite nanoparticles

Bare magnetite nanoparticles are often stabilised by surfactants or polymers to prevent their sedimentation and/or agglomeration in a solution.[90] In addition to this, bare iron oxides are prone to oxidation and degradation *in vivo* which can cause damage to DNA causing mutations.[91, 92]

Common stabilisers for magnetite nanoparticles include silica, various polymers and organic surfactants.[93-96] When polymers are used as stabilising agents for magnetic nanoparticles the polymer that is used is often chosen due to its physical properties, such as high water solubility. Poly(sodium-4-styrene sulphonate),[97] poly(diallyldimethylammonium chloride),[98] poly(ethyleneimine)[99] and PEG[96] have all been successfully used in previously reported works.

Thünemaan *et al* demonstrated that poly(ethyleneimine) (PEI) can absorb onto maghemite nanoparticles to act as a primary layer in a stabilisation system along with a poly(ethylene oxide)-co-poly(glutamic acid) secondary layer. PEI can absorb on the nanoparticle surface due to the electrostatic interaction between the numerous ammonium groups within the PEI structure and the oppositely charged surface ions on the maghemite.[100] Stabilised nanoparticles were prepared in a "layer by layer" approach, with bare particles prepared first, then coated by PEI, and then finally coated by the separately synthesised copolymer. Once the final polymer layer is in place, the primary PEI layer is effectively "glued" in place due to the steric stabilisation provided by the secondary layer. When placed into a physiologically mimetic medium (0.15 M sodium chloride solution) no change in particle size distribution was measured during the 30 day duration of the experiment.

PEO has also shown promise in the stabilisation of magnetite nanoparticles.[101-103] Riffle *et al* demonstrated the synthesis of PEO stabilised nanoparticles that remained dispersed in physiological conditions and possessed high magnetic saturation values.[102]

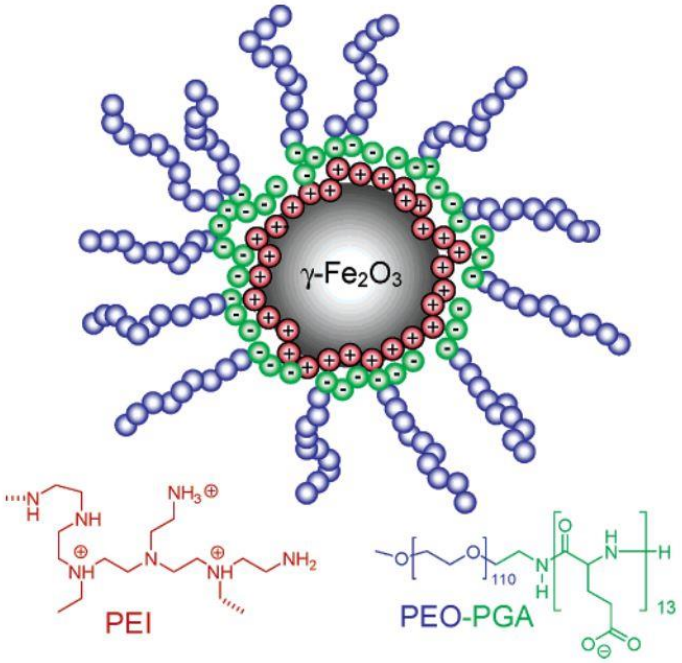

Figure 2.6 : Sketch of polymer coated maghemite nanoparticles and the associated polymer chemical structures prepared by Thünemaan *et al.*[99]

PEO polymer chains were immobilised onto magnetite particles through the electrostatic interactions of carboxylic acid groups that was were part of a triblock copolymer consisting of PEO tail blocks and a polyurethane based central segment. Nanocomposites produced by this method remained stable at pH values of 7 and lower, and also remained in solution for approximately one week at pH 8. Magnetic saturation values of stabilised particles were lower than of bulk magnetite, but remained in line with values reported of other stabilised magnetite indicating that PEO is not inherently detrimental as a stabiliser.

2.4.3 Nanoparticle contrast agents

Perhaps the most well-known use of magnetic nanoparticles is as contrast agents for magnetic resonance imaging (MRI). MRI is a technique that shares its base principles with NMR, which was briefly discussed in the previous chapter. Medically, it is used as a non-invasive imaging technique that utilises the same principle of magnetic moments to generate images of the internal structures of an organism.

Within the body there is a large number of proton as a result of the high water and lipid content of living organisms. When these protons are placed into a magnetic field there is an alignment of their magnetic moments either with the field (parallel) or against it (anti-parallel). There will always be a difference in the number of protons that align one way or the other due to the slightly higher energy requirement of the anti-parallel alignment. If a radio frequency (RF) pulse is then applied across the protons, they will become excited and de-align with the previously applied magnetic field. As the RF pulse only occurs briefly, the protons will eventually (detectibly) relax back into alignment with the external field, and after multiple measurements these relaxations can be used to create an image that is composed of proton densities. Relaxations occur either longitudinally (T_1), when energy from the excited nuclei is lost to the surroundings, or transversely (T_2), when the energy loss occurs as a results of interaction with other nuclei.

MR images can be improved through the usage of a contrast agent, a magnetic material that shortens the relaxation time of protons within the magnetic field, improving the resolution of the image. The key considerations for contrast agents are their solubility in water, and magnetic saturation. The solubility and stability of the particles is critical because it directly affects the contrast agent's interaction with the proton rich aqueous environment *in vivo*. Further to this, it is desirable that the particles remain stable for as long as possible *in vitro*, as it allows for a greater period of time between when the particles are prepared, and when they have to be used. A high magnetic saturation means that the particle generates a stronger magnetic field during the course of the experiment.

Various iron oxide contrast agents are already available commercially, and are stabilised by a range of polymers. Feridex is stabilised by dextran, Resovist by a carboxydextran, Lumirem by a siloxane, and Clariscan by a PEG composite.[104] The stabiliser that is chosen for the particles can dramatically affect their magnetic properties, with different coatings changing relaxivity values for T_1 or T_2 independently, so in order to achieve the desired results care must be taken in coating choice.

2.4.4 Magnetically targeted drug delivery

Whilst chemotherapy is already a highly effect treatment for numerous forms of cancer, it is a non-site-specific treatment, often highly detrimental to the patient.[105] Due to the inherently cytotoxic nature of the agents used in chemotherapy, when healthy cells come into contact with chemotherapeutics they are also destroyed. A solution to this would be a method of targeting these drugs specifically to the location of cancer cells. Magnetic nanocomposites have the potential to accomplish this through their stabilising shell which, can be functionalised in numerous ways, and their magnetic core, which enables guiding to a site via an external magnetic field.[106-109] The effect of this is to localise the drug to a specific region, lowering the detrimental effects on the rest of the system.

One of the earliest demonstrations of this technique was performed by Lübbe *et al*, who bound the anti-cancer agent "Epirubicin" to an iron oxide nanoparticles being stabilised by starch based polymers.[83] This drug-polymer-nanoparticle composite was held in proximity to the site of a tumour by an external magnetic field and after one to two weeks the appearance of the tumour had been reduced, which led to a complete loss of the growth.

An example that is more relevant to the work presented in this thesis was carried out by Ghosh *et al*, who used free radical polymerisation to produce magnetic nanospheres stabilised by a POEGMA-co-POEGMA surface network.[110] This system maintained the thermoresponsive nature of the POEGMA, which could be activated the application of an alternating magnetic field, heating up the nanoparticle cores. The nanospheres could also be readily taken up during cell activity studies, and showed minimal negative effects on cellular systems. This system shows great potential as a drug delivery vehicle and highlights the desirability of a POEGMA/iron oxide nanoparticle composite.

2.5 Conclusions

The potential medical applications of polymers and polymer-nanoparticle hybrids are enormous, with only a handful having been touched in this chapter.

By careful selection of monomer, polymers can be prepared which are able to react to external stimuli such as pH and temperature. The form of this response is normally a swelling or de-swelling of the polymer chains in response to their local environment, which when coupled with a carried molecular payload allows a triggered release when the stimulus is applied. This principle has been shown to be effective in biological systems where the complex architectures composed of copolymers or polymer-nanoparticle hybrids have been utilised to deliver drug payloads with less detrimental effects than would be observed if the drug was applied conventionally.

Magnetic nanoparticles play a crucial role in MR imaging, acting as contrast agents that improve the overall quality of images. These nanoparticles need to be stabilised in order to remain in solution for longer periods of time, and prevent their degradation from biological action. Stabilisation is often provided by polymers, with polyelectrolytes being of particular interest due to the electrostatic interactions they can have with oppositely charged surface ions on the nanoparticle.

2.6 References

1. D. J. Siegwart, J. K. Oh and K. Matyjaszewski, *Progress in Polymer Science*, 2012, **37**, 18-37.

2. J. K. Oh, D. J. Siegwart, H. I. Lee, G. Sherwood, L. Peteanu, J. O. Hollinger, K. Kataoka and K. Matyjaszewski, *J. Am. Chem. Soc.*, 2007, **129**, 5939-5945.

3. S. Ramakrishna, J. Mayer, E. Wintermantel and K. W. Leong, *Composites science and technology*, 2001, **61**, 1189-1224.

4. C. de las Heras Alarcón, S. Pennadam and C. Alexander, *Chemical Society Reviews*, 2005, **34**, 276-285.

5. Y. T. Li, Y. Q. Tang, R. Narain, A. L. Lewis and S. P. Armes, *Langmuir*, 2005, **21**, 9946-9954.

6. B. K. Nanjwade, H. M. Bechra, G. K. Derkar, F. Manvi and V. K. Nanjwade, *European Journal of Pharmaceutical Sciences*, 2009, **38**, 185-196.

7. T. M. Allen and P. R. Cullis, *Science*, 2004, **303**, 1818-1822.

8. J.-F. Berret, N. Schonbeck, F. Gazeau, D. El Kharrat, O. Sandre, A. Vacher and M. Airiau, *J. Am. Chem. Soc.*, 2006, **128**, 1755-1761.

9. H. K. Nguyen, P. Lemieux, S. V. Vinogradov, C. L. Gebhart, N. Guerin, G. Paradis, T. K. Bronich, V. Y. Alakhov and A. V. Kabanov, *Gene Ther.*, 2000, **7**, 126-138.

10. H. B. Na, I. C. Song and T. Hyeon, *Adv. Mater.*, 2009, **21**, 2133-2148.

11. S. A. Corr, S. J. Byrne, R. Tekoriute, C. J. Meledandri, D. F. Brougham, M. Lynch, C. Kerskens, L. O'Dwyer and Y. K. Gun'ko, *J. Am. Chem. Soc.*, 2008, **130**, 4214-4215.

12. M. Turk, S. Dincer, I. S. Yulug and E. Piskin, *J. Control. Release*, 2004, **96**, 325-340.

13. M. Krishnamoorthy, S. Hakobyan, M. Ramstedt and J. E. Gautrot, *Chemical Reviews*, 2014, **114**, 10976-11026.

14. X. Fan, L. Lin, J. L. Dalsin and P. B. Messersmith, *J. Am. Chem. Soc.*, 2005, **127**, 15843-15847.

15. A. Mizutani, A. Kikuchi, M. Yamato, H. Kanazawa and T. Okano, *Biomaterials*, 2008, **29**, 2073-2081.

16. K. Bertal, J. Shepherd, C. I. Douglas, J. Madsen, A. Morse, S. Edmondson, S. P. Armes, A. Lewis and S. MacNeil, *Journal of materials science*, 2009, **44**, 6233-6246.

17. J. Madsen, S. P. Armes, K. Bertal, H. Lomas, S. MacNeil and A. L. Lewis, *Biomacromolecules*, 2008, **9**, 2265-2275.

18. B. Jeong and A. Gutowska, *Trends in biotechnology*, 2002, **20**, 305-311.

19. A. S. Hoffman, P. S. Stayton, V. Bulmus, G. Chen, J. Chen, C. Cheung, A. Chilkoti, Z. Ding, L. Dong and R. Fong, *Journal of Biomedical Materials Research*, 2000, **52**, 577-586.

20. I. Y. Galaev and B. Mattiasson, *Trends in biotechnology*, 1999, **17**, 335-340.

21. J. M. Anderson and M. S. Shive, *Advanced drug delivery reviews*, 2012, **64**, 72-82.

22. T. D. Bugg, *Introduction to enzyme and coenzyme chemistry*, John Wiley & Sons, 2012.

23. H. R. Horton, L. A. Moran, R. S. Ochs, J. D. Rawn and K. G. Scrimgeour, *Principles of biochemistry*, Prentice Hall Upper Saddle River, 1996.

24. J. M. G. Cowie and V. Arrighi, *Polymers: chemistry and physics of modern materials*, CRC press, 2007.

25. J. M. Harris and R. B. Chess, *Nature Reviews Drug Discovery*, 2003, **2**, 214-221.

26. F. Veronese and J. M. Harris, *Advanced drug delivery reviews*, 2002, **54**, 453.

27. T. Yamaoka, Y. Tabata and Y. Ikada, *Journal of pharmaceutical sciences*, 1994, **83**, 601-606.

28. C. Mateo, J. Lombardero, E. Moreno, A. Morales, G. Bombino, J. Coloma, L. Wims, S. L. Morrison and R. Pérez, *Hybridoma*, 2000, **19**, 463-471.

29. J. Lyczak and S. Morrison, *Archives of virology*, 1994, **139**, 189-196.

30. R. M. Fielding, *Clinical pharmacokinetics*, 1991, **21**, 155-164.

31. W. T. Al-Jamal and K. Kostarelos, *Accounts of chemical research*, 2011, **44**, 1094-1104.

32. D. Lasic, D. Papahadjopoulos and G. Gregoriadis, *Journal*, 1998, 1-7.

33. R. Zhang, Y. Wang, F. S. Du, Y. L. Wang, Y. X. Tan, S. P. Ji and Z. C. Li, *Macromol. Biosci.*, 2011, **11**, 1393-1406.

34. M. A. Ward and T. K. Georgiou, *Polymers*, 2011, **3**, 1215-1242.

35. D. Schmaljohann, *Advanced drug delivery reviews*, 2006, **58**, 1655-1670.

36. Y. Qiu and K. Park, *Advanced drug delivery reviews*, 2012, **64**, 49-60.

37. V. Balamuralidhara, T. Pramodkumar, N. Srujana, M. Venkatesh, N. V. Gupta, K. Krishna and H. Gangadharappa, 2011.

38. Q. Yang, S. Wang, P. Fan, L. Wang, Y. Di, K. Lin and F.-S. Xiao, *Chemistry of Materials*, 2005, **17**, 5999-6003.

39. Y. J. Zhu and F. Chen, *Chemistry–An Asian Journal*, 2015, **10**, 284-305.

40. P. Gupta, K. Vermani and S. Garg, *Drug discovery today*, 2002, **7**, 569-579.

41. A. K. Gaharwar, N. A. Peppas and A. Khademhosseini, *Biotechnology and bioengineering*, 2014, **111**, 441-453.

42. K. R. Rao and K. P. Devi, *International journal of pharmaceutics*, 1988, **48**, 1-13.

43. L. H. Gan, P. Ravi, B. W. Mao and K. C. Tam, *Journal of Polymer Science Part A: Polymer Chemistry*, 2003, **41**, 2688-2695.

44. J. Tan, P. Ravi, H.-P. Too, T. A. Hatton and K. Tam, *Biomacromolecules*, 2005, **6**, 498-506.

45. B. H. Tan, K. C. Tam, Y. C. Lam and C. B. Tan, *Advances in colloid and interface science*, 2005, **113**, 111-120.

46. J. F. Lutz, O. Akdemir and A. Hoth, *J. Am. Chem. Soc.*, 2006, **128**, 13046-13047.

47. C. Porsch, S. Hansson, N. Nordgren and E. Malmström, *Polymer Chemistry*, 2011, **2**, 1114-1123.

48. J. F. Lutz, *Adv. Mater.*, 2011, **23**, 2237-2243.

49. H. Cheng, J. L. Zhu, Y. X. Sun, S. X. Cheng, X. Z. Zhang and R. X. Zhuo, *Bioconjugate Chem.*, 2008, **19**, 1368-1374.

50. H. Tan, C. M. Ramirez, N. Miljkovic, H. Li, J. P. Rubin and K. G. Marra, *Biomaterials*, 2009, **30**, 6844-6853.

51. R. M. Da Silva, J. F. Mano and R. L. Reis, *Trends in biotechnology*, 2007, **25**, 577-583.

52. C. Vasile, *Handbook of Polymer Blends and Composites*, Rapra Technology, 2003.

53. H. Wei, X.-Z. Zhang, Y. Zhou, S.-X. Cheng and R.-X. Zhuo, *Biomaterials*, 2006, **27**, 2028-2034.

54. H. Wei, X.-Z. Zhang, H. Cheng, W.-Q. Chen, S.-X. Cheng and R.-X. Zhuo, *J. Control. Release*, 2006, **116**, 266-274.

55. H. S. Shin, S. Y. Kim and Y. M. Lee, *Journal of Applied Polymer Science*, 1997, **65**, 685-693.

56. C. Y. Quan, H. Wei, Y. X. Sun, S. X. Cheng, K. Shen, Z. W. Gu, X. Z. Zhang and R. X. Zhuo, *J. Nanosci. Nanotechnol.*, 2008, **8**, 2377-2384.

57. D. X. Li, Q. He, Y. Cui, K. W. Wang, X. M. Zhang and J. B. Li, *Chem.-Eur. J.*, 2007, **13**, 2224-2229.

58. D. Schmaljohann, J. Oswald, B. Jørgensen, M. Nitschke, D. Beyerlein and C. Werner, *Biomacromolecules*, 2003, **4**, 1733-1739.

59. X.-Z. Zhang, D.-Q. Wu and C.-C. Chu, *Biomaterials*, 2004, **25**, 3793-3805.

60. H. Wei, X. Zhang, C. Cheng, S.-X. Cheng and R.-X. Zhuo, *Biomaterials*, 2007, **28**, 99-107.

61. Z. M. O. Rzaev, S. Dinçer and E. Pişkin, *Progress in Polymer Science*, 2007, **32**, 534-595.

62. H. G. Schild, *Progress in Polymer Science*, 1992, **17**, 163-249.

63. S. Aoshima and S. Kanaoka, in *Wax crystal control· nanocomposites· stimuli-responsive polymers*, Springer, 2008, pp. 169-208.

64. Y. Xia, N. A. D. Burke and H. D. H. Stöver, *Macromolecules*, 2006, **39**, 2275-2283.

65. R. Plummer, D. J. T. Hill and A. K. Whittaker, *Macromolecules*, 2006, **39**, 8379-8388.

66. H. Vihola, A. Laukkanen, H. Tenhu and J. Hirvonen, *Journal of pharmaceutical sciences*, 2008, **97**, 4783-4793.

67. H. Vihola, A.-K. Marttila, J. S. Pakkanen, M. Andersson, A. Laukkanen, A. M. Kaukonen, H. Tenhu and J. Hirvonen, *International journal of pharmaceutics*, 2007, **343**, 238-246.

68. V. Bütün, S. Armes and N. Billingham, *Polymer*, 2001, **42**, 5993-6008.

69. V. San Miguel, A. Limer, D. M. Haddleton, F. Catalina and C. Peinado, *Eur. Polym. J.*, 2008, **44**, 3853-3863.

70. N. Takeda, E. Nakamura, M. Yokoyama and T. Okano, *J. Control. Release*, 2004, **95**, 343-355.

71. Z. Hu, T. Cai and C. Chi, *Soft Matter*, 2010, **6**, 2115-2123.

72. M. S. Kim, H. Hyun, K. S. Seo, Y. H. Cho, J. Won Lee, C. Rae Lee, G. Khang and H. B. Lee, *Journal of Polymer Science Part A: Polymer Chemistry*, 2006, **44**, 5413-5423.

73. J. F. Lutz, *Journal of Polymer Science Part A: Polymer Chemistry*, 2008, **46**, 3459-3470.

74. J.-F. Lutz and A. Hoth, *Macromolecules*, 2006, **39**, 893-896.

75. M. A. Ward and T. K. Georgiou, *Journal of Polymer Science Part A: Polymer Chemistry*, 2010, **48**, 775-783.

76. W. Li, D. Wu, A. D. Schlüter and A. Zhang, *Journal of Polymer Science Part A: Polymer Chemistry*, 2009, **47**, 6630-6640.

77. C. Kojima, K. Yoshimura, A. Harada, Y. Sakanishi and K. Kono, *Journal of Polymer Science Part A: Polymer Chemistry*, 2010, **48**, 4047-4054.

78. W. Li, A. Zhang, K. Feldman, P. Walde and A. D. Schlüter, *Macromolecules*, 2008, **41**, 3659-3667.

79. D.-W. Wang, X.-M. Zhu, S.-F. Lee, H.-M. Chan, H.-W. Li, S. K. Kong, C. Y. Jimmy, C. H. Cheng, Y.-X. J. Wang and K. C.-F. Leung, *Journal of Materials Chemistry B*, 2013, **1**, 2934-2942.

80. S. P. Foy, R. L. Manthe, S. T. Foy, S. Dimitrijevic, N. Krishnamurthy and V. Labhasetwar, *ACS nano*, 2010, **4**, 5217-5224.

81. H. Y. Xie, C. Zuo, Y. Liu, Z. L. Zhang, D. W. Pang, X. L. Li, J. P. Gong, C. Dickinson and W. Zhou, *Small*, 2005, **1**, 506-509.

82. F. Márquez, G. M. Herrera, T. Campo, M. Cotto, J. Ducongé, J. M. Sanz, E. Elizalde, Ó. Perales and C. Morant, *Nanoscale research letters*, 2012, **7**, 1-11.

83. A. S. Lübbe, C. Bergemann, W. Huhnt, T. Fricke, H. Riess, J. W. Brock and D. Huhn, *Cancer research*, 1996, **56**, 4694-4701.

84. Z. R. Stephen, F. M. Kievit and M. Zhang, *Materials Today*, 2011, **14**, 330-338.

85. R. M. Cornell and U. Schwertmann, *The iron oxides: structure, properties, reactions, occurrences and uses*, John Wiley & Sons, 2006.

86. G. Goya, T. Berquo, F. Fonseca and M. Morales, *Journal of Applied Physics*, 2003, **94**, 3520-3528.

87. C. Bean and J. Livingston, *Journal of Applied Physics*, 1959, **30**, S120-S129.

88. H. S. Lee, W. C. Lee and T. Furubayashi, *Journal of Applied Physics*, 1999, **85**, 5231-5233.

89. R. Massart, *IEEE transactions on magnetics*, 1981, 1247-1248.

90. M. Chanana, Z. Mao and D. Wang, *Journal of biomedical nanotechnology*, 2009, **5**, 652-668.

91. H. L. Karlsson, P. Cronholm, J. Gustafsson and L. Moller, *Chemical research in toxicology*, 2008, **21**, 1726-1732.

92. T. Neuberger, B. Schöpf, H. Hofmann, M. Hofmann and B. Von Rechenberg, *Journal of Magnetism and Magnetic Materials*, 2005, **293**, 483-496.

93. T. K. Jain, M. A. Morales, S. K. Sahoo, D. L. Leslie-Pelecky and V. Labhasetwar, *Molecular pharmaceutics*, 2005, **2**, 194-205.

94. Y. Sun, L. Duan, Z. Guo, Y. DuanMu, M. Ma, L. Xu, Y. Zhang and N. Gu, *Journal of Magnetism and Magnetic Materials*, 2005, **285**, 65-70.

95. J. Chatterjee, Y. Haik and C.-J. Chen, *Journal of Magnetism and Magnetic Materials*, 2001, **225**, 21-29.

96. J.-F. Lutz, S. Stiller, A. Hoth, L. Kaufner, U. Pison and R. Cartier, *Biomacromolecules*, 2006, **7**, 3132-3138.

97. S. A. Corr, Y. K. Gun'ko, R. Tekoriute, C. J. Meledandri and D. F. Brougham, *The Journal of Physical Chemistry C*, 2008, **112**, 13324-13327.

98. K. W. Mattison, P. L. Dubin and I. J. Brittain, *The Journal of Physical Chemistry B*, 1998, **102**, 3830-3836.

99. A. F. Thünemann, D. Schütt, L. Kaufner, U. Pison and H. Möhwald, *Langmuir*, 2006, **22**, 2351-2357.

100. A. V. Dobrynin and M. Rubinstein, *Progress in Polymer Science*, 2005, **30**, 1049-1118.

101. X. Liu, Y. Guan, Z. Ma and H. Liu, *Langmuir*, 2004, **20**, 10278-10282.

102. L. Harris, J. Goff, A. Carmichael, J. Riffle, J. Harburn, T. St. Pierre and M. Saunders, *Chemistry of Materials*, 2003, **15**, 1367-1377.

103. A. Mukhopadhyay, N. Joshi, K. Chattopadhyay and G. De, *ACS applied materials & interfaces*, 2011, **4**, 142-149.

104. Y.-X. J. Wang, *Quantitative imaging in medicine and surgery*, 2011, **1**, 35.

105. P. G. Corrie, *Medicine*, 2008, **36**, 24-28.

106. C. Alexiou, R. J. Schmid, R. Jurgons, M. Kremer, G. Wanner, C. Bergemann, E. Huenges, T. Nawroth, W. Arnold and F. G. Parak, *European Biophysics Journal*, 2006, **35**, 446-450.

107. C. Sun, J. S. Lee and M. Zhang, *Advanced drug delivery reviews*, 2008, **60**, 1252-1265.

108. J. Dobson, *Drug development research*, 2006, **67**, 55-60.

109. O. Veiseh, J. W. Gunn and M. Zhang, *Advanced drug delivery reviews*, 2010, **62**, 284-304.

110. S. Ghosh, S. GhoshMitra, T. Cai, D. R. Diercks, N. C. Mills and D. L. Hynds, *Nanoscale research letters*, 2010, **5**, 195-204.

Chapter 3: Amide and ester initiated ATRP

3.1 Introduction

Atom transfer radical polymerisation (ATRP) has been shown to be a fantastic tool for the creation of well-defined, complex, polymer architectures from a wide array of monomer feedstocks and a large range of initiating moieties.[1-6] However, certain functional initiators have been shown to inhibit its efficacy, especially in the case of initiators containing amide bonds.[7-13] Whilst searching through the literature reveals many possible reasons behind this apparent problem, there are often cases where differing sources disagree directly with each other resulting in contradictory results.[7-11, 14-18]

The use of an amide bond within an initiator would be favourable for polymers whose application is in a biological environment due to the high bond strength when compared to the more ubiquitously used ester bond, and mimicry of peptide bonds found within living organisms. The successful use of amide bonds within a material also opens up additional synthetic routes that can be used either prior or post polymerisation that can increase functionalization beyond that which may be available to other initiating moieties.

This chapter outlines the synthesis of poly(oligo ethylene glycol) methyl ether methacrylate (POEGMA) materials by ATRP, using both a common ester containing initiator (ethyl 2-bromoisobutyrate) and an analogous amide initiator (2-bromo-2-methyl-*N*-propylpropanimde) and their subsequent characterisation by nuclear magnetic resonance spectroscopy (NMR) and size exclusion chromatography (SEC). Further to this the kinetics involved in the reaction were monitored using UV-visible spectroscopy in order to ascertain the difference in results, and the two initiators were compared using DFT modelling techniques. The reason for experimental differences between amide and ester initiators has never fully been discovered, and as such this investigation was launched to find the lack of efficacy of an amide bond. Finally, two different techniques (ARGET-ATRP and SET-LRP) were tested for the preparation of POEGMA to ascertain if they provided any benefit over conventional ATRP when using an amide initiator.

3.1.1 Poly(oligo ethylene glycol) methyl ether methacrylate (POEGMA)

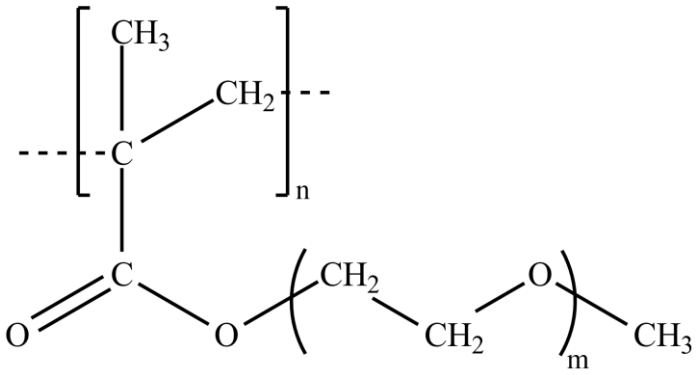

Figure 3.1 : A single OEGMA unit as part of a polymer chain. Differing molecular weights of OEGMA can be formed by varying the number of ethylene glycol units in the side chain, and the monomer is commercially available with a many different length chains. Typical values for *m* range from 4 to 32, providing a molecular weight range from 300 to 4000.

Poly(oligo ethylene glycol) methyl ether methacrylate is part of a family of polymers composed from a backbone of methyl methacrylate, each with differing numbers of ethylene glycol units found after the ester bond, as denoted by *m* in Figure 3.1 above. The applications of POEGMA have expanded greatly in the last few years, with copolymers of the material finding uses in a wide array of roles within bioengineering.[19] Two key reasons for this are that it both increases the protein resistance of materials it is applied to and that it also possesses a lower critical solution temperature (LCST). [20, 21]

The core of the "comb-like" POEGMA structure is a methyl methacrylate (MMA) backbone. Synthetically this is invaluable as MMA based polymerisations have been studied for decades using a wide range of different polymerisation mechanisms.[22-24] Specifically for ATRP, MMA was one of the first monomers investigated by both the Matyjaszewski and Sawamoto groups in the 1990s.[25, 26] Further to this, PMMA has been used extensively within the dental and medical industries due to its biocompatibility and low toxicity.[27]

By attaching polyethylene glycol (PEG) units to the side of this PMMA backbone the solubility of the polymer is dramatically improved. PMMA is insoluble in water, and even at low molecular weights will only form an emulsion. PEG on the other hand will readily dissolve in water with a solubility of around 630 mg/ml at 20 ^{o}C for polymers with a molecular weight averaging 8000.[28] The addition of this

pendant PEG chain to the MMA backbone creates a water soluble polymer with both hydrophobic and hydrophilic sections.

LCST is a reversible phenomenon that results in a polymer precipitating out of aqueous solution above a critical temperature, contrary to general practice where solubility increases as temperature rises. PEG has been shown to possess a LCST around 85 ^{o}C.[29-32] Work with poly(N-isopropylacrylamide) (PNIPAAm) has shown that the LCST of thermoresponsive polymers can be adjusted by increasing or decreasing the hydrophillicity of the polymer.[33-36] For POEGMA this can easily be carried out by changing the length of PEG chain attached to the PMMA backbone, or copolymerisation with another desired copolymer.[20]

The solubility of a system is controlled by the Gibbs energy of mixing (Gmix) and can be expressed as shown in Equation 3.1.

$$\Delta G_{mix} = \Delta H_{mix} - T\Delta S_{mix}$$

Equation 3.1

In order for spontaneous mixing to occur the Gmix must decrease, otherwise the components present will remain immiscible. Hydrogen bonding between water molecules and the hydrophilic components of the polymer can cause mixing to occur even though G_{mix} is positive, despite it being entropically unfavourable overall. Once above the LCST the material behaves as would be expected, as the additional energy within the system overcomes the relatively weak attraction from the hydrogen bonding (Figure 3.2). Various physical properties of the materials can affect the LCST, these include: the Đ, Mn, degree of branching and ratio of monomers present in copolymers.[37, 38]

Previous work by Lutz *et al.* has shown that copolymers of POEGMA and 2-(2-methoxyethoxy)ethyl methacrylate can exhibit LCSTs around 35 ^{o}C, and can be tuned to specific temperatures by adjusting the ratio of constituents.[20] This is interesting as this puts materials made of these polymers in the range of being responsive to changes within a living system.

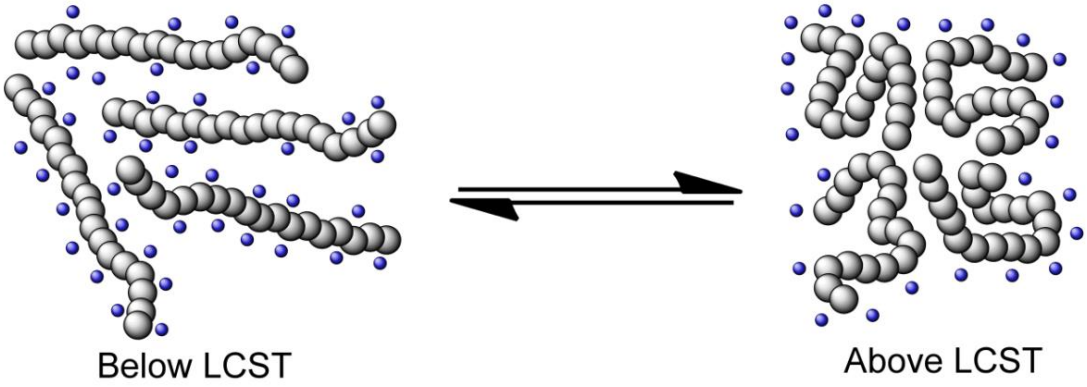

Figure 3.2 : For POEGMA in water below the LCST there is hydrogen bonding between the solvent and hydrophilic portions of the polymer. As the temperature increases above the LCST the hydrogen bonding that previously held the polymer soluble is no longer enough to keep the Gibbs free energy of the system negative. As polymers will only dissolve in a solvent when the Gibbs free energy decreases, the result is POEGMA precipitates out due to polymer chains collapsing and agglomerating into hydrophobic clusters pushing water molecules out into the bulk solvent.

The protein resistance of this material stems from the ethylene glycol structure and means antibodies *in vivo* cannot target materials coated with this polymer. This effect has been known about for decades and has been used successfully to "PEGylate" various therapeutics to increases both the bio-compatibility and bio-availability of drug release systems.[39] PEGylation is the process of attaching strands of polyethylene glycol to drugs in order to reduce renal clearance (the kidney's action of clearing waste from blood plasma) by reducing immunogenicity (the ability of a substance to provoke an immune response).[40-42]

3.1.2 Ethyl 2-bromoisobutyrate and 2-bromo-2-methyl-N-propylpropanimide

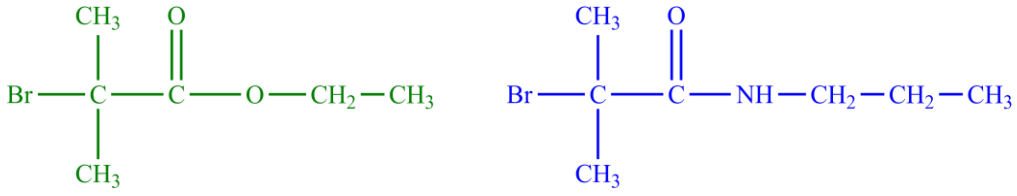

Figure 3.3 : Chemical structures of ethyl 2-bromoisobutyrate, in green, and 2-bromo-2-methyl-*N*-propylpropanimide, in blue. The amide structure is analogous to the ester, with the only difference being an additional CH_2 group following the amide bond.

Ethyl 2-bromoisobutyrate (EBriB) is a simple, cheap, initiator that has been used successfully for the ATRP of numerous monomers.[43] The terminal bromine, which acts as a leaving group to create a radical and allow polymerisation, is activated by the presence of an ester carbonyl adjacent to the α-carbon.[44] The effect of this is to delocalise the local electron cloud, enhancing the polarisation of the carbon-halide bond, and increasing the stability of the resulting radical that is formed.[44]

Matyjaszewski *et al* demonstrated using the polymerisation of MMA, that whilst EBriB has a comparatively lower reactivity than highly reactive initiators such as benzhydryl chloride, it still creates a fast rate of polymerisation, producing polymers with low dispersities and M_n close to theoretically expected (from the ratio of initiator to monomer).[44] However, where the rate of initiation in high reactivity initiators is faster than the rate of propagation of the monomer, instead of initiating radicals encountering dormant polymer chains, radical-radical recombination occurs, triggering irreversible terminations and the failure to initiate further chain growth. This in turns leads to a build-up of Cu(II) that slows down the rate of polymerisation considerably and produces low monomer conversion over comparably long periods of time. This is displayed in Scheme 3.1, where it is clear that if the rate of initiation (k_{init}) is greater than the rate of polymerisation (k_p) an excess of initiator radicals will

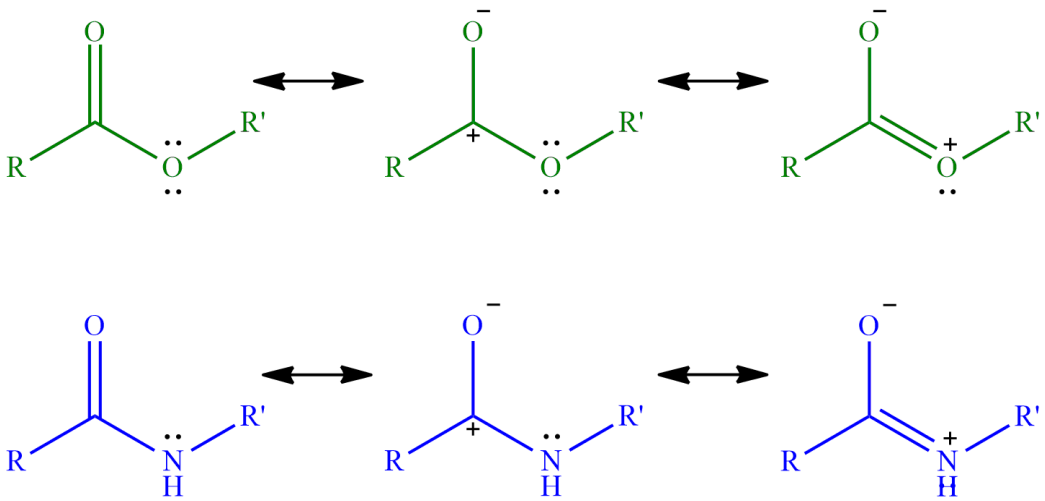

Figure 3.4 : Resonance structures for ester (green) and amide (blue) carbonyls. The delocalisation of the carbonyl electron cloud enables of the activation of halides bound to "R". It also has the effect of stabilising radical formation on "R" as the halide dissociates from the alkyl chain during polymerisation.

form, decreasing the chance of initiator and monomer interaction, and increasing the chance of termination occurring (k_t)

$$I - Br \xrightarrow{k_{init}} I\cdot + Br\cdot$$

$$P_n\cdot + M \xrightarrow{k_p} P_{n+1}\cdot$$

$$P_n\cdot + P_n\cdot \xrightarrow{k_{t1}} P_{n-n}$$

$$I\cdot + I\cdot \xrightarrow{k_{t2}} I - I$$

Scheme 3.1

The problems associated with amide based initators are well known and have been widely reported within the literature. Table 3.1 summarises some of these papers, and be can be found at the end of Section 3.1. The most common problems were poor initiator efficiencies that lead to higher than predicted molecular weights and slow polymerisations with low conversions.[9-15, 45] The efficiency of an initiator (I_{eff}) within a polymerisation can be calculated with Equation 3.2, where M_n is the observed molecular weight of a polymer, and $M_{n\ theo}$ is the theoretically calculated molecular weight derived from the masses of monomer and initator used, as well as monomer to polymer conversion.

$$I_{eff} = \frac{M_n}{M_{n\ theo}}$$

Equation 3.2

Teodorsecu *et al* initially suggested that the low conversions were not being triggered by the loss of active chains, but instead stemmed from a loss of activity in the catalytic system.[15] It was suggested that polymers produced still had end group activity, but reactions stopped due to the complete deactivation of the catalyst system.

One possible explanation for this was given by Limer *et al,* who stated that during the initial initiation step a high concentration of radicals was likely to form.[8] The result of this is radical-radical coupling and disproportionation in direct competition with the initiation and propagation of the ATRP. To control this it was suggested that lowering the temperature at the start of the reaction (to 25 ^{o}C), prior to heating to

reaction temperature (90 ^{o}C), would slow the rate of initation and this coupled with the usage of CuCl as opposed to CuBr would enable controlled polymers to be produced. This was used to synthesis polymers with molecular weights in good agreement of theoretical values and dispersites around 1.20.

Contrary to this however was the work of Adams *et al*, who found that the previously suggested method failed to produce controlled polymers when using oligopeptide-based initiators.[10] Using an initiator that was analagous to one reported by Limer *et al*, they found significant initiator remaining at the end of a reaction, and suggested that this may result from significant termination reactions in the early stages of the reaction despite attempts at thermally controlling the initiation step.

Finally, it has even been suggested that the prescence of amide bonds themselves can trigger poor polymerisation performance. Polymerisation of N,N-dimethylacrylamide using a range of initiating system all produced monomers with broad dispersities, low conversions and higher than expected molecular weights.[14, 16, 17]

Rademacher *et al* suggested that this may be due to Cu salts complexing to amide groups within the polymer chain, resulting in radical stablisation which retards the deactivations step in ATRP.[14] Without the deactivation step the rate of initiation becomes faster than propagation, and radical-radical terminations occur.

In this chapter ethyl 2-bromoisobutyrate (EBriB) will be compared with an analogous amide initiator, 2-bromo-2-methyl-*N*-propylpropanimide (MBrPA), for the ATRP of OEGMA in an effort to ascertain the reasons behind the clear differences in polymerisation rates and mechanisms at work, and to attempt to clarify the observed differences in the molecular weight parameters and physical characteristics of materials produced.

Table 3.1

Author/Date	Article Title	Amide Problem Listed	Reason Given for Problem/Possible Solution
Senoo *et al.*[17] (1999)	Living radical polymerization of N,N-dimethylacrylamide with $RuCl_2(PPh_3)$(3)-based initiating systems	Living radical polymerization of DMAA to give polymers with controlled molecular weights and [high] Đ > 1.6	Slow initiation and slow interconversion between the dormant and the radical species.
Rademacher *et al.*[14] (2000)	Atom transfer radical polymerization of N,N-dimethylacrylamide	Broad molecular weight distributions, poor agreement between theoretical and experimental M_n, [problems with] incremental monomer addition experiments and end group analysis.	Cu salts complex to the amide group of the chain ends and stabilize the radical. This stabilization retards the deactivation step in ATRP and produces an unacceptably high concentration of radicals which leads to spontaneous termination reactions.
Teodorescu *et al.*[15] (2000)	Controlled polymerization of (meth)acrylamides by atom transfer radical	The polymerization reached limited conversion, which could be enhanced by increasing the catalyst/initiator ratio.	The limited conversion is not due to the loss of the active chains, but rather to the loss of activity of the catalytic system. At this moment, it is still unclear the mechanism through which the catalyst is inactivated.

Author/Date	Article Title	Amide Problem Listed	Reason Given for Problem/Possible Solution
Neugebauer *et al.*[16] (2003)	Copolymerization of N,N-dimethylacrylamide with n-butylacrylate via atom transfer radical polymerization	Limited conversion of monomer to polymer indicating the occurrence of termination reactions or loss of the catalyst.	The limited conversion cannot be explained by a total decomposition of the growing centres, since this would provide polymers with much higher polydispersity. The lower molecular weight tailing in the GPC chromatogram suggests chain-breaking reactions
Li *et al.*[45] (2005)	Biomimetic stimulus-responsive star diblock gelators	Poor living character was achieved using an amide-based trifunctional initiator, but the analogous triester initiator gave reasonably well-defined thermo-responsive and pH-responsive star diblock copolymers.	Amide initiators have been reported to have poor efficiency, which leads to low monomer conversions and produce polymers with high polydispersities.
Limer *et al.*[8] (2006)	Amide functional initiators for transition-metal-mediated living radical polymerization	Amide-based initiators result in polymers which have a higher molecular weight than expected.	With amide initiators the initial initiation step likely occurs rapidly leading to a high concentration of free radicals, which results in radical-radical coupling/disproportionation in competition with initiation/propagation. A low temperature at the start of the reaction to 25 °C still allows initiation to proceed, but more slowly. The use of Cu(I)Cl as opposed to Cu(I)Br also reduces the rate of homolytic bond fission.

Author/Date	Article Title	Amide Problem Listed	Reason Given for Problem/Possible Solution
Adams *et al*.[10] (2009)	Oligopeptide-based amide functional initiators for ATRP	Amide-based initiators results in polymers which have a higher molecular weight than expected and a significantly higher polydispersity than those prepared from ester-based initiators.	In many cases significant initiator remains [after polymerisation], suggesting that either not all peptides successfully initiate polymerization or that significant termination reactions occur early in the reaction. This low initiator efficiency agrees with other reports for amino acid-based initiators.
Habraken *et al*.[11] (2009)	Peptide block copolymers by N-carboxyanhydride ring-opening polymerization and atom transfer radical polymerization: The effect of amide macroinitiators	ATRP macroinitiation from the polypeptides resulted in higher than expected molecular weights	Analysis of the reaction products and model reactions confirmed that this is due to the high frequency of termination reactions by disproportionation in the initial phase of the ATRP, which is inherent in the amide initiator structure.

3.2 Materials and Apparatus

3.2.1 Materials

Oligo(ethylene glycol methyl ether) methacrylate ($M_n \approx 360$, Sigma-Aldrich), triethylamine (≥99%, Sigma-Aldrich), copper (0) wire (1.0mm, 99.9%, Sigma-Aldrich), ethyl bromoisobutyrate (98%, Sigma-Aldrich) 4,4'-dinonyl-2,2'-bipyridine (97%, Sigma-Aldrich), 2,2'-bipyridine (98%, Sigma-Aldrich), copper (I) bromide (98%, Sigma-Aldrich), copper (I) chloride (99%, Sigma-Aldrich), copper (II) bromide (99%, Sigma-Aldrich), copper (II) chloride (99%, Sigma-Aldrich), propylamine (98%, Sigma-Aldrich), 2-bromo-2-methylpropanoyl bromide (98%, Sigma-Aldrich), sodium bicarbonate (analytical reagent grade, Fischer Scientific), activated charcoal (Sigma-Aldrich), aluminium oxide (activated, neutral, for column chromatography 50-200μm, Acros Organics), magnesium sulphate (97%, anhydrous, Acros Organics), methanol (analytical reagent grade, Fisher Scientific), *N,N,N',N',N''*-pentamethyldiethylenetriamine (99%, Sigma-Aldrich), *N*-Methyltrimethylacetamide (98%, Sigma-Aldrich), Ethyl trimethylacetate (99% Sigma-Aldrich), tin 2-ethylhexanoate (92.5-100%, Sigma-Aldrich), 2-propanol (HPLC grade, Fisher Scientific), toluene (laboratory grade, Fisher Scientific), diethyl ether (laboratory grade, Fisher Scientific), tetrahydrofuran (HPLC grade, Fisher Scientific), ethanol (analytical reagent grade, Fisher Scientific), and water (HPLC gradient grade, Fisher Scientific) were purchased and used without further purification. Dichloromethane (analytical reagent grade) was purchased from Fisher Scientific and immediately before use dried and distilled over calcium hydride. The deuterated solvents used for ^{13}C and ^{1}H NMR were d_1-chloroform, d_4-methanol or d_6-ethanol purchased from Cambridge Isotope Laboratories Inc. and were used as supplied.

3.2.2 Characterisation

^{1}H and ^{13}C NMR spectra were recorded using a JEOL ECS spectrometer (400 MHz) at 293 K in solutions of deuterated chloroform ($CDCl_3$), d_4-methanol or d_8-ethanol. Molecular weight parameters were recorded by size exclusion chromatography

(SEC) of THF solutions using two 5μm mixed C PLgel columns at 40°C and a Shodex RI-101 refractive index detector. The SEC system was calibrated using poly(methyl methacrylate) standards.

UV-visible spectra were recorded using either a Shimadzu UV-1800 spectrometer using quartz cuvettes with a path length of 10 mm. IR spectra were recorded using a Shimadzu IR-Affinity1 spectrometer equipped with a Golden Gate Diamond ATR.

3.3 Experimental

3.3.1 Synthesis of 2-bromo-2-methyl-*N*-propylpropanimide

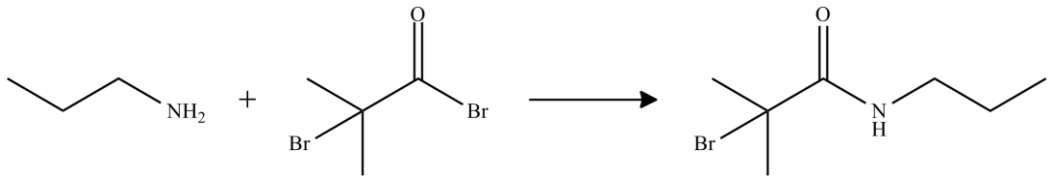

Scheme 3.2: Synthesis of 2-bromo-2-methyl-*N*-propylpropanimide (MBrPA)

In a typical synthesis: 2-bromo-2-methyl-propionyl bromide (MBrPBr) (6 g, 26.1 mmol) was dissolved in toluene (40 ml). In a second vessel, propylamine (1.54 g, 26.1 mmol) and triethylamine (0.330 g, 3.3 mmol) were dissolved in toluene (40 ml) and cooled to 0 °C in an ice bath. The solution of MBrPBr was added dropwise to the pre-chilled solution, and the resultant cloudy mixture was left stirring at 0 °C for three hours, then at room temperature for a further 10 hours. The completed reaction was passed through filter paper to remove any salts and then evaporated under reduced pressure to leave a viscous brown liquid. Pure MBrPA was recovered by redissolving the liquid in 40 ml of diethyl ether prior to passing it through a short alumina column. This solution was then washed five times against a 10% saturated solution of aqueous sodium hydrogen carbonate then left stirring overnight with 5 g of activated carbon and 5 g of anhydrous magnesium sulphate prior to filtration. The final product was collected under reduced pressure to yield a yellow liquid (58% yield) prior to analysis by NMR and FTIR.

^{1}H NMR δ_H(400 MHz; $CDCl_3$; ppm) 0.95 (3H, t, J=7.53, -CH_2-*CH_3*), 1.6 (2H, m, J=7.29, -CH_2-*CH_2*-CH_3), 1.95 (6H, s, (*CH_3*)$_2$C-) 3.25 (2H, q, J=6.92,5.93, NH-*CH_2*-CH_2-), 6.7 (1H, br s, *NH*)

^{13}C NMR δ_C(100 MHz; $CDCl_3$; ppm) 11 (-CH_2-*CH_3*), 23 (-CH_2-*CH_2*-CH_3), 34 ((*CH_3*)$_2$C-), 42 (NH-*CH_2*-CH_2-)

FTIR (ν_{max}/cm^{-1}) 3350s (NH) , 2940s (CH), 1740 (CO), 1460s (CH), 1370s (CH), 510w (CBr).

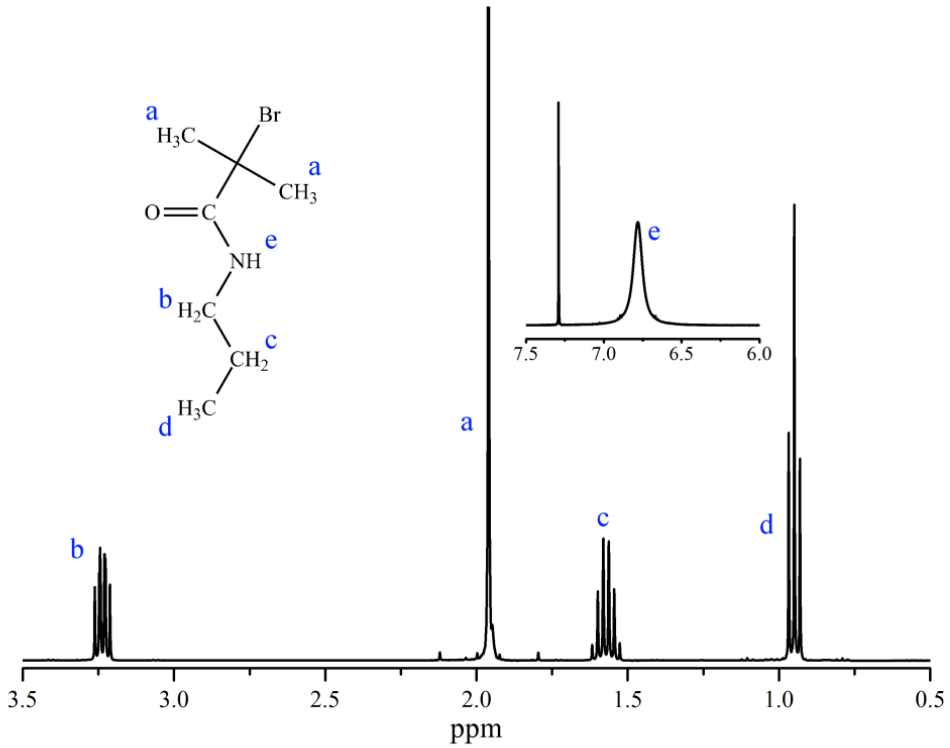

Figure 3.5 : ^{1}H NMR spectra of 2-bromo-2-methyl-*N*-propylpropanimide (amide initiator synthesised for ATRP), with proton signal assignments made corresponding to the structure displayed inset.

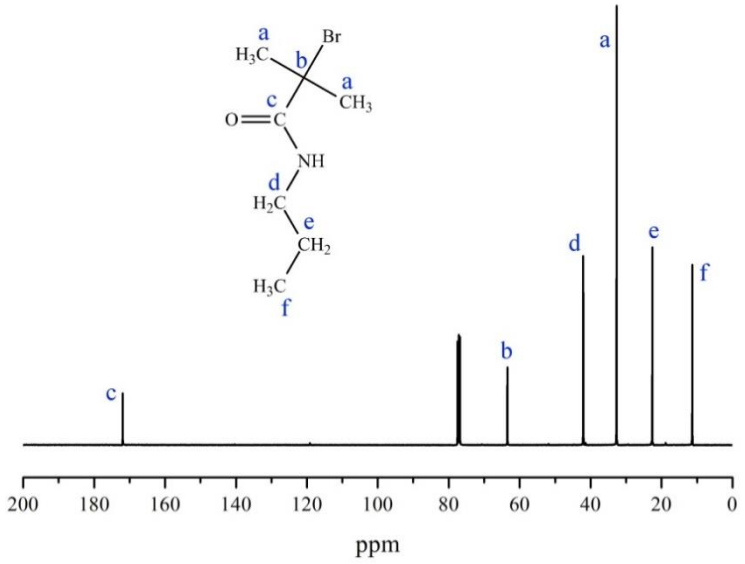

Figure 3.6 : ^{13}C NMR spectra of 2-bromo-2-methyl-*N*-propylpropanimide (amide initiator synthesised for ATRP), with carbon signal assignments made corresponding to the structure displayed inset.

3.3.2 Synthesis of POEGMA by ATRP

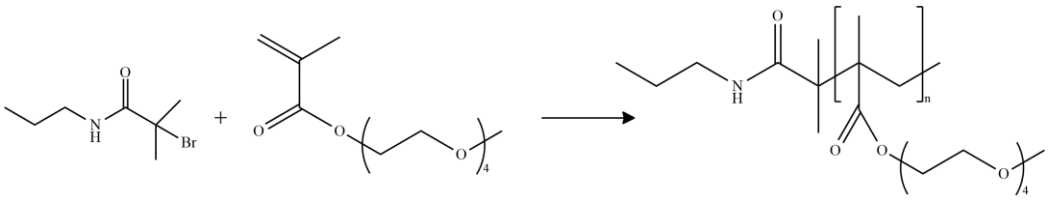

Scheme 3.3 : MBrPA as an ATRP initiator for OEGMA

A typical synthesis was as follows: A Schlenk tube containing OEGMA (M_n 300, 5 g, 18.1 mmol), CuCl (0.036 g, 0.362 mmol), 4,4'-dinonyl-2,2'-bipyridine (dNBpy) (0.2959 g, 0.724 mmol) and ethanol (15 ml) was sealed and degassed with nitrogen for 45 minutes. MBrPA (0.0507 mL, 0.362 mmol) or EBriB (0.053 mL, 0.362 mmol) was injected via gastight syringe and then left stirring at room temperature for 15 hours. 1mL samples were removed via syringe, exposed to air and then passed through a short alumina column to remove the catalytic system before being dried to

remove reaction solvent. They were then separately diluted in tetrahydrofuran (THF) for SEC, and $CDCl_3$ for NMR. At the end of polymerisation the full reaction was exposed to air then diluted with THF (40 mL), whereupon the reaction mixture turned from dark brown to green, and then passed through an alumina column to remove the catalytic system. The combined solution was added dropwise to an excess of cold, stirring hexane. The product precipitated as a clear viscous liquid and was collected by centrifuge prior to drying overnight under vacuum at 35 ^{o}C prior to SEC and NMR analysis.

The quantities of reactants, initiator, catalyst, solvent, and details of the products can be found in Tables: 3.2 – 3.5 in Section 3.4.2.

^{1}H NMR δ_H(400 MHz; $CDCl_3$; ppm) 0.8-1.1 (3H, br, -CH_2-C-*CH_3*), 1.7-2.0 (2H, br, CH_3-C-*CH_2*-), 3.1 (3H, br, CH_2-O-*CH_3*), 3.3-3.8 (4H, br, O-*CH_2*-*CH_2*-O), 4.1 (2H, br, C(=O)-O-*CH_2*)

^{13}C NMR δ_C(100 MHz; $CDCl_3$; ppm) 24-27 (CH_2-C-*CH_3*), 31-34 (CH_3-C-*CH_2*-), 57-60 (CH_3-*C*-CH_2-)/(CH_2-O-*CH_3*), 66-69 (O-*CH_2*-*CH_2*-O), 177-179 (*C*=*O*)

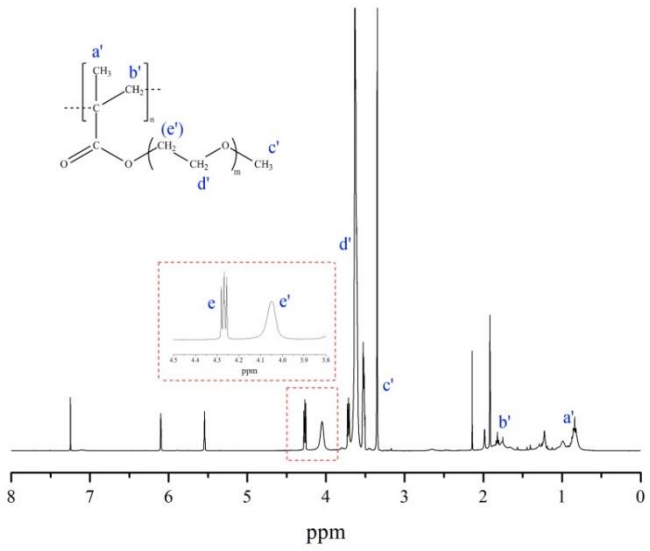

Figure 3.7 : ^{1}H NMR spectra of a MBrPA initiated POEGMA reaction mixture, with proton signal assignments made corresponding to the structure displayed inset. The ratio of proton e (monomer) to e' (polymer) was used to calculate monomer conversion. e' is specific to the first CH_2 group following the ester moiety in the side chain of POEGMA.

3.3.4 Synthesis of POEGMA by ARGET-ATRP

A typical synthesis was as follows: A Schlenk tube containing OEGMA (M_n 300, 4 g, 14.49 mmol), *N*,*N*,*N*′,*N*′,*N*′′-pentamethyldiethylenetriamine (PMDETA) (0.076 ml, 3.62 mmol), water (15 ml), $CuBr_2$ (0.0323 g, 0.145 mmol) and MBrPA (0.0507 mL, 0.362 mmol), was sealed and degassed with nitrogen for 45 minutes. Tin 2-ethylhexanoate ($Sn(EH)_2$) (0.0217 ml, 0.66 mmol) was injected via gastight syringe and then left stirring at room temperature for 20 hours. 1mL samples were removed via syringe, exposed to air and then passed through a short alumina column to remove the catalytic system before being dried to remove reaction solvent. They were then separately diluted in tetrahydrofuran (THF) for SEC, and $CDCl_3$ for NMR, although no successful polymerisation occurred (Table 3.8 in Section 3.4.3.1).

3.3.5 Synthesis of POEGMA by SET-LRP

A typical synthesis was as follows: A Schlenk tube containing OEGMA (M_n 300, 5 g, 18.1 mmol), *N*,*N*,*N*′,*N*′,*N*′′-pentamethyldiethylenetriamine (PMDETA) (0.076 ml, 3.62 mmol), MBrPA (0.0507 mL, 0.362 mmol), ethanol (15 ml), $CuBr_2$ (0.0081g, 0.06 mmol) and a magnetic stirring bar wrapped in copper wire held above the mixture, was sealed and degassed with nitrogen for 45 minutes. The reaction was initiated by lowering the copper wire into the reaction mixture below. 1mL samples were removed via syringe, exposed to air and then passed through a short alumina column to remove the catalytic system before being dried to remove reaction solvent. They were then separately diluted in tetrahydrofuran (THF) for SEC, and $CDCl_3$ for NMR. At the end of polymerisation the full reaction was exposed to air then diluted with THF (40 mL), whereupon the reaction mixture turned from dark brown to green, and then passed through an alumina column to remove the catalytic system. The combined solution was added dropwise to an excess of cold, stirring hexane. The product precipitated as a clear viscous liquid and was collected by centrifuge prior to drying overnight under vacuum at 35 ^{o}C prior to SEC and NMR analysis.
Results of these reactions can be found in Table 3.9 in Section 3.4.3.2.

^{1}H NMR δ_H(400 MHz; $CDCl_3$; ppm) 0.8-1.1 (3H, br, -CH_2-C-*CH_3*), 1.7-2.0 (2H, br, CH_3-C-*CH_2*-), 3.1 (3H, br, CH_2-O-*CH_3*), 3.3-3.8 (4H, br, O-*CH_2*-*CH_2*-O), 4.1 (2H, br, C(=O)-O-*CH_2*)

^{13}C NMR δ_C(100 MHz; $CDCl_3$; ppm) 24-27 (CH_2-C-*CH_3*), 31-34 (CH_3-C-*CH_2*-), 57-60 (CH_3-*C*-CH_2-)/(CH_2-O-*CH_3*), 66-69 (O-*CH_2*-*CH_2*-O), 177-179 (*C=O*)

3.3.6 UV-visible analysis

CuCl (4.14 mg, 0.042 mmol) or $CuCl_2$ (5.61 mg, 0.042 mmol) was placed in a quartz UV-VIS cell (1 cm path length) and purged with N_2. To the cell was added 3 mL of a degassed stock solution of 4,4'-dinonyl-2,2'-bipyridine (dNBpy) in ethanol (1.98 mg/mL, 0.0048 mmol/mL). The cell was sealed under nitrogen via a rubber septum. EBriB (0.006 mL, 0.042 mmol) or MBrPA (0.006 mL, 0.042 mmol) was injected into the cell through the septum via gas tight syringe. After vigorous shaking the cell was placed in the UV-VIS spectrometer for measurement. Measurements were taken every five minutes for a total of 50 minutes. In the case of the amide analogue, *N*-methyltrimethylacetamide (3.07 mg, 0.042 mmol) was added prior to the cell being sealed and degassed with nitrogen as normal.

3.3.7 Chemical modelling

Chemical modelling was carried out by Dr. Simon Holder at the University of Kent. Initial molecular conformations were assessed and minimised using the semi-empirical PM6 method through the CS MOPAC interface in ChemBio3D Ultra version 12.0.2 (Cambridgesoft).[46] All density functional theory (DFT) calculations were run using the GAMESS-US code version 11 (R1).[47] All minimum energy confirmations and frequencies were determined at the B3-LYP/6-31+G(d) level of theory at 298.15K.[48, 49] Single-point energy calculations were conducted with the BMK,[50] M06-2X[51] and B2GP-PLYP[52] functionals using the augmented triple-ξ Dunning aug-cc-pVTZ basis set[53] and unrestricted wave functions. DFT-D3 dispersion corrections were utilised in all cases;[54, 55] with additional parameters for the D3 corrections taken from the literature.[56, 57] Calculations in solvents were

performed using the conductor-like polarisable continuum model (C-PCM) combined with the universal solvation model (SMD) of Truhlar *et al*.[58]

3.4 Results

3.4.1 Synthesis of 2-bromo-2-methyl-*N*-propylpropanimide (MBrPA)

The synthesis of 2-bromo-2-methyl-*N*-propylpropanimide (MBrPA) was accomplished through the nucleophilic addition/elimination (S_N2) reaction of propylamine and 2-bromo-2-methyl-propionyl bromide (MBrPBr). Mechanistically this occurs through the nucleophilic attack of the carbonyl atom in MBrPBr by the lone pair of electrons on the nitrogen in the propylamine. The attack is specific to the bromine adjacent to the carbonyl due to the relative positivity of the carbonyl resulting from the C=O bond. The elimination reaction occurs with the ejection of a Br^- atom as the carbonyl bond reforms, which then causes the removal of a proton from the nitrogen, completing the formation of an amide bond.

This mechanism is well known, and was experimentally facile to perform; initially producing a dark brown liquid once solvent had been removed following the reaction and prior to any purification. Following purification steps (addition of activated

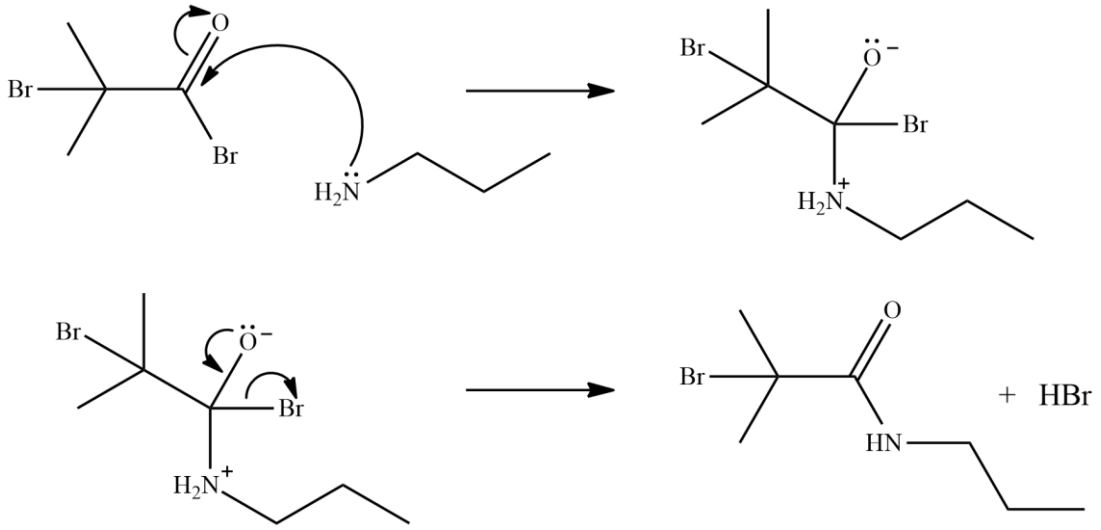

Scheme 3.4 : The mechanism for the synthesis of MBrPA as a result of a nucleophilic attack/elimination reaction.

carbon) the final product was recovered as a yellow liquid which showed a clean spectrum in ^{1}HNMR (Figure 3.5).

The ATRP of OEGMA was attempted using MBrPA as initiator, as will be discussed in Section 3.4.2, but early reactions had variable success rates leading to further investigation into the synthesis of the initiator. On close inspection of a new ^{1}HNMR spectrum of MBrPA, an additional signal at 1.9 ppm (2(CH_3)) was observed. The noticeable change in the signal relating to the dimethyl groups adjacent to ATRP initiation site, with no clear difference across the rest of the spectrum, strongly suggests the loss of the Br atom. This would account for some of the issues with ATRP reactions using the initially synthesised MBrPA, as with some initiator molecules lacking the Br atom they would not be able to participate in any polymerisations.

MBrPA was purified through sequential washings with sodium hydrogen carbonate, and following drying with anhydrous magnesium sulphate, filtration, and recollection, new ^{1}H and ^{13}C NMR spectra showed no sign of impurities. Previously MBrPA had been stored at room temperature in colourless glass sample jars, but the storage method was changed to keep it at low temperature (4 ºC), whilst wrapping the sample jar in foil to minimise UV exposure. ^{1}HNMR spectra were produced monthly following the introduction of these measures and showed no further sign of degradation.

3.4.2 Amide vs ester polymerisations by ATRP

The successful ATRP of OEGMA has previously been demonstrated in a range of solvents including water, methanol (MeOH), ethanol (EtOH), acetonitrile (MeCN), isopropanol (IPA), dimethyl sulfoxide (DMSO) and *N*,*N*-dimethylformamide (DMF).[6] Previous work within the group demonstrated that a 7:3 mix of IPA and water enabled the synthesis of well controlled POEGMA using ethyl 2-bromoisobutyrate (EBriB) as an initiator, so this was the solvent system first attempted with the ATRP of OEGMA using 2-bromo-2-methyl-*N*-propylpropanimde (MBrPA). All reactions proved unsuccessful, resulting in trial polymerisations using a range of solvents and the results of these experiments are displayed in Table 3.2.

Whilst the polymerisations initiated by EBriB (E1-3) were carried out successfully in all three solvent systems, the MBrPA initiated reactions (A1-5) were not as successful. Several attempts were made to carry out a polymerisation of OEGMA using MBrPA in the IPA/water (7:3) mixture, but the polymerisation solution invariably changed from a brown colour to green after 2-3 hours (A1 and A2, as well as others not listed). CuBr complexed to bipyridine (Bpy) in solution possesses a brown colouration, whilst $CuBr_2$ has a green hue. The colour of the solution changing to green could have been a result of the persistent radical effect (PRE), as $CuBr_2$ is generated at initiation, but the failure to synthesise any polymer suggests that the catalytic system was irreversibly deactivating in the IPA/water mixed solvent system.[59]

The polymerisations run in pure IPA (E2, A3, and A4) sometimes produced polymers; but they possessed drastically different degrees of success. E2 shows a low dispersity (1.19) and experimental molecular weight values in close agreement

Table 3.2: Amide and ester polymerisation using CuBr/Bpy catalyst system in a 1:2 ratio and 2:1 solvent to monomer ratio with varying solvents.

Sample ID	I	Solvent	Time (hrs)	$M_{n\,(exp)}$	$M_{n\,(theo)}$ [a]	Đ	Conv. (%) [b]
E1	Ester	IPA/water	12	11850	12150	1.17	87
E2	Ester	IPA	20	22700	21900	1.19	73
E3	Ester	EtOH	24	25300	26400	1.21	88
A1	Amide	IPA/water	24	n/a	n/a	n/a	n/a
A2	Amide	IPA/water	48	n/a	n/a	n/a	n/a
A3	Amide	IPA	48	8300	5250	1.56	35
A4	Amide	IPA	48	n/a	n/a	n/a	n/a
A5	Amide	EtOH	35	5520	3000	1.49	20
A6	Amide	EtOH	48	6130	5700	1.39	38

[a] $M_{n(theo)}$ was calculated by : [M]/[I] x $M_{n(0)}$ x % conversion.
[b] Conversion calculated by ^{1}H NMR

with theoretical values, as would be expected in a living polymerisation. A3 on the other hand only proceeded to 35% conversion after twice the time as E2, and produced a polymer with a broad dispersity, and a higher molecular weight than expected and A4 failed to polymerise.

Samples A5 and A6 were polymers produced using ethanol as solvent, and again the materials prepared were indicative of a lack of control within the polymerisation. Ethanol solvated reactions were however more successful overall, regardless of the quality of the materials produced, and generally proceeded to produce polymers instead of terminating before a polymerisation could take place.

It has previously been demonstrated that the solvent chosen for the ATRP of OEGMA can have a drastic effect over the level of control in the reaction.[6] Bergenudd *et al* carried out the ATRP of OEGMA, using CuBr/Bpy as the catalyst system, in a range of solvents including: water, IPA, DMSO and MeCN, and found that there was a rough correlation between the level of control in a reaction and the polarity of the solvent, with lower polarity solvents providing higher degrees of control.[6] Whilst IPA has a slightly lower relative polarity (0.617) when compared to EtOH (0.654) suggesting it would provide more control, it was decided to use EtOH as the solvent in subsequent ATRPs due to the increased success rate of EtOH solvated polymerisations.

The ligand used in the catalytic system is also known to affect the activation rate constant in ATRP.[60] Initial polymerisations were carried out using CuBr and bipyridine as a catalyst, as in many of the early ATRP systems.[5, 61] Whilst this produced good polymers for the ester initiated reactions with $M_{n(exp)}$ in close agreement to $M_{n(theo)}$, low dispersities, high conversions and an initiator efficiency close to 1, the amide initiated reactions took up to three times as long to create polymers with high dispersities and very low conversions. Further to this, molecular weights were much higher than anticipated in the MBrPA initiated polymerisations resulting from the poor initiator efficiency of the amide system. The results of some of these polymerisations are shown in Table 3.3.

As had been previously observed in the various solvent trial polymerisations, EBriB initiated polymerisations (E4-6) again showed high levels of control, even when targeting different degrees of polymerisation (50 for E4, 100 for E5 and E6). Samples A8-11 show results that are in close agreement with those previously

Table 3.3: Amide and ester polymerisation using CuBr/Bpy catalyst system in a 1:2 ratio and 2:1 solvent to monomer ratio.

Sample ID	I	[M]:[I]	Time (hrs)	$M_{n\ (exp)}$	$M_{n\ (theo)}$ [a]	Đ	Conv. (%) [b]	I_{eff} [c]
E4	Ester	50	24	11900	12150	1.31	81	1.02
E5	Ester	100	20	22700	23700	1.22	79	1.04
E6	Ester	100	24	23950	25200	1.29	84	1.05
A7	Amide	50	24	n/a	n/a	n/a	n/a	n/a
A8	Amide	50	34	2750	4050	1.3	27	1.47
A9	Amide	50	42	4300	3150	1.66	21	0.73
A10	Amide	50	48	6520	3600	1.45	24	0.55
A11	Amide	50	72	7130	4800	1.37	32	0.67

[a] $M_{n(theo)}$ was calculated by : [M]/[I] x $M_{n(0)}$ x % conversion.
[b] Conversion calculated by ^{1}H NMR
[c] Initiator efficiency calculated by: $M_{n(exp)}$ / $M_{n(th)}$

reported in the literature, with very low monomer to polymer conversions, high dispersities, and poor $M_{n(exp)}$ to $M_{n(theo)}$ agreement.[8, 10, 16] The reliability of the polymerisation in EtOH was again shown to be improved, with only one out of five experiments failing to react, as displayed with sample A7.

The literature suggested that changing to a system utilizing CuCl and dNBpy could help, as the catalyst may both improve the rate of polymerisation (as the k_{atrp} associated with dNBpy is higher than bpy) and also improve control over materials produced.[8, 62, 63] The results of these reactions are presented in Table 3.4 on the following page. The effect of using CuCl instead of CuBr is to reduce the relative rate of propagation of growing polymer chains in comparison to the initiating species.[64-67] This causes more control over the growing chains within the system, lowering dispersity and bringing molecular weights closer to those predicted ($M_{n(theo)}$). This is triggered by the higher bond dissociation energy of chlorine, slowing the rate of polymerisation.

Table 3.4 : Amide and ester polymerisation using CuCl/dNBpy catalyst system in a 1:2 ratio and 2:1 solvent to monomer ratio.

Sample ID	I	[M]/[I]	Time (hrs)	$M_{n\ (exp)}$	$M_{n\ (theo)}$ [a]	Đ	Conv. (%)[b]	[c]I_{eff}
E7	Ester	50	24	11100	11400	1.26	76	1.02
A12	Amide	50	20	19843	6000	1.31	40	0.30
A13	Amide	50	21	19288	8322	1.18	55	0.43
A14	Amide	50	28	20079	7950	1.33	53	0.40
A15	Amide	50	36	22067	7800	1.21	52	0.35
A16	Amide	50	36	18627	8904	1.18	59	0.48
A17	Amide	50	48	21749	11034	1.23	74	0.51
A18	Amide	50	70	18540	6900	1.29	46	0.37

[a]$M_{n(theo)}$ was calculated by : [M]/[I] x $M_{n(0)}$ x % conversion.
[b]Conversion calculated by ^{1}H NMR
[c]Initiator efficiency calculated by: $M_{n(exp)}$ / $M_{n(th)}$

The data shows that the system had been improved in some regards, with amide initiated polymerisations (A12-18) producing polymers with much higher molecular weights than observed in previous experiments. Whilst there was little difference within the results of an EBriB initiated system (E7 compared to E4-6), the majority of MBrPA reactions proceeded to >50% conversion. Whilst CuCl has a higher bond dissociation energy than CuBr, the increase of k_{act} resulting from the change of ligand was enough to offset any detrimental effect this would have on the overall reaction.[68] Amide initiated materials were still not as close to their theoretical molecular weights as the esters, generally still being double or more than the theoretical value, and initiator efficiencies dropped from around 60% to 30-50%, mirroring results that have previously been obtained in the literature.[8, 10, 14, 18]

In an effort to fully optimize the system the ratios of reagents were varied and further polymerisations carried out with the results displayed in Table 3.5. By increasing the ratio of solvent to monomer in the system further control was obtained over the system as the chance of any active radical meeting a dormant chain was again reduced.[6]

Table 3.5: Amide and ester optimization polymerisations using CuCl/dNBpy catalyst system and a 3:1 solvent to monomer ratio.

Sample ID	I	[M]/[I]	Time (hrs)	$M_{n\ (exp)}$	$M_{n\ (theo)}$[a]	Đ	Conv. (%)[b]	[c]I_{eff}
E8	Ester	50	20	12600	12000	1.17	80	0.95
E9	Ester	50	24	14877	13950	1.3	93	0.94
A19	Amide	50	48	13632	9410	1.26	63	0.69
A20	Amide	50	66	12390	9810	1.13	65	0.79
A21	Amide	50	70	19025	9600	1.19	64	0.50
A22	Amide	50	72	20780	9150	1.2	61	0.44
A23[d]	Amide	50	24	11730	6000	1.14	40	0.51
A24[d]	Amide	50	70	15240	5280	1.23	35	0.35

[a]$M_{n(theo)}$ was calculated by : [M]/[I] x $M_{n(0)}$ x % conversion.
[b]Conversion calculated by ^{1}H NMR
[c]Initiator efficiency calculated by: $M_{n(exp)}$ / $M_{n(th)}$
[d]Ligand to copper ratio 1:1

The ratio of ligand to copper was also varied in a pair of experiments (A23 and A24); however the results showed a much lower monomer conversion than with the otherwise identical experimental systems. This is to be expected as with half as many ligands for complexing much of the CuCl will not be dissolved due to its low solubility in polar solvents, meaning even fewer radicals are present and able to propagate the reaction.

The optimized system of 3:1 EtOH to monomer and 2:1 dNBpy to CuCl as catalyst system was then utilised as part of a sampled reaction in order to monitor the livingness of the system. Pseudo first order kinetic plots of both an amide and ester initiated reaction were produced from the data collected, and are displayed in Figures 3.8 and 3.9 on the following page. In a fully "living" reaction it is expected that both molecular weight against conversion, and $\ln(M_0/M)$ over time will produce a linear series of data points. As expected, the ester initiated reaction displays strongly living characteristics, with a decent linear fit on the pseudo first order plot (Figure 3.8). The start of the amide polymerisation appears to possess living characteristics, but after 20 hours the plot becomes non-linear. This plateauing has been explained in

the literature by the loss of the catalytic system by irreversible oxidation, causing termination of

propagating polymer chains.[69] Even within the system optimized for the ATRP of OEGMA using an amide initiator the ester initiated polymerisation occurs at a much faster rate than the amide. Polymers of a similar molecular weight were produced in

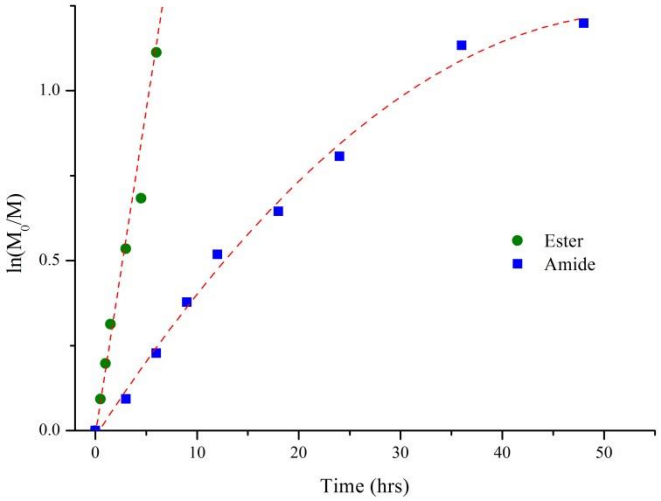

Figure 3.8 : Pseudo first order plot displaying $\ln(M_0/M)$ over time during the ATRP of OEGMA using an EBriB (green) and MBrPA (blue) as initiators and the optimized reaction system developed for amide initiators.

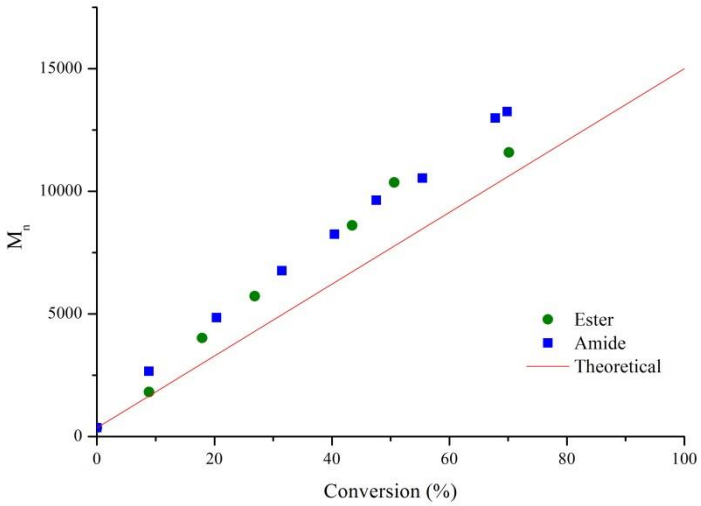

Figure 3.9 : A plot displaying molecular weight of POEGMA over time during the ATRP of OEGMA using an EBriB (green) and MBrPA (blue) as initiators and the optimized reaction system developed for amide initiators. The red line indicates the theoretical value expected in an ideal system.

6 and 48 hours by the ester and amide respectively, meaning that the rate of polymerisation of for EBriB is around 8 times faster than MBrPA.

3.4.2.1 UV-visible analysis of amide and ester initiators

The rate at which both initiators produce radicals was monitored by UV-visible spectroscopy where the main peak at 440 nm corresponds to Cu(I)Cl and as radicals are produced absorption decreases as Cu(I) is converted into Cu(II), in line with the processes occurring in Equation 3.3.

$$CuCl + R-Cl \xrightarrow{k_{act}} CuCl_2 + R\cdot$$

$$R\cdot + R\cdot \xrightarrow{k_t} R-R$$

Equation 3.3

A typical spectra series is displayed in Figure 3.10, clearly showing the drop in absorption at 440 nm. Correspondingly, at 740nm a peak is expected to appear as a result of the creation of Cu(II)Cl_2 (as has been shown in the literature).[70, 71]

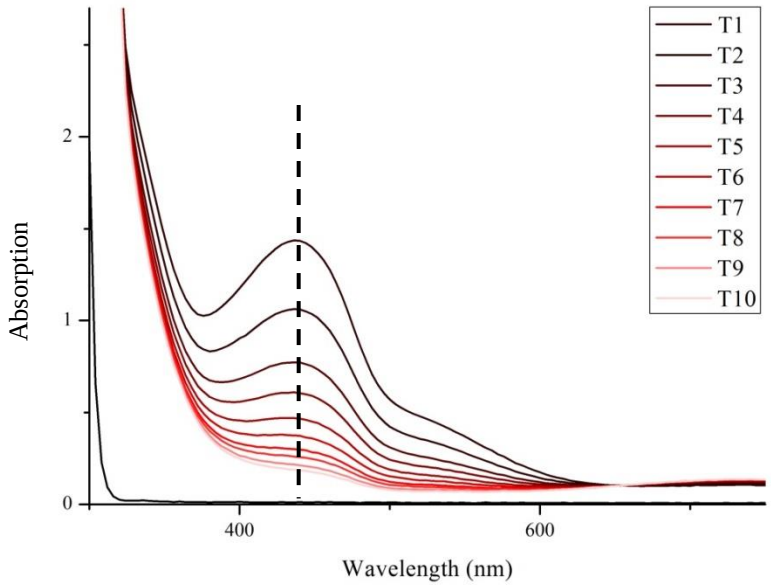

Figure 3.10 : Plot of UV-visible spectra produced by the addition of EBriB to a solution of CuCl complexed by dNBpy in ethanol. The dotted line is centred on the peak assigned decline of Cu(I) in the solution (440 nm).

This was achieved experimentally by placing CuCl, dNBpy, and EtOH in a quartz cuvette and then adding either the amide or ester initiators (the full procedure is explained in Section 3.3.3). UV spectra were recorded every 5 minutes, for a total of 50 minutes, with each individual experiment being repeated 3 times.

The plot of the data derived from the λ_{max} of the spectra is displayed in Figure 3.11, but it was impossible to elucidate a difference between the two initiators from this data, but when a first order plot is constructed (Figure 3.12), it is clear that the ester initiator is producing radicals (CuCl peak decaying) faster than the amide initiator. This implies that the rate of activation for the ester is higher than the amide, or:

$$k_{act(ester)} > k_{act(amide)}$$

Equation 3.4

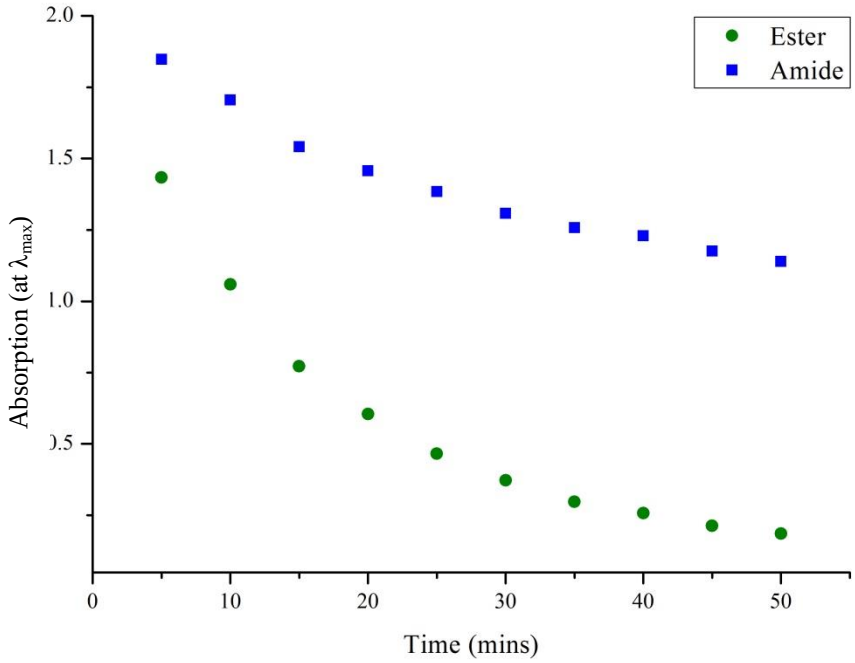

Figure 3.11: Plot of absolute data points at 440 nm derived from UV-visible spectra of ATRP initiators in a CuCl/dNBpy solution.

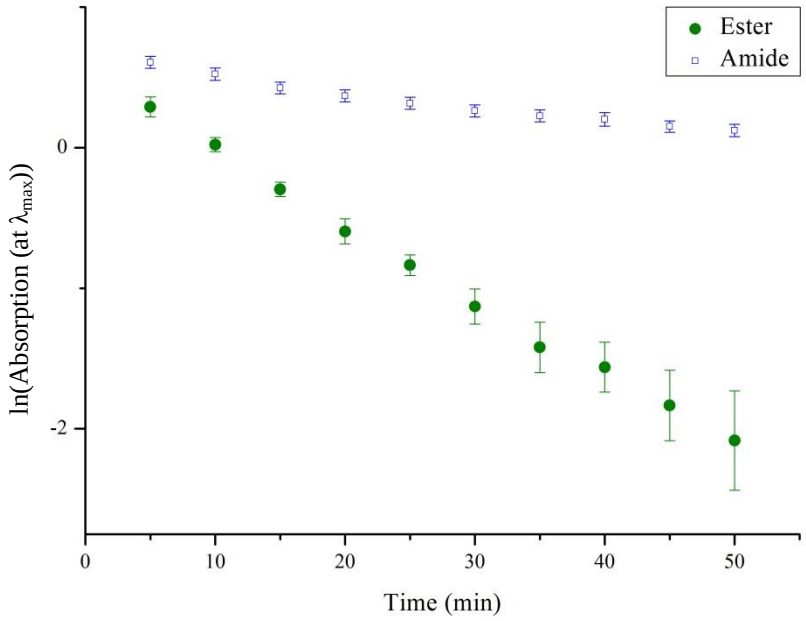

Figure 3.12: A plot displaying ln(absorbance at 440 nm) against time for amide and ester initiators. MBrPA (blue) clearly displays a shallower gradient than EBriB, indicating that the rate of activation for the ester is higher.

One explanation given for this effect in the literature is a complexation between the N-H bond in amide initiators, and copper catalyst present in the system.[18] This can be tested simply by placing CuCl in the presence of an amide bond without any other ligand. CuCl is insoluble in polar solvents, so any solvation of the metal halide must be the result of complexation with the amide bond. *N*-methyltrimethylacetamide (MTMEA) was used as for the study, as it is analogous to the amide initiator but without a bromine atom which would initiate a reaction. This was compared against a solution of CuCl in ethanol alone, and also a solution of CuCl, dNBpy and ethanol

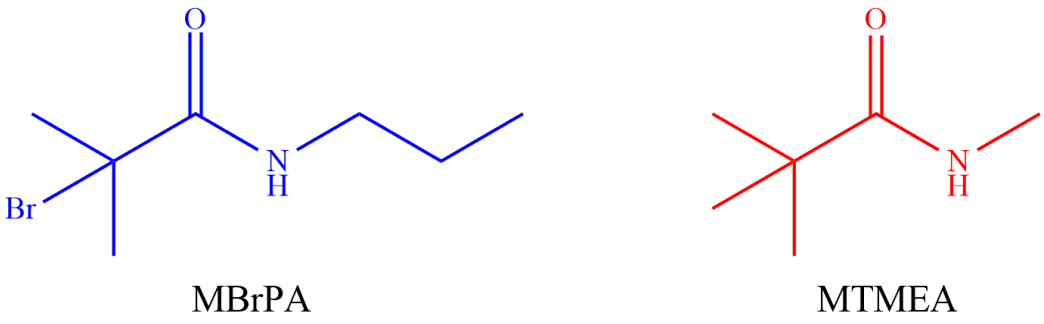

Figure 3.13: Structure of MBrPA (blue), and *N*-methyltrimethylacetamide (MTMEA, red). The structure of MTMEA is roughly analogous to MBrPA, but does not contain a bromine atom.

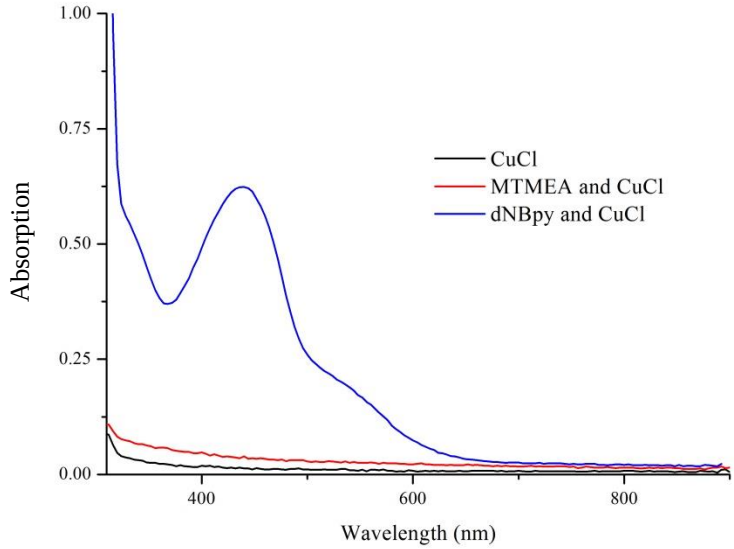

Figure 3.14 : UV-VIS data for: CuCl and only ethanol (black), CuCl with dNBpy in ethanol (red), and CuCl with MTMEA in ethanol (blue).

(Figure 3.14). Without any additives CuCl is insoluble in the solvent, and with a good ligand (dNBpy) the absorption value at 440 nm rises to 0.7-0.8. MTMEA has negligible effect, with the copper halide remaining insoluble, clearly showing that MTMEA, and by inference the amide bond within it, does not complex with CuCl. Another reason given within the literature for the ineffectiveness of amide initiators is that the amide bond can somehow interrupt the catalytic process simply by being present;[14] as such, any reaction with an amide present would be impaired. Again this is experimentally simple to test by adding MTMEA to an ester initiated kinetic study. As a control, an ester analogue (ethyl trimethylacetate, ETMEA) was

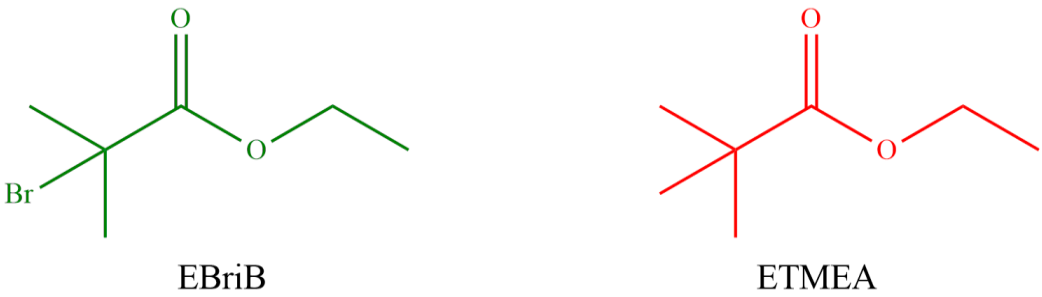

Figure 3.15: Structure of EBriB (green), and Ethyl trimethylacetate (ETMEA, red).

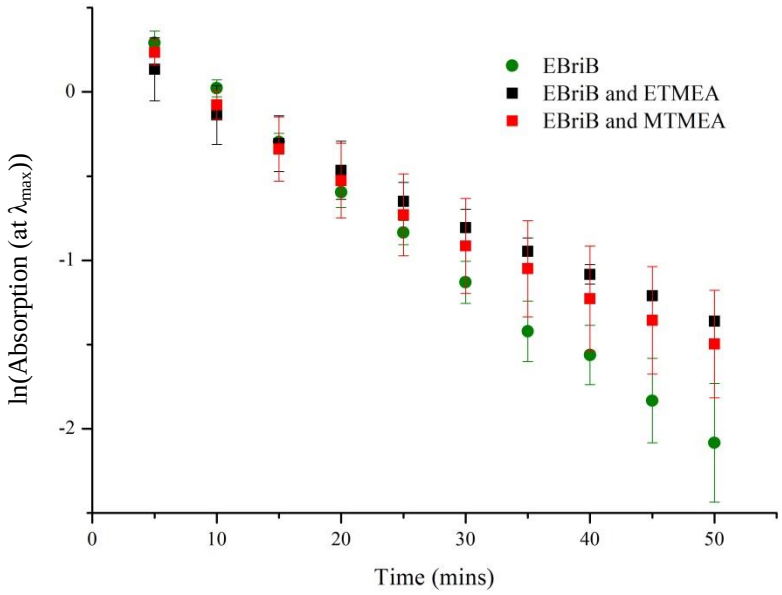

Figure 3.16: First order plot UV-visible data at 440nm corresponding to using the ester initiator (green), the ester initiator with ETMEA (black) and the ester initiator with MTMEA (red).

also added to an identical reaction, the results of these experiments are displayed in Figure 3.16. The original data for EBriB from Figure 3.11 is shown as a reference for the rate of radical formation. Clearly, both the ETMEA and MTMEA have a detrimental effect on the rate at which absorption decays, as displayed by the shallower gradient on both of their plots. However, the amount by which the decay is diminished was very similar whether it was an unreactive ester (ETMEA) or an unreactive amide (MTMEA) moiety added to the system. This is suggestive that it is merely the presence of additional molecules within the solutions causing the effect, not specifically the amide.

A further explanation for the lower amide activity could be that the amide initiator speeds up the rate of disproportionation of CuCl, to create Cu(0) and $CuCl_2$, similar to the effect that is proposed to be occurring within a single electron transfer living radical polymerisation (SET-LRP).[9, 72]

$$2Cu(I)X \xrightarrow{k_{dis}} Cu(0) + Cu(II)X_2$$

Equation 3.5

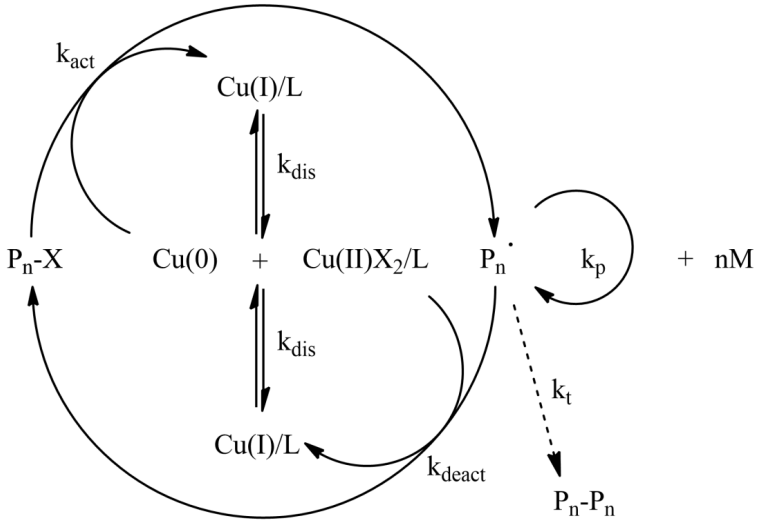

Scheme 1.14 : The proposed mechanism for SET-LRP. The disproportionation of Cu(I) occurs spontaneously within the solution providing Cu(0) species to activate the alkyl halide and allow polymerisation.

Within a SET-LRP reaction it is proposed that Cu(0) activates the alkyl halide to produce a radical, instead of the Cu(I) species as in a conventional ATRP. The Cu(0) is rapidly created *in situ* by the disproportionation of Cu(I)Cl to $Cu(II)Cl_2$ and Cu(0).[73] The advantage of this mechanism is that the spontaneous generation of $Cu(II)Cl_2$ (propagating chain deactivators) enables an increased level of control within the system as the persistent radical effect (PRE) is bypassed.[74] In a conventional ATRP $Cu(II)Cl_2$ would not be present in the reaction at initiation, but early stage bimolecular terminations of propagating chains lead to a build-up of "persistent" $Cu(II)Cl_2$ which proceeds to mediate the rest of the polymerisation.[59] SET-LRP avoids these early termination reactions by generating the mediating Cu(II) species at reaction onset. It has previously been shown that the solvent choice for the reaction has a large effect over whether SET-LRP occurs.[74] Percec *et al* demonstrated that the polymerisation of methyl acrylate in DMSO possessed characteristics of SET-LRP (>98% polymer bromine functionality indicating few bimolecular terminations), but if reaction conditions remained constant and MeCN was used as solvent the reaction had characteristics in line with conventional ATRP (80% bromine functionality at 86% monomer conversion).[74] In addition to this, SET-LRP have also been demonstrated to be occurring within water and alcohol systems,[75, 76] which suggests that in principle the rapid disproportionation of Cu(I)Cl

could be occurring within the system that was optimized for the ATRP of OEGMA using an amide initiator (ethanol, CuCl/dNBpy). This can be tested experimentally by adding initiator to a solution containing Cu(0) and a ligand. If the Cu(0) is attacking the alkyl halide of the initiator a signal corresponding to the generation of $Cu(II)Cl_2$ would be expected to appear, this signal has been demonstrated to occur around 740 nm.[70]

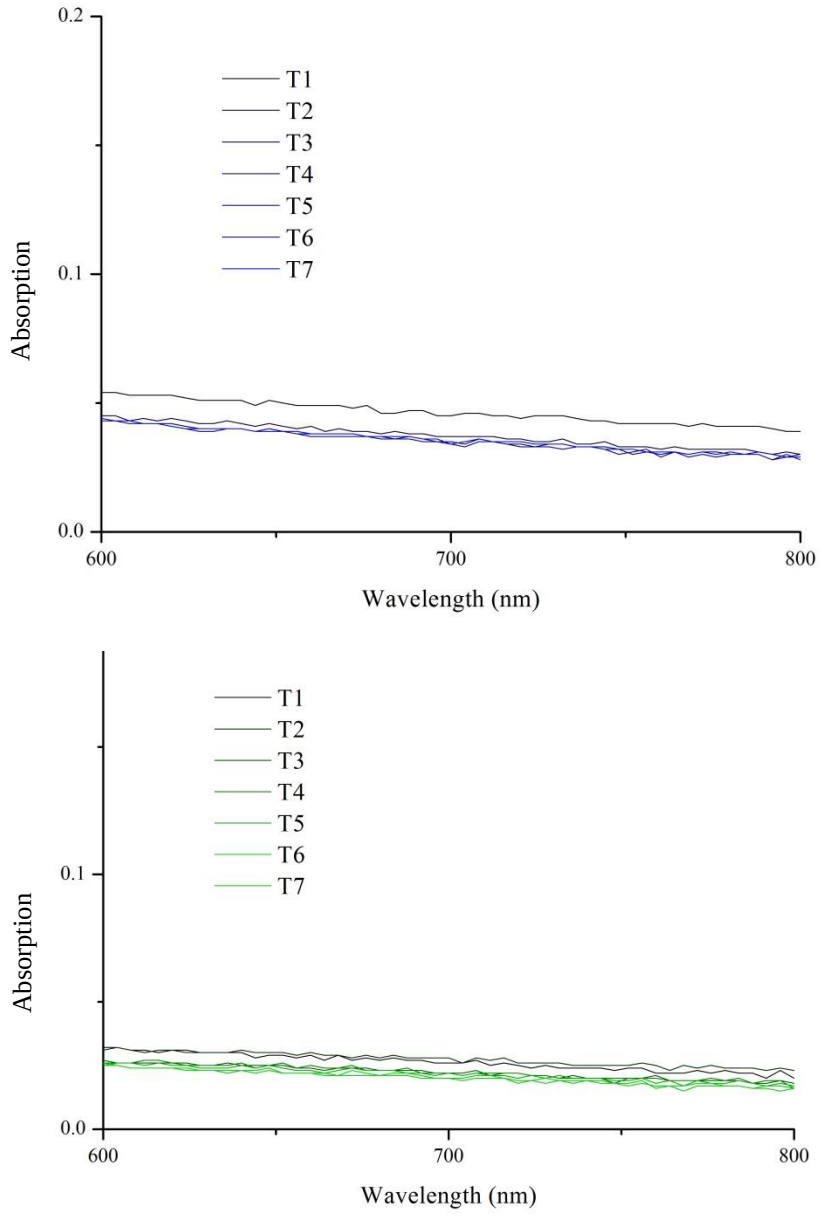

Figure 3.17 : VIS spectra showing the wavelength where $Cu(II)Cl_2$ is expected to appear (around 740 nm) for $Cu_{(0)}$ in ethanol with dNBpy. The top spectra displays the addition of MBrPA (blue), and EBriB is displayed on the bottom (green)

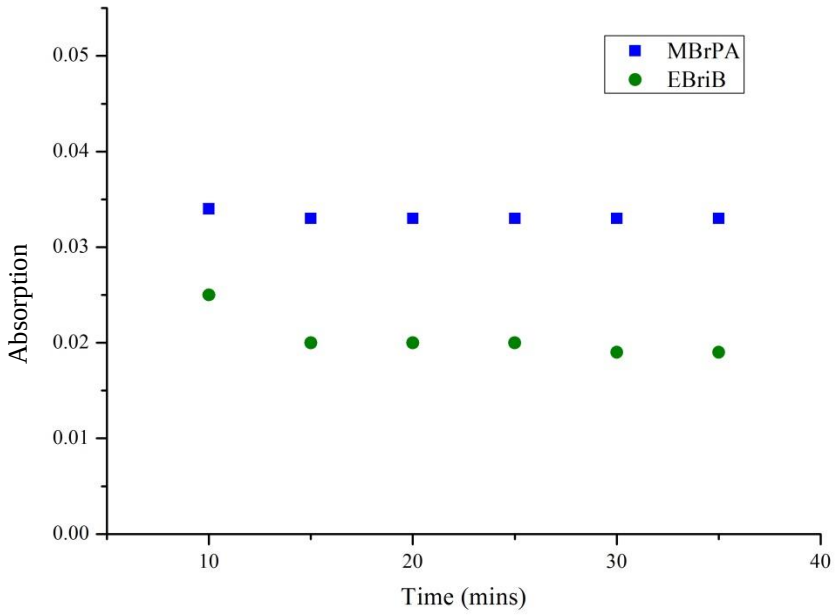

Figure 3.18 : A plot of the data produced from the VIS spectra of Cu(0) in ethanol with dNBpy. The absorption at 740 nm is shown for MBrPA (blue) and EBriB (green).

The spectra produced by these experiments are displayed in Figure 3.17 on the previous page, whilst the absorption at 740 nm for each spectrum is displayed in Figure 3.18 above. It is clear that there does not appear to be any disproportionation from either initiator under these conditions and there is no increase or decrease in absorption for either initiator. It should be noted that the Cu(0) powder that was added to each of the cuvettes was observed to simply settle at the bottom. Further to this, no colour change was observed in either of the cuvettes, whilst in all previous experiments the generation of Cu(II) species through the loss of Cu(I) had been accompanied by a colour change from brown to green, as was also observed during the ATRP of OEGMA.

Matyjaszewski *et al* demonstrated a method where the k_{atrp} value for an initiator can be calculated by observing the concentration of Cu(II) against time.[70, 71] By monitoring the increase of the Cu(II) peak absorption at 740 nm following the addition of an initiator to a solution containing CuCl, dNBpy and ethanol, the value of k_{atrp} can be obtained using Equations 3.6 and 3.7.

$$F([Cu(II)]) = \frac{C_0^{\ 2}}{3(C_0 - [Cu(II)])^3} - \frac{C_0}{(C_0 - [Cu(II)])^2} + \frac{1}{C_0 - Y}$$

Equation 3.6

$$k_{atrp} = \sqrt{\frac{Gradient}{k_t}}$$

Equation 3.7

The spectra produced by these experiments are displayed in Figure 3.20, whilst the plots derived from the spectra and Equation 3.6 are displayed in Figure 3.19 below. It should be noted that because the extinction coefficient that was used as a reference for determining the concentration of Cu(II) was for a bpy/$CuCl_2$ system, rather than the dNBpy with mixed halide (bromo-initiators with copper chlorides) system used here, the assumption of a constant extinction coefficient for the Cu(II) complex may not be valid. However the relative values between the initiators should still be revealing, as any error will be applied equally to both sets of results.

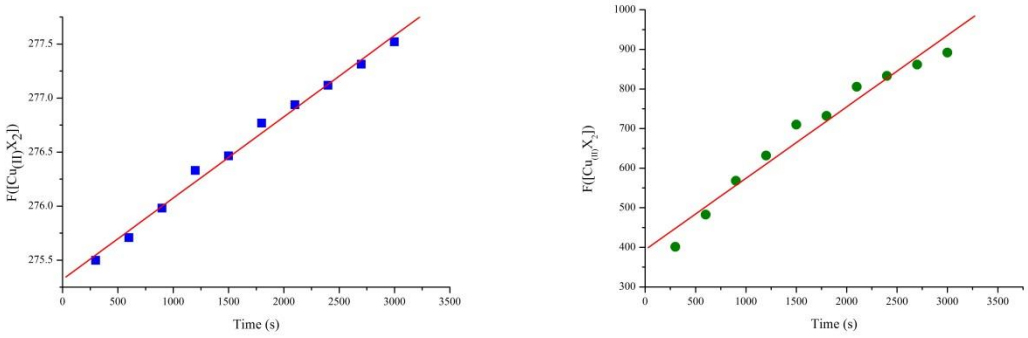

Figure 3.19 : Plots derived from Equation 3.2 by monitoring the rise in absorption at 740nm corresponding to Cu(II) species being generated by the amide (left) and ester (right) initiators using Cu(I)Cl/dNBpy in ethanol.

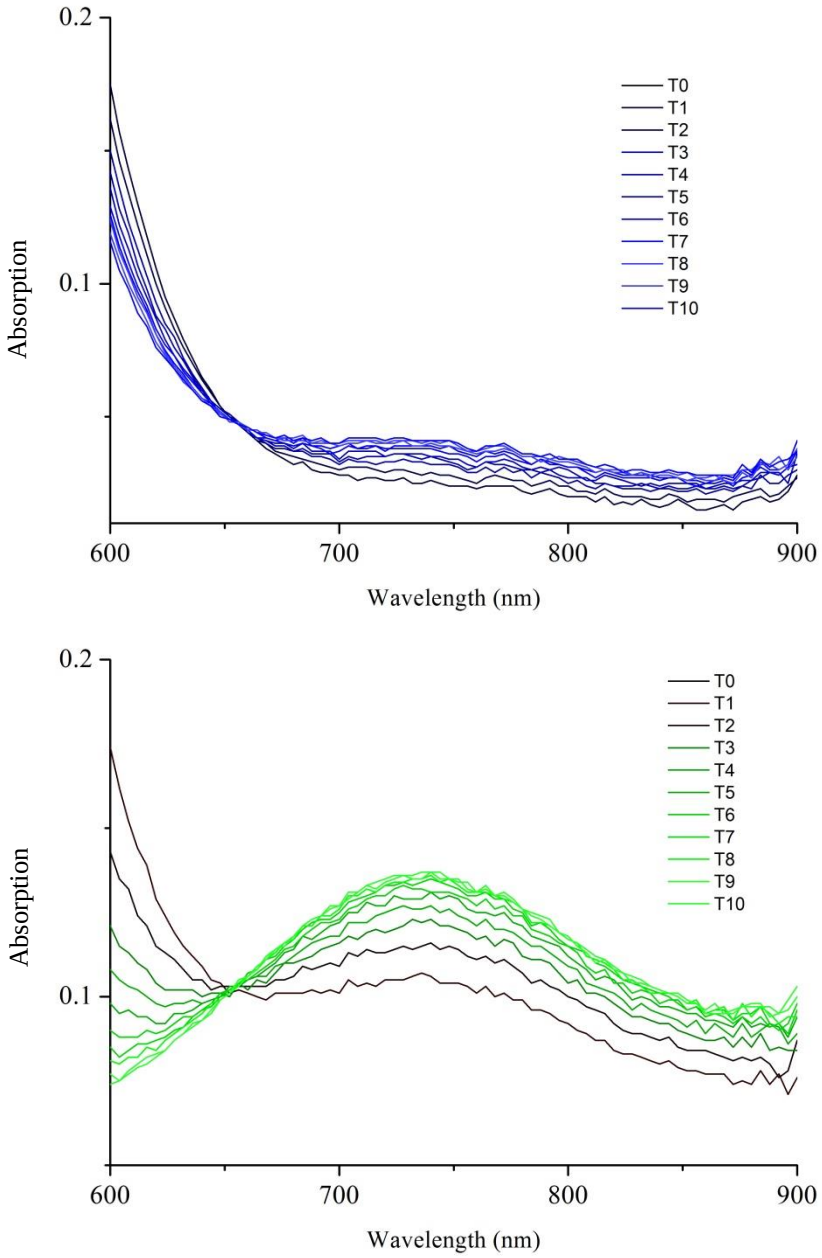

Figure 3.20 : VIS spectra showing the increase in signal relating to the generation of $Cu(II)Cl_2$ following the addition of MBrPA (blue, top) and EBriB (green, bottom).

k_{atrp} values for the initiators were calculated at 5.37×10^{-7} for the amide initiator, and 8.32×10^{-6} for the ester. This means that the activity of the ester is around 15 times greater than that of the amide, going a long way towards explaining the frequent observations of low initiator efficiencies within amide initiated polymerisation.

The k_{atrp} of EBriB has previously been reported as 1.0 x 10^{-5} using tris[(2-pyridyl)methyl]- amine (TPMA) as a ligand and CuBr in MeCN as solvent.[77] This value is only 1.2 times larger than the value calculated in this experiment (8.32 x 10^{-6}), implying a level of confidence in the result. The difference between the two values is to be expected because whilst the same initiator was used, the other reagents in the previously published experiment were varied.

To further understand this result, and attempt to actually explain rather than observe the difference between amide and ester initiated system, quantum chemical calculations were performed on model systems.

3.4.2.2 DFT modelling of amide and ester initiators and analogues

DFT calculations were carried out on a selection of chemicals analogous to EBriB and MBrPA. Methyl 2-bromo-2-methylpropanoate (MBriP), N-methyl 2-bromo-2-methylpropanamide (MBriPA), N,N-dimethyl 2-bromo-2-methylpropanamide (MBriPA2), methyl 2-chloro-2-methylpropanoate (MCliP) and N-methyl 2-chloro-2-methylpropanamide (MCliPA) were all tested, and their structures are displayed in figure 3.21 on the following page.

Geometries of the molecules were optimized using the B3LYP functional with the 6-31+Gd basis set that has previously been used to analyze ATRP initiators.[77-80] The B3LYP functional is known to give inaccurate values for thermo-chemical calculations, especially in free bond dissociation energies, so additional functionals were utilized for the free energy calculations.[81, 82] Both the BMK and M06-2X functionals have been reported to give good results for bond dissociation energy calculations, [50, 51, 82-86] and the double-hybrid functional B2G-PLYP has been reported to be accurate for thermo-chemical calculations.[52, 57, 87] For all of the calculations Grimme's D3 dispersion energy correction was employed as it has been shown to improve the results of bond dissociation energies as well as thermochemical values for most functionals,[54, 57, 88] and the *aug*-cc-pVTZ basis set was used.[53] Reference values for ΔH and ΔG for the dissociation of the carbon-bromine bond were taken from work previously published by Coote *et al*.[80]. The

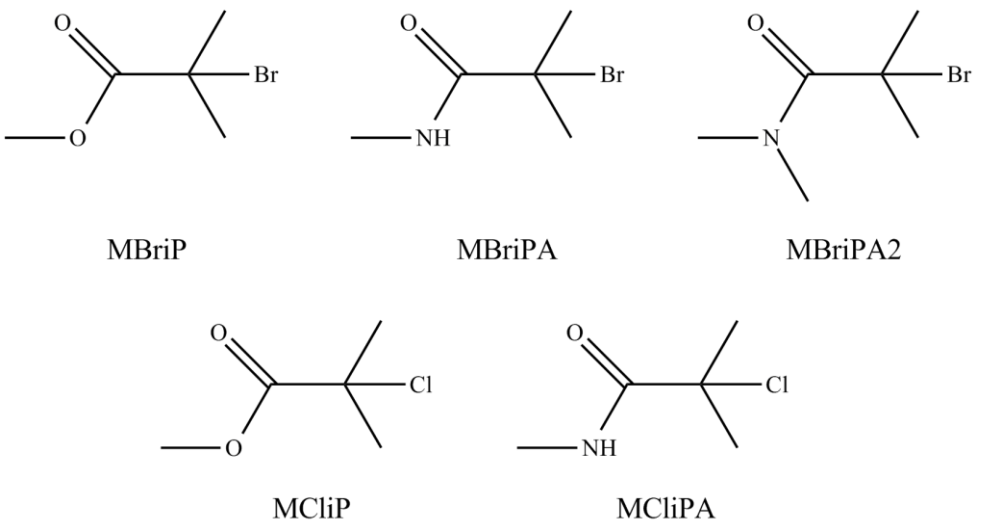

Figure 3.21: Structures of the molecules used in DFT calculations.

data produced from these calculations compared to literature values is displayed in Table 3.6 on the following page.

The closest values for ΔH and ΔG when compared to the literature were calculated using the BMK functional (UHF), reiterating that this function is of great value for low cost bond dissociation energy calculations. Regardless of the absolute values that were calculated for all the molecules, of particular significance were the results pertaining to the amide and ester initiators (MBriP and MBriPA), which showed a large difference in bond dissociation energy (BDE) between the two molecules. Apart from in the B3LYP results, values obtained were very consistent, with an overall average difference in BDE of -21.7kJ mol^{-1} with a mean standard deviation of only 1.25kJ mol^{-1} between the different methods.

Within the literature it has been stated that the BDE values for ATRP initiators are the major factor for the equilibrium constants for activation of the initiators by the copper catalysts.[77] If everything remains equal in terms of reaction conditions and reagents, then the relative BDE values can be used to evaluate the relative reactivity of initiating species.

Table 3.6 : Summary of the results from the DFT calculations, calculated at 298.15K in the gas phase. All values are in kJ mol^{-1}.

	R-Br → R• + Br•					
Compound		B3-LYP[a]	BMK[b]	M06-2X[b]	B2G-PLYP[b]	lit[c]
MBriP	ΔG	185.0	217.8	206.5	207.7	221.2
	ΔH	230.1	263.0	251.6	252.8	258.5
MBriPA	ΔG	208.9	239.8	226.4	228.7	NA
	ΔH	251.0	282.0	268.6	270.8	NA
ΔGG		-23.9	-22.0	-19.9	-21.0	
MBriPA2	ΔG	195.4	228.3	216.1	216.2	NA
	ΔH	238.8	271.8	259.6	259.7	NA
ΔGG		-10.4	-10.5	-9.6	-8.5	
MCliP	ΔG	225.9	276.0	265.6	254.2	278.5
	ΔH	271.7	321.7	311.3	299.9	315.3
MCliPA	ΔG	254.0	301.2	289.9	279.6	NA
	ΔH	296.8	343.9	332.6	322.3	NA

[a]6-31+G(d).
[b]*aug*-cc-pVTZ-D3.
[c]Calculated at the G3(MP2)-RAD level of theory at 298K in the gas phase.[80]

With the values shown here, a difference of -21.7kJ mol^{-1} between the initiators corresponds to the ester being roughly 6335 times more active than the amide:

$$\frac{k_{atrp(MBriPA)}}{k_{atrp(MBriP)}} = 0.000158$$

As a comparison, MBriPA2, an analogue of the amide initiator but with tertiary amide bond as opposed to a secondary, gave an average BDE of -9.53kJ mol^{-1}. This means that the ester is only 47 times more active than this secondary amide:

$$\frac{k_{atrp(MBriPA2)}}{k_{atrp(MBriP)}} = 0.00214$$

It has previously been reported that the k_{atrp} values for the secondary ATRP initiators ethylbromopropanoate and 2-bromo-*N*,*N*-diethylpropanamide were 0.30 and 0.044 respectively, having been derived experimentally.[89] This equates to the ester being only 7 times more active than the amide and as such should imply that for MBrPA (the initiator used in the ATRP of OEGMA in Section 3.4.2), where the difference to the ester was 6335 times, the polymerisation should not occur at all, and if it did, would have no controlled characteristics at all. Looking at the results of the chloride based initiators shows that if an active amide initiator molecule reacts with $Cu(II)Cl_2$ then the newly formed alkyl chloride is unlikely to be able to take part in any further reactions for the duration of the polymerisation as the BDE required to cleave the C-Cl bond is 61.4kJ mol^{-1} higher than for the C-Br bond.

This low initiation activity for amides should mean that polymerisations proceed extremely slowly, and would result in an initiator with extremely low efficiency due to the difficulty the amide initiator has when forming a stable radical as its halide dissociates. This was observed in polymerisations of OEGMA, where the amide initiator often took double or more time to produce polymers of the same molecular weight as those by the ester. The higher BDE of the amide structure compared to the ester shows that it is easier for the catalytic system to activate the ester initiator, where less energy is required to remove the halide and form a radical. The fact that these amides are less reactive than esters is not surprising, as it has been reported previously that they have lower radical stabilisation energies than their ester equivalents.[79] What is interesting is that the BDE difference between the molecules analysed in these calculations is so much larger.

One possible reason for this could be to do with the minimal energy conformations that these three molecules assume. As is shown in Figure 3.22, the C-Br bond angles for MBriP (top left) and MBriPA2 (bottom) to the plane of COO and CON are around 77^o and 65^o respectively. Whereas for MBriPA (top right) the angle is only around 4^o. This appears to be caused by an intramolecular H-Br hydrogen bond. This is a phenomenon that has been observed before with α-Br bonds in aromatic amides.[90] This hydrogen bond appears to have the effect of strengthening the carbon-bromine bond, and thereby increasing its bond dissociation energy.

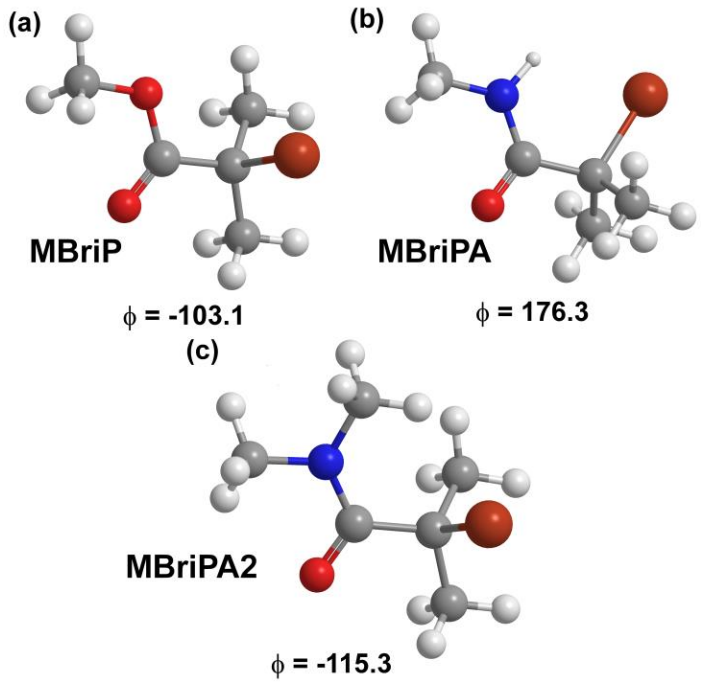

Figure 3.22: Optimised minimum energy conformations (B3LYP/6-31+G(d)) with O=C-C-Br dihedral angles obtained for model initiators.

The most obvious reason for the significant difference between the UV-visible results and quantum chemical calculations is that the UV data were recorded in a solvent (ethanol), which the calculations were were carried out in the gas phase, with no considerations taken for a solvent system. In order to investigate this a further set of calculations were carried out at the BMK/*aug*-cc-pVTZ level, making use of the universal solvation model of Truhlar *et al.*[58]

Xylene was chosen to act as a non-polar solvent due to its lack of hydrogen bonding and was compared against ethanol, which was used as the reaction solvent in the optimized polymerisations using MBrPA and OEGMA. Figure 3.24 shows the calculated results for ΔH and ΔG across both solvents and in the gas phase, with Table 3.7 giving details of k_{atrp} and ΔG relative to the ester initiator. There is a significant drop in the enthalpies when moving from the gas phase to the xylene system for both MBriP and MBriPA. MBriPA2 decreases in ΔH making the same change, but actually gains a small amount of ΔG. There does not appear to be any change for the ester initiator when moving from the non-polar xylene solvent into the polar ethanol environment, whereas the amides both show further drops in ΔG and ΔH when moving to more polar systems.

Table 3.7: Calculated (BMK/*aug*-cc-pVTZ) relative differences in BDFEs and relative k_{atrp} values for the amide initiators from the ester initiator.

Compound		Gas	Xylene	Ethanol
MBriP	$\Delta\Delta G^a$	0	0	0
	$K/K_0{}^b$	1	1	1
MBriPA	$\Delta\Delta G^a$	-20.4	-12.6	-6.6
	$K/K_0{}^b$	0.000264	0.00626	0.0710
MBriPA2	$\Delta\Delta G^a$	-10.5	-15.2	-5.5
	$K/K_0{}^b$	0.0144	0.00216	0.107

[a]Difference between ΔG for compound relative to ΔG for ester initiator (MBriP).
[b]K/K_0 = ratio of k_{atrp} for compound to k_{atrp} for ester (MBriP)

MBriPA and MBriPA2 were calculated to be around 14 and 9 times less reactive than MBriP when in ethanol. The value for MBriPA fits extremely well with previous experimental results, where in the UV analysis MBrPA was around 15 times less reactive than EBriB. It is clear that whilst solvation in a polar protic environment drastically increases the rate of activation of the amide structures for ATRP, their reactivity is still less than that of the esters. Significant solvent effects such as this have been noticed before (DMF vs DMSO).[11, 91]

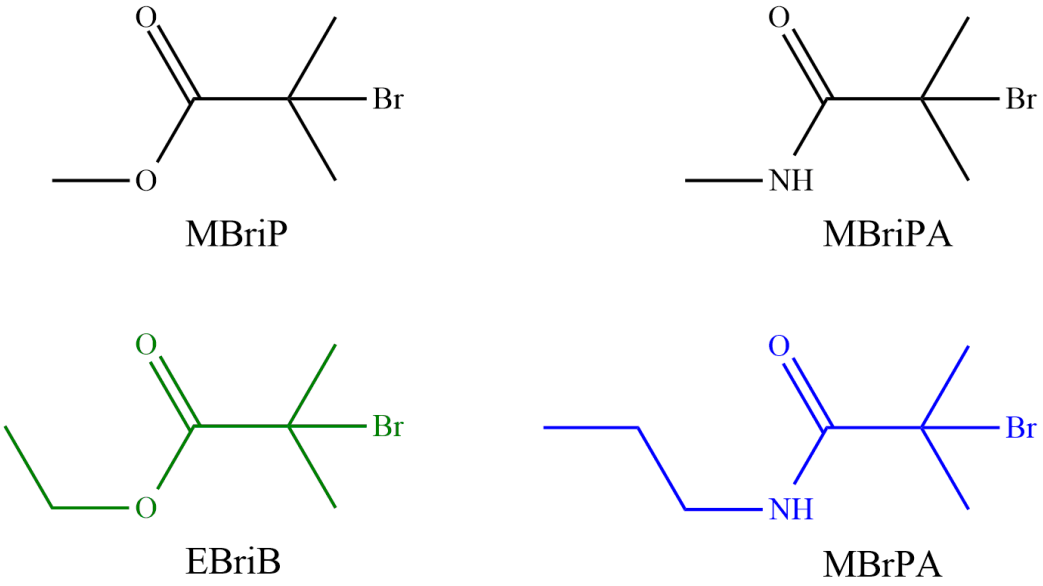

Figure 3.23 : Structures of molecules used for calculations (top) compared to the structures of the two initiators used for the ATRP of OEGMA in Section 3.4.2

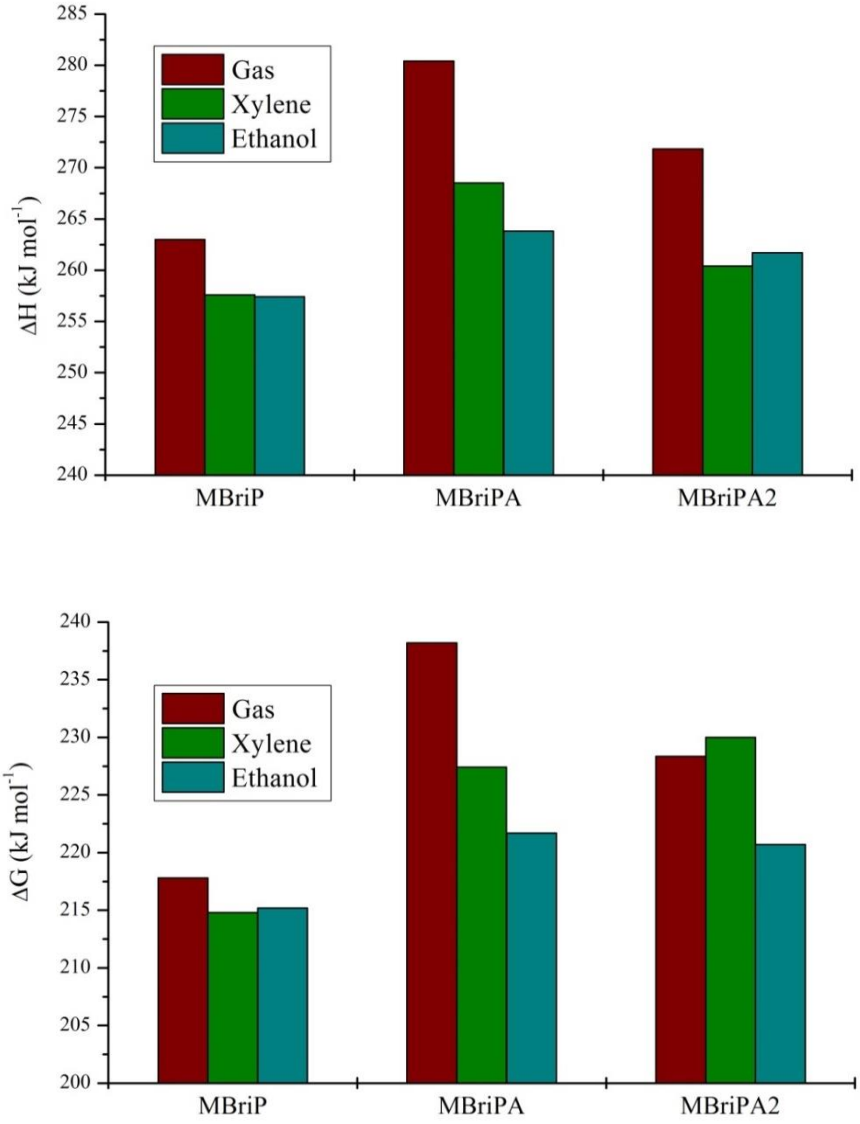

Figure 3.24 : Free energies and bond dissociation energies for model initiators in solvents calculated at the BMK/*aug*-cc-pVTZ//B3LYP/6-31+G(d) level of theory.

3.4.3 ARGET-ATRP and SET-LRP of OEGMA using MBrPA

In addition to the main body of work on the ATRP of OEGMA proposed in this chapter, several reactions were carried out using both an activator regenerated by electron transfer ATRP (ARGET-ATRP) and single electron transfer living radical polymerisation (SET-LRP) conditions.

3.4.3.1 ARGET-ATRP of OEGMA

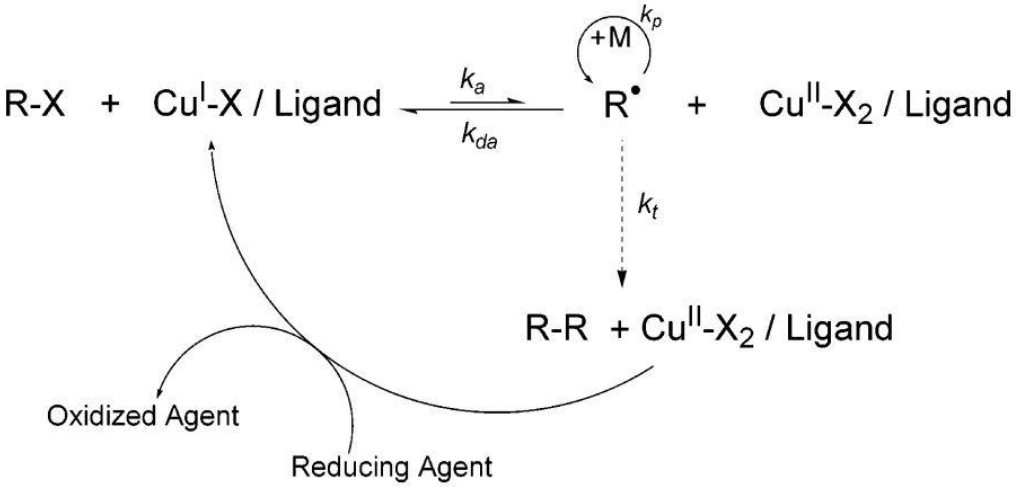

Scheme 1.12: Proposed mechanism for ARGET-ATRP.[91]

Activator regenerated by electron transfer ATRP (ARGET-ATRP) is a variant of ATRP that makes use of a reducing agent to mitigate the persistent radical effect.[92, 93] The result of this is that any Cu(II) species that form within the reaction are reduced back to Cu(I), and the total amount of copper halide that is required in the system is lowered. Common reducing agents that have been used include: tin 2-ethylhexanoate ($Sn(EH)_2$), ascorbic acid and glucose.[92, 94] ARGET-ATRP has also demonstrated ability to mitigate the adverse effects of any oxygen within the polymerisation, with some reported polymerisations progressing without any specific effort to remove oxygen from the system.[95, 96]

Whilst the reaction conditions that were developed for the ATRP of OEGMA using MBrPA enabled successful polymerisations in most cases, some reactions still did not proceed at all, and in these cases the reaction mixture was observed to change from a brown colour to green soon after initiation. Two reasons proposed for this effect occurring were an overly rapid generation of Cu(II) species upon initiation as a result of termination reactions, or oxygen being present within the reaction atmosphere despite practices being in place to stop this (degassing the reagents with nitrogen for 45 minutes). "Freeze-pump-thaw" is a technique that is often used to reduce the oxygen content of a reaction flask, but using this process did not improve the success rate of polymerisations compared to only degassing with nitrogen.

It has been demonstrated that ARGET-ATRP can be used for the synthesis of POEGMA in both alcohol and aqueous solutions.[97, 98] It was suggested that the utilisation of ARGET-ATRP would provide a higher rate of success for polymerisations due to the observed build-up of Cu(II) species on initiation being reduced back to active Cu(I) species.

$Sn(EH)_2$ was chosen as the reducing agent as it has frequently been used in successful ARGET-ATRP.[92, 93, 96] *N*,*N*,*N*′,*N*″,*N*″-pentamethyldiethylenetriamine (PMDETA) was also used in this reaction as it has been shown to be an effective ligand for the ARGET-ATRP of methacrylates and is readily available commercially.[97-99] The results of these reactions are displayed in Table 3.8 below. The polymerisation was attempted three times, with both varying degrees of polymerisations targeted and different lengths of reaction time. None of the reactions produced polymers that could be analysed by SEC as any product was indistinguishable from the reaction mixture at initiation. Upon initiation the reactions possessed a green colouration that persisted throughout the duration of the polymerisation. This was expected due to the increased amount of Cu(II) species within the system at initiation when compared to a conventional ATRP.

The reason for reactions being unsuccessful was unclear, as experimental conditions similar to those used in these experiments have previously produced polymers were low dispersities and controlled molecular weights.[99] It was proposed that the failures were again due to the amide initiator, where the C-Br bond dissociation energy was high enough that activation of the initiator was unfavourable with the specific

Table 3.8: ARGET-ATRP of OEGMA using $Sn(EH)_2$, PMDETA, $CuBr_2$, water and MBrPA

Sample ID	I	[M]/[I]	Time (hrs)	$M_{n(exp)}$	$M_{n(theo)}$[a]	Conversion (%)[b]
ARG1	Amide	50	24	n/a	n/a	0
ARG2	Amide	100	36	n/a	n/a	0
ARG3	Amide	100	72	n/a	n/a	0

[a]$M_{n(theo)}$ was calculated by : [M]/[I] x $M_{n(0)}$ x % conversion.
[b]Conversion calculated by ^{1}H NMR

components of the system that had been changed over that used in conventional ATRPs, mainly the ligand as PMDETA, and the solvent as water. Whilst quantum calculations had suggested that polar protic solvents (such as water) increase the activity of amide initiators, earlier ATRPs carried out in an IPA/water mix had also all been unsuccessful, indicating this solvent systems incompatibility with amide initiators.

3.4.3.2 SET-LRP of OEGMA

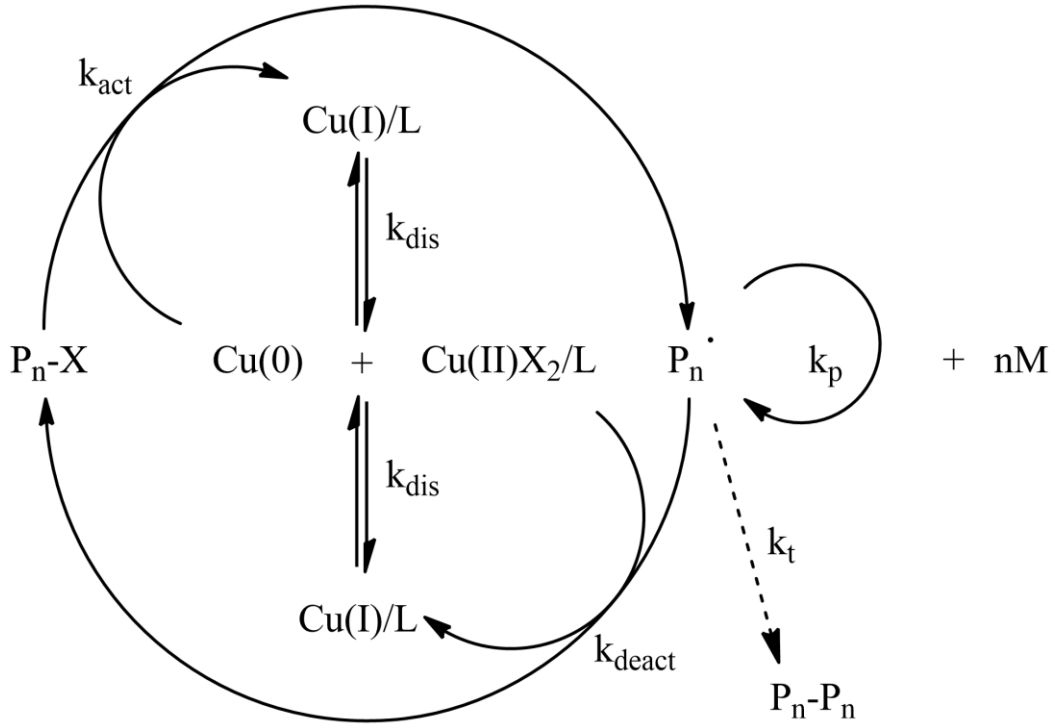

Scheme 1.14 : The proposed mechanism for SET-LRP.

Single electron transfer living radical polymerisation (SET-LRP) revolves around the rapid *in situ* disproportionation of Cu(I) species to Cu(0) and Cu(II), and it is the Cu(0) species that activate the alkyl halide initiator to trigger polymerisation. The Cu(II) formed fulfils the same role as in conventional ATRP, by acting as a deactivator to a propagating radical. This method has been demonstrated to rapidly synthesise controlled polymers from a range of vinyl monomers.[100]

Amide initiated ATRP of OEGMA generally took double or more time to produce polymers with similar molecular weights to those initiated by an ester (Table 3.5,

Section 3.4.2). SET-LRP polymerisations occur rapidly, often completing in minutes, as opposed to hours as in ATRP.[101] Due to the rapid rate of polymerisation that SET-LRP provides, it was decided to attempt the SET-LRP of OEGMA using MBrPA (amide initiator from Section 3.4.2) in experimental conditions similar to those previously reported for the polymerisation of methyl methacrylates.[74, 75] These conditions were: ethanol as solvent, Cu(0) wire wrapped around a stirrer bar, PMDETA as ligand, $CuBr_2$ as radical deactivator, and the reaction carried out at room temperature. Results from these polymerisations are displayed in Table 3.9, with a pseudo first order kinetic plot of a reaction shown in Figure 3.24 on the following page.

Upon initiation all polymerisations appeared colourless and then changed to a light blue indicating the formation of Cu(I), apart from SET3 which remained colourless for the duration. The delay in Cu(I) generation, an induction period, is an effect that has been observed previously and is a explained by the presence of oxygen within the system.[101] Whilst this would be detrimental in conventional ATRP, its effect is diminished in SET-LRP as Cu(0) will react with oxygen to form copper oxide, which can initiate and disproportionate itself, but at a much lower rate than Cu(0). Polymers synthesised in SET1, SET2, and SET4 invariably possessed broad dispersities, low conversions, and molecular weights considerably larger than theoretical values. In fact, the values recorded were consistently worse in these

Table 3.9: SET-LRP of OEGMA using MBrPA as initiator in ethanol, using: PMDETA, Cu(0) wire, and $CuBr_2$.

Sample ID	I	[M]/[I]	Time (mins)	$M_{n\ (exp)}$	$M_{n\ (theo)}$ [a]	Đ	Conv. (%) [b]
SET1	Amide	50	240	56000	4541	1.40	29
SET2	Amide	50	240	48450	3341	1.45	21
SET3	Amide	100	240	n/a	n/a	n/a	0
SET4	Amide	100	180	37200	4991	1.39	32

[a] $M_{n(theo)}$ was calculated by : [M]/[I] x $M_{n(0)}$ x % conversion.
[b] Conversion calculated by ^{1}H NMR

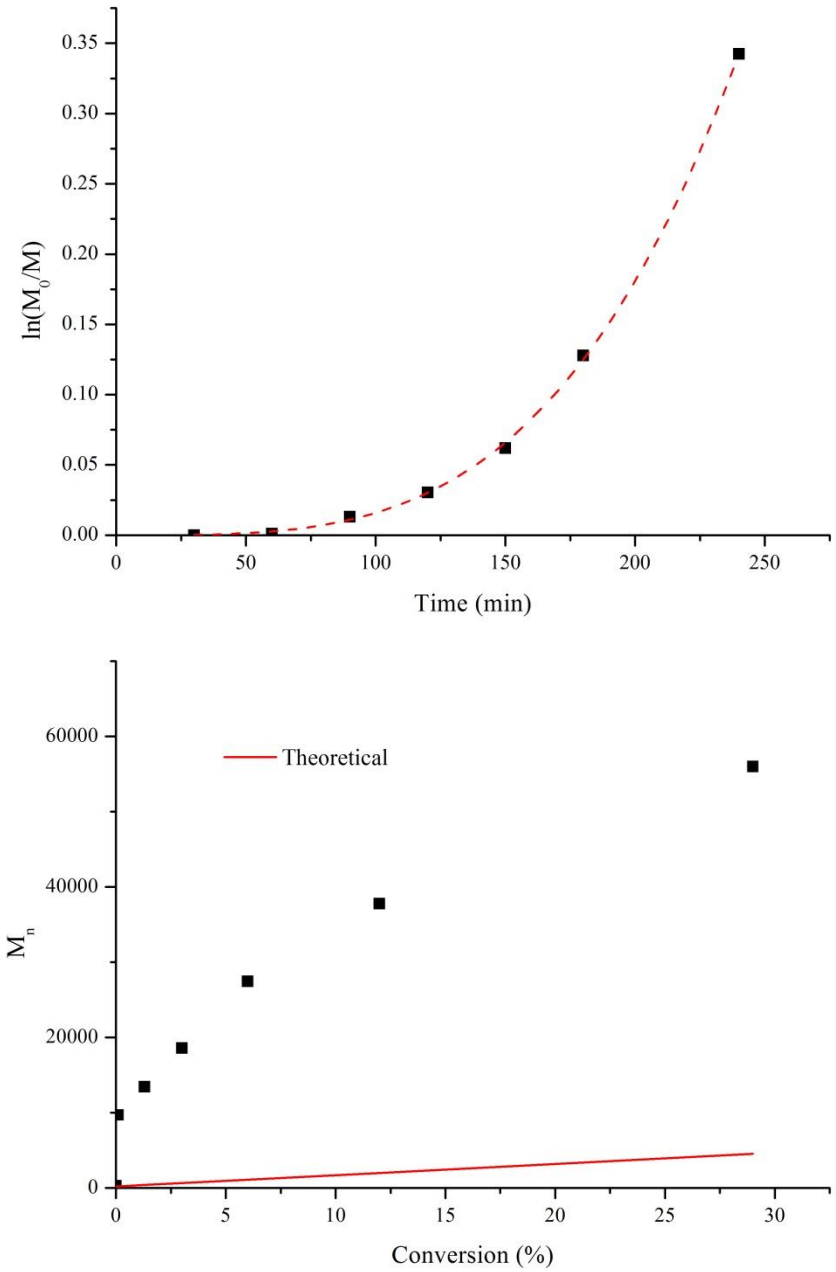

Figure 3.24 : Pseudo first order kinetics plot (top) and molecular weight against time (bottom) for SET-LRP of OEGMA using MBrPA as initiator.

SET-LRP than the equivalent polymers prepared by ATRP using MBrPA across all measured characteristics. The pseudo first order kinetic plot highlights the non-living nature of the reaction (Figure 3.24). This is confirmed by observation of the plot displaying molecular weight against conversion, where the data possesses little linearity and each sample had a molecular weight that was significantly larger than the theoretically calculated value.

Whilst the polymers produced by SET-LRP were in no measure "controlled", reactions were generally successful in the production of POEGMA without any optimisation of the system, and high molecular weight polymers (>M_n 30000) were prepared in a time period measured in minutes rather than hours or days as in ATRP. Further research into evaluating the ideal reaction conditions could enable SET-LRP to be a valuable tool in the synthesis of POEGMA using an amide initiator.

3.5 Conclusions

To conclude, OEGMA has successfully been polymerised using ATRP with both a common, frequently used ester initiator (EBriB) and a novel analogous amide initiator (MBrPA) that was synthesised specifically for the polymerisation. Whilst the amide polymerisations were initially not as successful as the ester, by careful control of the experimental conditions the system was optimised to produce polymers that were a lot closer to having ideal "living/controlled" characteristics.

The reason for the discrepancy between the two initiators was analysed by both UV-visible spectroscopy and by quantum chemical calculations to determine bond dissociation energies. Whilst initial UV-visible investigations failed to validate previous reasons given in the literature for the lack of control in amide initiated polymerisations, the k_{atrp} of both EBriB and MBrPA was calculated by using a method that had been reported by Matyjaszewski *et al*.[70, 71] This value of k_{atrp} was in close agreement with density function theory calculations that were performed once solvent effects of the reaction environment were taken into consideration.

It appears that the key reason for the amide initiators having such a low efficiency is that the bond dissociation energy of amides is much higher than that of analogous esters. This means that polymerisation of methacrylates using amide based initiators will always suffer from slow reaction times and relatively poor control due to the difficulty in cleaving the carbon halide bond in an amide initiator. The higher bond dissociation energy of the amide might stem from an intramolecular H-Br bond, and this effect can be somewhat mitigated by using a polar protic solvent.

By looking at the bond dissociation energies of some chlorine based initiators, it is highly likely that if there is any deactivation of amide initiator molecules by a copper(II) chloride complex (creating an C-Cl bond) then that molecule is effectively terminated to any other significant reactions for the duration of the polymerisation, as the bond dissociation energy is larger than for C-Br bonds. This backs up the experimental data of Adams *et al* who detected evidence of unreacted amide initiator even when polymerisations had proceeded to high conversions.[10]

Both ARGET-ATRP and SET-LRP were evaluated for the synthesis of POEGMA as each technique has qualities that would be beneficial for polymerisation. It has been demonstrated with ARGET-ATRP that the amount of catalyst required for polymerisation is lower than in a conventional ATRP.[92] Further to this, ARGET-ATRP is a robust polymerisation system as it provides some mitigation to the effects of oxygen within the reaction.[96, 102] Unfortunately the ARGET-ATRP of OEGMA using MBrPA failed to synthesise any polymer, possibly as a result of changing the solvent and ligand used for the reaction. SET-LRP showed more potential, and was used to prepare three polymers with high molecular weights in reactions that were significantly faster than ATRP, but without any controlled characteristics. If reaction conditions were optimised, then SET-LRP could become a much faster method for the production of controlled POEGMA using MBrPA.

3.6 References

1. W. A. Braunecker and K. Matyjaszewski, *Progress in Polymer Science*, 2007, **32**, 93-146.

2. V. Coessens, T. Pintauer and K. Matyjaszewski, *Progress in Polymer Science*, 2001, **26**, 337-377.

3. D. J. Siegwart, J. K. Oh and K. Matyjaszewski, *Progress in Polymer Science*, 2012, **37**, 18-37.

4. K. Matyjaszewski and N. V. Tsarevsky, *Nature chemistry*, 2009, **1**, 276-288.

5. J. S. Wang and K. Matyjaszewski, *Macromolecules*, 1995, **28**, 7901-7910.

6. H. Bergenudd, G. Coullerez, M. Jonsson and E. Malmstrom, *Macromolecules*, 2009, **42**, 3302-3308.

7. H. Rettig, E. Krause and H. G. Börner, *Macromol. Rapid Commun.*, 2004, **25**, 1251-1256.

8. A. Limer and D. M. Haddleton, *Macromolecules*, 2006, **39**, 1353-1358.

9. P. M. Wright, G. Mantovani and D. M. Haddleton, *Journal of Polymer Science Part A: Polymer Chemistry*, 2008, **46**, 7376-7385.

10. D. J. Adams and I. Young, *J. Polym. Sci. Pol. Chem.*, 2008, **46**, 6082-6090.

11. G. J. M. Habraken, C. E. Koning and A. Heise, *J. Polym. Sci. Pol. Chem.*, 2009, **47**, 6883-6893.

12. K. Y. Baek, M. Kamigaito and M. Sawamoto, *Journal of Polymer Science Part A: Polymer Chemistry*, 2002, **40**, 1937-1944.

13. Y. Mei, K. L. Beers, H. M. Byrd, D. L. VanderHart and N. R. Washburn, *J. Am. Chem. Soc.*, 2004, **126**, 3472-3476.

14. J. T. Rademacher, R. Baum, M. E. Pallack, W. J. Brittain and W. J. Simonsick, *Macromolecules*, 2000, **33**, 284-288.

15. M. Teodorescu and K. Matyjaszewski, *Macromol. Rapid Commun.*, 2000, **21**, 190-194.

16. D. Neugebauer and K. Matyjaszewski, *Macromolecules*, 2003, **36**, 2598-2603.

17. M. Senoo, Y. Kotani, M. Kamigaito and M. Sawamoto, *Macromolecules*, 1999, **32**, 8005-8009.

18. S. Monge and D. M. Haddleton, *Eur. Polym. J.*, 2004, **40**, 37-45.

19. C. de las Heras Alarcón, S. Pennadam and C. Alexander, *Chemical Society Reviews*, 2005, **34**, 276-285.

20. J. F. Lutz, O. Akdemir and A. Hoth, *J. Am. Chem. Soc.*, 2006, **128**, 13046-13047.

21. W. Feng, S. P. Zhu, K. Ishihara and J. L. Brash, *Biointerphases*, 2006, **1**, 50-60.

22. W. Zimmt, *Journal of Applied Polymer Science*, 1959, **1**, 323-328.

23. R. M. Fitch, M. B. Prenosil and K. J. Sprick, 1969.

24. S. Balke and A. Hamielec, *Journal of Applied Polymer Science*, 1973, **17**, 905-949.

25. M. Kato, M. Kamigaito, M. Sawamoto and T. Higashimura, *Macromolecules*, 1995, **28**, 1721-1723.

26. J.-S. Wang and K. Matyjaszewski, *J. Am. Chem. Soc.*, 1995, **117**, 5614-5615.

27. R. Q. Frazer, R. T. Byron, P. B. Osborne and K. P. West, *Journal of long-term effects of medical implants*, 2005, **15**.

28. S. Aldrich, *Polyethylene glycol Product Information*, 2015.

29. M. S. Kim, H. Hyun, K. S. Seo, Y. H. Cho, J. Won Lee, C. Rae Lee, G. Khang and H. B. Lee, *Journal of Polymer Science Part A: Polymer Chemistry*, 2006, **44**, 5413-5423.

30. Z. Hu, T. Cai and C. Chi, *Soft Matter*, 2010, **6**, 2115-2123.

31. J. A. Yoon, C. Gayathri, R. R. Gil, T. Kowalewski and K. Matyjaszewski, *Macromolecules*, 2010, **43**, 4791-4797.

32. C. R. Becer, S. Hahn, M. W. Fijten, H. M. Thijs, R. Hoogenboom and U. S. Schubert, *Journal of Polymer Science Part A: Polymer Chemistry*, 2008, **46**, 7138-7147.

33. K. B. Doorty, T. A. Golubeva, A. V. Gorelov, Y. A. Rochev, L. T. Allen, K. A. Dawson, W. M. Gallagher and A. K. Keenan, *Cardiovascular Pathology*, 2003, **12**, 105-110.

34. M. C. Hacker, L. Klouda, B. B. Ma, J. D. Kretlow and A. G. Mikos, *Biomacromolecules*, 2008, **9**, 1558-1570.

35. H. Feil, Y. H. Bae, J. Feijen and S. W. Kim, *Macromolecules*, 1993, **26**, 2496-2500.

36. X. Yin, A. S. Hoffman and P. S. Stayton, *Biomacromolecules*, 2006, **7**, 1381-1385.

37. V. Aseyev, H. Tenhu and F. M. Winnik, in *Self Organized Nanostructures of Amphiphilic Block Copolymers II*, Springer, 2011, pp. 29-89.

38. O. V. Borisov, E. B. Zhulina, F. A. Leermakers and A. H. Müller, in *Self organized nanostructures of amphiphilic block copolymers I*, Springer, 2011, pp. 57-129.

39. J. F. Lutz, *Adv. Mater.*, 2011, **23**, 2237-2243.

40. F. Veronese and J. M. Harris, *Advanced drug delivery reviews*, 2002, **54**, 453.

41. F. F. Davis, *Advanced drug delivery reviews*, 2002, **54**, 457-458.

42. A. Abuchowski, J. R. McCoy, N. C. Palczuk, T. van Es and F. F. Davis, *Journal of Biological Chemistry*, 1977, **252**, 3582-3586.

43. K. Matyjaszewski, *Macromolecules*, 2012, **45**, 4015-4039.

44. K. Matyjaszewski, J.-L. Wang, T. Grimaud and D. A. Shipp, *Macromolecules*, 1998, **31**, 1527-1534.

45. Y. T. Li, Y. Q. Tang, R. Narain, A. L. Lewis and S. P. Armes, *Langmuir*, 2005, **21**, 9946-9954.

46. J. J. Stewart, *Journal of Molecular modeling*, 2007, **13**, 1173-1213.

47. M. W. Schmidt, K. K. Baldridge, J. A. Boatz, S. T. Elbert, M. S. Gordon, J. H. Jensen, S. Koseki, N. Matsunaga, K. A. Nguyen and S. Su, *Journal of Computational Chemistry*, 1993, **14**, 1347-1363.

48. A. D. Becke, *The Journal of Chemical Physics*, 1993, **98**, 1372-1377.

49. C. Lee, W. Yang and R. G. Parr, *Physical Review B*, 1988, **37**, 785.

50. A. D. Boese and J. M. Martin, *The Journal of Chemical Physics*, 2004, **121**, 3405-3416.

51. Y. Zhao and D. G. Truhlar, *Theoretical Chemistry Accounts*, 2008, **120**, 215-241.

52. A. Karton, A. Tarnopolsky, J.-F. Lamere, G. C. Schatz and J. M. Martin, *The Journal of Physical Chemistry A*, 2008, **112**, 12868-12886.

53. T. H. Dunning Jr, *The Journal of Chemical Physics*, 1989, **90**, 1007-1023.

54. S. Grimme, J. Antony, S. Ehrlich and H. Krieg, *The Journal of Chemical Physics*, 2010, **132**, 154104.

55. R. Peverati and K. K. Baldridge, *Journal of Chemical Theory and Computation*, 2008, **4**, 2030-2048.

56. L. Goerigk and S. Grimme, *Journal of Chemical Theory and Computation*, 2011, **7**, 3272-3277.

57. L. Goerigk and S. Grimme, *Physical Chemistry Chemical Physics*, 2011, **13**, 6670-6688.

58. A. V. Marenich, C. J. Cramer and D. G. Truhlar, *The Journal of Physical Chemistry B*, 2009, **113**, 6378-6396.

59. H. Fischer, *Chemical Reviews*, 2001, **101**, 3581-3610.

60. W. Tang and K. Matyjaszewski, *Macromolecules*, 2006, **39**, 4953-4959.

61. J. S. Wang, D. Greszta and K. Matyjaszewski, *Abstr. Pap. Am. Chem. Soc.*, 1995, **210**, 227-PMSE.

62. K. Matyjaszewski, S. Coca, S. G. Gaynor, M. L. Wei and B. E. Woodworth, *Macromolecules*, 1998, **31**, 5967-5969.

63. N. V. Tsarevsky, W. A. Braunecker, A. Vacca, P. Gans and K. Matyjaszewski, *Macromol. Symp.*, 2007, **248**, 60-70.

64. D. A. Shipp, J.-L. Wang and K. Matyjaszewski, *Macromolecules*, 1998, **31**, 8005-8008.

65. K. Matyjaszewski, D. A. Shipp, J.-L. Wang, T. Grimaud and T. E. Patten, *Macromolecules*, 1998, **31**, 6836-6840.

66. J.-D. Tong, G. Moineau, P. Leclere, J.-L. Brédas, R. Lazzaroni and R. Jérôme, *Macromolecules*, 2000, **33**, 470-479.

67. X. S. Wang and S. P. Armes, *Macromolecules*, 2000, **33**, 6640-6647.

68. S. Patai, *The chemistry of the carbon-halogen bond*, John Wiley & Sons, 1973.

69. K. Matyjaszewski and J. Xia, *Chemical Reviews*, 2001, **101**, 2921-2990.

70. W. Tang, N. V. Tsarevsky and K. Matyjaszewski, *J. Am. Chem. Soc.*, 2006, **128**, 1598-1604.

71. W. A. Braunecker, N. V. Tsarevsky, A. Gennaro and K. Matyjaszewski, *Macromolecules*, 2009, **42**, 6348-6360.

72. V. Percec, T. Guliashvili, J. S. Ladislaw, A. Wistrand, A. Stjerndahl, M. J. Sienkowska, M. J. Monteiro and S. Sahoo, *J. Am. Chem. Soc.*, 2006, **128**, 14156-14165.

73. D. Konkolewicz, Y. Wang, M. Zhong, P. Krys, A. A. Isse, A. Gennaro and K. Matyjaszewski, *Macromolecules*, 2013, **46**, 8749-8772.

74. G. Lligadas, B. M. Rosen, M. J. Monteiro and V. Percec, *Macromolecules*, 2008, **41**, 8360-8364.

75. G. Lligadas and V. Percec, *Journal of Polymer Science Part A: Polymer Chemistry*, 2008, **46**, 2745-2754.

76. N. H. Nguyen, B. M. Rosen and V. Percec, *Journal of Polymer Science Part A: Polymer Chemistry*, 2010, **48**, 1752-1763.

77. W. Tang, Y. Kwak, W. Braunecker, N. V. Tsarevsky, M. L. Coote and K. Matyjaszewski, *J. Am. Chem. Soc.*, 2008, **130**, 10702-10713.

78. A. A. Isse, A. Gennaro, C. Y. Lin, J. L. Hodgson, M. L. Coote and T. Guliashvili, *J. Am. Chem. Soc.*, 2011, **133**, 6254-6264.

79. M. L. Coote, C. Y. Lin, A. L. Beckwith and A. A. Zavitsas, *Physical Chemistry Chemical Physics*, 2010, **12**, 9597-9610.

80. C. Y. Lin, M. L. Coote, A. Gennaro and K. Matyjaszewski, *J. Am. Chem. Soc.*, 2008, **130**, 12762-12774.

81. H. Kruse, L. Goerigk and S. Grimme, *The Journal of organic chemistry*, 2012, **77**, 10824-10834.

82. E. I. Izgorodina, M. L. Coote and L. Radom, *The Journal of Physical Chemistry A*, 2005, **109**, 7558-7566.

83. A. S. Menon, G. P. Wood, D. Moran and L. Radom, *The Journal of Physical Chemistry A*, 2007, **111**, 13638-13644.

84. I. Y. Zhang, J. Wu, Y. Luo and X. Xu, *Journal of Chemical Theory and Computation*, 2010, **6**, 1462-1469.

85. R. J. O'Reilly, A. Karton and L. Radom, *International Journal of Quantum Chemistry*, 2012, **112**, 1862-1878.

86. Y. Zhao and D. G. Truhlar, *The Journal of Physical Chemistry A*, 2008, **112**, 1095-1099.

87. A. Tarnopolsky, A. Karton, R. Sertchook, D. Vuzman and J. M. Martin, *The Journal of Physical Chemistry A*, 2008, **112**, 3-8.

88. B. Chan and L. Radom, *The Journal of Physical Chemistry A*, 2012, **116**, 4975-4986.

89. W. Tang and K. Matyjaszewski, *Macromolecules*, 2007, **40**, 1858-1863.

90. Y.-Y. Zhu, L. Jiang and Z.-T. Li, *CrystEngComm*, 2009, **11**, 235-238.

91. S. Steig, F. Cornelius, P. Witte, B. B. Staal, C. E. Koning, A. Heise and H. Menzel, *Chem. Commun.*, 2005, 5420-5422.

92. W. Jakubowski, K. Min and K. Matyjaszewski, *Macromolecules*, 2006, **39**, 39-45.

93. W. Jakubowski and K. Matyjaszewski, *Angewandte Chemie*, 2006, **118**, 4594-4598.

94. H. Dong and K. Matyjaszewski, *Macromolecules*, 2008, **41**, 6868-6870.

95. L. F. Zhang, Z. P. Cheng, S. P. Shi, Q. H. Li and X. L. Zhu, *Polymer*, 2008, **49**, 3054-3059.

96. K. Matyjaszewski, H. Dong, W. Jakubowski, J. Pietrasik and A. Kusumo, *Langmuir*, 2007, **23**, 4528-4531.

97. C. Porsch, S. Hansson, N. Nordgren and E. Malmström, *Polymer Chemistry*, 2011, **2**, 1114-1123.

98. A. Simakova, S. E. Averick, D. Konkolewicz and K. Matyjaszewski, *Macromolecules*, 2012, **45**, 6371-6379.

99. Y. Kwak and K. Matyjaszewski, *Polymer international*, 2009, **58**, 242-247.

100. V. Percec, T. Guliashvili, J. S. Ladislaw, A. Wistrand, A. Stjerndahl, M. J. Sienkowska, M. J. Monteiro and S. Sahoo, *J. Am. Chem. Soc.*, 2006, **128**, 14156-14165.

101. B. M. Rosen and V. Percec, *Chemical Reviews*, 2009, **109**, 5069-5119.

102. K. Min, W. Jakubowski and K. Matyjaszewski, *Macromol. Rapid Commun.*, 2006, **27**, 594-598.

Chapter 4: PEI-*graft*-POEGMA

4.1 Introduction

As has been discussed in the previous chapters, the field of polymer science has expanded dramatically since the middle of the 1990s as new techniques were developed for the synthesis of novel polymers conforming to complex architectures.[1-3] One area that has seen a surge of interest is the biomedical field, where polymers can be produced to react to specific triggers that exist *in vivo*.[4-9]

4.1.1 Bio-applications for polymers

By utilising one or more polymers that can react to external stimuli, "smart" materials can be developed to fulfil specific roles. These roles can include, but are not limited to; polymer coatings to increase bioavailability of drug molecules, targeted drug delivery systems (DDS) for localised treatments *in vivo*, magnetic resonance imaging (MRI) contrast agents, and separation techniques.[11-16]

Due to the modular way in which polymers composites can be assembled, one possible method for synthesising "smart" materials is by covalently bonding complete polymer chains to functional substrates. For many years magnetic nanoparticles have held a leading role in medical diagnosis, acting as contrast agents in MRI. The fundamentals of MRI lie in the same processes which occur in ^{1}H NMR, utilising a strong magnetic field to align protons within the sample. A radio frequency (RF) pulse is then applied across the field, causing the protons to shift alignment, then "relax" back to their aligned state after the RF signal is removed. This relaxation causes a small emission of further RF from the affected protons, which can be detected and used to eventually make an image.[17]

MR images can be improved up by the utilisation of contrast agents, magnetic materials whose presence changes the rate at which protons will relax, bringing about an increase in resolution.[18, 19] In general the agents used are either compounds of gadolinium or iron oxides, depending on the specific image that is required. There are a wide range of contrast agents available on the market, but

most share two key properties: high stability in water and high magnetic saturation. Water stable particles can be dispersed into solutions more readily, ensuring that the material can come into contact with protons in the body. Magnetic saturation is a measure of how strong a magnetic field the particle will exhibit during the experiment, increasing their contrast effect.

Beyond their MR contrast effect, magnetic nanoparticles can also be used as a substrate for hyperthermia, a process that uses high temperatures to kill localised areas of cancer cells.[20, 21] By exposing the particles to an alternating magnetic field, heat builds up within the particles due to a combination of Brownian motion, direct thermal activation, and reversal of the particle's local magnetic field by the strong external field. If this particle is at or near the site of a tumour, then the heating effect could reach temperatures high enough to cause cell death. Even without inducing cell death, this thermal effect can trigger the activation of thermally responsive materials *in situ*; potentially delivering payloads of therapeutics directly to the site they are required.

Several drug delivery systems are already on the market, treating a range of conditions that vary from fungal infections (AmBisome), to cancer (Bexxar), and even hepatitis (PEG-Intron).[22-24] Polymer drug delivery systems (DDS) offer many advantages over introducing unprotected therapeutics into a person.[25, 26] They can be passively targeted by attaching moieties or DNA that are programed for specific biological overexpression. This minimises the amount of a drug that has to be in the living system by making it region-specific. A secondary effect of this is an improvement in the therapeutic index of the drug, by possibly lowering the total amount of therapeutic agent required, and decreasing any toxic effect. Also, the presence of a protective polymer coating enables the usage or therapeutics that would be unable to survive *in vivo* for any great period of time.

4.1.2 Polymers used for biological applications

The numbers of polymers that are being investigated for medical applications is numerous, many of which have been discussed in the previous chapters. For this

work, research was carried out using poly(oligo ethylene glycol) methyl ether methacrylate (POEGMA) and polyethyleneimine (PEI).

4.1.2.1 Poly(oligo ethylene glycol) methyl ether methacrylate (POEGMA)

As mentioned in Chapter 3, POEGMA is part of a group of polymers containing a methyl methacrylate backbone, with ethylene glycol units forming side chains to create a brush-like structure.

It is of interest within this application because it has been shown to increase the protein resistance in materials it is bound to, and it also possesses a lower critical solution temperature (LCST) whilst being highly soluble in water.[27-29] These properties would be invaluable for the creation of a multifunctional detection/delivery system. Increased protein resistance enables the system to remain *in vivo* for longer, whilst the LCST can be triggered in order to release any drugs being carried by the system.

The thermoresponsive nature of POEGMA can be fine-tuned by copolymerisation with 2-(2-methoxyethoxy)ethyl methacrylate (MEO_2MA).[30] $PMEO_2MA$ exhibits an LCST around 26 ºC, making it unsuitable for *in vivo* applications. The LCST of POEGMA is dependent on the length of ethylene oxide units, a length of eight or nine units exhibits an LCST around 90 ºC. Lutz *et al* showed that by varying the degree of copolymerisation the LCST can be fine-tuned between the LCSTs of the homopolymers. At 8% OEGMA the copolymer produced exhibited a LCST 37 ºC, directly in the range of biological systems.[30]

4.1.2.2 Polyethyleneimine (PEI)

PEI is a polymer composed of ethylene units interspersed by primary, secondary and/or tertiary amines. PEI can come as four distinct forms; linear, branched, hyperbranched, and dendritic. In a linear arrangement the majority of amines are secondary, except possibly a primary amine at either end of the chain. Branched structures have a mix of amines as secondary and tertiary to create some branching, and as a dendrimer there are many tertiary amines creating a perfect

star shaped structure. In a hyperbranched system there are also multiple tertiary amine sites, but the structure is not uniformly branched at each successive amine. Whilst dendrimers are desirable for a number of applications, the synthesis of perfect structures is often costly and time consuming.[31] Due to this, branched and hyperbranched structures are often used, as they offer many of the same advantages as dendrimers, and are widely available commercially.

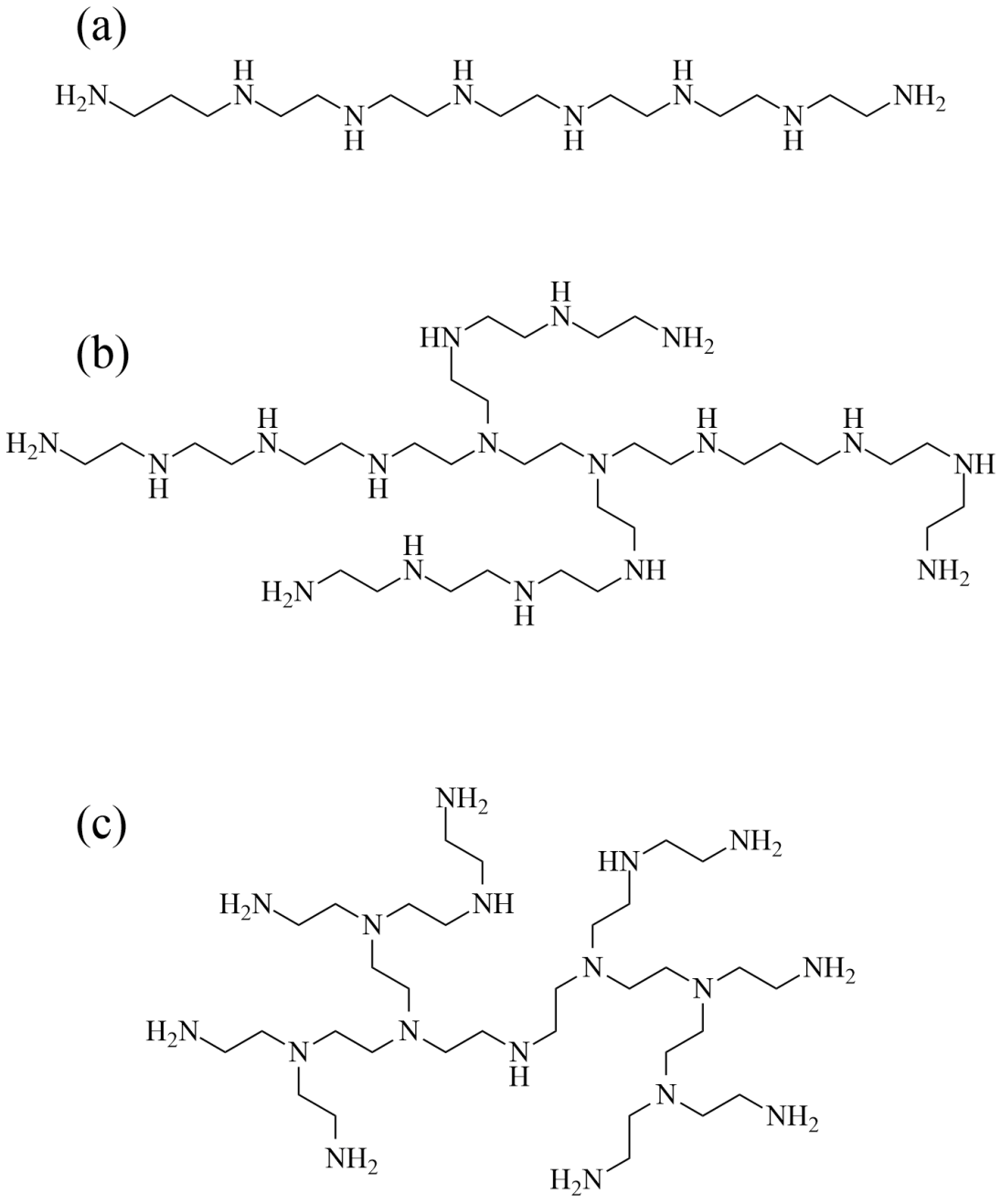

Figure 4.1 : Three different types of molecular structures that PEI can conform to, (a) linear, (b) branched, and (c) hyperbranched.

It has previously been shown that PEI can be absorbed onto the surface of magnetite nanoparticles in order to act as the first layer of a particle stabilisation system where poly(ethylene oxide)-*co*-poly(glutamic acid) acted as a secondary layer.[32] It has also been noted by several groups that aqueous stabilisation of prepared nanoparticles can be obtained by using a combination of PEI and polyethylene glycol, or polyethylene oxide. [33-35] Due to the large number of ammonium groups within the PEI structure, it is inherently cytotoxic, due to the possible electrostatic interactions with phosphate groups within DNA. These interactions have also led to interest in PEI as a gene therapy agent, which has been investigated previously.[36-38]

PEI has been successfully copolymerised with thermoresponsive polymers (poly(*N*-isopropylacrylamide) (PNIPAAm), or PNIPAAm-based copolymers, in order to produce controlled medical release systems.[39, 40] Quan *et al* synthesised a PNIPAAm based copolymer coupled to PEI that exhibited a thermal response. This was then used in drug loading experiments and showed a temperature triggered controlled release of the loaded drug payload.[39] Cheng *et al* synthesised a separate PNIPAAm based copolymer via free radical polymerisation then coupled it to PEI. The material produced possessed a LCST at 38 ºC, and had an improved DNA transfection efficiency when compared to the unmodified PEI.[40]

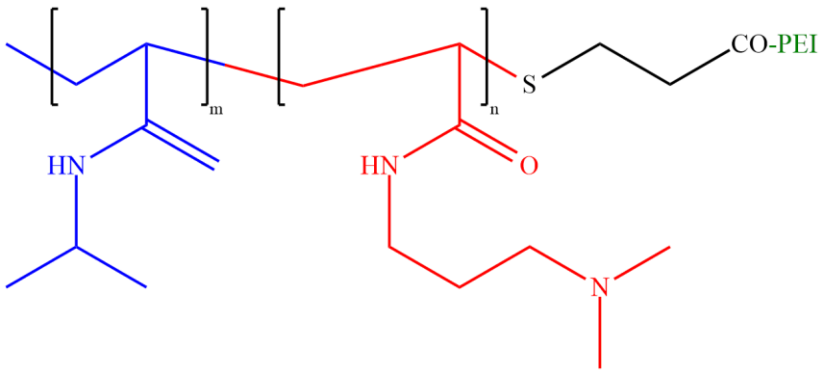

Figure 4.2 : Illustration of the (PNIPAAM-*co*-PNDAPM)-*b*-PEI structure synthesised by Cheng *et al*.[41]

4.1.3 PEI-*graft*-POEGMA stabilised nanoparticles

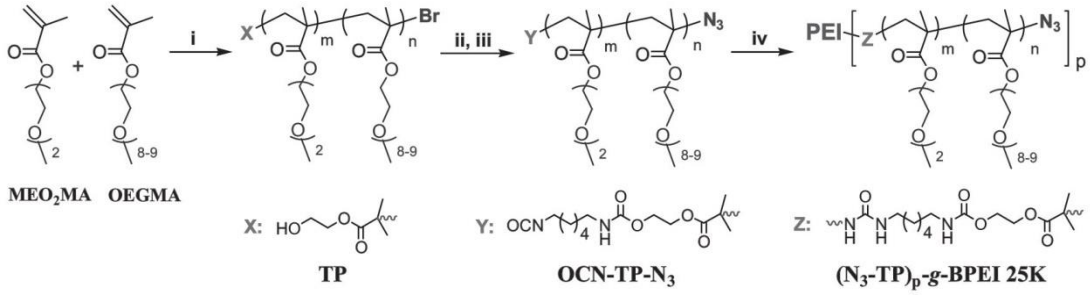

Scheme 4.1: Synthetic route used by Zhang et al for the synthesis of PEI-*g*-P(MEO_2MA-*co*-OEGMA). (i) CuBr/$CuBr_2$, PMDETA, THF, 2'-hydroxyethyl-2-bromoisobutyrate, 70 ºC, 12 h. (ii) NaN_3, room temp., 20 h. (iii) $OCN(CH_2)_6NCO$, $CHCl_3$, DIEA, reflux, 16 h. (iv) PEI (M_n 25k, branched), $CHCl_3$, 12 h.[42]

PEI-*graft*-POEGMA based materials have previously been synthesised through a multistage reaction wherein the copolymer was synthesised first, then coupled to the PEI.[41]

Initially Zhang *et al* carried out atom transfer radical polymerisation (ATRP) to synthesise P(MEO_2MA-*co*-OEGMA), producing copolymers similar to those reported by Lutz *et al*.[30, 41] The bromine end group was then changed to azido group, in order to avoid side reactions during coupling to the PEI. This was achieved by the addition of NaN_3 in DMF, in a darkroom environment. Next, the other end of the copolymer was modified to produce isocyanate functionality. This was carried out using a modified version of Kissel *et al*'s method.[42] Finally, the copolymer was coupled to the PEI by dissolving PEI in chloroform, and adding the copolymer (also dissolved in chloroform) to it dropwise. The resulting solution was then refluxed at 70 ºC under nitrogen for 20 hours prior to precipitation into diethyl ether to collect the product.[41] Whilst this method was successful at creating a gene delivery vehicle, it relied on multiple steps, and includes reaction conditions that require exacting control of temperature, atmosphere and light.

One advantage of this system however is that it avoided any requirement to use ATRP with an amide based initiator. As detailed in Chapter 3, amide initiators for ATRP have proven to cause many problems, including low initiator efficiencies that cause higher than predicted molecular weights, and slow polymerisations with variables rates.[43-49].

In this chapter an alternative method to produce PEI-*graft*-POEGMA will be outlined (Scheme 4.2). PEI (branched, M_n 600) was modified with an ATRP initiating moiety to produce a macroinitiator for the ATRP of OEGMA. This method only relies on two synthetic steps, and utilised the robust nature of ATRP under relatively mild conditions, and the knowledge of how to minimize the detrimental effects of amide initiators for ATRP, to produce well defined polymers that possessed low dispersities and a range of molecular weights. Furthermore, these polymers retained the thermoresponsive effect provided by the POEGMA segment, and still possessed the ability to transfect DNA due to the PEI core. Finally the PEI-*graft*-POEGMA was used as a stabiliser for superparamagnetic nanoparticles, which retained the same characteristics of particles prepared in the absence of the polymer.
The results of this method were published in 2014.[50]

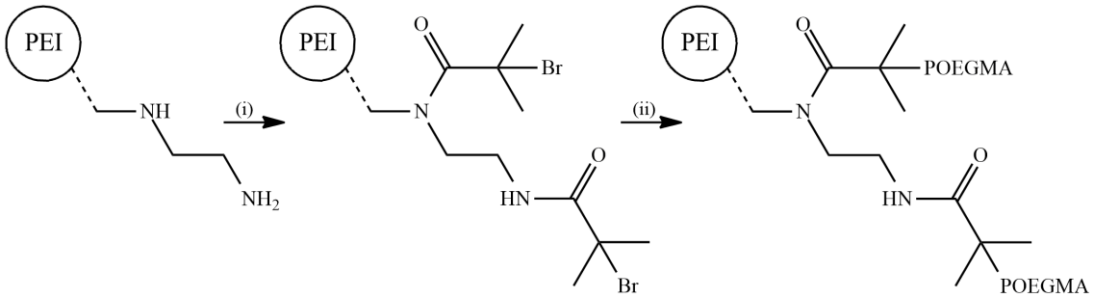

Scheme 4.2 : Outline of the novel, facile, two-step synthesis of PEI-*graft*-POEGMA. (i): Functionalization of PEI macro-initiator: Et_3N, DCM, $BrC(CH_3)_2COBr$, 0 ºC, 24 h. (ii): ATRP of OEGMA using PEI macro-initiator: OEGMA, CuCl, dNBpy, EtOH, 48 h.

4.2 Materials and Apparatus

4.2.1 Materials

Oligo(ethylene glycol methyl ether) methacrylate (M_n 360, Sigma-Aldrich), triethylamine (99 %, Sigma-Aldrich), copper (I) bromide (98 %, Sigma-Aldrich), 2-bromo-2-methylpropanoyl bromide (98 %, Sigma-Aldrich), *N*,*N*′,*N*″,*N*″-Pentamethyldiethylenetriamine (99 %, Sigma-Aldrich), ethidium bromide (≥95 %, Sigma-Aldrich), low molecular weight DNA from salmon sperm (≤5 %

protein, Sigma-Aldrich), sodium bicarbonate (analytical reagent grade, Fisher Scientific) aluminium oxide (activated, neutral, for column chromatography 50-200 μm, Acros Organics) magnesium sulphate (97 %, anhydrous, Acros Organics) methanol (analytical reagent grade, Fisher Scientific), tetrahydrofuran (analytical reagent grade, Fisher Scientific) and ethanol (analytical reagent, Fisher Scientific), Polyethyleneimine, branched (M_n 600, 99 %, Đ 1.08, Polysciences Inc.) were purchased and used without further purification. Dichloromethane (analytical reagent grade) was purchased from Fisher Scientific and immediately before use was dried and distilled over calcium hydride. Ferric chloride ($FeCl_3$) and ferrous sulphate heptahydrate ($FeSO_4.7H_2O$) were purchased from Riedel-deHaen and sodium hydroxide (NaOH) was purchased from J.T. Baker. All were analytical grade and used without further purification. Distilled water for DLS was obtained from a Millipore MilliQ Ultrapure water filtration system.

4.2.2 Characterisation

^1H and ^{13}C NMR spectra of the polymers were recorded using a JEOL ECS spectrometer (400 MHz) at 25 °C in solutions of deuterated chloroform ($CDCl_3$), d_4-methanol or d_6-ethanol. Molecular weight parameters were recorded by size exclusion chromatography (SEC) of THF solutions using two 5 μm mixed C PLgel columns at 40 °C and a Shodex RI-101 refractive index detector. The SEC system was calibrated using poly(methyl methacrylate) standards.

DLS measurements were performed on the PEI-*graft*-POEGMA stabilised nanoparticle dispersions, and PEI-*graft*- POEGMA DNA complexes, using a Malvern Zetasizer Nano ZS with Dispersion Technology Software (DTS) version 5.0 software. All measurements of 10 scans were repeated three times and the average at each temperature reported.

Fluorescence data was recorded using a FluroMax-2 fluorometer at an excitation wavelength of 500nm, scanning from 530 nm to 700 nm at a 1 nm increment, using a 950 v lamp.

Particle sizes, distributions and morphologies of the nanoparticles and were analysed by Cem Atlan under the supervision of Nico Sommerdijk and Seyda

Bucak, Particles were analysed by FEI Tecnai G2 Sphera Transmission electron microscope (TEM) operating at 200 kV by drying 30uL of samples on carbon coated 200 mesh copper grids. Phase identification of synthesized nanoparticles was obtained by Rigaku X-Ray diffractometer (XRD) by scanning 2-theta range of 20^{o} to 70^{o} at room temperature with 0.02 theta increments per 10 sec. Magnetic properties of both bare and PEI-b-POEGMA coated particles were analysed by Vibrating Sample Magnetometer at dry state and room temperature.

4.3 Experimental

4.3.1 Synthesis of Poly(ethyleneimine)-*graft*-(2-bromo-2-methyl)propanamide

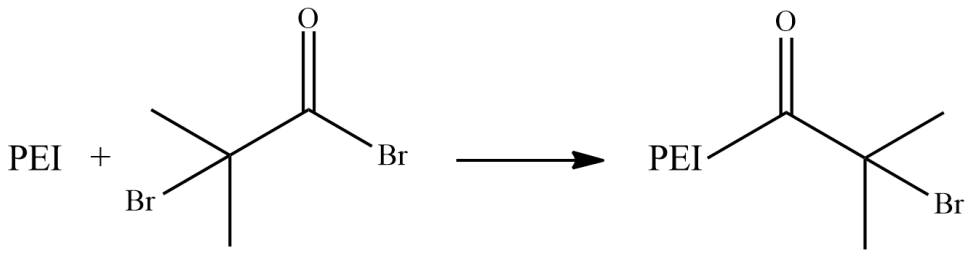

Scheme 4.3 : Synthesis of PEI-graft-(2-bromo-2-methyl)propanamide, macroinitiator for ATRP of OEGMA

PEI Mw 600 (5 g, 0.0083 mol) and triethylamine (1.5 ml, 0.011 mol) were dissolved in 200 ml of dichloromethane and placed into an ice bath at 0 ^{o}C and left stirring. 2-bromo-2-methylpropanoyl bromide (15 g, 0.0653 mol), pre dissolved in 100 ml of dichloromethane, was added dropwise to this mixture. The resulting solution was left stirring at 0 ^{o}C for 3 hours and then stirring at room temperature for a further 18 hours. The solution was filtered to remove solids and then evaporated to leave a yellow viscous oil which was re-dissolved in 40 ml of dichloromethane. This was washed five times against a 10% saturated solution of sodium bicarbonate then left stirring over night with 3 g of activated charcoal and 5 g of anhydrous magnesium sulphate. Finally this was filtered again to remove solids before being dried under vacuum (yield 61%) prior to NMR analysis.

^{1}H NMR δ_H(400 MHz; $CDCl_3$; ppm) 1.65 (3H, br, ((CH_3)$_2$C-)), 2.45 (2H, br, -N-CH_2-CH_2-NH-), 2.6 (2H, br, -CH_2-CH_2-NH-), 3.2 (4H, br, -NH-CH_2-CH_2-NH- / -N-CH_2-CH_2-N-), 3.45 (2H, br, -NH-CH_2-CH_2-NH-C=O), 3.6 (2H, br, -CH_2-CH_2-NH-C=O)

^{13}C NMR δ_C(100 MHz; $CDCl_3$; ppm) 32 ((CH_3)$_2$C-), 38 (-NH-CH_2-CH_2-NH- / C=O-NH-CH_2-CH_2), 41-50 (C=O-NH-CH_2-CH_2-NH / -NH-CH_2-CH_2-NH- / -N-CH_2-CH_2-NH-), 50-58 (-N-CH_2-CH_2-NH- / -N-CH_2-CH_2-N- / (CH_2)$_2$C-)), 172 (C=O-NH)

4.3.2 Synthesis of Poly(ethyleneimine)-*graft*-poly(oligo ethylene glycol) methyl methacrylate

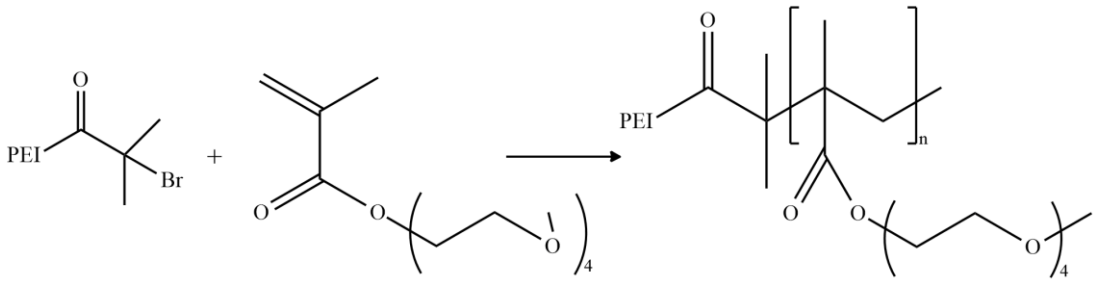

Scheme 4.4 : PEI macroinitiator for the ATRP of OEGMA

A typical synthesis was as follows: A Schlenk tube containing OEGMA (Mn 300, 5 g, 18.1 mmol), CuCl (0.036 g, 0.362 mmol), 4,4'-dinonyl-2,2'-bipyridine (dNBpy) (0.2959 g, 0.724 mmol) and ethanol (14 ml) was sealed and degassed with nitrogen for 45 minutes. PEI-initiator in ethanol (0.1 g/ml) was injected via a gastight syringe and then left stirring at room temperature under nitrogen for 48 hours. At timed intervals 1 mL samples were removed via syringe, exposed to air and then passed through a short alumina column to remove the catalytic system then diluted in THF for SEC and $CDCl_3$ for NMR. The polymer was isolated by dropwise addition of the THF solution to an excess of cold, stirred hexane. The product precipitated as a green viscous liquid and was collected by centrifuge prior to drying overnight under vacuum at 35 ^{o}C before SEC and NMR analysis. Results of these reactions can be found in Table 4.1 in Section 4.4.2.

^{1}H NMR δ_H(400 MHz; $CDCl_3$; ppm) 0.75-1.1 (3H, br, *atactic*, -CH2-C-*CH_3*), 1.75 (2H, br, -*CH_2*-C-), 3.5 (3H, br, -CH_2-O-*CH_3*), 3.6 (4H, br, -O-*CH_2*-*CH_2*-), 4.1 (2H, br, -C=O-O-*CH_2*-)

^{13}C NMR δ_C(100 MHz; $CDCl_3$; ppm) 24-27 (CH_2-C-*CH_3*), 31-34 (CH_3-C-*CH_2*-), 57-60 (CH_3-**C**-CH_2-)/(CH_2-O-*CH_3*), 66-69 (O-*CH_2*-*CH_2*-O), 177-179 (*C=O*)

4.3.3 UV-visible analysis of PEI-*graft*-POEGMA dialysis

PEI-*graft*-POEGMA (0.2 g in 10 ml of deionised water) was placed into a holder, and enclosed securely behind dialysis tubing. A tank containing 4 L of water and 10 ml of *N*,*N*,*N′*,*N″*,*N″*-pentamethyldiethylenetriamine was prepared, and set mixing with a magnetic stirrer flea. The sample holder was then added to the dialysis tank, and allowed to dialyse submerged for the required time. 2 ml samples of the water/ligand solution were removed and placed into a quartz cuvette with 10 mm path length, then analysed by UV-visible spectrometry to monitor the dialysis. Finally the dialysed polymer sample was recovered by removing the holder from the dialysis tank, and then diluting the sample with 100 ml of methanol. Excess anhydrous magnesium sulphate was added to the methanol and left overnight to remove water. Finally, this solution was filtered to remove solids, and then the product was collected under vacuum to recover the dialysed polymer.

4.3.4 DNA complexation with PEI-*graft*-POEGMA monitored by DLS and ethidium bromide assay

DNA complexation of PEI-*graft*-POEGMA was carried out in collaboration with Tom Ashton as part of a MChem project at the University of Kent.

4.3.4.1 DLS of DNA-polymer complex and LCST determination

Aqueous solutions (1 wt%) of PEI (M_n 600), PEI-*graft*-POEGMA (M_n 26500), DNA (from salmon sperm), and PEI-*graft*-POEGMA complexed with DNA were prepared using deionised water. Each sample was incubated at 25 ^{o}C in a quartz cuvette with path length 10 mm for two minutes prior to analysis.

4.3.4.2 Ethidium bromide assay of DNA-polymer complex

2 ml of a 1 µg/ml solution of ethidium bromide in distilled water was added to a quartz cuvette with path length 10 mm. 0.2 ml of a 0.15 mg/ml solution of DNA in distilled water was added by syringe to the cuvette prior to sealing and mixing. A 0.02 mg/ml solution of PEI or PEI-*graft*-POEGMA was added in 20µl increments and the resulting emission spectra recorded.

4.3.5 Synthesis of magnetite nanoparticles stabilised with PEI-graft-POEGMA

Nanoparticles were synthesised by Cem Altan and U. Ecem Yarar under the supervision of Nico Sommerdijk and Seyda Bucak as part of a collaboration between: Yeditepe University (Turkey), Eindhoven University of Technology (The Netherlands), and the University of Kent (England).

Typically $FeCl_3$ (0.141 g) and $FeSO_4 \cdot 7H_2O$ (0.121 g) were dissolved in distilled water (40 ml) which was deaerated by bubbling with nitrogen for 30 minutes to remove any dissolved oxygen. The solution was then stirred for 15 minutes for complete mixing under nitrogen gas. A solution of PEI-*graft*-POEGMA (P1 in Table 4.1) (38 mg) in aqueous NaOH (0.257 g in 10 ml) was added to the iron salts solution rapidly and solution changes colour from orange to black immediately. The resulting solution was then stirred at room temperature for 30 minutes. The particles were collected with a handheld magnet and centrifuged 2 times after washing with water. The final precipitate was then dried in a vacuum oven overnight at 60 °C. The magnetite nanoparticles without stabilizer were prepared in an identical procedure but without PEI-*graft*-POEGMA.

4.4 Results

4.4.1 Synthesis of Poly(ethyleneimine)-*graft*-(2-bromo-2-methyl)propanamide (PEI-macroinitiator/PEI-Br)

4.4.1.1 Structure of commercially bought PEI

In order to assess the result of the synthesis of the PEI-macroinitiator, the structure of the commercially available PEI had to be determined. The manufacturer's description for branched PEI with a M_n 600 stated that there was a ratio of 25:50:25 between primary, secondary and tertiary amine groups within the polymer. In order to verify this, a combination of ^{1}H, ^{13}C, and two dimensional NMR techniques were used.

Von Harpe *et al* previously reported ^{13}C assignments for PEI, which were used to determine the actual ratio of amine groups present within the purchased PEI by

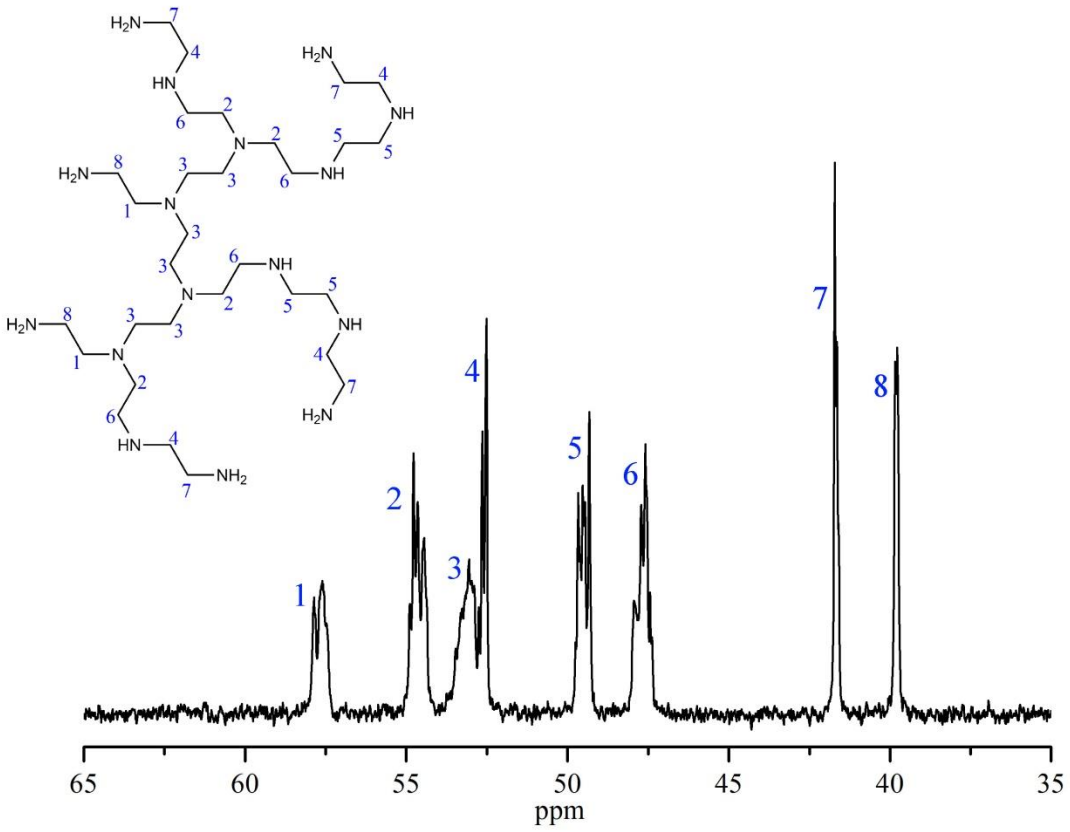

Figure 4.3 : ^{13}C NMR spectra of PEI (M_n 600) with peaks assigned from literature. Inset shows an approximate PEI structure that fits the calculated average ratio of 1º, 2º and 3º amines.

using Equation 4.1, where "*A*" denotes the signal intensity for the relevant numbered peak.[51]

$$1°:2°:3° = (A_7 + A_8) : \frac{(A_4 + A_5 + A_6)}{2} : \frac{(A_1 + A_2 + A_3)}{3}$$

Equation 4.1

The calculated results from the ^{13}C NMR spectrum on the previous page (Figure 4.3) give a ratio of 42.5 : 37.1 : 20.4 for 1º, 2º and 3º amine groups respectively. This approximates to six 1º, six 2º and four 3º amines per PEI (M_n 600) molecule, a significant deviation from the 25:50:25 ratio that had been supplied by the manufacturer. The structure of PEI that is shown in Figure 4.3 (and the

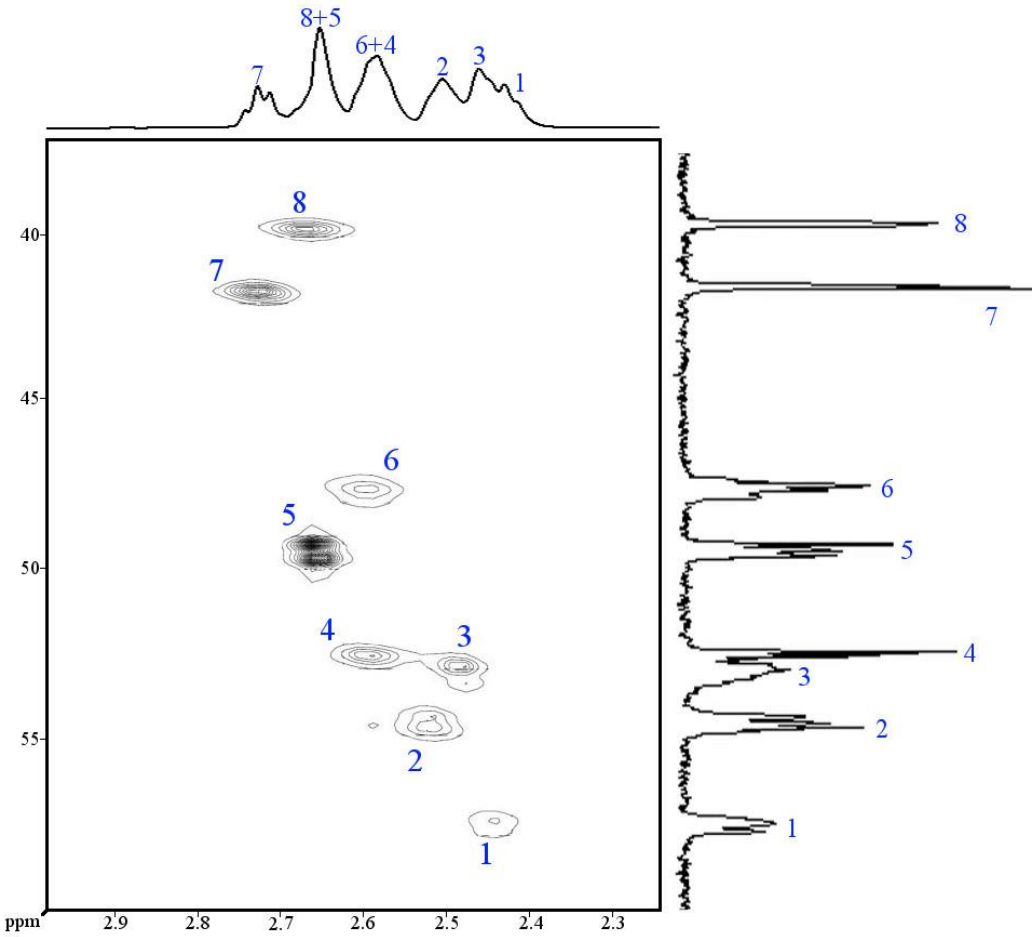

Figure 4.4 : Two dimensional HMQC NMR of PEI (M_n 600). ^{1}H NMR is displayed on the x-axis at the top, with ^{13}C NMR displayed on the y-axis on the right. Contours that appear on the main body of the spectra denote directly bonded carbon-proton nuclei.

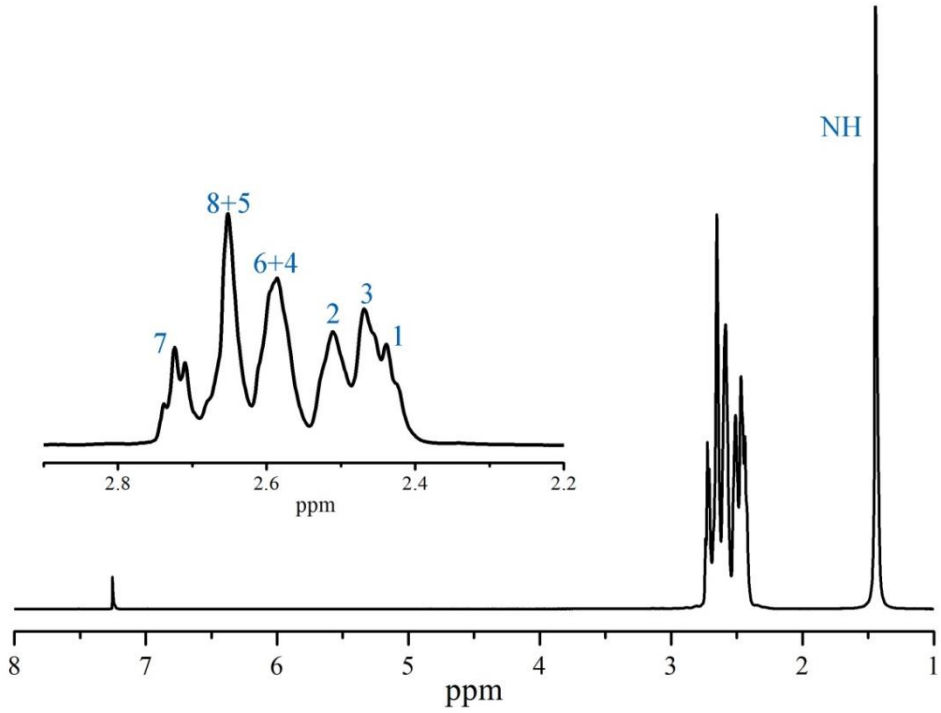

Figure 4.5 : ^{1}H NMR spectra of PEI (M_n 600) with peaks assigned. Assignments were made from peak correlations discovered in Figure 4.4, and protons groups were labelled in accordance with the structure shown in Figure 4.3 previously.

PEI-macroinitiator structure in Figures 4.6 and 4.7) is an approximation only; it serves as a guideline to illustrate the closest structure possible that can be constructed using this calculated average of amine sites.

Previously, the ^{1}H NMR structure of PEI (M_n 600) had not been assigned due to the complex collection of peaks that overlap between 2.3 and 2.8 ppm. Using 2D NMR techniques (heteronuclear multiple-quantum correlation, HMQC) the ^{1}H NMR spectrum could be assigned due to the elucidation of carbon-proton nuclei. The 2D HMQC spectrum produced is displayed on the previous page in Figure 4.4, whilst the assigned ^{1}H NMR spectrum is given in Figure 4.5 above.

4.4.1.2 Synthesis of PEI-macroinitiator

The synthesis of the PEI-macroinitiator was carried out by the careful addition of 2-bromo-2-methylpropanoyl bromide to a solution of PEI, with both reagents dissolved in dichloromethane (DCM). After being purified and collected under

reduced pressure the PEI-macroinitiator had the appearance of a dark brown, highly viscous liquid. Whilst the method that is fully described in Section 4.3.1 (and in Scheme 4.5), shows the process that was eventually used to repeatedly synthesise the initiator, the reaction had to first be fully developed.

Initially the synthesis was carried out in methanol (MeOH), as the manufacturer's description listed this specific PEI as soluble in low alcohols. After the reaction had been completed and the product collected, it was redissolved into DCM in order for it to be washed against an aqueous sodium

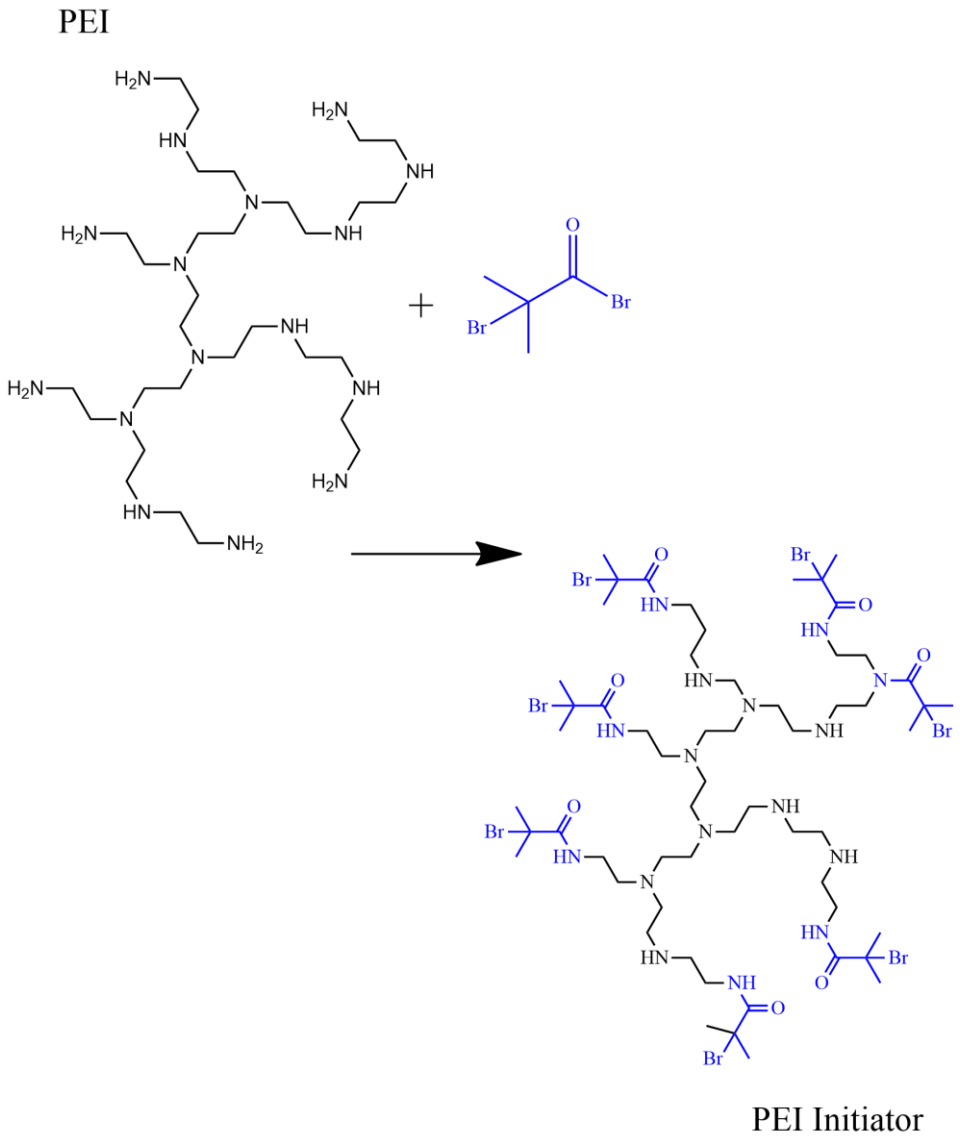

Scheme 4.5 : The synthetic route to produce the PEI initiator from an unmodified branched PEI with a molecular weight of 600. The ATRP initiating sites are highlighted in blue and result from the reaction of primary and (some) secondary amine sites on the PEI structure.

hydrogen carbonate solution. Due to the initiators solubility in both MeOH and DCM, it was decided to just use DCM for further reactions, removing one purification step. Unlike the synthesis of 2-bromo-2-methyl-*N*-propylpropanimde (MBrPA, amide initiator from Chapter 3) the addition of activated charcoal did not appear to reduce the colouration of the macro-initiator during purification. The same storage measures were adopted for the PEI-macroinitiator as had been used for MBrPA, namely the material being keep at a low temperature (4 ºC) and left out of direct sunlight. Due to its high viscosity it was impossible to inject a neat amount of PEI-macroinitiator through a septum into an ATRP reaction vessel. Instead, solutions of PEI-macroinitiator in ethanol were prepared, as it had been shown (in Chapter 3) to be the solvent of choice for amide initiated ATRPs of OEGMA.

The overall molecular structure of the PEI-macroinitiator and the unmodified PEI are comparable, with only some amine moieties being converted to amide ATRP initiator sites, whilst the core structure of the PEI remains unchanged. This is represented in Figure 4.6. Comparing the ^{1}H and ^{13}C NMR spectra of the starting PEI and the synthesised PEI-macroinitiator, the average number of sites available for ATRP initiation could be determined per PEI molecule. Integration of the area between 2.38 ppm and 2.75 ppm on the starting PEI ^{1}H NMR spectrum (Figure 4.6) gave a signal intensity that was referenced to a known number of protons derived from the calculated average structure. Likewise, the peak centred at 1.9 ppm on the PEI-macroinitiator is the result of the dimethyl group adjacent to the initiating bromine atom for ATRP. The ratio of these two signal intensities could be corrected to give an average the number of ATRP initiating sites per PEI molecule; 6.6.

Due to the complex nature of the NMR spectra, and the fact that the predicted structure of PEI and PEI-macroinitiator are only averages, the location of individual ATRP initiation sites within the PEI molecules are difficult to discern. However, the ratio of 1º, 2º and 3º amine sites had been previously determined: six 1º, six 2º, and four 3º.

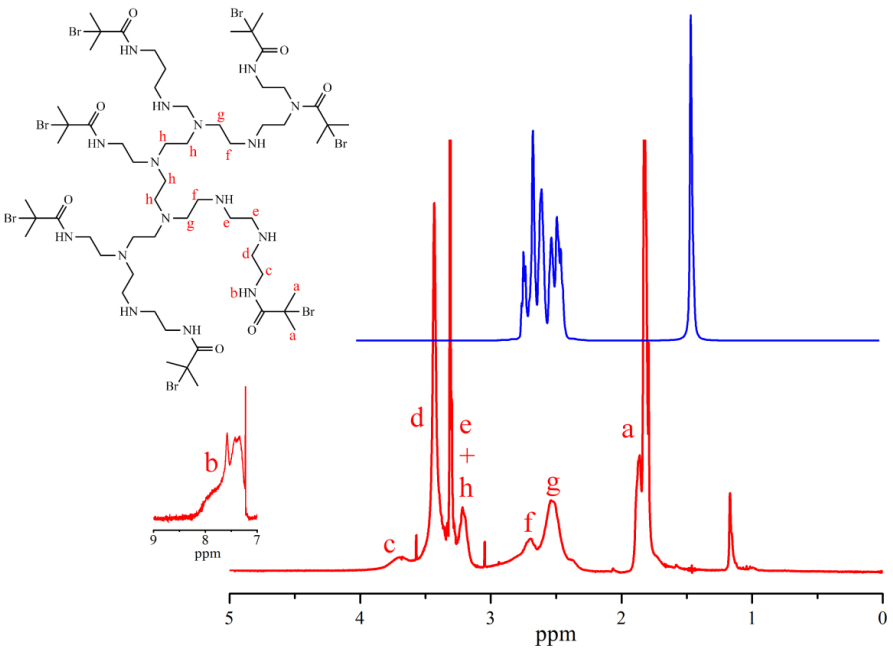

Figure 4.6 : ^{1}H NMR spectra of PEI M_n 600 (top, in blue) and PEI-macroinitiator (bottom, in red). The signal labelled "a" clearly shows the presence of the dimethyl group associated with the ATRP initiating bromine. "b" is also shown at 7.5 ppm, and is indicative of the presence of an N-H proton as part of an amide bond

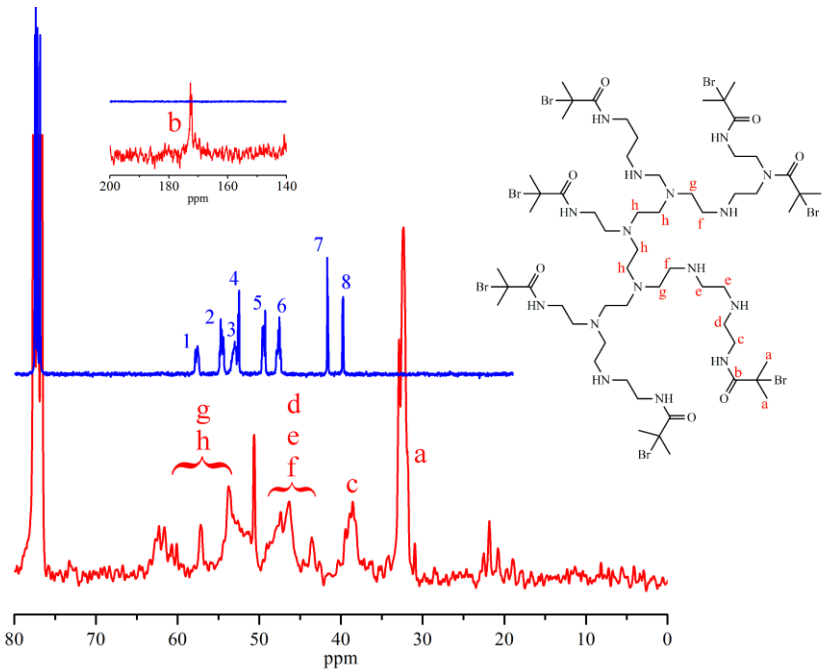

Figure 4.7 : ^{13}C NMR spectra of PEI M_n 600 (top, in blue) and PEI-macroinitiator (bottom, in red). "a" and "b" show the presence of the dimethyl and amide carbons respectively. The shift of carbon 4 (from figure 4.1) to "d" is indicative of some of the 2º amine sites reacting, due to its adjacency to the 2º amine site.

The disappearance of signals corresponding to carbons 7 and 8 in the ^{13}C spectrum of the PEI-macroinitiator suggests that all 1º amine sites have reacted and now provide an amide function. The number of initiation sites calculated (6.6), means that it is clear that some of the 2º amine sites must also have reacted. This can be observed again on the ^{13}C spectrum of the PEI-macroinitiator by noticing the shift in the signal corresponding to carbon 4 (which is adjacent to a 2º amine and carbon 7) from 52.5 ppm in the starting PEI, to around 45 ppm on the macroinitiator.

4.4.2 Synthesis of PEI-*graft*-POEGMA

With the successful synthesis of a PEI-macroinitiator, the ATRP of OEGMA was carried out using the experimental conditions that were outlined for amide initiated ATRP in Chapter 3. It was demonstrated that for the ATRP of OEGMA using MBrPA, the ideal reaction used CuCl and dNBpy as the catalyst system, and ethanol as the solvent in a 3:1 ratio with monomer. This was shown to enable polymerisations with higher monomer conversions, producing polymers with narrower dispersities, and more controlled molecular weight parameters, than had been attainable with other reagents or conditions. It was thought that the same results would carry over to polymerisations using the PEI-macroinitiator due to the grafted initiating moieties being analogous to MBrPA. The results of the polymerisations using the PEI-macroinitiator were a series of polymers with differing molecular weights, and dispersities at or below 1.4. These results are displayed in Table 4.1.

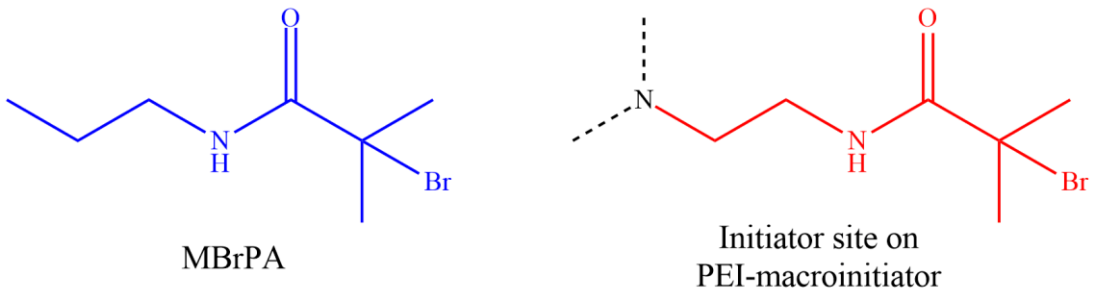

Figure 4.8 : Structures of MBrPA (blue, amide initiator from chapter 3) and one ATRP initiation site in the PEI-macroinitiator (red).

Table 4.1 : Amide and PEI-macroinitiator (PEI-Br) polymerisations using CuCl/dNBpy catalyst system and a 3:1 solvent monomer ratio.

Sample ID	I	[M]/[I]	$M_{n\,(exp)}$	$M_{n\,(SEC\ Triple)}$[a]	$M_{n\,(th)}$[b]	Đ	Conv. (%)[c]
A1	Amide	50	12400	-	10700	1.12	64
P1	PEI-Br	50	15150	-	1150	1.23	7.5
P2	PEI-Br	50	27350	26500	13700	1.40	83
P3	PEI-Br	50	47200	-	10400	1.40	63
P4	PEI-Br	100	30850	28400	19500	1.25	59
P5	PEI-Br	100	32150	-	32700	1.27	99
P6	PEI-Br	50	n/a	n/a	n/a	n/a	n/a

[a]SEC M_n determined from triple-detection SEC.
[b]$M_{n(th)}$ was calculated by : [M]/[I] x $M_{n(0)}$ x % conversion.
[c]Conversion calculated by ^{1}H NMR

Sample A1 corresponds to a reaction that was initiated by MPBrPA (as a reference) and shows a low dispersity with experimental molecular weight values close to those predicted theoretically, as was expected from the optimised reaction conditions. Samples P1-6 were initiated by the PEI macroinitiator and produced much more variable results. P1 displays an extremely low conversion for the molecular weight of the polymer produced, because of this there is a large discrepancy between theoretical and experimental molecular weight values. This is likely to be caused by early termination reactions occurring during the polymerisation before propagation can occur. Adams *et al* have previously observed that following polymerisations using amide initiators there are high levels of unreacted initiator,[46] and bond dissociation calculations in Chapter 3 suggest this might result from $Cu(II)Cl_2$ species reacting with initiation sites before propagation to a polymer chain can occur. Samples P2-5 were more successful, with monomer conversion amounts generally reaching over 60 %.

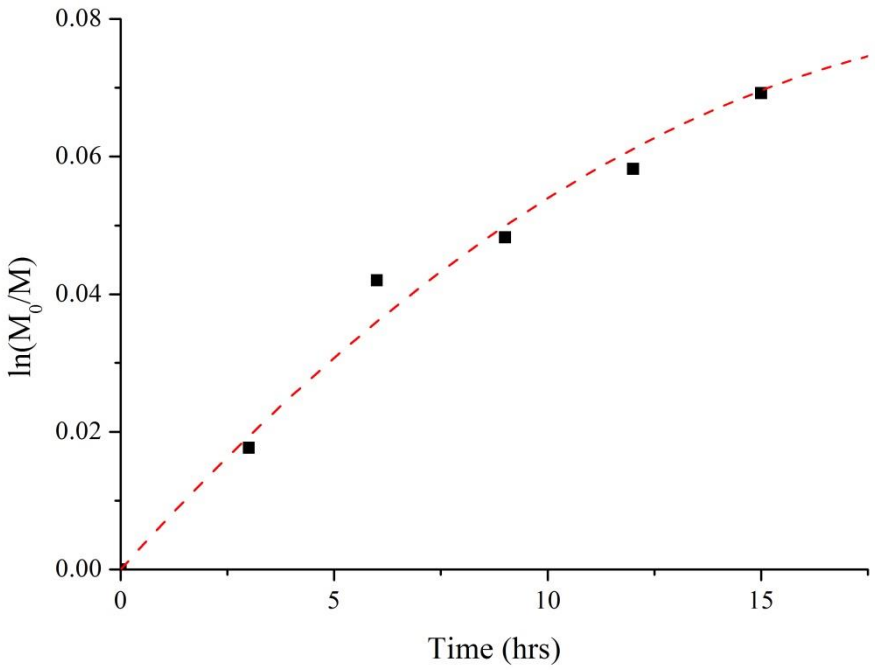

Figure 4.9 : Pseudo first order plot of sample P1 displaying $\ln(M_0/M)$ over time during the ATRP of OEGMA using the PEI-macroinitiator. Similar to amide polymerisations in chapter three the plot has a clearly non-linear trend indicative of early termination reactions

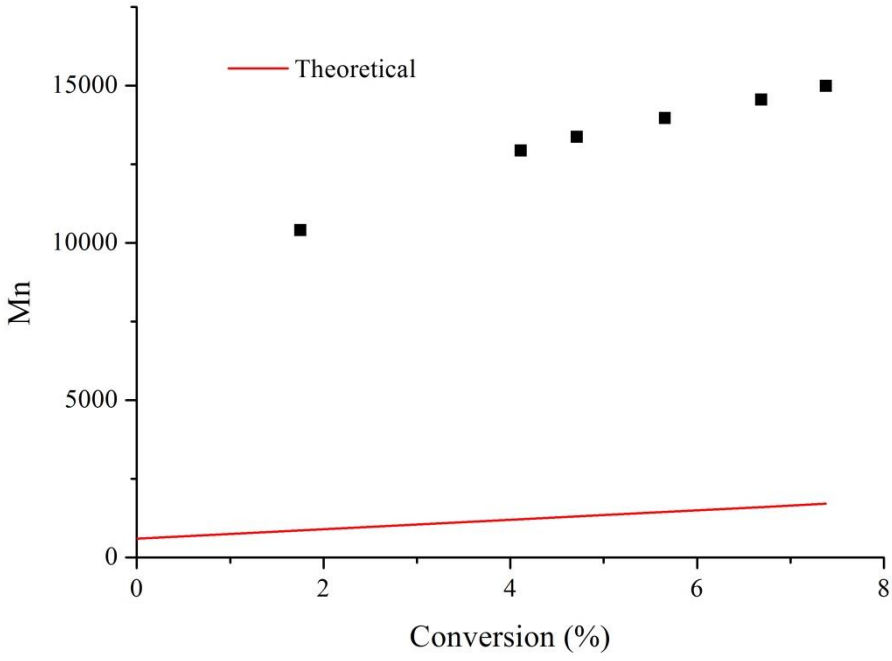

Figure 4.10 : A plot displaying the molecular weight of PEI-graft-POEGMA (P1) over time during a sampled ATRP using the PEI-macroinitiator. Due to the extremely low conversion of monomer the experimental values for M_n were much l higher than theoretical values

P6 represents a polymerisation that failed to produce a polymer. Similarly to several of the reactions that were carried out in Chapter 3, not every ATRP using the PEI-macroinitiator was successful. Generally an unsuccessful reaction exhibited a colour change from brown to green following initiation, which could either be the result of losing control of the nitrogen atmosphere within the reaction vessel, or an irreversible build-up of $Cu(II)Cl_2$ due to termination reactions before propagation could occur.

SEC triple-detection was used on samples P2 and P4 in order to determine whether there was any significant difference when compared to conventional single channel SEC. Conventional SEC (listed as "$M_{n\ exp}$" in Table 4.1) was carried out using a Shodex RI-101 refractive index detector, calibrated against linear poly(methyl methacrylate) (PMMA) standards. However, PEI-*graft*-POEGMA possesses a hyperbranched structure, with a PEI core providing on average 6.6 sites for OEGMA chains to polymerise from. SEC triple-detection utilises a concentration detector (normally refractive index or ultra violet), alongside a light scattering detector, and a viscometer. In this setup the viscometer is calibrated against a universal standard, derived from known values

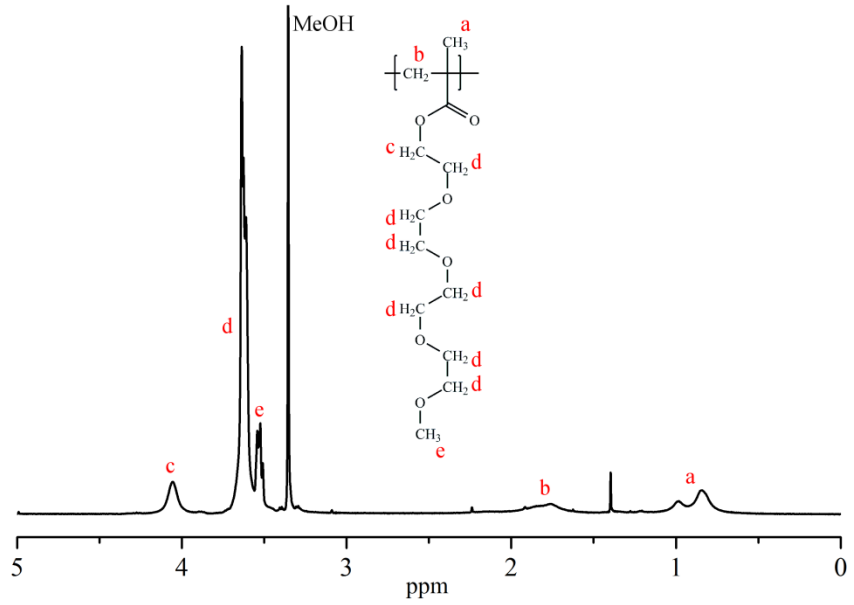

Figure 4.11 : ^{1}H NMR spectra of precipitated PEI-*graft*-POEGMA (PII) sample with peak assignment. Peak "a" displays splitting due to the atactic nature of the MMA backbone in the polymer chain. Consecutive methylene groups along the chain are not magnetically equivalent, giving rise to the appearance more than one signal.

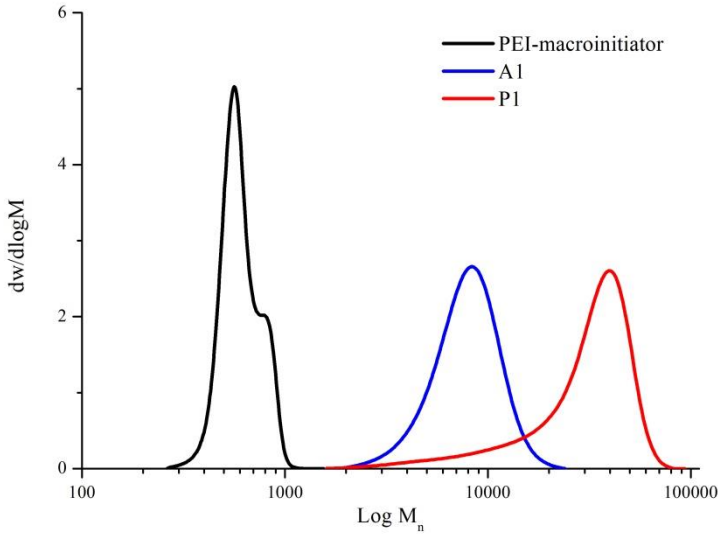

Figure 4.12 : Conventional SEC molecular weight distributions for the PEI-macroinitiator (black, left), sample A1 (blue, middle), and P1 (red, right).

that are independent from the properties of polymers to be analysed, and the light scattering result provides an absolute value for molecular weight. Whilst long-chain branching can have a more profound effect on SEC results, short-chains (as are often found in ATRP) normally have a smaller impact.[52]

SEC triple-detection provided M_n values that showed only a 3.1% difference for sample P2, and 7.9% difference for sample P4. Even though there is a significant difference in molecular structure between the linear PMMA standards and synthesised PEI-*graft*-POEGMA, the maximum chain length possible for POEGMA to reach from the PEI core is only 15 units, assuming 6.6 initiating sites, in the highest M_n sample: P5. These short-chains do not appear to be long enough to cause significant deviation in results between SEC triple-detection and SEC single detection; however SEC triple-detection did supply lower M_n values for both samples, suggesting conventional SEC tends to slightly overestimate the actual M_n in these branched polymers.

4.4.2.1 Copper removal from PEI-*graft*-POEGMA

Figure 4.13 : A portion of sample P1, showing the green colour of the polymer that persisted following passage through alumina columns and precipitation into hexane.

Samples of PEI-*graft*-POEGMA produced possessed a green colouration even after multiple passages through columns and precipitations. This was due to the copper catalyst from the ATRP forming a complex with the PEI core, an effect that has been widely reported previously.[53, 54] Complexation occurs due to the numerous amine nitrogen atoms present within the structure, which can act as electron donors in order to chelate metal ions.[55] In fact, PEI has been previously used as part the catalyst system for the ATRP of MMA in an effort to produce a recoverable catalyst.[56]

In attempt to remove the copper from the PEI-*graft*-POEGMA samples, a dialysis system was setup, with the polymer dissolved in water behind dialysis tubing, and then placed into a tank with a competitive catalyst. Initially EDTA

Figure 4.14 : PMDETA/water dialysis tank after 48 hours. The polymer sample was dissolved in water within the holder, behind dialysis tubing. The blue colouration is due to the presence of chelated copper ions.

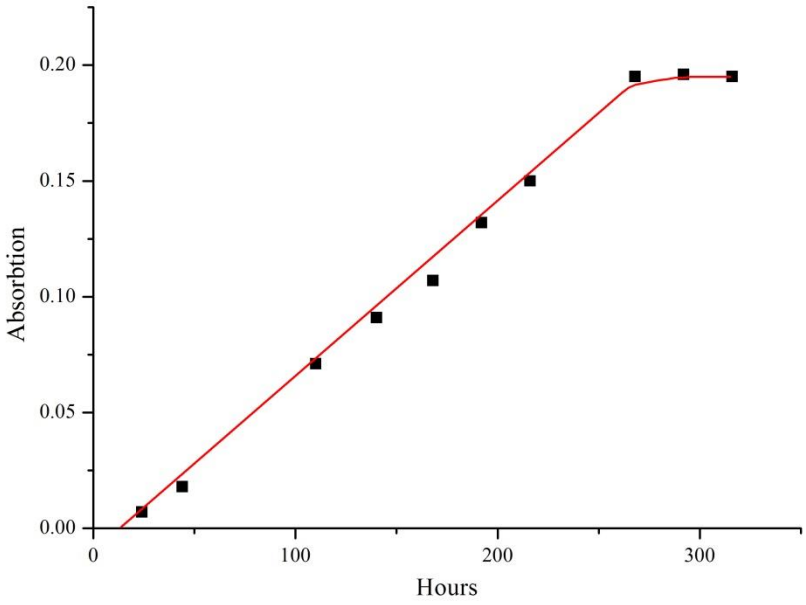

Figure 4.15 : Plot showing the increasing absorption of the signal relating to Cu(II) over time. After two weeks of dialysis no further increase in intensity was observed.

(20 g in 4L of water) was used in order to create the concentration gradient, as it had been reported that EDTA can compete against PEI to form complexes with copper.[55] After leaving the dialysis running for 24 hours, then replacing the EDTA/water solution and running the dialysis for a further 48 hours, the polymer was recollected but still possessed a green colour. The dialysis was repeated using N,N,N',N',N''-pentamethyldiethylenetriamine (PMDETA) (10 ml in 4L of water) as the competing ligand. This time after 24 hours the tank of ligand/water turned light blue, indicative of copper complexation with the PMDETA, as is shown in Figure 4.14. The external solution was replaced, and then samples were taken from the PMDETA/water solution for UV analysis.

PMDETA/water samples were recovered over the following 320 hours (two weeks), until the UV signal associated with Cu(II) species stopped increasing, as show in Figure 4.15 above. Again the polymer was recovered, yielding a green viscous liquid. Samples of dialysed and non-dialysed polymer were analysed by UV spectrometry to determine if any significant reduction in copper had occurred, with the spectra displayed in Figure 4.16.

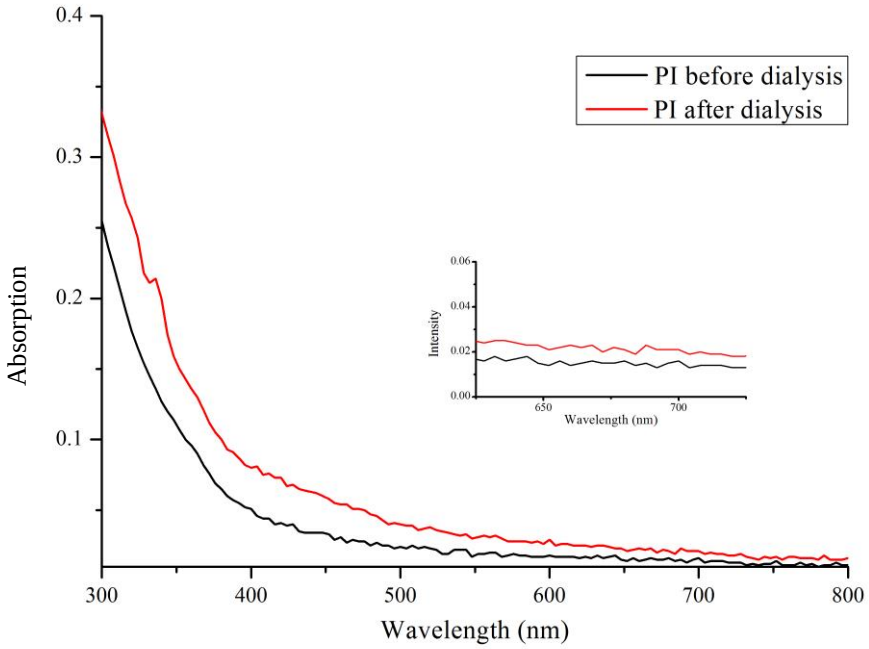

Figure 4.16 : UV visible spectra of PI before (black) and after (red) dialysis with PMDETA/water. The inset shows the region around 684 nm where a peak relating to Cu(II) species was present in the presence of PMDETA.

The UV spectra of the PEI-*graft*-POEGMA before and after dialysis show small differences in absorption due to minor concentration disparity and the spectra do not display any sort of absorption above 500 nm that would be expected if there was chelated copper (II) species in the sample. Despite this, both samples still possessed a distinct green hue. A further method of determining the concentration of copper remaining in the samples would be atomic absorption spectroscopy, but instead a study was performed to determine how detrimental the presence of copper was to the binding sites present in the PEI.

4.4.3 Determination of PEI-*graft*-POEGMA DNA complexation

4.4.3.1 Ethidium bromide exclusion assay

Whilst the green colouration of both the un-dialysed and dialysed polymer, and the blue colouration of the dialysis solution both indicate the presence of

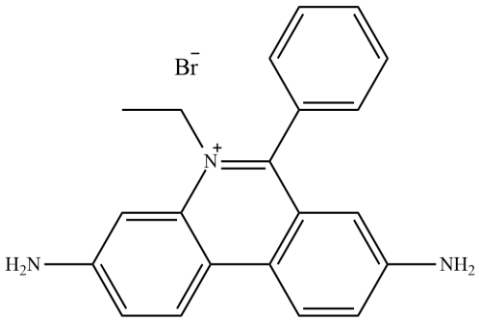

Figure 4.17 : Chemical structure of ethidium bromide (EthBr).

remaining catalytic system (copper), UV-visible spectroscopy was unable to provide answers to how much copper was present, or whether it would affect the ability of the polymer for applications requiring electron donation from the amines in the PEI core. Instead, an investigation into the ability of the PEI-*graft*-POEGMA to complex DNA would elucidate how active the PEI amine sites remained after ATRP with OEGMA.

PEI is well known for its ability to form complexes with DNA due to the large number of proton donation sites resulting from numerous amine groups within the structure.[37, 41, 57] A common method of determining the ability of a molecule to complex with DNA uses fluorescence spectroscopy to perform an ethidium

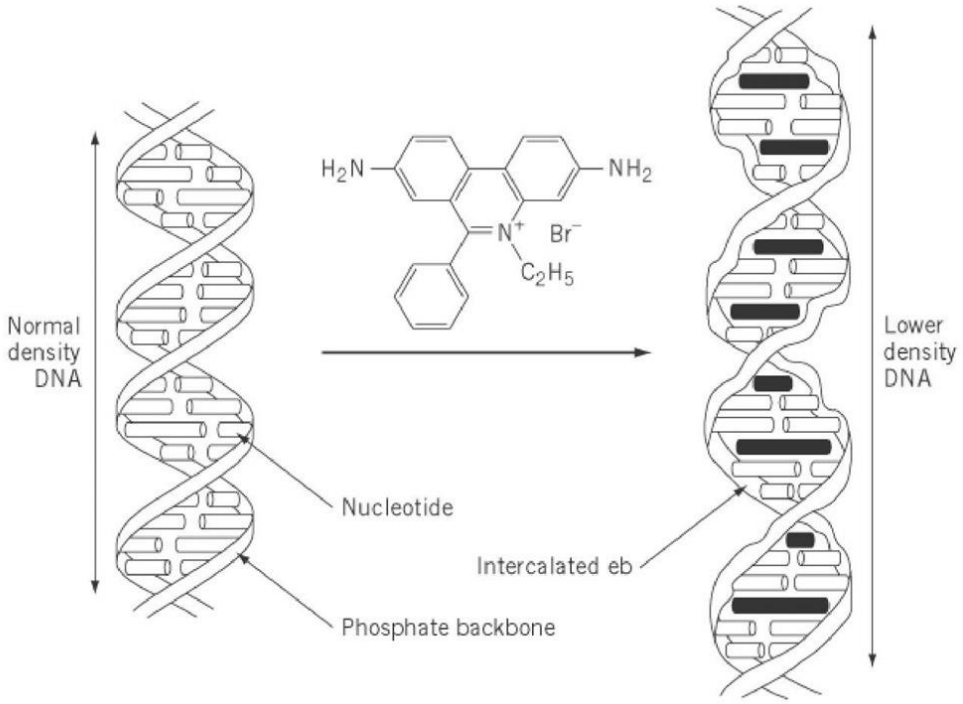

Figure 4.18 : Illustration showing the intercalation of EthBr into a strand of DNA. The presence of the EthBr causes an elongation of the DNA strand as it fits between adjacent nucleotide base pairs.[60]

bromide (EthBr) exclusion assay.[58-60] EthBr is inherently UV fluorescent due to its aromatic structure, this fluorescence increases in an aqueous solution when EthBr intercalates between DNA strands, due to it having entered a hydrophobic area away from the solvent. Without DNA intercalation, EthBr molecules are quenched by the aqueous solvent, and the fluorescence is reduced. When something that can complex with DNA is added to the system, such as PEI, the EthBr is forced to dissociate from intercalation, triggering the re-quenching of the molecule, and lowering the observed fluorescence. Intercalation of DNA occurs when the heteroaromatic EthBr molecule is inserted between adjacent nucleotide base pairs of a DNA strand.[58, 60, 61] Specifically, hydrogen bonding occurs between the 3,8 amino substiuents of the EthBr molecule and the phosphate groups present in the DNA.

To carry out the exclusion assay solutions of EthBr in distilled water were prepared and placed in a quartz cuvette. A DNA and water solution was added to this and then gently mixed before recording the initial fluorescence intensity. The PEI and PEI-graft-POEGMA were then added to the DNA/EthBr solution in portions and with each addition a new emission spectrum was produced, as is described in section 4.3.4.2. At the start of each experiment the cuvette contained 0.002mg of EthBr, 0.004mg of DNA, and 0.4 µg of polymer were added with each separate addition, with no correction for the difference in M_n between the materials made at this time. The generic emission spectra produced

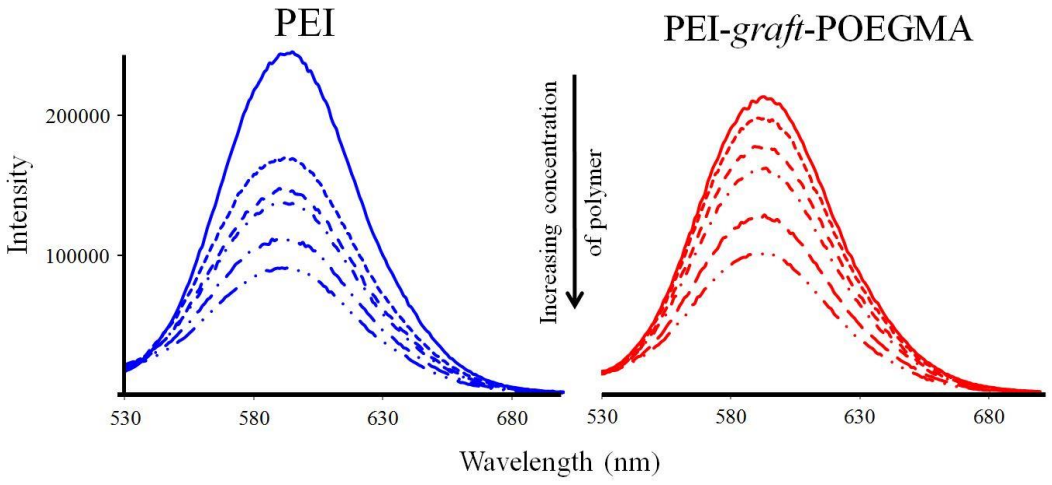

Figure 4.19 : Generic emission spectra produced by EthBr exclusion assay of PEI M_n600 (left, blue) and PEI-*graft*-POEGMA PIII (right, red). As the amount of polymer increases within the system fluorescence quenching occurs in both samples and the overall signal intensity decreases.

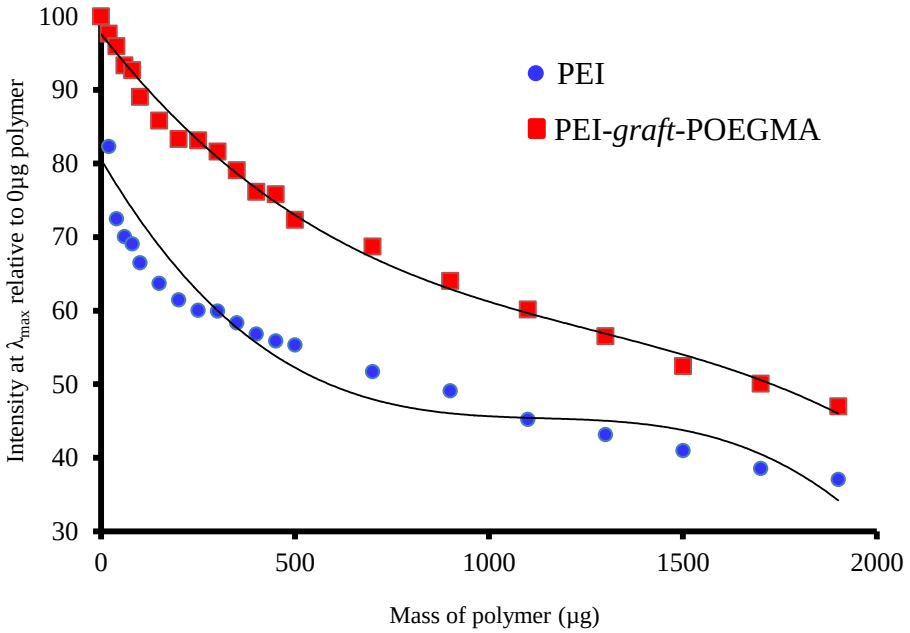

Figure 4.20 : UV-fluorescence plots of the signal intensity relative to the starting intensity (where 100 is purely EthBr/DNA. The PEI M_n 600 sample is displayed as blue, whilst the PEI-*graft*-POEGMA sample is shown as red. The overall DNA quantity remains constant in the sample, as polymer is added EthBr is forced out of intercalation triggering a loss of fluorescence relative to the starting value.

by the polymer additions are displayed in Figure 4.19, and a plot of the fluorescence intensity relative to the starting fluorescence (without either polymer) is given in Figure 4.20. It is clear that the intensity of the spectra decreased with the addition of both PEI and

PEI-*graft*-POEGMA. As more of the polymer was added into the sample, EthBr dissociated from DNA and entered the aqueous environment, triggering a loss of fluorescence as quenching occurred.

Whilst the overall intensity loss for the PEI sample was greater than that of the PEI-*graft*-POEGMA at a given mass of polymer added, the molecular weights of the two samples were vastly different. The PEI sample had a M_n of 600, whilst the PEI-*graft*-POEGMA sample had a M_n of 27350 (sample P2 in Table 4.1). This means that for every 1 µg of sample P2 added to the EthBr solution, there was around 46 µg of PEI in the equivalent sample of unmodified PEI. Additional emission spectra were produced after remaking polymer solutions so that they contained equivalent weight percentages with respect to PEI core. The plots constructed from the data (Figure 4.21) indicate that the PEI-*graft*-

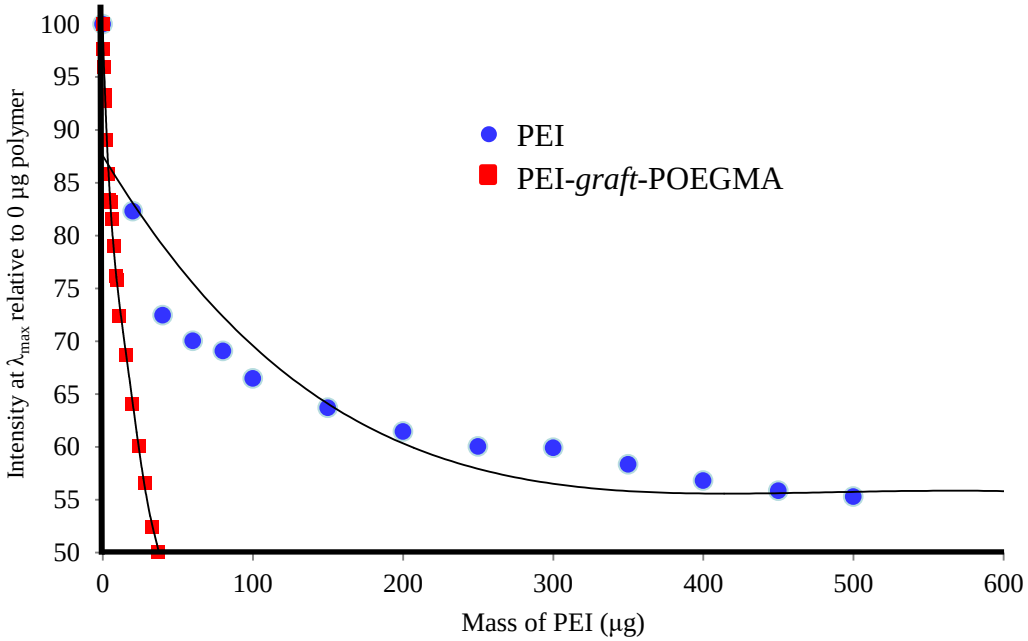

Figure 4.21 : UV-fluorescence plots of the signal intensity relative to the starting intensity (where 100 is purely EthBr/DNA) against the corrected mass of PEI within the two samples. The PEI M_n 600 sample is displayed as blue, whilst the PEI-*graft*-POEGMA sample (PII) is shown as red. PII clearly displays a greater efficiency at displacing EthBr from DNA as evidenced by the rapid loss of signal intensity in the copolymer spectrum

POEGMA has a significantly increased efficiency at displacing intercalated EthBr from DNA when compared to the unmodified PEI. It has previously been reported by Cheng *et al*, that PNIPAAm based PEI copolymers can exhibit comparable, or even higher, transfection efficiencies when compared to unmodified PEI.[40] From the data presented here the transfection efficiency for PEI-graft-POEGMA appears to be orders of magnitude higher than the unmodified hyperbranched PEI. In fact, the large increase in efficiency was so surprising that further investigation into this result would have been desirable in case of experimental error; but unfortunately this was not carried out due to completion of the associated masters program.

4.4.3.2 DLS measurements of Polymer DNA complexes

An alternative method to valdiating the ability of PEI-*graft*-POEGMA to complex with DNA is by using dynamic light scattering (DLS), which gives a size distribution profile of particles in a solution. 0.01 mg/ml samples were prepared of PEI, PEI-*graft*-POEGMA and DNA, as well as 0.01 mg/ml PEI or

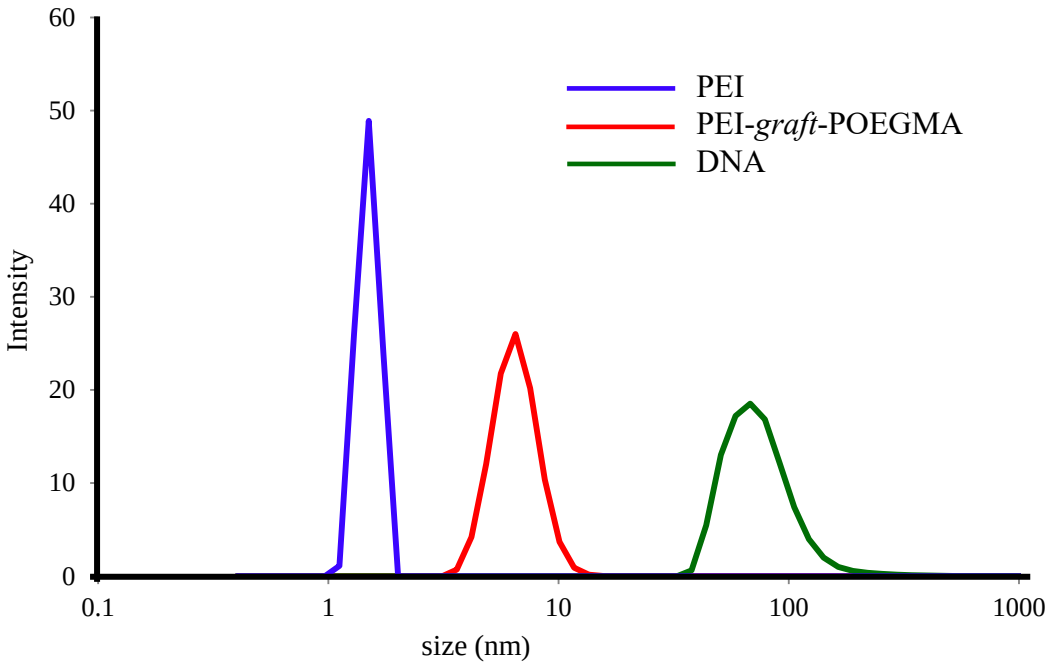

Figure 4.22 : Plot produced from DLS data showing number average size distributions for PEI (blue – 1.5 nm), PEI-*graft*-POEGMA (red – 6.5 nm), and DNA (green – 65 nm)

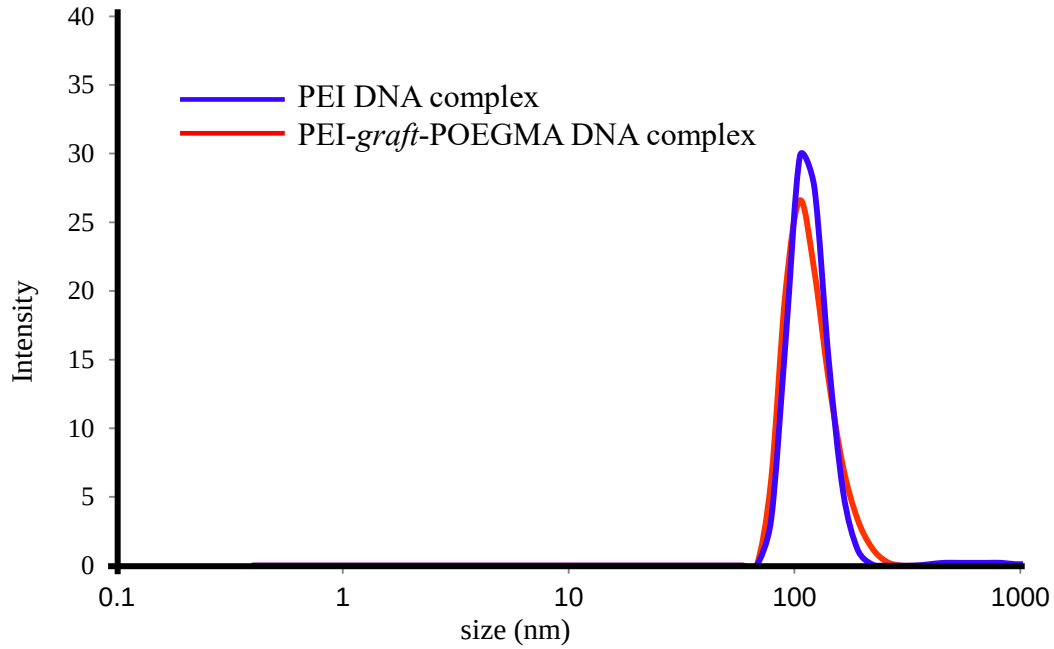

Figure 4.23 : Plot produced from DLS data showing number average size distributions of PEI with DNA (blue – 105 nm) and PEI-*graft*-POEGMA with DNA (red – 105 nm). The disappearance of signals at 1.5 nm and 6.5 nm for PEI and PEI-*graft*-POEGMA respectively, indicate that both polymers are forming complexes with the DNA.

Table 4.2 : DLS measurements of PEI, PEI-*graft*-POEGMA and DNA samples

Sample	Number average size (nm)
PEI	1.5
PEI-*graft*-POEGMA	6.5
DNA	65
PEI + DNA	105
PEI-*graft*-POEGMA + DNA	105

PEI-*graft*-POEGMA with 0.02mg/ml of DNA samples, and then subjected to DLS at 25 ºC after 2 minutes of incubation. Size distributions produced from these samples can be seen on the following page in Figures 4.22 and 4.23, with specific number average data points displayed in Table 4.2

As expeceted, Figure 4.22 shows that unmodified PEI had the smallest individual particle size, with a number average of 1.5 nm. PEI-*graft*-POEGMA was larger than unmodified PEI due to the increased volume associated with grafter POEGMA

chains, and measured 6.5 nm. Finally the DNA sample possessed the largest individual size at 68 nm.

The size distibution plot of PEI with DNA and PEI-graft-POEGMA with DNA both suggest that the polymers are forming complexes with the DNA. The disappearance of signals at 1.5 nm and 6.5 nm in figure 4.23 implies that there is no polymer left in solution that is not complexing to DNA. This is reinforced by the prescence of a single peak for each sample centred at 105 nm, suggesting a small hydrodynamic expansion as the polymers complex to the DNA, which can be attributed to the known elongation of DNA strands as intercalation occurs.[58, 59, 61]

This data, and the EthBr exclusion assay, was performed by Tom Ashton under supervision of Simon Holder.

4.4.4 Characterisation of PEI-*graft*-POEGMA stabilised magnetic nanoparticles

With the data provided by DNA complexation implying that PEI-*graft*-POEGMA still had active amine sites, a sample was sent to collaborators (Cem Atlan and U. Ecem Yarar) for the preparation of polymer stabilised magnetic nanoparticles.

The coprecipitation method for the preparation of magnetic nanoparticles has been widely reported for the creation of randomly oriented crystalline particles, that possess various morphologies and sizes in the 10 nm range.[62] This method was successfully used to synthesise superparamagnetic nanoparticles with, and

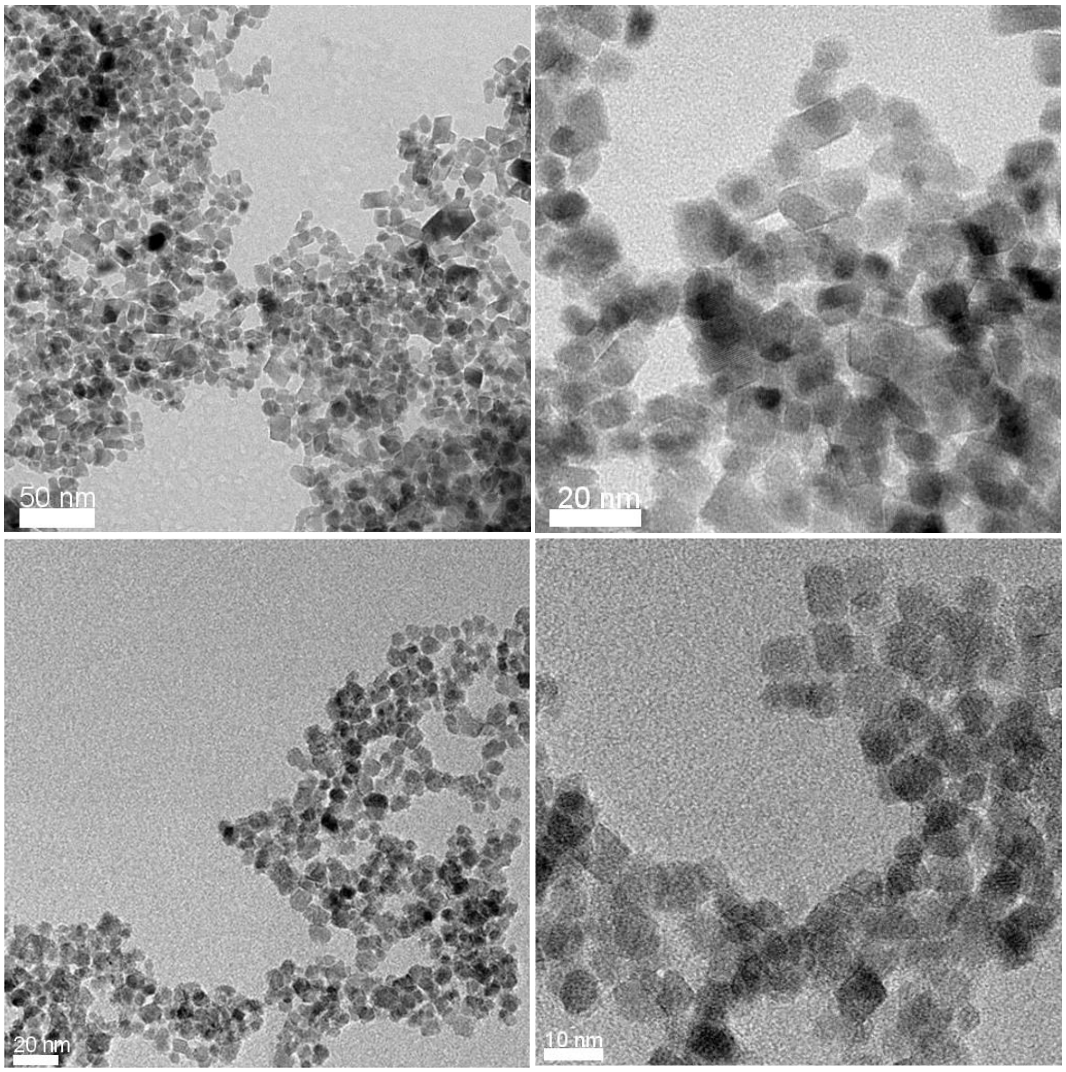

Figure 4.24 : TEM images of bare (top), and polymer stabilised (bottom) magnetic nanoparticles. Both pairs of images show that particles prepared share the same general morphology, size distributions also being similar across both samples.

without, PEI-*graft*-POEGMA (sample P2 in Table 4.1) acting as a stabiliser. The morphologies of synthesised particles were analysed using transmission election microscopy (TEM), with images produced displayed in Figure 4.24. Size, and size distribution, of prepared particles was calculated by measuring 150 individual particles and determined that bare particles had an average diameter of 7.9 nm (standard deviation: 1.5 nm), whilst stabilised particles had an average diameter of 7.4 nm (standard deviation: 1.35 nm).

X-ray diffraction analysis of the stabilised particles (Figure 4.25) shows that the spectrum produced has characteristic peaks that can be assigned to magnetite and/or maghemite, without the presence of any other iron oxide phases, matching closely to a spectrum produced by simulation for magnetite/maghemite. Peaks on XRD spectra correspond to the intensity of reflected x-rays as the sample is rotated through a range of angles, and specific iron oxide phases will display high counts (generating peaks) depending on their crystal structure.[63]

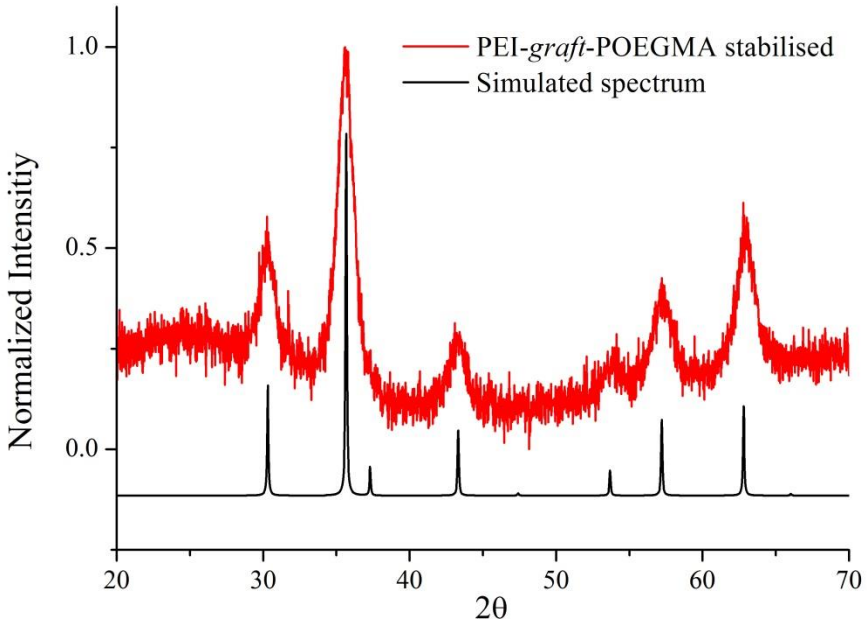

Figure 4.25 : XRD spectrum of PEI-*graft*-POEGMA stabilised magnetic nanoparticles (red) and a simulated spectrum for magnetite/maghemite nanoparticles. The polymer stabilised spectrum closely matches the simulated spectrum with obvious peak broadening arising from the non-uniform nature of prepared particles.

The magnetic properties of saturation magnetization, remenance and coercivity of the PEI-*graft*-POEGMA stabilised particles were compared to the bare particles using vibrating sample magnetometry. Figure 4.26 shows the spectra produced, with both hysteresis loops showing no coercivity or remenance, indicating that both materials are of a superparamagnetic nature. Polymer stabilised particles were found to have a saturation magnetisation of 40.7 emu/g, whereas for bare particles it was 48 emu/g, which is less than bulk magnetite. This discrepancy is most likely due to the polymer stabiliser due to the fact that both samples are of similar size and morphology. It has previously been shown that particles with different coatings can have low magnetisation values due to the non-magnetic surface coating that is surrounding the iron oxide core.[64]

Magnetic nanoparticles that were prepared were dispersed into distilled water by sonication immediately after synthesis. Polymer stabilised particles remained stable in suspension over a period of days, whilst bare particles aggregated and precipitated in a matter of minutes, as is displayed in the photographs shown in Figure 4.27.

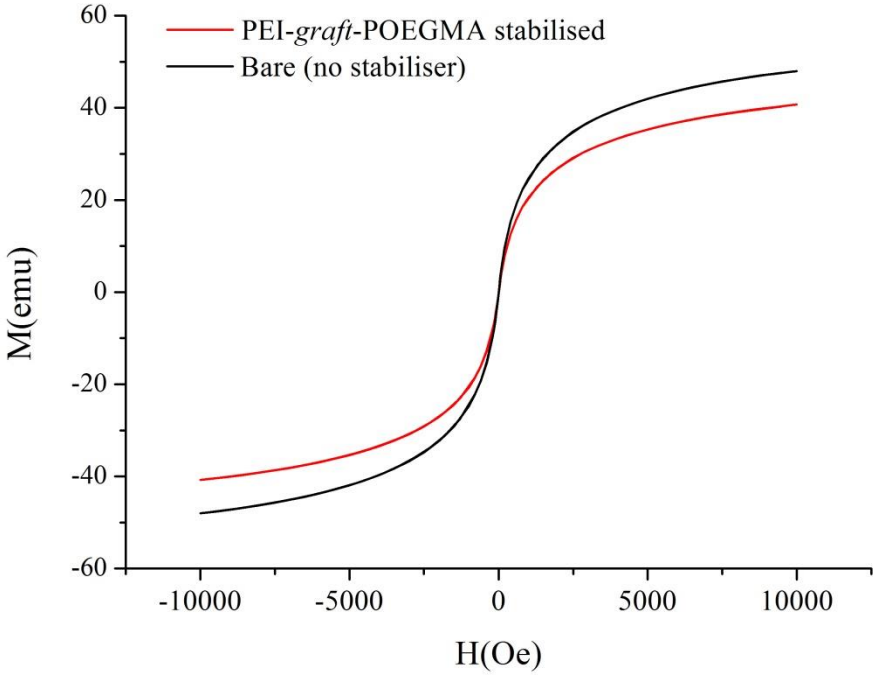

Figure 4.26 : Magnetisation curves of PEI-graft-POEGMA stabilised (red), and bare (black) iron oxide nanoparticles. Both samples show hysteresis loops indicative of superparamagnetism due to the lack of coercivity or remenance.[10]

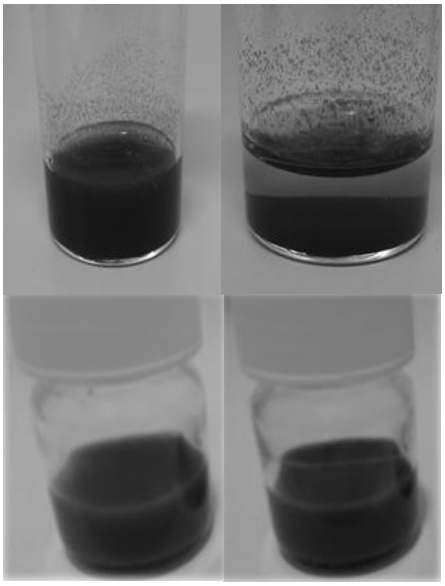

Figure 4.27 : Bare (top) and polymer stabilised (bottom) nanoparticles in distilled water. After 30 minutes the bare particles precipitated out of suspension (top right), whilst PEI-*graft*-POEGMA stabilised particles remained in suspension for days.

4.4.5 LCST of PEI-*graft*-POEGMA and thermoresponsive nature of PEI-*graft*-POEGMA stabilised nanoparticles

In Chapter 3 the ability of hydrophilic polymers to possess a LCST was discussed. Below this temperature a single phase molecular solution exists, and above it the polymer precipitates out of solution as it becomes hydrophobic. Solubility in water is lost as hydrogen bonds between the water molecules and the polymer break, causing the polymer to precipitate into a cloudy dispersion at the cloud point temperature: T_{CP}.[65-68] Previously, copolymers prepared partly from hydrophilic polymers have been used to create thermoresponsive materials due to this effect, as copolymers synthesised often share a similar LCST to the homopolymers used.[4, 67, 68]

1 wt% solutions of two polymers from table 4.1 (A1 and P3) and PEI-*graft*-POEGMA stabilised iron oxide nanoparticles in water were analysed by DLS and by visual monitoring in order to characterise the LCST of the prepared materials, the results of which are displayed in Figure 4.28 on the following

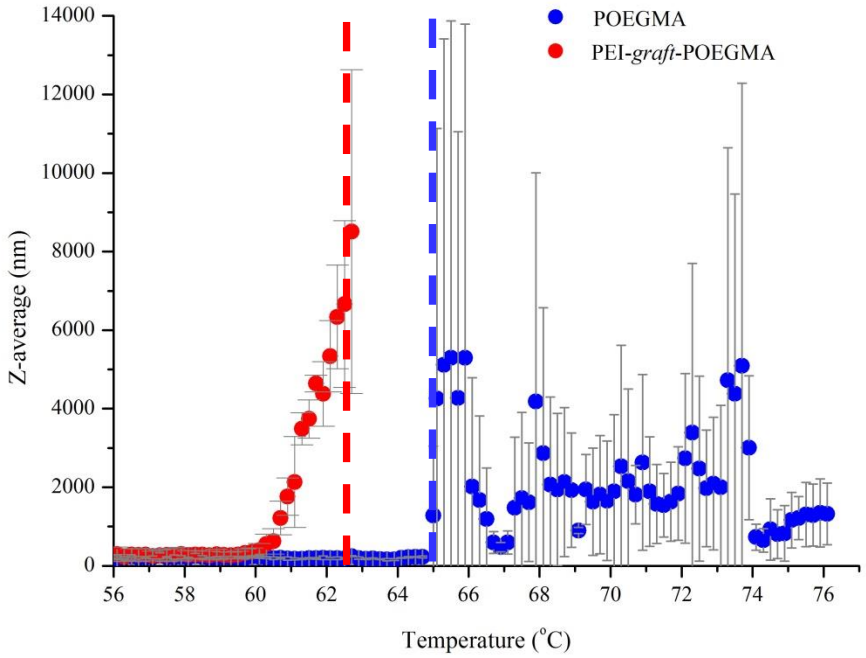

Figure 4.28 : DLS results for 1 wt% aqueous solutions of POEGMA (blue) and PEI-*graft*-POEGMA, vertical dashed lines indicate the temperature at which clouding of the solution was visible to the eye. "Z-average" (y-axis) is an intensity weighted mean of the hydrodynamic volume of the particles present.

page. At the T_{CP} of the sample particle sizes increase as the polymer precipitates, this is observable by DLS, and can be visually observed by the solution changing to a cloudy dispersion. Previous work has shown that POEGMA has a T_{CP} around 64 ºC, and this value can be controlled by adjusting the M_n of the polymer, its concentration in solution, or the specific architecture of the polymer.[29, 69]

A1, the linear POEGMA homopolymer, displayed a T_{CP} at 65 ºC when observed visually, and within the DLS data this temperature coincides with when the z-average size distribution of particles became non-uniform and increased in diameter. The variation in sizes that POEGMA particles displayed above 65 ºC implies that as the formerly hydrophilic section of the polymer chain collapse the created clusters are agglomerating in random distributions.

A T_{CP} of 65 ºC is in close agreement with literature values reported for POEGMA with similar overall molecular weights and side chain lengths. P3, PEI-*graft*-POEGMA, observed an increase in z-average size distributions that begun at 60.5 ºC when measured by DLS, but was not observed visually until 63

ºC. This lower T_{CP} value when compared to the homopolymer is not entirely surprising due to the fact that PEI is not known to possess a LCST, and the end-group polarity of a polymer is known to affect LCST.[70-72]

PEI-*graft*-POEGMA stabilised nanoparticles displayed significantly different properties. Even as the sample was incubated at room temperature before heating, there was considerable light scattering, and the z-average (particle diameters) had large standard deviations even over the course of multiple measurements (Figure 4.29). Three distinct phases of diameter were observed within the sample as the temperature was increased; a low diameter range below 40 ºC, a transition phase between 40 ºC and 52 ºC, and a higher diameter phase above 52 ºC. The same average distribution of particle diameters was observed at the same temperatures, over a series of repeated cycles of heating and cooling. Below 40 ºC particles displayed an average diameter of 59 ± 18 nm, which is around eight times larger than measured by TEM (7.4 ± 1.5 nm). This is indicative of particles forming clusters when suspended in aqueous solution as the increase is too large to be attributed to the hydrodynamic radius increase that would be expected from the addition of polymer to the surface of the particle. After heating to a temperature of 75 ºC particles showed an increase in average size to 92 ± 14 nm. The size change occurred over a temperature range of 40 to 52 ºC, with an inflection point of 46 ºC, as can be seen in Figure 4.31. No visual clouding of the solution was observed at any of the measured temperatures.

The LCST of a polymer has been shown to affected by macromolecular architecture, monomer ratio and polydispersity.[73] For POEGMA coated particle systems, such as gold nanoparticles or polystyrene micelles, distinct size effects have been noted.[74, 75] Holder *et al* showed that triblock (ABA) copolymers of POEGMA (A) and polystyrene (B) have a significantly lower T_{CP} (around 11 ºC) than POEGMA homopolymers over the same M_n range.[74] Ieong *et al* demonstrated that nanoparticle structures with a thermoresponsive shell observe a decrease in T_{CP} as the diameter of the particle increases. This was attributed to changes in in the polymer packing density due to the constrained nature of the system.[75] In these previously reported systems, precipitation of the polymer was always a result of raising the temperature above the T_{CP}, something that was not observed with PEI-*graft*-POEGMA polymer stabilised nanoparticles. In this instance, there was no full particle precipitation associated with temperature

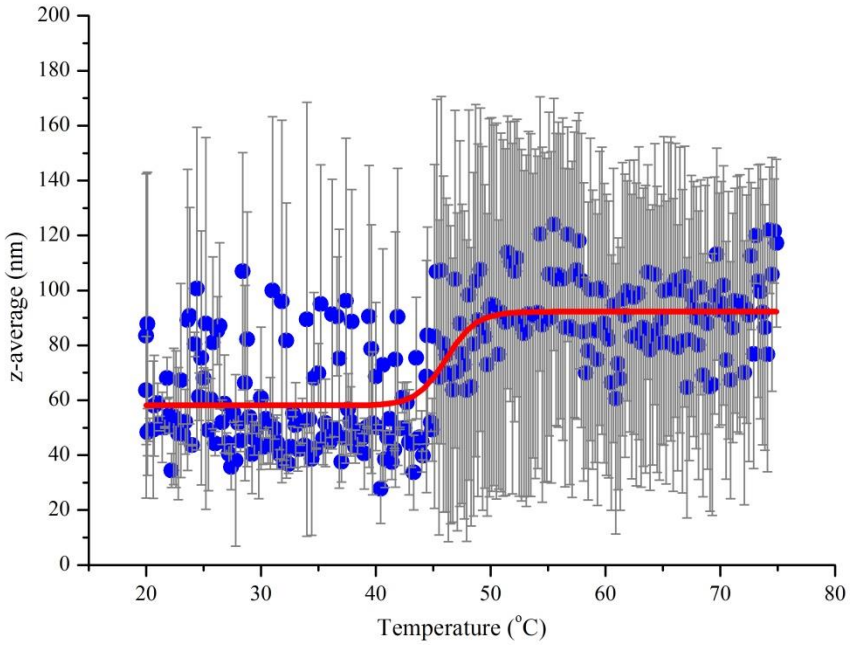

Figure 4.29 : DLS results for 1 wt% aqueous solutions of PEI-*graft*-POEGMA stabilised nanoparticles showing the variation in particles sizes as temperature changed.

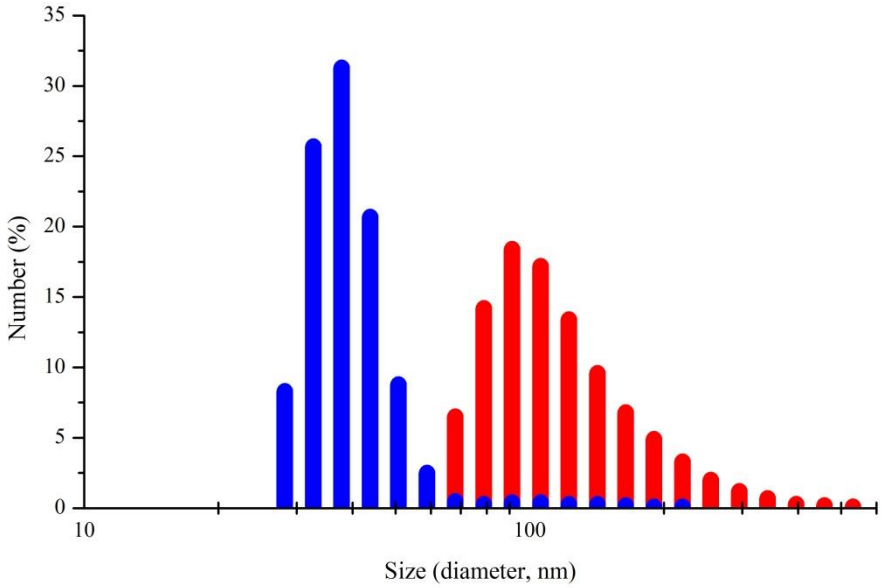

Figure 4.30 : DLS results for PEI-*graft*-POEGMA stabilised nanoparticles showing size distributions at 20 ºC (blue) and 50 ºC (red).

change, even with an increase in average particle size, and no full T_{CP} was observable by DLS or visible clouding.

Iron oxide magnetic nanoparticles forming clusters in solution is a well-known phenomenon, and recently experimental effort has been directed towards controlling the size of clusters, and their morphology.[76-79] A facile route to controllable magnetic nanoparticle clusters with tuneable cluster size would be desirable for a range of applications including: sealants, damping agents, and separation aids.[80-83] From the individual particle size measured from TEM (figure 4.17), and assuming that the particles are irregularly packed in a spherical conformation,[84] the average cluster size of PEI-graft-POEGMA stabilised magnetic nanoparticles increases from around 300 particles to 1200 particles across the temperature range from 20 to 75 ºC.

4.5 Conclusions

A facile synthetic route for the preparation of PEI-*graft*-POEGMA was developed utilising a commercially available branched PEI as a starting point.

The purchased PEI was analysed by conventional and two dimensional NMR techniques to elucidate its structure, and the number of primary, secondary and tertiary amines present was determined to be different from what was reported by the supplier. The branched PEI was used to synthesise a poly-amide ATRP macro initiator that was used in the polymerisation of OEGMA.

PEI-*graft*-POEGMA synthesised via ATRP had low dispersities (<1.4), but experimentally observed M_n values were not in close agreement to theoretically expected results. Whilst PEI-*graft*-POEGMA samples remained green after repeated methods to purify them (most likely due to the presence of copper from the ATRP catalytic system), the ability of the polymer to complex DNA was not hindered, and even surpassed the transfection efficiency of unmodified PEI at equivalent weight percentages. This suggested that any copper being chelated by the amine core of the polymer was in very small quantities.

PEI-*graft*-POEGMA demonstrated its utility by its ready use as a stabiliser in the preparation of superparamagnetic nanoparticles. Particles stabilised by the polymer showed no deviation in magnetic characteristics when compared to un-

stabilised particles prepared by the same method. Stabilised particles remained in suspension over a timescale of days, whereas un-stabilised particles were observed to agglomerate rapidly and settle out of suspension in a matter of minutes.

The thermoresponsive nature of POEGMA was transferred to PEI-*graft*-POEGMA and PEI-*graft*-POEGMA stabilised magnetic nanoparticles. A sample of PEI-*graft*-POEGMA possessed a T_{CP} of 60.5 ºC, around 5 ºC lower than a POEGMA homopolymer of the same M_n. PEI-*graft*-POEGMA stabilised magnetic nanoparticles showed a thermally induced increase in particle cluster size from 59 nm to 93 nm at 46 ºC, which was both fully reversible and repeatable.

4.6 References

1. L. H. Sperling, *Introduction to physical polymer science*, John Wiley & Sons, 2015.

2. R. K. O'Reilly, *Polymer international*, 2010, **59**, 568-573.

3. K. Matyjaszewski and J. Xia, *Chemical Reviews*, 2001, **101**, 2921-2990.

4. M. A. Ward and T. K. Georgiou, *Polymers*, 2011, **3**, 1215-1242.

5. S. Ramakrishna, J. Mayer, E. Wintermantel and K. W. Leong, *Composites science and technology*, 2001, **61**, 1189-1224.

6. A. K. Gaharwar, N. A. Peppas and A. Khademhosseini, *Biotechnology and bioengineering*, 2014, **111**, 441-453.

7. M. Krishnamoorthy, S. Hakobyan, M. Ramstedt and J. E. Gautrot, *Chemical Reviews*, 2014, **114**, 10976-11026.

8. J. D. Andrade, *Surface and Interfacial Aspects of Biomedical Polymers: Volume 1 Surface Chemistry and Physics*, Springer Science & Business Media, 2012.

9. J. K. Oh, D. J. Siegwart, H. I. Lee, G. Sherwood, L. Peteanu, J. O. Hollinger, K. Kataoka and K. Matyjaszewski, *J. Am. Chem. Soc.*, 2007, **129**, 5939-5945.

10. D. C. Jiles, *Introduction to magnetism and magnetic materials*, CRC press, 1998.

11. A. K. Gupta and M. Gupta, *Biomaterials*, 2005, **26**, 3995-4021.

12. M. Chanana, Z. Mao and D. Wang, *Journal of biomedical nanotechnology*, 2009, **5**, 652-668.

13. C. Alexiou, R. J. Schmid, R. Jurgons, M. Kremer, G. Wanner, C. Bergemann, E. Huenges, T. Nawroth, W. Arnold and F. G. Parak, *European Biophysics Journal*, 2006, **35**, 446-450.

14. Z. R. Stephen, F. M. Kievit and M. Zhang, *Materials Today*, 2011, **14**, 330-338.

15. F.-Y. Cheng, C.-H. Su, Y.-S. Yang, C.-S. Yeh, C.-Y. Tsai, C.-L. Wu, M.-T. Wu and D.-B. Shieh, *Biomaterials*, 2005, **26**, 729-738.

16. S. Bucak, S. Sharpe, S. Kuhn and T. A. Hatton, *Biotechnology progress*, 2011, **27**, 744-750.

17. J. P. Hornak, *Basics of NMR*, Rochester Institute of Technology, Center for Imaging Science, 1997.

18. H. B. Na, I. C. Song and T. Hyeon, *Adv. Mater.*, 2009, **21**, 2133-2148.

19. C. F. Geraldes and S. Laurent, *Contrast media & molecular imaging*, 2009, **4**, 1-23.

20. J.-P. Fortin, C. Wilhelm, J. Servais, C. Ménager, J.-C. Bacri and F. Gazeau, *J. Am. Chem. Soc.*, 2007, **129**, 2628-2635.

21. F. Sonvico, S. Mornet, S. Vasseur, C. Dubernet, D. Jaillard, J. Degrouard, J. Hoebeke, E. Duguet, P. Colombo and P. Couvreur, *Bioconjugate Chem.*, 2005, **16**, 1181-1188.

22. J. Adler-Moore, *Bone marrow transplantation*, 1993, **14**, S3-7.

23. J. M. Vose, *The Oncologist*, 2004, **9**, 160-172.

24. P. Glue, R. Rouzier-Panis, C. Raffanel, R. Sabo, S. K. Gupta, M. Salfi, S. Jacobs, R. P. Clement and T. H. C. I. T. Group, *Hepatology*, 2000, **32**, 647-653.

25. T. M. Allen and P. R. Cullis, *Science*, 2004, **303**, 1818-1822.

26. K. Cho, X. Wang, S. Nie and D. M. Shin, *Clinical cancer research*, 2008, **14**, 1310-1316.

27. D. C. Popescu, R. Lems, N. A. Rossi, C. T. Yeoh, J. Loos, S. J. Holder, C. V. Bouten and N. A. Sommerdijk, *Adv. Mater.*, 2005, **17**, 2324-2329.

28. J. F. Lutz, *Adv. Mater.*, 2011, **23**, 2237-2243.

29. J. F. Lutz, O. Akdemir and A. Hoth, *J. Am. Chem. Soc.*, 2006, **128**, 13046-13047.

30. J.-F. Lutz and A. Hoth, *Macromolecules*, 2006, **39**, 893-896.

31. B. K. Nanjwade, H. M. Bechra, G. K. Derkar, F. Manvi and V. K. Nanjwade, *European Journal of Pharmaceutical Sciences*, 2009, **38**, 185-196.

32. A. F. Thünemann, D. Schütt, L. Kaufner, U. Pison and H. Möhwald, *Langmuir*, 2006, **22**, 2351-2357.

33. X. Liu, Y. Guan, Z. Ma and H. Liu, *Langmuir*, 2004, **20**, 10278-10282.

34. L. Harris, J. Goff, A. Carmichael, J. Riffle, J. Harburn, T. St. Pierre and M. Saunders, *Chemistry of Materials*, 2003, **15**, 1367-1377.

35. A. Mukhopadhyay, N. Joshi, K. Chattopadhyay and G. De, *ACS applied materials & interfaces*, 2011, **4**, 142-149.

36. H. K. Nguyen, P. Lemieux, S. V. Vinogradov, C. L. Gebhart, N. Guerin, G. Paradis, T. K. Bronich, V. Y. Alakhov and A. V. Kabanov, *Gene Ther.*, 2000, **7**, 126-138.

37. O. Boussif, F. Lezoualch, M. A. Zanta, M. D. Mergny, D. Scherman, B. Demeneix and J. P. Behr, *Proc. Natl. Acad. Sci. U. S. A.*, 1995, **92**, 7297-7301.

38. M. Turk, S. Dincer, I. S. Yulug and E. Piskin, *J. Control. Release*, 2004, **96**, 325-340.

39. C. Y. Quan, H. Wei, Y. X. Sun, S. X. Cheng, K. Shen, Z. W. Gu, X. Z. Zhang and R. X. Zhuo, *J. Nanosci. Nanotechnol.*, 2008, **8**, 2377-2384.

40. H. Cheng, J. L. Zhu, Y. X. Sun, S. X. Cheng, X. Z. Zhang and R. X. Zhuo, *Bioconjugate Chem.*, 2008, **19**, 1368-1374.

41. R. Zhang, Y. Wang, F. S. Du, Y. L. Wang, Y. X. Tan, S. P. Ji and Z. C. Li, *Macromol. Biosci.*, 2011, **11**, 1393-1406.

42. H. Petersen, P. M. Fechner, D. Fischer and T. Kissel, *Macromolecules*, 2002, **35**, 6867-6874.

43. H. Rettig, E. Krause and H. G. Börner, *Macromol. Rapid Commun.*, 2004, **25**, 1251-1256.

44. A. Limer and D. M. Haddleton, *Macromolecules*, 2006, **39**, 1353-1358.

45. P. M. Wright, G. Mantovani and D. M. Haddleton, *Journal of Polymer Science Part A: Polymer Chemistry*, 2008, **46**, 7376-7385.

46. D. J. Adams and I. Young, *J. Polym. Sci. Pol. Chem.*, 2008, **46**, 6082-6090.

47. G. J. M. Habraken, C. E. Koning and A. Heise, *J. Polym. Sci. Pol. Chem.*, 2009, **47**, 6883-6893.

48. Y. Mei, K. L. Beers, H. M. Byrd, D. L. VanderHart and N. R. Washburn, *J. Am. Chem. Soc.*, 2004, **126**, 3472-3476.

49. K. Y. Baek, M. Kamigaito and M. Sawamoto, *Journal of Polymer Science Part A: Polymer Chemistry*, 2002, **40**, 1937-1944.

50. A. Kleine, C. L. Altan, U. E. Yarar, N. A. Sommerdijk, S. Bucak and S. J. Holder, *Polymer Chemistry*, 2014, **5**, 524-534.

51. A. von Harpe, H. Petersen, Y. Li and T. Kissel, *J. Control. Release*, 2000, **69**, 309-322.

52. M. Gaborieau and P. Castignolles, *Analytical and bioanalytical chemistry*, 2011, **399**, 1413-1423.

53. L. Steinmann, J. Porath, P. Hashemi and Å. Olin, *Talanta*, 1994, **41**, 1707-1713.

54. B. L. Rivas and K. E. Geckeler, in *Polymer Synthesis Oxidation Processes*, Springer, 1992, pp. 171-188.

55. W. Maketon, C. Z. Zenner and K. L. Ogden, *Environmental science & technology*, 2008, **42**, 2124-2129.

56. Z. Shen, Y. Chen, H. Frey and S.-E. Stiriba, *Macromolecules*, 2006, **39**, 2092-2099.

57. M. Turk, S. Dincer and E. Piskin, *J. Tissue Eng. Regen. Med.*, 2007, **1**, 377-388.

58. F. J. Meyer-Almes and D. Porschke, *Biochemistry*, 1993, **32**, 4246-4253.

59. S. Nafisi, A. A. Saboury, N. Keramat, J.-F. Neault and H.-A. Tajmir-Riahi, *Journal of Molecular Structure*, 2007, **827**, 35-43.

60. Ethidium Bromide, http://what-when-how.com/molecular-biology/ethidium-bromide-molecular-biology/, (accessed 11/9/2014).

61. J. Ren, T. C. Jenkins and J. B. Chaires, *Biochemistry*, 2000, **39**, 8439-8447.

62. A. H. Lu, E. e. L. Salabas and F. Schüth, *Angewandte Chemie International Edition*, 2007, **46**, 1222-1244.

63. H. P. Klug and L. E. Alexander, *X-ray diffraction procedures*, Wiley New York, 1954.

64. Y. Yuan, D. Rende, C. L. Altan, S. Bucak, R. Ozisik and D.-A. Borca-Tasciuc, *Langmuir*, 2012, **28**, 13051-13059.

65. P. Bahadur and K. Pandya, *Langmuir*, 1992, **8**, 2666-2670.

66. P. D. Huibers, V. S. Lobanov, A. Katritzky, D. Shah and M. Karelson, *Journal of colloid and interface science*, 1997, **187**, 113-120.

67. M. Almgren, P. Bahadur, M. Jansson, P. Li, W. Brown and A. Bahadur, *Journal of colloid and interface science*, 1992, **151**, 157-165.

68. W. Brown, K. Schillen, M. Almgren, S. Hvidt and P. Bahadur, *The Journal of Physical Chemistry*, 1991, **95**, 1850-1858.

69. J. F. Lutz, *Journal of Polymer Science Part A: Polymer Chemistry*, 2008, **46**, 3459-3470.

70. S. Huber, N. Hutter and R. Jordan, *Colloid and Polymer Science*, 2008, **286**, 1653-1661.

71. A. Miasnikova and A. Laschewsky, *Journal of Polymer Science Part A: Polymer Chemistry*, 2012, **50**, 3313-3323.

72. J. Du, H. Willcock, J. P. Patterson, I. Portman and R. K. O'Reilly, *Small*, 2011, **7**, 2070-2080.

73. V. Aseyev, H. Tenhu and F. M. Winnik, in *Self Organized Nanostructures of Amphiphilic Block Copolymers II*, Springer, 2011, pp. 29-89.

74. S. J. Holder, G. G. Durand, C. T. Yeoh, E. Illi, N. J. Hardy and T. H. Richardson, *J. Polym. Sci. Pol. Chem.*, 2008, **46**, 7739-7756.

75. N. S. Ieong, K. Brebis, L. E. Daniel, R. K. O'Reilly and M. I. Gibson, *Chem. Commun.*, 2011, **47**, 11627-11629.

76. R. Sondjaja, T. A. Hatton and M. K. Tam, *Journal of Magnetism and Magnetic Materials*, 2009, **321**, 2393-2397.

77. A. Ditsch, P. E. Laibinis, D. I. Wang and T. A. Hatton, *Langmuir*, 2005, **21**, 6006-6018.

78. J.-F. Berret, N. Schonbeck, F. Gazeau, D. El Kharrat, O. Sandre, A. Vacher and M. Airiau, *J. Am. Chem. Soc.*, 2006, **128**, 1755-1761.

79. S. A. Corr, S. J. Byrne, R. Tekoriute, C. J. Meledandri, D. F. Brougham, M. Lynch, C. Kerskens, L. O'Dwyer and Y. K. Gun'ko, *J. Am. Chem. Soc.*, 2008, **130**, 4214-4215.

80. K. Raj and R. Moskowitz, *Journal of Magnetism and Magnetic Materials*, 1990, **85**, 233-245.

81. I. Šafařík and M. Šafaříková, *Journal of Chromatography B: Biomedical Sciences and Applications*, 1999, **722**, 33-53.

82. G. D. Moeser, K. A. Roach, W. H. Green, P. E. Laibinis and T. A. Hatton, *Industrial & Engineering Chemistry Research*, 2002, **41**, 4739-4749.

83. S. Bucak, D. A. Jones, P. E. Laibinis and T. A. Hatton, *Biotechnology progress*, 2003, **19**, 477-484.

84. C. Song, P. Wang and H. A. Makse, *Nature*, 2008, **453**, 629-632.

Chapter 5: Conclusions and future work

5.1 Conclusions

The main focus of the work presented within this thesis was to develop a system that enabled the successful usage of amide initiators for ATRP, and to determine the specific reasons for the previously reported failures of amide initiated systems. To this end, a novel amide based ATRP initiator (*N*-methyl 2-bromo-2-methylpropanamide) with a chemical structure similar to a widely used ester initiator (Ethyl 2-bromoisobutyrate) was synthesised.

These initiators were used in a series of polymerisations with OEGMA, which used differing reagents and/or ratios of reagents until they produced polymers with similar molecular weight parameters and kinetic characteristics that were at considered at least partially "living". The optimised conditions proposed in this work are ethanol as solvent in a 3:1 ratio with the monomer, CuCl and 4,4'-dinonyl -2,2'-bibpyridine as the catalyst system. Using these reagents, samples of POEGMA were synthesised using the amide initiator that had dispersities as low as 1.13 and molecular weights that were in close agreement to theoretical values. The pseudo-first-order kinetic plot that is often used to judge the livingness of a reaction possessed some linearity, but was observed to plateau as reactions continued indicating irreversible termination reactions were occurring. In addition to this, even within these optimised conditions amide initiated polymerisations proceeded much more slowly than when the analogous ester was used, often taking up to eight times as long to produce polymers of comparative molecular weight.

The difference between reaction kinetics was investigated through both UV-visible spectroscopy and quantum chemical calculations. Some of the previous proposed reasons for the poor performance of amide initiators were measured by UV-visible spectroscopy, but there did not appear to be any evidence of: catalyst complexation to the amide bond,[1] interruption of the catalytic system by the amide bond,[2] or a faster rate of disproportionation of Cu species in the presence

of an amide bond,[3] when these reaction conditions were used. This supports the conclusion of Adams *et al*, which was that any amide complexation was not significant.[4] Using a method previously published within the literature,[5] the rate of atom transfer polymerisation (k_{atrp}) could be calculated by observing the rate that Cu(II) species were generated. The result of this calculation stated that the activity of the ester initiator (8.32×10^{-6}) was fifteen times higher than the amide (5.37×10^{-7}). The value calculated for the ester was in close agreement to previous data reported for the same molecule but under different reaction conditions.

Quantum chemical calculations indicated that the bond dissociation energy of the halogen in the amide initiator was much larger than that of the analogous amide (Δ-22 kJ mol^{-1}). This difference equated to the ester initiator being 6335 times more reactive than the amide if no solvent effects were taken into consideration. The minimal energy conformations of amide and ester molecules suggested that there may be intramolecular hydrogen bonding occurring within the amide which acts to stabilise the alkyl halide bond. By running the calculation again whilst taking account of solvent effects, it was discovered that a polar solvent (ethanol) could reduce the difference in bond dissociation energies between amide and ester initiators so that the ester was only fourteen times more reactive than the amide. This is most likely as a result of hydrogen bonding with the solvent interrupting any intramolecular hydrogen bonding, reducing the stabilisation effect on the alkyl halide bond. The value of "fourteen time more active" fits in close proximity to the results that was calculated by UV-visible spectroscopy ("fifteen times more active").

Whilst the synthesis of a polyethyleneimine-*graft*-POEGMA had previously been reported in the literature,[6] a novel synthetic route was proposed here that utilises much less rigorous reaction conditions and contains fewer synthetic steps. The foundation of this synthesis was the one-step modification of a commercially available branched polyethyleneimine (PEI) into an ATRP macroinitiator through functionalisation of the PEI's numerous amine groups. In order to characterise the macroinitiator, the molecular structure of the starting PEI had to be determined. Through a combination of ^{1}H, ^{13}C and HMQC NMR with carbon

peak assignments taken from literature values,[7] it was calculated that there were approximately six primary, six secondary and four tertiary amines present in an average PEI molecule with a M_n of 600. This varied from the manufacturer's specification which stated that amine sites were present in a 25 : 50 : 25 ratio of primary, secondary and tertiary amines respectively. From analysis of the ^{1}H and ^{13}C NMR spectra of the functionalised PEI it was calculated that post functionalisation, each average PEI-macroinitiator molecule provided 6.6 ATRP initiation sites, resulting from the conversion of all primary amines as well as some of the secondary amines in the base material.

The PEI-macroinitiator was successfully used in the ATRP of OEGMA using the optimised conditions that were discovered previously for amide initiated ATRP. Polymers produced by this method displayed dispersities less than 1.4, but molecular weight values were invariably higher than those predicted. Post reaction it proved difficult to remove the ATRP catalyst system from the synthesised polymers, resulting in prepared samples of PEI-*graft*-POEGMA possessing a distinct green colouration indicative of the presence of copper. Despite multiple precipitations, repeated passages through silica columns, and dialysis with ligands that were known to be effective in copper removal, samples invariably remained green.

PEI is known for its ability to transfect DNA as a result of the large number of amine sites within its structure that can interact electrostatically with the phosphate groups with DNA. The ability of PEI-*graft*-POEGMA to form similar complexes with DNA was monitored using dynamic light scattering and fluorometry, with both sets of experiments indicating that complexation occurs. The result of the fluorometry was particularly intriguing as it suggested PEI-*graft*-POEGMA is orders of magnitude more effective at DNA transfection than the unmodified PEI.

Samples of PEI-*graft*-POEGMA were sent to collaborators and used as stabilisers in the synthesis of superparamagnetic nanoparticles. Particles produced in these syntheses shown no significant deviation in any characteristic when compared to particles prepared in the absence of the polymer. The lower

critical solution temperature (LCST) of a linear POEGMA homopolymer was compared to that of the PEI-*graft*-POEGMA, and polymer stabilised nanoparticle. The homopolymer possessed an LCST of 65 ºC, in close agreement to the previously reported value in the literature of 64 ºC,[8] whilst the copolymer retained the thermoresponsive activity provided by the POEGMA segment and possessed an LCST of 60.5 ºC. The thermal response of the nanoparticles was notably different, and can be summarised over three temperature ranges. Between 20 to 40 ºC there is already considerable scattering recorded and even over repeated measurements data showed large standard deviations. The average particle diameter was 59 ± 18nm, which is considerably large than the value measure by transmission electron microscopy (7.4 ± 1.5 nm), indicating that the particles are forming clusters in solution. Over the temperature range from 40 to 52 ºC the average size of the particles increases, with an inflection point at 46 ºC. Above 52 ºC the average size of particles was recorded to be 92 ± 14 nm, potentially indicating a fourfold increase in cluster size assuming irregular packing in a perfect sphere. All of these thermal changes were fully reversible and repeated cycles of heating and cooling showed identical behaviour.

Finally, the stability of PEI-*graft*-POEGMA stabilised nanoparticles was demonstrated by dispersing samples of stabilised and bare particles in solution. The unstabilised particles were observed to settle aggregate and settle out of solution in a matter of minutes, whilst stabilised particles stayed dispersed in solution over days.

5.2 Future work

The most significant further work that can be proposed from this thesis is to use the optimised reaction conditions that were developed for amide initiators in ATRP using different monomers. Whilst POEGMA is an extremely versatile monomer, a major advantage of ATRP is its ability to polymerise such a broad range of monomers. The combination of amide functionality and differing monomer units opens up numerous potential applications.

In addition to this, a brief investigation into single electron transfer living radical polymerisation (SET-LRP) was carried out and described in Chapter 3. Whilst the polymers produced possessed poor dispersity, low conversion of monomer to polymer, and much higher molecular weights than theoretically calculated, the rates of polymerisation were much fast than with conventional ATRP suggesting it may be an efficient route to higher molecular weights of amide initiated polymers so long as a measure of control can be introduced.

The novel synthesis of a poly-amide initiator for ATRP from a commercially available branched PEI allows for the ready functionalisation of polyethyleneimine. Again, further polymerisations with differing monomers are something that could be investigated as the utility of PEI-*graft*-POEGMA has already been demonstrated.

Perhaps the most surprising result in this work was the apparent improvement in DNA transfection efficiency that PEI-*graft*-POGMA possessed over unmodified PEI. This is an area that needs to be investigated more thoroughly as the potential of a transfection agent that is orders of magnitude higher than previously used materials is highly desirable.

The preparation of superparamagnetic nanoparticles that undergo cluster size transitions as a result of temperature variation could be used as a targeted drug delivery system. Magnetic hyperthermia is known to be achievable by exposing iron oxide nanoparticles to oscillating magnetic fields, and if a therapeutic agent could be embedded, encapsulated or conjugated to PEI-*graft*-PEOGMA stabilised nanoparticles then a multi-functional drug delivery system would be created. This system could be targeted through the application of an external magnetic field, and then the controlled release of its payload could be activated using magnetic hyperthermia. Whilst the temperature at which these materials undergo cluster size transition is currently slightly too high for *in vivo* usage (46 ^{o}C), the copolymerisation of OEGMA with a monomer such as 2-(2-methoxyethoxy)ethyl methacrylate should lower this temperature, highlighting the need to attempt polymerisation from the PEI-macroinitiator with monomers other than OEGMA.

5.3 References

1. J. T. Rademacher, R. Baum, M. E. Pallack, W. J. Brittain and W. J. Simonsick, *Macromolecules*, 2000, **33**, 284-288.

2. M. Teodorescu and K. Matyjaszewski, *Macromol. Rapid Commun.*, 2000, **21**, 190-194.

3. A. Limer and D. M. Haddleton, *Macromolecules*, 2006, **39**, 1353-1358.

4. D. J. Adams and I. Young, *J. Polym. Sci. Pol. Chem.*, 2008, **46**, 6082-6090.

5. W. A. Braunecker, N. V. Tsarevsky, A. Gennaro and K. Matyjaszewski, *Macromolecules*, 2009, **42**, 6348-6360.

6. R. Zhang, Y. Wang, F. S. Du, Y. L. Wang, Y. X. Tan, S. P. Ji and Z. C. Li, *Macromol. Biosci.*, 2011, **11**, 1393-1406.

7. A. von Harpe, H. Petersen, Y. Li and T. Kissel, *J. Control. Release*, 2000, **69**, 309-322.

8. J.-F. Lutz and A. Hoth, *Macromolecules*, 2006, **39**, 893-896.